Experimental Transmission of Dispersion Managed Solitons

Ian Stuart Penketh

Doctor of Philosophy

The University of Aston in Birmingham

Jaunary, 2000

The University of Aston in Birmingham

Experimental Transmission of Dispersion Managed Solitons

Ian Stuart Penketh

Doctor of Philosophy

January 2000

This thesis investigates the feasibility of soliton transmission at 1550nm over standard fibre. This is done using a dispersion compensating fibre module in each amplifier span to compensate for the high dispersion. The basic principles of soliton propagation in optical fibre are discussed within this thesis, followed by and an introduction to advantages of dispersion management. In the experimental chapter single channel transmission results are presented at 10Gbit/s and 40Gbit/s. At 10Gbit/s the effects of dispersion management on the power dispersion relationship for solitons are investigated. The detrimental effects of soliton-soliton interactions, which are increased due to the greater overlap between breathing solitons are discussed. A technique for reducing the soliton-soliton interactions through amplifier positioning is presented as a solution to this problem. The experiments demonstrate the feasibility of using standard fibre for transmission over trans-oceanic distances at 10Gbit/s. The 40Gbit/s experiment demonstrates transmission over sufficient distance for an terrestrial system. Also contained within this thesis are experimental results showing transmission of solitons over dispersion shifted fibre using a novel technique that makes use of the non-linear polarisation rotation of the soliton in the fibre. This is used to generate the effect of saturable absorption, allowing transmission distances of 200,000km to be achieved.

The experiments were conducted using a single span recirculating loop. The operation of the loop and the measurement techniques used to analyse transmission performance are all presented within this thesis.

Additional key words and phrases

Solitons, Dispersion Management, Optical fibre communications, standard fibre, non-linear polarisation rotation, saturable absorption.

Acknowledgements

Throughout the 3 years of my research at Aston, I've been supported by the Photonics Research Group at Aston University, and would like to acknowledge these people here.

Professor Nick Doran who has been my supervisor has provided guidance, and help in learning the underlying concepts behind the work in this thesis. Thanks must also go to Paul Harper and Steven Alleston who I worked closely and collaborated with in the experimental work. Finlay Knox, Andrew Gloag and Ian Phillips were helpful when developing my experimental skills during my first year.

I would also like to thank Donald Govan, Anne Niculae and J.H.B. Nijhof who provided simulations results to support my research, these results are used in the experimental chapters 5, 6, 7 and 8. Lee Richardson provided several simulation results to support the theory in chapters 2 and 3.

I would also like to thank Bert Biggs who gave excellent technical support with matters around the Lab. Finally I would like to take the opportunity to thank the other members of the research group not mentioned here for general help and sharing of knowledge.

Table of Contents

Table of Figures

Chapter 1

Introduction

1.1 Communications

The development of low loss fibres has provided a medium with potentially huge bandwidth, and it is these fibres that provide the fundamental infrastructure of the world wide communications network. This network consists of point to point transmission lines of up to 1000km for terrestrial links, and of the order of several thousand kilometres for transoceanic links. The last decade has seen services such as the Internet and E-mail emerge as practical methods of communicating, buying and selling products. The growth of these services will ensure that the demand for greater communication bandwidth will continue for the foreseeable future. To continue to meet this demand research is on going into increasing the bandwidth of these communication links. Two fundamental techniques used in telecommunication to increase the data rates across these transmission lines are Time-Division-Multiplexing (TDM) and Wavelength-Division-Multiplexing (WDM). Time division multiplexing can be achieved electrically. However it is sometimes more convenient to do this with the optical signal, since it avoids the problems of expensive high speed electronics, in which case this is referred to as Optical-Time-Division-Multiplexing (OTDM), and involves the interleaving of different channels in the time domain. This can only be achieved with channels of pulse (return to zero) format, and requires sufficient mark to space ratio to avoid intersymbol interference.

Wavelength division multiplexing is used to transmit signals at different frequencies (or wavelength) in the available bandwidth. By modulating multiple data channels on to multiple carrier waves the channels can be transmitted simultaneously across the transmission medium to the receiver, where a band pass filter and a photodiode are used to extract the channels individually. This modulation can be achieved by either electrically modulating a CW light source or by modulating the CW light externally to the light source with a light intensity modulator. These multiplexing techniques are commonly used in commercial systems today and will continue to be important in the future of high data rate communications.

1.2 Optical fibre

There are several different types of optical fibre which have different refractive index profiles such as Gaussian, triangular and multiple cladding, but for the simplicity of this introduction only step index fibre is discussed here. A schematic of such a profile is shown in Figure 1-1. A centre core and surrounding cladding make up the basic structure of the fibre. The refractive index difference Δn at the interface between the fibre core n_1, and cladding n_2 largely prevents the radiation of light into the surrounding environment. The value of Δn is typically around $4x10^{-3}$, and the values of n_1 and n_2 are around 1.45.

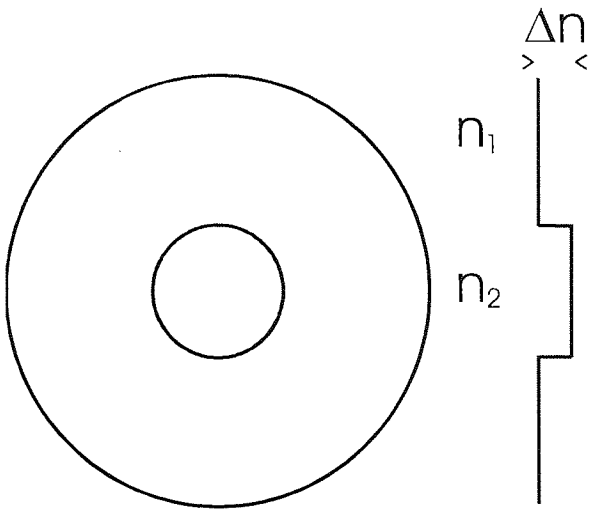

Figure 1-1 The refractive index profile transverse to the fibre axis of step index fibre. The inner core having a greater refractive index n_2 than the outer cladding refractive index n_1. The typical refractive index difference Δn is around $4x10^{-3}$.

The size of the core is an important feature in supporting propagating waves. This together with the refractive index of the core and cladding define the waveguide parameter V for a given wavelength of the light. This is given by Equation 1-1.

$$V = \frac{2\pi a}{\lambda}\sqrt{n_1^{\,2} - n_2^{\,2}}$$

Equation 1-1

where a is the radius of the core and λ is the wavelength of the propagating light. The value of the waveguide parameter determines the number of propagation modes that will be supported in the fibre. In this thesis all the experiments were carried out using fibre that supports only the fundamental mode and is referred to as single mode fibre. For single mode propagation the design of the fibre should be such that $V<2.405$[1][2]. As a result of the low waveguide parameter in single mode fibre, there is a lower cut off point λ_c for the wavelengths the fibre will support, this is given by

$$\lambda > \frac{2\pi a}{2.405}\sqrt{n_1^2 - n_2^2}$$

Equation 1-2

The depth of the cladding does not effect the waveguide parameter provided that it is large enough to fully support the modes of the fibre. For given values of n_1 and n_2, the waveguide parameter is dependent on the core radius. In single mode fibre this is typically between 2-4μm, much smaller than the typical core radius of multimode fibre in the range of 25-30μm. The disadvantage of single mode fibre is that the small core makes it difficult to couple light into the fibre, adding complexity and cost to the manufacture of compatible components. However it is necessary to use this type of fibre for long distance communications at high data rates to avoid the limitations of modal dispersion, which would otherwise make such systems impossible.

1.3 Fibre Loss

The fundamental limitation of transmission in any medium (including optical fibre) is power loss. Without loss there would be no need for amplification and the effects of noise that accompany it. The loss in fibre is defined by Equation 1-3.

$$\alpha = -\frac{1}{L}\ln\frac{P_o}{P_i}$$

Equation 1-3

where α is the loss coefficient, P_i is the input power to the fibre, P_o is the output power of fibre, and L is the length of the fibre. Often for conveniences the loss is expressed in decibels per km, which is given by

$$Loss(dB) = -\frac{10}{L}\log\frac{P_o}{P_i}$$

Equation 1-4

This loss is wavelength dependent and is a result of the combination of several characteristics. These are divided into two types, intrinsic loss and extrinsic loss. The graph in Figure 1-2 shows the loss curves of these characteristics along with the total loss with wavelength.

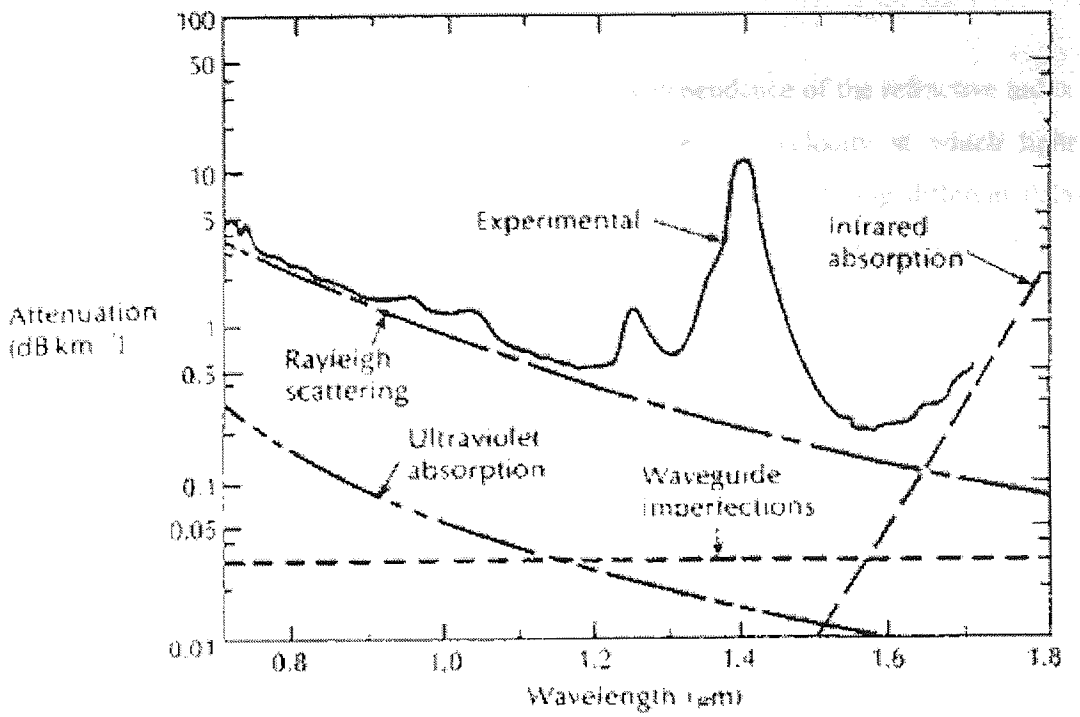

Figure 1-2 Measured attenuation with wavelength for single mode fibre. Also included are some of the loss individual loss mechanisms shown by the dashed lines.[3][4]

Rayleigh scattering contributes to the majority of the intrinsic loss of the fibre, this is proportional to λ^{-4} and is thus dominant at short wavelengths (less than 1.2μm). The intrinsic loss of material absorption dominates above 1.6μm. The presence of OH impurities in the fibre causes the majority of extrinsic loss. This produces several absorption peaks at 745nm, 950nm, 1400nm and the fundamental peak at 2700nm. These absorption peaks divide what are commonly referred to as telecommunication windows. These windows are centred at 850nm, 1300nm and 1550nm, and correspond to the first, second and third telecommunications windows respectively. Previous systems have used the 1300nm window, but modern systems use the 1550nm window to take advantage of the low fibre loss of 0.2dB/km.

1.4 Chromatic dispersion

Chromatic dispersion is an effect that causes different wavelengths of light to travel at different velocities within a medium. Since any signal with modulation will have a finite bandwidth (or range of wavelengths), this effect is particularly important in communications. The dispersion effect will cause a signal to broaden or distort with transmission as a result of the different components of the spectrum travelling at different velocities and arriving at their destination at different times. There are two sources of dispersion in an optical fibre these are the material dispersion and the waveguide dispersion, and are discussed below.

1.4.1 Material Dispersion

Material dispersion is a result of the frequency dependence of the refractive index n(ω) of the material itself. The refractive index determines the velocity at which light will propagate and thus results in different frequency components suffering different delays as they propagate through a medium. The frequency dependence of the refractive index can be approximated by a Sellmeier equation as below[5].

$$n^2(\omega) = 1 + \sum \frac{B_j \omega_j^2}{\omega_j^2 - \omega^2}$$

Equation 1-5

Where B_j is the strength of the j^{th} resonant frequency ω_j of the material. For the case of bulk silica these values have been obtained experimentally and are found to be[5] B_1 = 0.6961663, B_2 = 0.4079426, B_3 = 0.8974794, λ_1 = 0.0684043μm, λ_2 = 0.1162414 μm, λ_3 = 9.896161μm. Inserting these values into Equation 1-5 and plotting this equation as a function of λ, (where $\omega=2\pi c/\lambda$) shows this wavelength dependence of the refractive index.

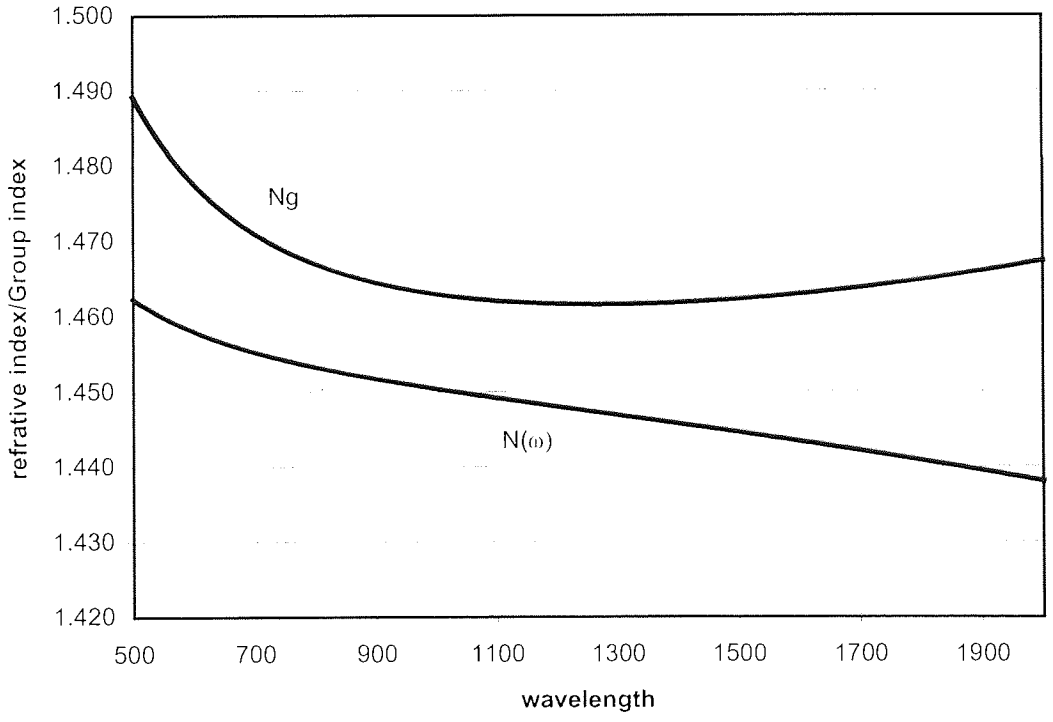

Figure 1-3 Refractive n(ω) index and Group index Ng for bulk silica against wavelength. This plot is taken from Equation 1-5.

For a monochromatic wave propagating through a material there will be points of constant phase. These points of constant phase will travel at a phase velocity v_p, which is given by

$$v_p = \frac{\omega}{\beta}$$

Equation 1-6

Where ω is the angular frequency of the wave and β is the propagation coefficient given as

$$\beta = n(\omega)\frac{2\pi}{\lambda}$$

Equation 1-7

With λ being the wavelength and $n(\omega)$ the refractive index. This wavelength dependence of β can be expanded as a Taylor series about a central frequency ω_0 and written as

$$\beta(\omega) = n(\omega)\frac{\omega}{c} = \beta_0 + \beta_1(\omega - \omega_0) + \frac{1}{2}\beta_2(\omega - \omega_0)^2 + ...$$

Equation 1-8

Where β_0, β_1, β_2 and β_3 are the inverse group velocity, group velocity, dispersion and dispersion slope respectively. These coefficents are given by

$$\beta_m = \left(\frac{d^m\beta}{d\omega^m}\right)_{\omega=\omega_0}$$

Equation 1-9

Where m is the m^{th} coefficient of the Taylor series. It is the β_2 term that is responsible for the dispersion in optical fibre. A modulated signal can be thought of as a number of closely spaced waves that propagate in a packet. This packet can be observed to propagate at a group velocity given by

$$v_g = \frac{\delta\omega}{\delta\beta}$$

Equation 1-10

The group delay of this packet is the inverse of the group velocity and corresponds to the β_1 term in Equation 1-8. This can be written as

$$v_g = \frac{c}{\left(n - \lambda \frac{dn}{d\lambda}\right)}$$

Equation 1-11

The function on the denominator being the group index, which can also be written as

$$n_g = \left(n + \omega \frac{dn}{d\omega}\right)$$

Equation 1-12

Therefore β_1 is given by

$$\beta_1 = \frac{1}{v_g} = \frac{n_g}{c} = \left(n + \omega \frac{dn}{d\omega}\right)\frac{1}{c}$$

Equation 1-13

And the β_2 term is the rate of change of the β_1 term with respect to frequency and is given by the equation

$$\beta_2 = \frac{1}{c}\left(2\frac{dn}{d\omega} + \omega \frac{d^2 n}{d\omega^2}\right) \approx \frac{\omega}{c}\frac{d^2 n}{d\omega^2} \approx \frac{\lambda^3}{2\pi c^2}\frac{d^2 n}{d\lambda^2}$$

Equation 1-14

The graph in Figure 1-4 shows a plot of the material dispersion with wavelength. The curve can be seen to cross the zero at 1270nm. This point is commonly referred to as the dispersion zero and divides two regimes known as the normal and anomalous dispersion. In the anomalous dispersion the value of β_2 is negative (seen above 1270nm), where as in the normal dispersion the value of β_2 is positive (seen below 1270nm). Although at dispersion zero the β_2 term is zero this does not mean that the dispersion is zero, it is then necessary to take into account the higher order dispersion. In the normal regime the lower wavelengths travels slower than the higher wavelengths, while the opposite is true in the anomalous regime.

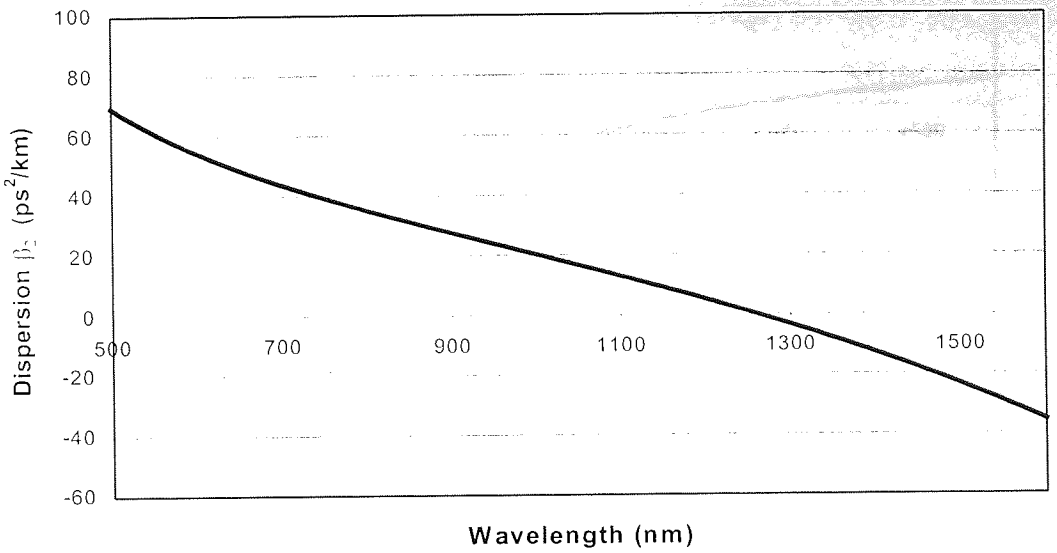

Figure 1-4 Dispersion for bulk silica with wavelength with the value of the dispersion crossing the zero axis at 1270nm (dispersion zero). With the Normal dispersion being below this point and the anomalous dispersion above this point.

It is often more convenient for experimental purposes to work with units of ps/nm km. The dispersion is then written as the derivative of the group delay with respect to wavelength as shown below.

From Equation 1-12 it can be shown that

$$\tau_g = \frac{1}{v_g} = \frac{n_g}{c} = \frac{1}{c}\left(n + \omega\frac{dn}{d\omega}\right) = \frac{1}{c}\left(n - \lambda\frac{dn}{d\lambda}\right)$$

Equation 1-15

Since the dispersion is given as the rate of change of group index with respect to wavelength, D_m (D_2 for bulk silica)can be written as

$$D_m = \frac{d\tau_g}{d\lambda} = \frac{1}{c}\left[\frac{dn}{d\lambda} - \left(\frac{dn}{d\lambda} + \frac{d^2n}{d\lambda^2}\right)\right],$$

Equation 1-16

which evaluates to

$$D_m = -\frac{\lambda}{c}\frac{d^2n}{d\lambda^2}$$

Equation 1-17

This Material dispersion is shown in Figure 1-5 in terms of ps/nm km.

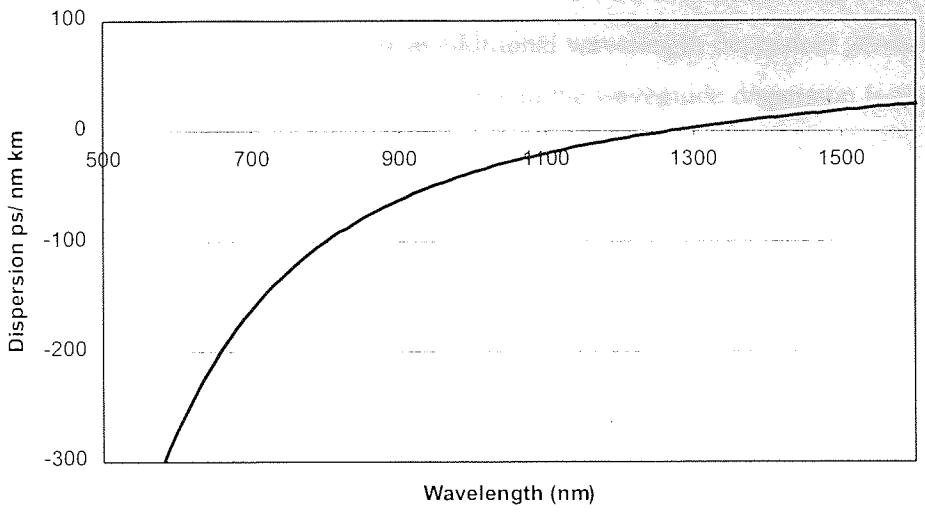

Figure 1-5 Material dispersion vs wavelength for bulk silica in ps/nm km (D_m).

The relationship between dispersion in ps^2/km (β_2) and dispersion in ps/nm km (D_2) is given by

$$D_2 = -\frac{2\pi c}{\lambda^2}\beta_2$$

Equation 1-18

where λ is the wavelength of interest and c is the speed of light.

1.4.2 Waveguide Dispersion

The dispersion in an optical fibre differs slightly from that previously discussed for bulk silica. In optical fibres the dispersive properties of the fibre structure must also be taken into consideration. Equation 1-1 (introduced at the beginning of this chapter) shows the wavelength dependence of the waveguide parameter V (or normalised frequency), which is small for high wavelengths and larger for lower wavelengths. This results in a waveguide dispersion that contributes to the overall dispersion of the fibre. To understand this waveguide dispersion physically it is useful to define the effective refractive index n_{eff}. which is given by

$$n_{eff} = \frac{\beta}{k}$$

Equation 1-19

Where β is the propagation constant of the wavelength in the fibre and k is the propagation constant in a vacuum. At high wavelengths the propagating mode in the fibre penetrates into the cladding and thus the cladding refractive index has a large bearing on n_{eff}.

At shorter wavelengths the light is more confined to the core and thus the n_{eff} is more closely matched to that of the core. This leads to an additional wavelength dependent group delay and thus an additional dispersion. The group delay due to the waveguide dispersion is given as[6]

$$\tau_g = \frac{1}{c}\left[N_{gclad} + \Delta n \frac{d(Vb)}{dV} \right]$$

Equation 1-20

Where N_{gclad} is the group index of the cladding and Δn is the refractive index difference between the core and cladding. d(Vb)/dV is the mode delay function, where V is the normalised frequency defined in Equation 1-1 and b is the normalised propagation coefficient which can be defined as[7]

$$b = 1 - \frac{U^2}{V^2}$$

Equation 1-21

Where $V^2 = U^2 + W^2$, with U and W being the eigenvalues in the core and cladding (sometimes referred to as the radial propagation constant and cladding decay parameter). For single mode step index fibre W can be defined as[8]

$$W(V) = 1 - 0.9960$$

Equation 1-22

and therefore b can be written as

$$b(V) = \left(1.1428 - \frac{0.9960}{V} \right)^2$$

Equation 1-23

To an accuracy of 0.2% for normalised frequency V between 1.5 and 2.5. Figure 1-6 shows a plot of the effective refractive index as a function of wavelength compared with those of the core and cladding.

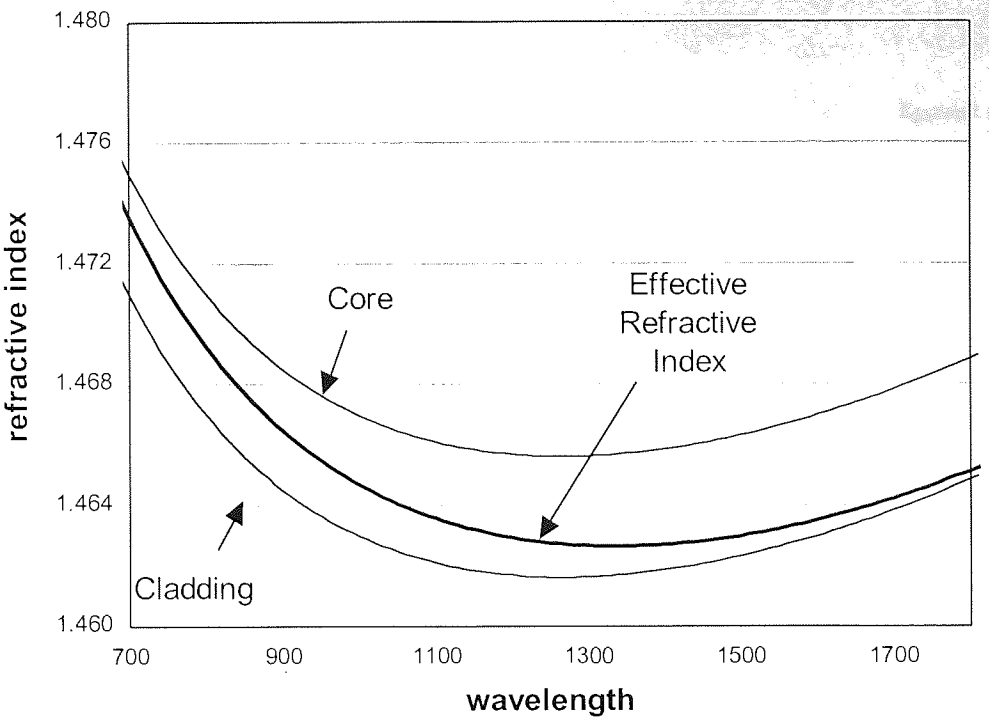

Figure 1-6 Wavelength dependence of the effective refractive index due to the fibre structure (for standard fibre) for given refractive indexs of the core and cladding. At high wavelengths a larger proportion of the propagation mode is contained within the cladding of the fibre, thus having an effective refractive index more closely matched to that of the cladding. At lower wavelength the core has a greater influence on the effective refractive index since the propagating mode in more confined to the core.

As with material dispersion the waveguide dispersion can be written in ps/nm km such that D_w is given by

$$D_w = \frac{d\tau_g}{d\lambda}$$

Equation 1-24

Substituting in $d\omega$ for $d\lambda$

$$D_w = -\frac{\omega}{\lambda}\frac{d\tau_g}{d\omega}$$

Equation 1-25

And substitute in Equation 1-20

$$D_w = -\frac{\omega}{\lambda}\frac{d}{d\omega}\frac{1}{c}\left[N_{g2} + \Delta n\frac{d(Vb)}{dV}\right]$$

Equation 1-26

Which evaluates to

$$D_w = -\frac{\omega \Delta n}{\lambda c}\frac{d}{d\omega}\left(\frac{d(Vb)}{dV}\right)$$

Equation 1-27

From Equation 1-1

$$d\omega = \frac{c}{a\sqrt{n_1^2 - n_2^2}}dV$$

Equation 1-28

Thus from Equation 1-27 D_w can be written as

$$D_w = -\frac{(n_1 - n_2)}{c\lambda}\frac{\omega a\sqrt{n_1^2 - n_2^2}}{c}\frac{d^2(Vb)}{dV \cdot dV}$$

$$= -\left(\frac{n_1 - n_2}{c\lambda}\right)V\frac{d^2(Vb)}{dV^2}$$

Equation 1-29

This waveguide dispersion contribution is shown in Figure 1-7 in terms of ps/nm km.

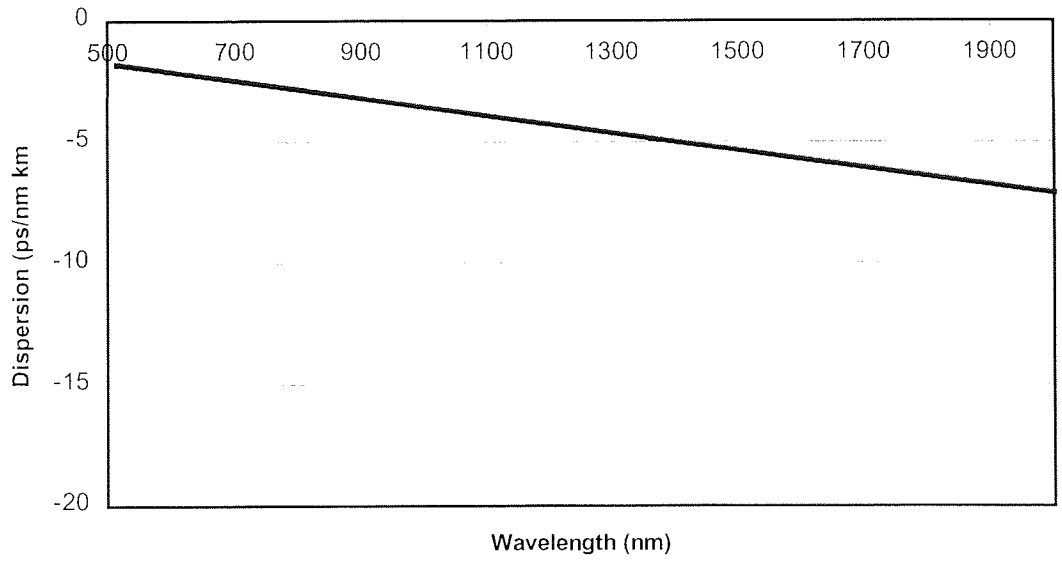

Figure 1-7 the dispersion contribution of the waveguide for standard fibre in ps/nm km.

1.4.3 Total Chromatic dispersion

The total chromatic dispersion is the supposition of both material and waveguide dispersion and is given as

$D = D_m + D_w$

Figure 1-8 shows a plot of the material dispersion, waveguide dispersion and the total dispersion with respect to wavelength.

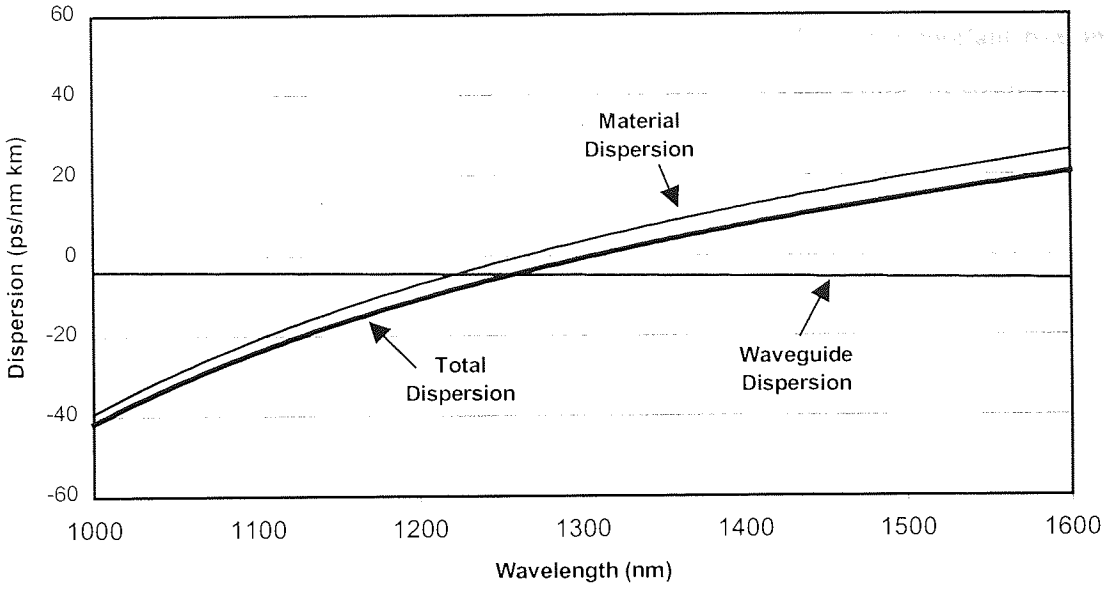

Figure 1-8 the material dispersion and the waveguide dispersion, and the combined dispersion for standard fibre, giving a dispersion zero close to 1300nm.

The effect of the waveguide dispersion is to shift the dispersion zero of the material to higher wavelengths. The reduction of the core size increases the waveguide dispersion and further shifts the dispersion zero to even higher wavelengths. It is waveguide dispersion that is used to manufacture dispersion shifted fibres where the dispersion zero of the fibre can be shifted to 1.55μm (the third telecommunications window). However the small core size associated with these fibres increases the loss. This can be overcome by using graded index fibre[9].

1.5 Non-linearity in optical fibre

Applying a large electromagnetic field to any dielectric will result in a non-linear response. In optical fibre this is seen as an intensity dependent refractive index change and is often represented by the equation below[10].

$$n(\omega, I) = n_0(\omega) + n_2 I$$

Equation 1-30

Where $n_0(\omega)$ is the linear component of the refractive index and n_2 is the intensity dependent component (non-linear component). As was discussed previously in section 1.4 the

value of the $n_0(\omega)$ is typically around 1.45. The value of n_2 taken to be around 2.5×10^{-16} cm^2/W. The typical operating powers within optical fibres tend to be in the region of a few milliwatts. At first glance this makes the contribution of n_2 seem insignificant. However when taking into account the small area of between 20 and 40μm^2 that the light is guided within, and the low loss of the fibre, this value becomes significant and plays an important role in fibre communications. In dispersion compensating fibre which is used in the experiments in Chapter 5, Chapter 6 and Chapter 8 the size of the core is smaller which results in even higher non-linear effect.

1.6 Fibre Birefringence

Despite its name, single mode fibre actually supports two propagation modes. These two modes of the fibre are orthogonally polarised to each other. For perfectly cylindrical geometry these modes have the same propagation velocities. In practice however the imperfect fabrication of the fibre will always result in a small deviation from the ideal geometry. These defects give rise to slightly different propagation constants or refractive indexes for the two modes which are referred to here as the x and y axis. The difference between the propagation coefficients of the fibre is known as modal birefringence. And is defined as

$$B = \frac{\lambda\left|\beta_x - \beta_y\right|}{2\pi} = \left|n_x - n_y\right|$$

Equation 1-31

It can be shown that the power between these modes is exchanged periodically along the fibre[11]. This period is referred to as the beat length L_B and is given as

$$L_B = \frac{2\pi}{\left|\beta_x - \beta_y\right|} = \frac{\lambda}{B}$$

Equation 1-32

There are occasions when it is desired that the light maintains its polarisation along the fibre. This can be achieved with polarisation maintaining fibre that has a large degree of birefringence such that the small random changes do not effect the polarisation of the field. Large birefringence can be introduced through elliptically shaped core and cladding, or by the introduction of stress through an axis of the fibre. For sustained polarisation along the fibre it is required that linear polarised light is launched at either one of the fast or slow axes.

1.7 Erbium Doped Fibre Amplifiers

One of the most important developments in recent years has been the Erbium doped fibre amplifier[12]. These amplifiers have a large optical bandwidth in the 3rd telecommunications window (1.55μm). The gain medium for these amplifiers consists of fibre doped with rare earth Erbium. This dopent results in several absorption peaks in the optical spectrum. By applying a pump source to the fibre at one of these wavelengths, electrons can be excited into higher energy states so that they can decay to release photons at a different wavelength. The efficiency of this process varies from absorption peak to absorption peak, with 980nm and 1480nm being the most efficient..

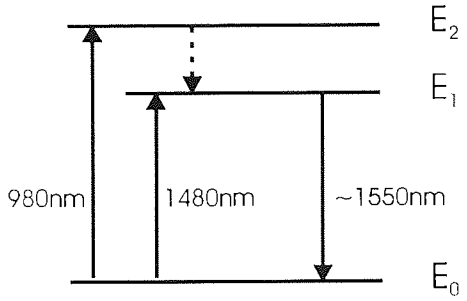

Figure 1-9 Energy level states and transition necessary for amplification, pumping at 980nm or 1480nm causes electrons to transfer into higher energy states E_1 and E_2 respectively. The 980nm has an additional transition from E_2 to E_1.

Figure 1-9 shows an energy state diagram with the transitional states of the electrons in the amplifying process. The 1480nm-pump power excites electrons from energy state E_0 into the energy state E_1. The electrons then emit photons in the 1530-1560nm region during the transition back to E_0. This transition can happen either by random spontaneous emission or by stimulation from a signal photon in the 1530-60nm region to provide amplification. Pumping at 980nm causes the electrons to be excited into a higher state E_2 from which there is a non-radiative decay to E_1. From state E_1 the electrons decay in the same way as for pumping at 1480nm. These EDFAs can provide gains greater than 25dB and a saturated output power of more than 22dBm. The expansion of the bandwidth of these amplifiers has been the subject of much research. Erbium doped fluoride fibre amplifiers have been found to give greater flatter bandwidth and have been the subject of much research[12]. The ever increasing trend towards more channels with higher data rates will result in this Erbium 1530-1560nm band (known as the C-band) of these amplifiers being completely filled. Consequently there has been recent work on a new Erbium band in the range 1570-1610nm, which can be achieved through Tellurite based erbium doped fibre[14]. Other amplifier designs have produced gain in the 1460-1510nm range[15]. These amplifiers could be used in parallel with the conventional C-band amplifiers to extend the available bandwidth to cover a region from 1460nm to 1610nm. The other important issue with regards to Erbium doped amplifiers is the flatness of the gain.

For a WDM system an uneven gain could result in a selected few wavelength channels receiving the majority of the power. This would result in low signal power for the other channels which would then result in a poor signal to noise ratio at the receiver. This is often overcome with gain flattening gratings[16][17].

1.8 Modulation Formats

There are predominantly two modulation formats that are the subject of research, these are non-return to zero (NRZ), and return to zero (RZ - pulse format). A particular form of RZ format is the soliton format, which is the focus of this thesis. These are formed through a balance between dispersion and non-linearity. An illustration of the time domain profile of these two formats is shown in Figure 1-10. For NRZ systems a high voltage represents a one and a low voltage represents a zero, for RZ systems the presence and absence of a pulse represents a one and a zero respectively.

Figure 1-10 Intensity profile of NRZ and RZ modulation formats. NRZ showing a stepwise profile, and RZ showing a pulse profile.

The main difference behind the operation of these systems is that the NRZ format is linear and must avoid the penalties of non-linearity by limiting the maximum operating power. Soliton format however makes use of the non-linearity (combined with the dispersion) in the fibre to produce stable pulses. The predominately used format in optical fibre communication systems is NRZ while RZ is being used in the most recently installed oceanic systems, but the soliton format is being proposed as possible alternative. Each of these formats have their own advantages and disadvantages. The more rapid modulation of the soliton format results in a greater spectral bandwidth than the RZ and NRZ formats. This greater bandwidth is undesirable when considering wavelength division multiplexing. The greater bandwidth requires greater channel spacing in the spectral domain. This will reduce the spectral efficiency of the available bandwidth by reducing the number of channels. However greater transmission distances are possible with soliton format[18][19]. Additionally,

unlike soliton format the non-linearity in the fibre is undesirable for linear formats, this is largely avoided by keeping the optical power propagating in the fibre low enough to avoid the non-linearity. This is a major problem when considering multiple wavelength channels, since the total power of all the channels must be less than this non-linear limit. If the number of channels in a system is doubled the power in each channel must be halved to maintain the same total power. Since solitons make use of this non-linearity this limitation does not apply, and each channel can maintain the same power regardless of the number of other channels.

Other advantages of the soliton and RZ formats are that they are more tolerant to the effects of polarisation mode dispersion[20] (which is higher in older fibre currently installed in the ground), and are compatible with optical processing techniques, such as optical time division multiplexing (OTDM) and optical switching and routing. OTDM allows operation at data rates above the capabilities of the electronic components. These optical domain routing and switching techniques could provide an alternative to current electrical nodes which will be the bottle neck of future networks.

1.9 Thesis Overview - Transmission over standard fibre

Since the development of optical amplifiers particularly the erbium doped fibre amplifier (EDFA) [12], there has been an interest in developing passive repeater free all optical transmission links. Older transmission links use electrical 3R repeater stages placed periodically across the transmission line. These repeaters Re-time, Re-shape & Re-generate the signal. The disadvantage of these systems is that they are both complex and expensive. This is due to the need to convert from the optical domain into the electrical domain where the signal is re-timed and re-shaped before being converted back into optical domain (re-generated) for transmission to the next repeater. This process is performed at every repeater stage along the link. These repeaters are also fixed in data rate making the upgrade to higher data rates difficult and expensive, since every repeater would need to be replaced. For a WDM system a separate repeater would be required for each channel at every repeater stage of the transmission link. This would make such systems impractically expensive. It is these disadvantages that provide the motivation behind the move from the 3R regenerator's to passive all optical transmission links. In these all optical systems the amplification is performed with an optical amplifier, typically an EDFA (discussed in section 1.6). The broad gain spectrum of EDFAs also makes them very attractive for Wavelength Division Multiplexing (WDM) systems, which are used in the most recently installed systems and are seen as the future of terabit and higher data rate communication systems. These erbium doped fibre amplifiers are passive making these points bit rate independent. This will remove some of the complications of upgrading to higher data rates.

While newer systems already utilise EDFAs, there is still an interest in replacing the regenerators in older presently installed links so that higher data rates can be used. A large proportion of the fibre in the ground today is standard fibre. This fibre was originally designed for transmission within the 1.3μm window (2nd communication window), as due to cost effectiveness this was the operating wavelength of the components at the time of installation. The EDFAs operate within the 1.5μm communication window (3rd telecommunication window) covering a broad range from 1530-1560nm. At these wavelengths standard fibre has a very high dispersion (In the region of 16ps/(nm km)). Such a high dispersion poses many problems that must be taken into account when considering the upgrade of these systems. The next chapter in this thesis defines a linear relationship between dispersion and stable power for a soliton. As a results of this relationship the powers required to produce a stable soliton for a dispersion of 16ps/nm km are not practical. There are several other undesirable characteristics that are more pronounced at high dispersion such as soliton-soliton interaction, Gordon Haus jitter, and electro-striction. The high dispersion also brings about a problem specific to the average soliton concept. A requirement of this is that the amplifier spacing must be much less than soliton period. As will be defined in the next chapter, the soliton period is inversely proportional to the dispersion of the fibre, and is significantly reduced at high dispersions. For standard fibre with a dispersion of 16ps/nm km and a pulse width of 15ps this would be reduced to 9km, which is not a practical amplifier span for a commercial transmission links. Failure to meet this requirement limits the maximum distance of error free transmission to only a few hundred km's[21]. These dispersion dependent characteristics are discussed further in Chapter 2.

Optical phase conjugation has been proposed as a solution to this problem[22][23], this involves the spectral inversion of the signal part way down the transmission line. As a result the spectral broadening that occurs in the first section of the link is reversed in transmission in the second half of the link. This method has been demonstrated successfully[24][25] but adds complexity to the system. Other methods involve periodic dispersion compensation. This can be done with fibre Bragg gratings[26][27][28], which used in reflection can be manufactured to produce different transmission path lengths for different wavelengths. However the most promising method to date is periodic dispersion compensation by inserting lumped lengths of high negative dispersion fibre along the transmission line. This technique is often referred to as dispersion management, and is the method of most interest in this thesis. The use of dispersion management to overcome the limitations of high dispersion in standard fibre has been the subject of much research[29][30][31][32]. These transmission systems give rise to the dispersion-managed soliton, which has many benefits over that of the uniform soliton particularly with the enhanced power. The high local dispersions are also known to be

beneficial in WDM systems, these will be discussed later in Chapter 3 of this thesis. Chapter 4 introduces the experimental setup used for the transmission experiments in the remainder of this thesis. The main focus of this thesis is single channel transmission of solitons using dispersion management over standard fibre, with the aim being to demonstrate the feasibility of upgrading currently installed standard fibre systems. It will also show in this thesis that standard fibre may also be practical for the installation of future systems for transoceanic transmission at 10Gbit/s and for terrestrial transmission at 40Gbit/s. These experiments are discussed in chapters 5, 6, 7 and 8. Chapters 5 and 6 are standard fibre relevant experiments at 10Gbit/s using lumped dispersion compensation modules. Chapter 5 investigates the dispersion tolerance of such a system, and demonstrates stable propagation at zero dispersion and in the normal regime (additional to the anomalous regime). Chapter 6 investigates the increased effect of soliton-soliton interactions in such strong dispersion management. In this experiment the soliton-soliton interaction effect is found to be the limiting factor of error free transmission. This chapter also shows that the interaction effect can be reduced by optimising the amplifier position within the map. Through this technique error free transmission up to 16,500km is demonstrated, which is the furthest distance over standard fibre using any modulation format without inline control. The experiment in Chapter 7 utilises polarisation rotation in the fibre with a polarisation discriminating element to demonstrate the benefits of saturable absorption. Distances of 200,000km error free transmission are observed over a 26km dispersion map containing a combination of mainly dispersion shifted and standard fibre. Similarly to Chapter 5 and Chapter 6, Chapter 8 is also based on the same standard fibre system however this is at the operating rate of 40Gbit/s demonstrating transmission over terrestrial transmission distances (up to a thousand kilometres).

Chapter 2

Soliton theory

2.1 Introduction

In order to study the propagation of pulses in optical fibre, an accurate mathematical model is required which can represent the propagation characteristics. The main characteristics that must be included in this equation are the fibre loss, the group velocity dispersion and the fibre non-linearity. When deriving this propagation equation (known as the non-linear Schrodinger equation - NLSE) only the first order effects of dispersion and non-linearity will be considered, but a more rigerous derivation is avalable in Ref[33]. However, for completeness there is a small section on the higher order contributions to the propagation equation in section 2.3.4 of this chapter. A stable solution in the form of a pulse for this NLSE model is presented in section 2.3.3. In section 2.3.4 of this chapter, several important soliton characteristics applicable to practical transmission systems will be discussed.

2.2 Derivation of the Non-linear Schrodinger Equation

The starting point for the derivation of the Non-linear Schrodinger Equation is the standard wave equation shown below which is derived from Maxwells equations.

$$\nabla^2 E - \frac{1}{c^2}\frac{\partial^2 E}{\partial t^2} = \mu_0 \frac{\partial^2 P_L}{\partial t^2} + \mu_0 \frac{\partial^2 P_{NL}}{\partial t^2}$$

Equation 2-1

Where E(r,t) is the electric field, c is the speed of light, μ_0 is the permeability of free space. P_L and P_{NL} are the linear and non-linear parts of the induced polarisation $P(r,t) = P_L(r,t) + P_{NL}(r,t)$. These linear and non-linear induced polarisations are related to the electric field through the dielectric tensors $\chi^{(1)}$ and $\chi^{(3)}$ respectively. To simplify the derivation, there are several assumption that must be made. Firstly, it must be assumed that P_{NL} is a small perturbation to P_L, and it is assumed that the polarisation is maintained along the fibre, thus allowing a scalar approximation. It is also assumed that the optical signal is monochromatic,

ie $\Delta\omega << \omega$. $\Delta\omega$ being the bandwidth of the signal and ω being the central frequency. *E(r,t)* can then be split into rapid and slowly varying components and written in the form

$$E(r,t) = \frac{1}{2}\hat{x}\left[\overline{E}(r,t)\exp(-i\omega_0 t) + c.c\right]$$

Equation 2-2

Where $\overline{E}(r,t)$ is the slowly varying envelope function on a carrier wave of frequency ω_0, *c.c* denotes the complex conjugate and $\hat{x}$ is the polarisation unit vector. The polarisation components P_L and P_{NL} may also be expressed in the same way as Equation 2-2.

Further simplification is achieved if it is assumed that the non-linear response is instantaneous, this allows the dispersion of $\chi^{(3)}$ to be neglected. This assumption is valid for pulse widths greater than 100 femto seconds. To obtain a wave equation for the function $\overline{E}(r,t)$ it is convenient to operate in the Fourier domain. By taking ε_{NL}, the non-linear component of the dielectric constant to be constant, the Fourier transform of *E(r,t)* which is defined as

$$E(r,\omega-\omega_0) = \int_{-\infty}^{\infty}\overline{E}(r,t)\exp(i(\omega-\omega_0)t)dt$$

Equation 2-3

is found to satisfies the Fourier domain wave equation

$$\nabla^2\widetilde{E} + \varepsilon(\omega)k_0^2\widetilde{E} = 0$$

Equation 2-4

Where $k_0 = 2\pi/\lambda$ is the propagation coefficient, and $\varepsilon(\omega)$ is the dielectric constant whose real and imaginary parts are related to $\overline{n}(\omega)$ and $\alpha(\omega)$. This can be used to define the refractive index $\overline{n}(\omega)$. However since the refractive index is intensity dependent through the non-linear component of the dielectric, it is usually written in the form

$$\overline{n}(\omega) = n(\omega) + n_2\left|\overline{E}\right|^2,$$

Equation 2-5

where $n(\omega)$ is the linear component of the refractive index and n_2 is the non-linear component that is defined as

$$n_2 = \frac{3}{8n}\chi^{(3)}_{xxxx}$$

Equation 2-6

It is the dependence of $\bar{n}(\omega)$ on the square of the electric field in Equation 2-5 that gives rise to non-linear effects such as Self Phase Modulation (SPM).

Equation 2-4 can be further solved by separation of variables to give a solution of the form

$$\tilde{E}(r,\omega-\omega_0) = F(x,y)\tilde{A}(Z,\omega-\omega_0)\exp(i\beta_0 Z)$$

Equation 2-7

Where $\tilde{A}(Z,\omega-\omega_0)$ is a slowly varying function with Z, and *F(x,y)* is the mode distribution transverse to the fibre. For a single mode fibre this is the distribution of the fundamental mode, and can be approximated by a Gaussian function. In the first order theory this is unaffected by the non-linear changes in refractive index which is thus ignored below. Thus by substituting Equation 2-7 into Equation 2-4 the propagation equation can be written as

$$\frac{\partial\tilde{A}}{\partial Z} = i\left[\beta(\omega)+\Delta\beta-\beta_0\right]\tilde{A}$$

Equation 2-8

$\Delta\beta$ can be determined by evaluating the modal distribution function F(x,y) and the refractive index difference Δn. The solution of the slowly varying amplitude $\tilde{A}(Z,\omega-\omega_0)$ can then be found by taking the inverse transform of this equation and expanding $\beta(\omega)$ as a Taylor series.

$$\beta(\omega) = \beta_0 + (\omega-\omega_0)\beta_1 + \frac{1}{2}(\omega-\omega_0)^2\beta_2 + \frac{1}{6}(\omega-\omega_0)^3\beta_3 + \ldots.$$

Equation 2-9

where ω_0 is the central frequency and

$$\beta(\omega) = \left[\frac{\partial^n\beta}{\partial\omega^n}\right]_{\omega=\omega_0}$$

Equation 2-10

β_0, β_1, β_2, β_3, are the propagation constant, the inverse group velocity, group velocity dispersion and dispersion slope respectively. The cubic and higher order terms in this expansion are ignored in this derivation since they are negliable when $\Delta\omega << \omega_0$. The cubic term is significant when β_2 (GVD) is close to or equal to zero. Substituting into Equation 2-8, and evaluating $\Delta\beta$ to obtain terms of loss α and non-linearity n_2, the equation becomes

$$\frac{\partial A}{\partial Z}+\beta_1\frac{\partial A}{\partial t}+\frac{i}{2}\beta_2\frac{\partial^2 A}{\partial t^2}+\frac{\alpha}{2}A=i\gamma|A|^2A$$

Equation 2-11

Where the non-linear coefficient gamma is defined as.

$$\gamma=\frac{n_2\omega_0}{cA_{eff}}\left[W^{-1}km^{-1}\right]$$

Equation 2-12

and A_{eff} is the effective area of the fibre, which is determined by factors such as the area of the core, the area of the cladding and the refractive index difference between the core and cladding. A_{eff} is typically between 50μm and 80μm when operating in the 1.5μm window with single mode fibre. n_2 is typically taken to be 2-3x$10^{-22}$$m^2/V^2$

A further modification is made to Equation 2-11 with the substitution

$$T=t-\frac{Z}{v_g}=t-\beta_1 Z$$

Equation 2-13

This adds a moving reference point of the pulse that propagates at the group velocity $V_g = 1/\beta_1$. The equation then become

$$i\frac{\partial A}{\partial Z}=-\frac{i}{2}\alpha A+\frac{1}{2}\beta_2\frac{\partial^2 A}{\partial T^2}-\gamma|A|^2A$$

Equation 2-14

Equation 2-14 is commonly referred to as the General Non-linear Schrodinger equation and is the basis of the analysis of propagation in the next section. The derivation of this equation has come about by neglecting the higher order terms of dispersion and non-linearity. The effects of the higher order terms are negligible for the experiments considered in this thesis, however these effects will be discussed briefly, later in this chapter.

2.3 Analysis of the Non-linear Schrodinger Equation

In this section the Non-Linear Schrodinger Equation derived previously is analysed. In order to do this two length scales are defined which are refered to as the non-linear length given as

$$L_{NL} = \frac{1}{\gamma P_0}$$

Equation 2-15

And the Dispersion length which is given as

$$L_D = \frac{\tau_0^2}{|\beta_2|}$$

Equation 2-16

From these two lengths four further regimes of the NLSE are defined which will be considered separately for a transmission system of length L. These regimes are

1) $L << L_D$, $L << L_{NL}$: This is where neither the non-linearity nor dispersion have any signifficant roll to play on a propagating signal. This regime requires no further analysis in this chapter.
2) $L << L_{NL}$, $L \geq L_D$: In this regime the effect of dispersion dominates over non-linearity and results in temporal broadening of a signal with a finite bandwidth, this is the first regime discussed in this chapter within section 2.3.1 on Group Veocity Dispersion.
3) $L << L_D$, $L \geq L_{NL}$: In this regime the effect of non-linearty dominates over dispersion, this gives rise effects such as Self Phase Modulation which leads to spectral broadening. This regime will be discussed in section 2.3.2 on Self-Phase-Modulation.
4) $L \geq L_D$, $L \geq L_{NL}$: This is the final regime discussed where both the non-linearity and dispersion play a significant role in the transmission of the signal. This gives rise to the stable pulse phenomena known as the soliton, and is discussed in The soliton solution in section 2.3.3

2.3.1 Group Velocity Dispersion

In this section the case where the dispersion characteristic of the fibre dominates is considered, and the non-linear effects are ignored. Therefore Equation 2-17 below is satisfied, with the dispersion length being much shorter than the non-linear length.

$$\frac{L_D}{L_{NL}} = \frac{\gamma P_0 \tau_0^2}{|\beta_2|} << 1$$

Equation 2-17

To ensure this criteria is met the non-linear coefficient γ is set to zero. Thus, the non-linear term (the last term) of Equation 2-14 can be removed and the NLSE can then be written as

$$i\frac{\partial A}{\partial Z} = -\frac{i}{2}\alpha A + \frac{1}{2}\beta_2 \frac{\partial^2 A}{\partial T^2}$$

Equation 2-18

The effect of loss has no influence on the dispersion and can be normalised out of the equation by substituting in *U(Z,T)* for *A(Z,T)* where

$$A(Z,T) = \sqrt{P_0}\exp\left(-\frac{\alpha Z}{2}\right)U(Z,T)$$

Equation 2-19

The NLSE equation then simplifies to

$$i\frac{\partial U}{\partial Z} = \frac{1}{2}\beta_2 \frac{\partial^2 U}{\partial T^2}$$

Equation 2-20

A solution for this equation can be found when operating in the Fourier domain. This requires a Fourier transform of $U(Z,T)$ to produce $\tilde{U}(Z,\omega)$ whose relationship is given by

$$U(Z,T) = \frac{1}{2\pi}\int_{-\infty}^{\infty}\tilde{U}(Z,\omega)\exp(-i\omega T)d\omega$$

Equation 2-21

Substituting $\tilde{U}(Z,\omega)$ into Equation 2-14 the NLSE becomes

$$i\frac{\partial \tilde{U}}{\partial Z} = -\frac{1}{2}\beta_2\omega^2\tilde{U}$$

Equation 2-22

The homogenous solution of this equation is found to be

$$\tilde{U}(Z,\omega) = \tilde{U}(0,\omega)\exp\left(\frac{i}{2}\beta_2\omega^2 Z\right),$$

Equation 2-23

where the exponent is a phase term with the phase change given by

$$\Phi = \frac{\beta_2 \omega^2 Z}{2}$$

Equation 2-24

This solution shows the effect of GVD alone, which causes a phase change of all the frequency components of the initial signal $\tilde{U}(0,\omega)$ proportional to the propagation distance Z. This solution shows that these phase changes vary as the square of the frequency through the ω^2 term. However these phase changes are not time dependent and thus will not introduce extra frequency components to the spectrum, but will however change the pulse profile during propagation.

The general time domain solution can be found by substituting this equation into Equation 2-21 to give

$$U(Z,T) = \frac{1}{2\pi} \int_{-\infty}^{\infty} \tilde{U}(0,\omega) \exp\left[\frac{i}{2}\beta_2 \omega^2 Z - i\omega T\right] d\omega$$

Equation 2-25

Where the initial condition $\tilde{U}(0,\omega)$ is found by the Fourier transform of $U(Z,T)$ when Z =0 and is given in Equation 2-26 below.

$$\tilde{U}(0,\omega) = \int_{-\infty}^{\infty} U(0,T) \exp(i\omega T) dT$$

Equation 2-26

In order to analyse the effect of dispersion on a pulse after transmission, a pulse with an initial Gaussian profile was used. The mathematical form of a Gaussian pulse lends itself to this mathematical analysis, because it is easily intergrable. The form of this function at the initial launch point is given by

$$U(0,T) = \exp\left(-\frac{T^2}{2\tau_0^2}\right)$$

Equation 2-27

Where τ_0 is the half width 1/e intensity point of the initial pulse. For a Gaussian this is related to Full Width Half Maximum (FWHM) pulse width by $T_{FWHM}=2(\ln 2)^{1/2}\tau_0$ which simplifies to $T_{FWHM}=1.665\tau_0$

Substituting Equation 2-27 into Equation 2-26 to find the Fourier transform of the initial waveform (and substituting this into Equation 2-25 to determine the function of the pulse in the time domain). The solution then evaluates to

$$U(Z,T)=\left(\frac{\tau_0^2}{\tau_0^2-i\beta_2 Z}\right)^{\frac{1}{2}}\exp\left(-\frac{T^2}{2(\tau_0^2-i\beta_2 Z)}\right)$$

Equation 2-28

The solution shows that the pulse maintains a Gaussian shape as it propagates. However, the pulse broadens temporally with transmission, with the width of the pulse as a function of Z given below

$$\tau_Z=\tau_0\sqrt{1+\left(\frac{Z}{L_D}\right)^2}$$

Equation 2-29

where $L_D=\tau_0^2/|\beta_2|$. This equation shows that increasing the dispersion increases the amount of broadening that takes place. From the L_D term it can also be seen that pulse broadening is governed by the initial pulse width and that a shorter initial pulse broadens much more quickly. This is shown in Figure 2-1 where three Gaussian pulses of initial widths 1, 2 and 4 are plotted using Equation 2-29 with β_2 set to 1. The pulse width of the shortest pulse broadens significantly more with distance than the other pulses.

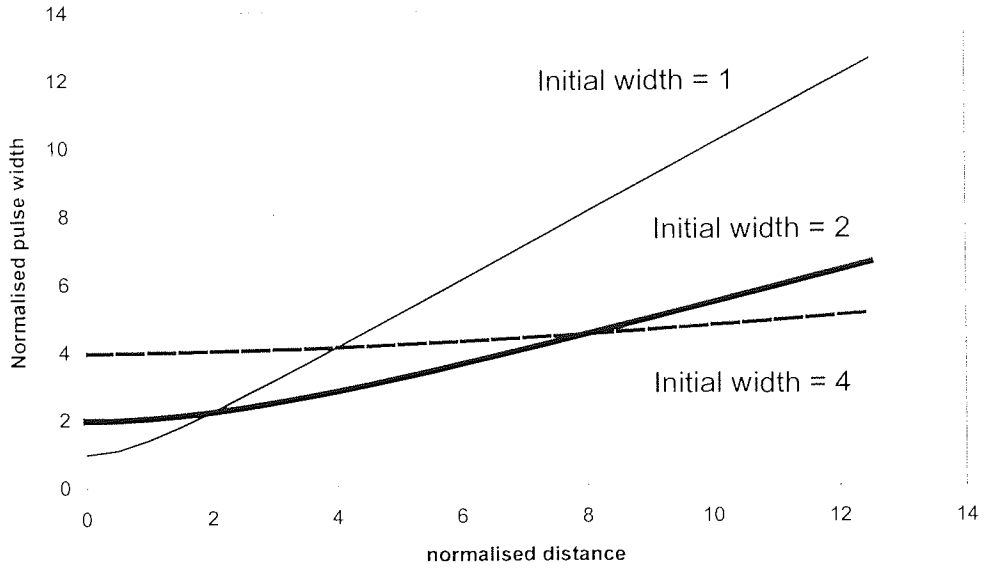

Figure 2-1 A plot of Equation 2-29 for three different Gaussian pulses with initial pulse widths of 1, 2 and 4, propagating in unity dispersion ($\beta_2 = 1$).

Comparing the solution in Equation 2-27 with the original pulse function, it can clearly be seen that the pulse frequency components have been subject to a phase change. This phase

change can be determined mathematically by separating the equation into its amplitude and phase components into the form shown below

$$U(Z,T) = |U(Z,T)| \exp(i\phi(Z,T))$$

Equation 2-30

The phase component extracted using this equation is found to be.

$$\phi(Z,T) = -\frac{\mathrm{sgn}(\beta_2)\left(\frac{Z}{L_D}\right)T^2}{1+\left(\frac{Z}{L_D}\right)^2\tau_0^2} + \tan^{-1}\left(\frac{Z}{L_D}\right)$$

Equation 2-31

Where sgn(β_2) signifies the sign of β_2. The instantaneous frequency change across the pulse is give by the time differentiation of this equation and is therefore

$$\delta\omega = -\frac{\partial\phi}{\partial T} = 2\frac{\mathrm{sgn}(\beta_2)\left(\frac{Z}{L_D}\right)}{1+\left(\frac{Z}{L_D}\right)^2}\frac{T}{\tau_0^2}$$

Equation 2-32

This equation shows that the frequency shift acquired is linear across the pulse. The pulse broadening can be understood physically from the fact that different frequency components travel at different velocities due to the dispersion. Since the pulse is a form of modulation, there will always be a finite spectrum of frequencies that will travel at different velocities and thus disperse in time. The pulse broadening depends on the initial pulse width, which can be understood from the fact that shorter pulses have a more rapid modulation, which in turn results in a broader spectrum of frequencies. This broader spectrum of frequenices only serves to increase the effect of dispersion. This pulse broadening due to dispersion is often referred to as chirp, since there is an instantaneous frequency chirp across the profile of the pulse. There are therefore two signs of chirp that a pulse can acquire corresponding to the two different dispersion regimes, $\beta_2 > 0$ (Normal) , or $\beta_2 < 0$ (anonalous). In the first case the chirp results in the red components traveling faster than the blue components of the signal spectrum, while the opposite is true in the anomalous regime. It can be seen from Equation 2-32 that a chirp free Gaussian pulse, launched into the fibre will

broaden by equal amounts in the normal and anomalous regimes (ie the broadening effect is independent of the sign of β_2). The effect is somewhat different if the input pulse already has chirp. Considering here the effect of launching a Gaussian pulse that is linearly chirped and whose function is

$$U(0,T) = \exp\left[-\frac{(1+iC)}{2}\frac{T^2}{T_0^2}\right]$$

Equation 2-33

Where C is the chirp parameter. By repeating the previous process, the function of the pulse with propagation distance Z is derived as

$$U(z,T) = \sqrt{\frac{T_0^2}{T_0^2 - i\beta_2 z(1+iC)}}\exp\left[-\frac{(1+iC)T_0^2}{2[T_0^2 - i\beta_2 z(1+iC)]}\right]$$

Equation 2-34

from which the broadening factor with distance is given by the function.

$$\frac{T_1}{T_0} = \sqrt{\left(1+\frac{C\beta_2 z}{T_0^2}\right)^2 + \left(\frac{\beta_2 z}{T_0^2}\right)^2}$$

Equation 2-35

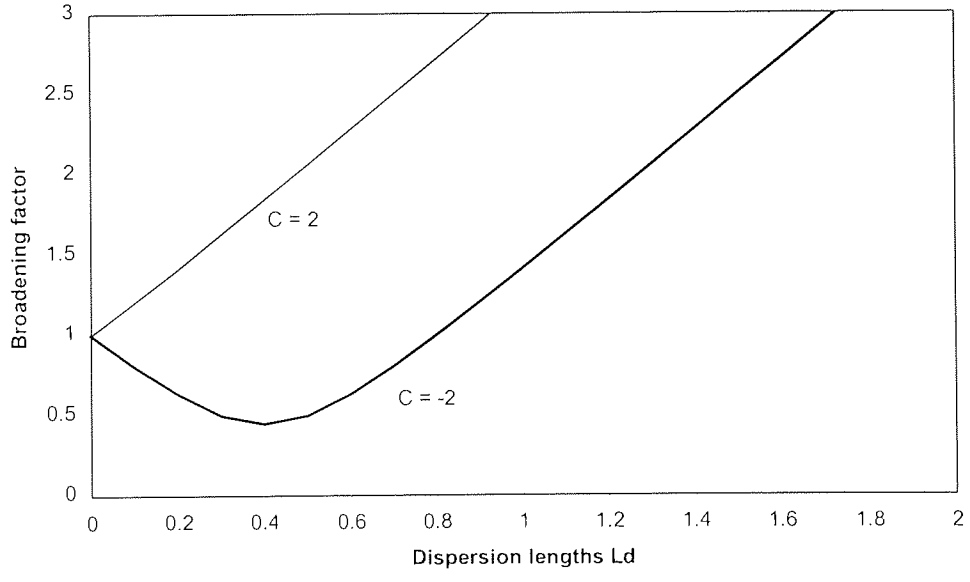

Figure 2-2 The broadening factor with transmission distance in the Normal dispersion for a pulse with different sins of chirp. The two lines represent initial chirps of –2, and 2. The pulse with positive chirp undergoes compression before broadening

The graph above shows the broadening factor with distance for two opposite initial chirps for a Gaussian shaped pulse launched in Normal dispersion (β_2 being positive). For the case when the pulse is positively chirped, broadening occurs immediately with transmission. When the pulse is launched with a negative chirp it under goes a narrowing process before it broadens with transmission. This is as a result of the chirp being imposed by the normal disperison fibre being opposite to that already present on the pulse. In the initial transmission the pulse undergoes a narrowing process as the original chirp is counter-acted during propagation.

2.3.2 Self Phase Modulation

In this section the effects of dispersion are neglected, so that we only consider the effects of Self Phase Modulation (SPM) from the non-linearity component of the NLS equation. For this, the dispersion length is considered to be much greater then the non-linear length and Equation 2-36 below is satisfied.

$$\frac{L_D}{L_{NL}} = \frac{\gamma P_0 \tau_0^2}{|\beta_2|} >> 1$$

Equation 2-36

This is achieved by setting the value of β_2 to 0 in Equation 2-14. Again as with the previous section the amplitude loss function is normalised with

$$A(Z,T) = \sqrt{P_0}\exp\left(-\frac{\alpha Z}{2}\right)U(Z,T)$$

Equation 2-37

and the NLSE becomes

$$\frac{\partial U}{\partial Z} = \frac{i}{L_{NL}}\exp(-\alpha Z)|U|^2 U$$

Equation 2-38

It is important to note that although the amplitude is normalised the loss coefficent is still present in this equation since it has an effect on the non-linearity. This equation can easily be solved to give the solution

$$U(Z,T) = U(0,T)\exp(i\phi_{NL}(Z,T))$$

Equation 2-39

Where U(0,T) is the initial waveform at Z=0. And the phase component is given by

$$\phi_{NL}(Z,T) = |U(0,T)|^2 \frac{Z_{eff}}{L_{NL}}$$

Equation 2-40

The effective transmission distance Z_{eff} (which is smaller than Z due to the power loss and therefore reduced non-linearity) is given by

$$Z_{eff} = \frac{1}{\alpha}\left[1 - \exp(-\alpha Z)\right]$$

Equation 2-41

The maximum phase shift of the pulse occurs at the centre T=0 and has a magnitude of

$$\phi_{\max} = \frac{Z_{eff}}{L_{NL}} = \gamma P_0 Z_{eff}$$

Equation 2-42

Where P_0 is the peak power of the pulse and γ is the non-linear coefficient. From this equation the non-linear length is defined as the effective distance over which $\phi_{max} = 1$ ($Z_{eff} = L_{NL}$) for non-linearity acting alone.

By differentiating Equation 2-40 with respect to time, a frequency chirp imposed on the pulse can be given by Equation 2-43. This chirp is found to increase with distance. It is also time dependent and will thus generate new frequency components with propagation, ultimately causing spectral broadening. This is a contrast with GVD, which broadens the pulse temporally, but does not effect the spectrum of the pulse.

$$\delta\omega = -\frac{\partial \phi_{NL}}{\partial T} = -\frac{\partial |U(0,T)|^2}{\partial T}\frac{Z_{eff}}{L_{NL}}$$

Equation 2-43

Again as with the dispersion effect let us consider the effect of launching a pulse, this time a super Gaussian profile pulse with an initial field given by

$$U(0,T) = \exp\left[-\frac{1}{2}\left(\frac{T}{T_0}\right)^{2m}\right]$$

Equation 2-44

where m is the order of the super Gaussian pulse (m=1 for Gaussian). The self phase modulation induces a frequency shift on the pulse and is given as

$$\delta\omega = \frac{2m}{T_0}\frac{Z_{eff}}{L_{NL}}\left(\frac{T}{T_0}\right)^{2m-1}\exp\left[-\left(\frac{T}{T_0}\right)^{2m}\right]$$

Equation 2-45

Equation 2-45 is plotted for m=1,2 and 4 on the graph in Figure 2-3 along with the respective pulse profiles.

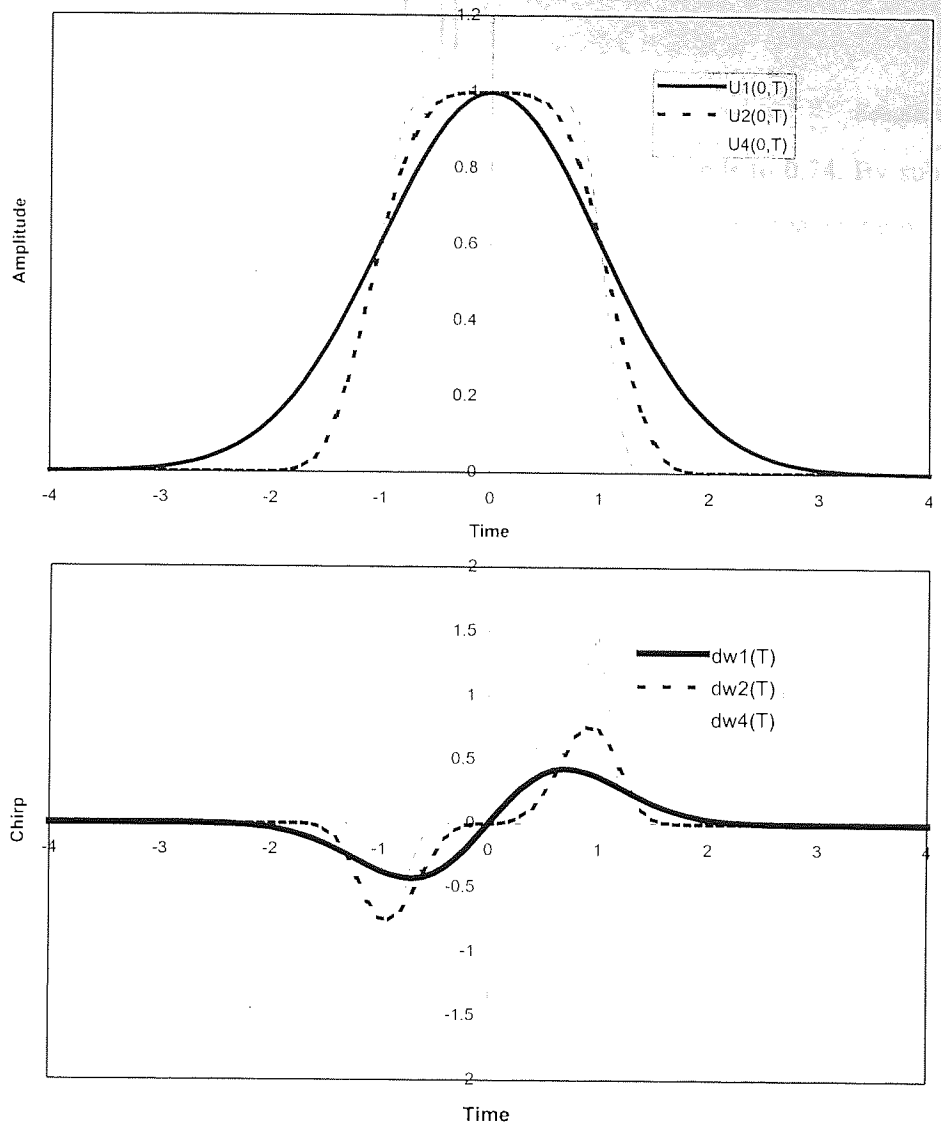

Figure 2-3 The effect of transmission of a pulse with a unit width T_0 and effective transmission distance equal to the non-linear length L_{NL}. The top graph shows the amplitude of the three Gaussian pulses, while the bottom graph shows the induced chirp caused by the differential phase change across the Gaussian pulses. The thick black line represents the 1st order Gaussian (m=1). While the thick dashed line and the thin dashed line, represent the 2nd and 4th order Gaussian pulses respectively.

It can clearly be seen from the graph that the frequency chirp is greater for steeper edges of the pulse. The amount of spectral broadening can be determined from the maximum value of $\delta\omega$. This can be calculated from Equation 2-43 by setting its derivative to zero. Thus $\delta\omega_{max}$ is given as

$$\delta\omega_{max} = \frac{fm}{T_0}\phi_{max}$$

Equation 2-46

Where ϕ_{max} is given by $\phi_{max} = Z_{eff}/L_{NL} = \gamma P_0 Z_{eff}$ and f is a constant which is given by

$$f = 2\left(1-\frac{1}{2m}\right)^{1-1/2m}\exp\left[-\left(1-\frac{1}{2m}\right)\right]$$

Equation 2-47

For m = 1, f is equal 0.86, For greater values of m this tends to 0.74. By substituting $\Delta\omega$ for $1/T_0$ (as $\Delta\omega=1/T_0$ where $\Delta\omega$ is the 1/e half width). The spectral broadening becomes

$$\delta\omega_{max} = 0.86\Delta\omega\phi_{max}$$

Equation 2-48

For a Gaussian (m=1).

2.3.3 The soliton solution

In the previous two sections, GVD and SPM were considered individually. In this section the case is considered where both of these characteristics act together, thus having the dispersion length and non-linear length roughly equal in distance. The loss coefficient α is set to zero to simplify the equation. The NLSE can then be written as

$$i\frac{\partial A}{\partial Z} = \frac{1}{2}\beta_2\frac{\partial^2 A}{\partial T^2} - \gamma|A|^2 A$$

Equation 2-49

To simplify calculations further, three normalised substitutions are introduced into Equation 2-49, these are shown below.

$$u = N\frac{A}{\sqrt{P_0}} \qquad z = \frac{Z}{L_D} \qquad \tau = \frac{T}{\tau_0}$$

Equation 2-50

Where N is defined as

$$N^2 = \frac{L_D}{L_{NL}} = \frac{\gamma P_0 \tau_0^2}{|\beta_2|}$$

Equation 2-51

Equation 2-49 then becomes

$$i\frac{\partial u}{\partial z} + \frac{1}{2}\frac{\partial^2 u}{\partial \tau^2} + |u|^2 u = 0$$

Equation 2-52

The sign of the dispersion is taken to be anomalous or negative ($\text{sgn}(\beta_2) = -1$). For the normal dispersion regime the dispersive term (2^{nd} term) is negative. Equation 2-52 can be solved using the inverse scattering method in terms of eigenvalues, which was first proposed by Gardner et al[34], and was used by Zakharov and Shabat[35] to solve the NLSE. The technique is beyond the scope of this thesis, and here the solution will only be quoted. Consider the 1^{st} order solution of the NLSE, since it is the 1^{st} order (fundamental) solution with N=1 that is of most interest in optical fibre communications. This is the case in which there is only one eigenvalue solution. Higher order solitons also exsist but have some undesirble pulse splitting characteristics. The solution has the general form

$$u(z,\tau) = 2\zeta \sec h(2\zeta\tau)\exp(2i\zeta^2 z)$$

Equation 2-53

where ζ is the eigenvalue and determines the soliton amplitude. Normalising u(0,0), by setting $2\zeta = 1$, the fundamental soliton solution is reached, which is of the form of a hyperbolic secant and is given below.

$$u(z,\tau) = \sec h(\tau)\exp\left(iz/2\right)$$

Equation 2-54

From Equation 2-49, the relationship between the peak power, pulse width and the dispersion for the N=1 soliton is given as

$$P_0 = \frac{|\beta_2|}{\gamma\tau_0^2}$$

Equation 2-55

This proportional relationship between power and dispersion is particularly important in practical systems, since lower dispersion results in lower stable peak power. At zero dispersion the soliton peak power goes to zero. This together with the noise generated by the amplifier places a lower limit on the operating dispersion in a real system.

The further solutions to the NLSE are

$$u(0,\tau) = N \sec h(\tau)$$

Equation 2-56

Where N is an integer related to the order of the soliton. For higher order solitons, the required peak pulse power must be N^2 times greater than the peak power of the fundamental soliton. These higher order solitons have a peculiar evolution process, where pulse splitting occurs during transmission only for the pulses to reform back into the original shape. This happens periodically with distance $Z = m\pi$, where m is an integer. This period is referred to as the soliton period and in physical units is given as

$$Z_0 = \frac{\pi}{2} L_D = \frac{\pi}{2} \frac{\tau_0^2}{|\beta_2|}$$

Equation 2-57

The relationship between τ_0 and τ_{fwhm} for a hyperbolic sechant is given by

$$\tau_{fwhm} = 2\ln\left(1+\sqrt{2}\right)\tau_0$$

Equation 2-58

To understand the reason for the stable solution it is useful to consider the sign of the chirps that would other wise be induced by the SPM and GVD. The sign of the chirp induced by GVD is dependent on the sign of the dispersion coefficient. The chirp on the pulse resulting from SPM is always of the same sign since the frequency shift is opposite to the gradient of the pulse power profile (For a pulse there is always a positive gradient on the leading edge and a negative gradient on the trailing edge). In the anomalous dispersion regime these two sources of the chirp are opposed and can cancel out to produce a stable soliton. In the normal regime however, the chirps induced on the pulse due to SPM and GVD are of the same sign and thus accumulate with transmission and do not cancel out.

2.3.4 Higher order effects

The analysis of the NLSE in the previous sections of this chapter was carried out while neglecting the higher order effects. The inclusion of these effects adds extra terms to the general NLSE. By including the 3rd order dispersion and higher order non-linearity terms of self steepening and self frequency shift the NLSE becomes[35]

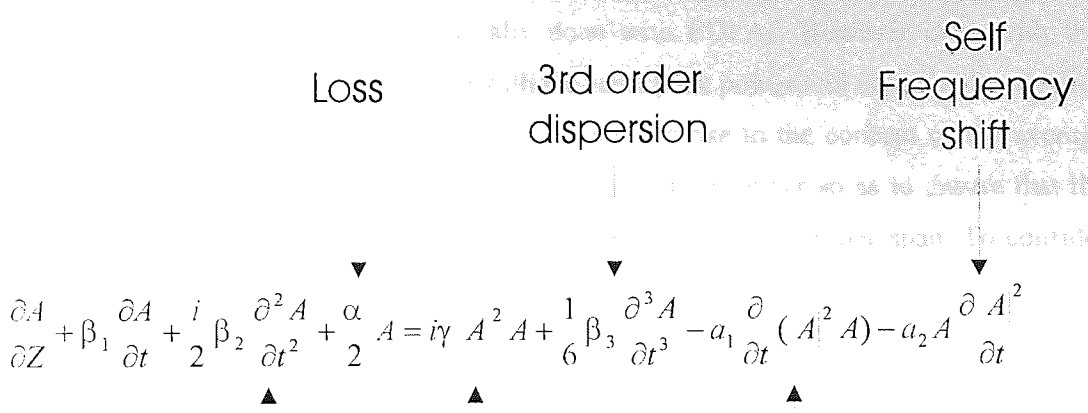

These extra terms become important when dealing with very short pulses (less than 100fs). The 3rd order dispersion is also generally required when operating close to the dispersion zero. The necessity to include this term for short pulses arises from the broad spectrum of the pulse. The 3rd order dispersion without the presence of non-linearity and β_2 set to zero, has the effect of generating oscillations on either the tails or leading edge of the pulse (depending on the sign of β_3), but these oscillations are significantly reduced in the presence of β_2. The self-steepening term arises as a result of the intensity dependence of the group velocity, which causes the peak of the pulse to shift towards the trailing edge, resulting in a steepening of the trailing edge of the pulse. Theoretically without dispersion this would continue until the point, where there is an infinitely sharp rising edge of the pulse, referred to as the optical shock. However in practice this never happens since the GVD term will start to dominate as the pulse edge gets sharper and the spectral width increases. As with the β_3 term the self-frequency shift term becomes significant for short pulses due to the broad spectral width. The source of the frequency shift is Raman gain which can amplify the lower frequency components with energy from the higher frequency components, thus causing a self frequency shift of the pulse energy towards higher wavelengths. The physical reason behind this effect comes from the retarded non-linear response.

2.3.5 Effect of loss and amplification (Average soliton)

In the previous section a stable solution was discussed for the NLSE. This stable solution neglected the effects of loss in the fibre. A pulse launched into the fibre with the same peak power as that that would be required for the loss less case, would experience attenuation as it propagates along the fibre. This in turn would reduce the non-linearity component in the NLSE and allow the dispersive term in Equation 2-14 to dominate, causing the pulse to broaden. This problem of loss is overcome by periodic amplification along the

transmission line. In practice this is usually done with EDFAs. However even with this discrete periodic amplification, launching with the same peak power will not give the required balance between non-linearity and dispersion. This gives rise to the concept of the average soliton[37][38][39], which involves launching pulses with higher power so as to ensure that the non-linearity and dispersion are exactly balanced over an entire amplifier span. To consider the effects of loss in the NLSE, Equation 2-14 is used, this time with α not equal to 0.

$$i\frac{\partial u}{\partial z}+\frac{1}{2}\frac{\partial^2 u}{\partial \tau^2}+|u|^2 u=-i\Gamma u$$

Equation 2-59

The loss has been normalised with Γ. Where Γ is defined as

$$\Gamma=\frac{\alpha}{2}L_D$$

Equation 2-60

To compensate for the loss of the fibre span, the input field and output field must be related by

$$u_2(mz_a)=G^{\frac{1}{2}}u_1(mz_a)\ ,$$

Equation 2-61

where u_1 is the field before the j^{th} amplifier and u_2 is the field at the output of the amplifier,G is defined as

$$G=e^{2\Gamma z_a}$$

Equation 2-62

And z_a is defined as

$$z_a=\frac{L_a}{L_D}\ ,$$

Equation 2-63

where L_a is the amplifier spacing. The amplifiers can be considered discrete compared with the amplifier span since the amplifiers are typically 10s of metres long compared with the span length (10s of km). Thus the transformation below is introduced

$$u(z,\tau) = \Lambda(z)R(z,\tau)$$

Equation 2-64

and equation becomes

$$i\frac{\partial R}{\partial z} + \frac{1}{2}\frac{\partial^2 R}{\partial \tau^2} + \Lambda^2(z)|R|^2 R = 0$$

Equation 2-65

Where

$$\Lambda(z) = \Lambda(0)e^{-\Gamma(z-ma)}$$

Equation 2-66

This shows an exponentially decaying energy between amplifiers, periodically along the transmission line. To achieve the balance between non-linearity and dispersion the average power is set equal to that of the lossless case. Then launch power $\Lambda^2(0)$ that is required is given as

$$\left\langle \Lambda^2(z) \right\rangle = \frac{1}{Z_a}\int_0^{z_a} \Lambda^2(z)dz = 1$$

Equation 2-67

Substituting in Equation 2-66 and evaluating gives

$$\Lambda^2(0) = \Lambda_0^2 = \frac{2\Gamma z_a}{1-e^{-2\Gamma z_a}} = \frac{G\ln G}{G-1}$$

Equation 2-68

The launch peak power for the soliton is then defined as

$$P_0 = \Lambda_0^2 \frac{|\beta_2|}{\gamma\tau_0^2}$$

Equation 2-69

If the amplifier period is short compared with the soliton period then this is a good approximation. As a guide it is desirable that the amplifier spacing meets the requirement $Z_a<8(Z_0)/10$[40]. Not meeting this requirement results in radiation of dispersive waves which can be amplified and limit the maximum transmission distance[41]. The dispersion power relationship discussed in section 2.3.3 and the signal to noise constraint discussed later in this chapter place a lower limit on the dispersion term. This has a serious implication on the amplifier spacing for short pulses that are required for high data rates. Two methods of overcoming this problem are discussed in Chapter 3. The result of the higher launch power is that the non-linearity dominates over the first part of the span until the pulse power has fallen below the average power, where the dispersion dominates until the next amplifier. This is illustrated in Figure 2-4. The average power is shown by the dotted line.

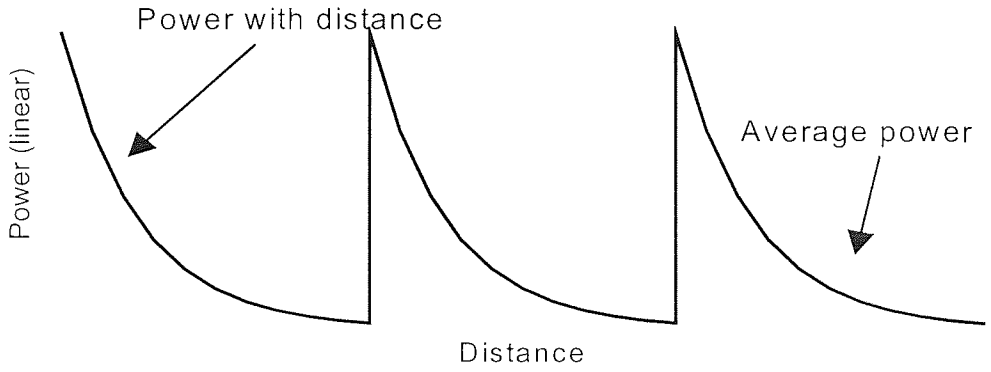

Figure 2-4 Loss and Amplification of soliton during propagation, The soliton average power is shown with a dotted line.

2.4 Soliton transmission characteristics

In the design of a practical soliton transmission system many factors must be considered. There are several system parameters, which govern transmission limitations. Pulse width, pulse power, pulse separation and amplifier spacing are just some the parameters which influence the transmission through effects such as Signal to noise ratio, Gordon Haus jitter, Electrostriction, Soliton-soliton interactions, Cross phase modulation and Birefringence. These characteristics are discussed in this section along with how they limit the system and how they can be reduced.

2.4.1 Signal to Noise ratio

One of the main limiting factors arising from the introduction of amplification comes from the required signal to noise ratio at the receiver. This problem is predominately as a

result of the noise generated by the amplifiers which combines with the signal. This ratio must be kept above a certain value to ensure error free transmission. The signal to noise ratio of a signal at the receiver is the signal power divided by the noise power, and can be written as

$$SNR = \frac{\left\langle i_{sig}^2 \right\rangle}{\left\langle i_{noise}^2 \right\rangle}$$

Equation 2-70

Where i_{sig} and i_{noise} are the currents of the signal and noise respectively. There are many sources of this noise at the receiver. These include the beating of the signal (signal spontaneous) and ASE frequencies (spontaneous-spontaneous), the shot noise and the thermal noise of the receiver. It is the former two sources of noise from the amplifier that are of most concern. The signal to noise ratio due to this beating is given by[42]

$$SNR = \frac{\left(\frac{eS_0}{(h\nu)}\right)^2}{\left(\frac{eS_0}{(h\nu)}\right)^2 S_0 N_a F_0} = \frac{S_0}{4N_a F_0}$$

Equation 2-71

Where S_0 is the signal power out of the amplifiers, h is Planks constant, e is the charge on an electron, ν is the frequency of the signal, N_a is the number of amplifiers the signal has passed through. F_0 is the noise figure for a given bandwidth B and is defined as

$$F_0 = (G-1)\mu h\nu B \,,$$

Equation 2-72

where μ is the inversion factor of the amplifiers and G is the gain. Substituting this into Equation 2-71 the signal to noise ratio can then be written as

$$SNR = \frac{S_0}{4N_a(G-1)\mu hB}$$

Equation 2-73

This equation shows the proportional relationship between the signal power and the Signal to Noise Ratio (SNR) of the receiver, where B is taken to be the bandwidth of the signal. For a given system this places a lower limit on the operating power. From section

2.3.3 a proportional relationship between soliton power and the operating dispersion was derived. Therefore it is this lower power limit that places a lower limit on the dispersion of the transmission line. This has major implications when considering effects such as Gordon Haus jitter. In practice for error free operation (an error rate of less than 10^{-9}) a signal to noise ratio of no less than 23dB is required.

Although it is not clear from Equation 2-73, it is possible to reduce the signal to noise ratio at the receiver by reducing the amplifier spacing. While this would increase N_a (the number amplfiers), the reduction in loss per amplifier would mean a reduction in the gain by a greater factor. For example a 6000km system with an amplifier span of 60km would require a gain of 12dB to compensate for the fibre loss (assuming the loss of fibre to be 0.2dB/km). Halving the amplifier span to 30km would mean doubling the number of amplifiers, however this would also mean that the gain G is reduced by a quarter (6dB). From Equation 2-73 it can be seen that the overall effect would be to increase the SNR at the receiver. In a practical system however, it is more desirable that amplifier spans be as long as possible to reduce the cost of the system.

2.4.2 Gordon-Haus jitter

Another major problem resulting from the generation of ASE through amplification is Gordon Haus jitter[43]. The resilience of solitons to perturbation results in some of the ASE that is released by the amplifiers being absorbed during propagation. The absorbed noise has an effect on the soliton amplitude, the temporal position, the soliton phase and the soliton frequency (wavelength). It is this last effect which is particularly detrimental to long distance transmission. The absorption of ASE results in small random changes in the central wavelength of the solitons. The effect of GVD translates these random wavelength changes into random velocity changes of the pulses. These in turn result in an r.m.s. timing jitter at the receiver as pulses move temporally from the centre of their bit slot. These temporal shifts increase as a function of distance. We define here the change in temporal position for a pulse as the group delay $\Delta\tau_g$ due to a frequency change $\Delta\omega$ over one amplifier span as[44]

$$\Delta\tau_g = \beta_2 L_a \Delta\omega \quad ,$$

Equation 2-74

where L_a is the amplifier spacing. By considering the distribution of the random varations in temporal position over a full system with multiple amplifiers, an estimate of the random timing jitter can be derived as

$$\left\langle t_N^2 \right\rangle = \frac{2\pi n_2 N_{sp} |\beta_2| hc(G-1)L^3}{9\tau_0 \lambda^2 A_{eff} L_a \Lambda_0^2}$$

Equation 2-75

Where N_{sp} is the spontaneous emission factor of the amplifier, h is planks constant, L_a is the amplifier spacing and G is the amplifier gain. This shows that the jitter increases with length as a function of $L^{3/2}$.

In order to avoid errors the pulse arrival times must coincide with a time window τ_w, which is typically taken to be one third of the bit window. Assuming a Gaussian distribution of arrival times, for an error rate of less than 10^{-9} the maximum tolerable variance $<\tau_N^2>$ is given by[45]

$$\left\langle t_N^2 \right\rangle \leq \left(\frac{t_w}{6.1} \right)^2$$

Equation 2-76

Combining this equation with Equation 2-75, the maximum distance of error free transmission L_{max} due to Gordon Haus jitter can be determined for a given a set of parameters. This is shown in Equation 2-77 below.

$$L_{\max}^3 = 0.1372 \frac{\tau_{fwhm} t_\omega^2 A_{eff} L_a \Lambda_0^2}{N_{SP} n_2 D_2 h(G-1)}$$

Equation 2-77

The terms of D_2 and τ_{fwhm} terms are included through the substitution of Equation 1-18 and Equation 2-58. The maximum distance of error free transmission is given as

$$L_{\max} = \frac{0.5158}{R} \left[\frac{k_F k_\omega{}^2 A_{eff} L_a \Lambda_0^2}{N_{SP} n_2 D_2 h(\exp(\alpha L_a) - 1)} \right]^{1/3}$$

Equation 2-78

The Gordon Haus effect is one of the major limiting factors of long distance soliton transmission and its suppression has been the subject of much research. One method is to reduce the random frequency changes that occur by suppressing the ASE released by the amplifiers. This can be achieved by either frequency dependent gain characteristics of the inline amplifiers[46], or by placing band pass filters periodically in the transmission line[47]. This will remove the majority of ASE that would otherwise be absorbed by the solitons

during propagation. The effect of including a filter results in the jitter being reduced by a function f(x). Where f(x) is defined as[48]

$$f(x) = \frac{2}{3x^2}\left[2x - 3 + 4\exp(-x) - \exp(-2x)\right]$$

Equation 2-79

and x is proportional to distance L and is a function of the excess gain required to compensate for the extra loss of the filter. When $x >> 1$, Equation 2-79 can be approximated by

$$f(x) \sim \frac{3}{x^2}$$

Equation 2-80

This leads to a more linear relationship between timing jitter and distance. There are two factors that determine the optimum bandwidth of the filter. Firstly the bandwidth is required to be as narrow as possible to remove as much ASE as possible. However additionally to the extra insertion loss of the filter, a narrow bandwidth would incur an extra loss on the soliton by attenuating the outer edges of the spectrum. This extra loss must then be compensated for by extra gain, which in turn leads to the generation of more noise from the amplifier. By reducing the bandwidth of the filter, the eventual limiting factor of transmission will be the SNR. This leaves a compromise between the limitation of the SNR and the limitation of Gordon Haus jitter.

The graph in Figure 2-5 shows the increase in timing jitter with distance for a 10Gbit/s system. The dispersion is 0.5ps/nm km and the pulse width is 20ps. The amplifier span is 50km and the loss of the fibre is taken to be 0.2dB/km. This compares the timing jitter increase with distance for an unfiltered system with that of a system consisting of a filter in every span. It can clearly be seen that there is a more linear increase in timing jitter for the filtered system as oppose to the $L^{3/2}$ function of the non-filtered system.

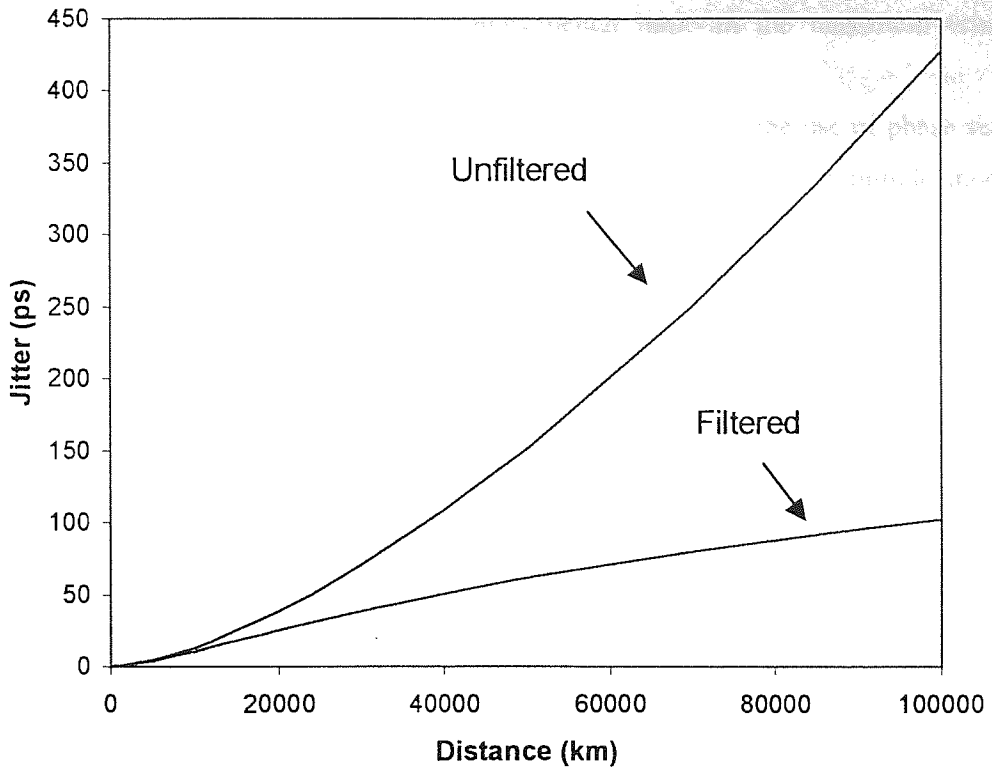

Figure 2-5 Timing jitter vs distance for a 10GBit/s system with 20ps pulses, a dispersion of 0.5ps/nm km, and a 50km amplifier span. The loss of the fibre assumed to be 0.2 dB/km. The first curve shows the increase in jitter as a function of $L^{3/2}$. The second curve shows a more linear trend with jitter suppressed.

A technique referred to as sliding guiding filters has been the subject of investigation, numerical studies have found that a greater degree of jitter reduction can be achieved[49][50][51] and has been successfully demonstrated experimentally[52][53][54][55]. This technique involves the introduction of small shifts in the central wavelength of the band pass filters along the transmission line. Through the resilience of the soliton and its ability to generate new frequencies, this leads to the central wavelength of the soliton being guided in small increments to a different wavelength as it propagates. The ASE does not respond to such guiding and is therefore filtered out as the pass band moves to a different wavelength. This reduces the timing jitter to a function of $L^{1/2}$ with transmission distance. An extension to this technique which is more efficient in terms of spectral bandwidth is the use of zig-zag sliding guiding filters, where the soliton frequency is shifted up and down in frequency[56]. These techniques add to the complication of the system design, since it would require the manufacture of a large number of filters each with different and very specific central wavelengths which are required to be inserted into the transmission line in the correct order.

Another method of reducing jitter is to reduce the dispersion (D_2 term) that appears in denominator of Equation 2-77. At lower dispersions there is a lower rate of change of velocity with respect to wavelength and as a result, the random wavelength shifts have a reduced effect on the velocities of the pulses. Unfortunately the pulse power – dispersion relationship

first discussed in section 2.3.3 places a lower limit on the system dispersion due to the Signal to Noise ratio constraint. This places a fundamental limit on the maximum error free transmission distance due to Gordon Haus Jitter.

Other techniques of reducing timing jitter have investigated the use of phase sensitive amplifiers[57][58] to reduce these temporal shifts, while placing inline amplitude modulator periodically in the transmission line have been shown to increase transmission distances almost indefinitely[59]. The use of a phase modulator at a point within the transmission line has also been investigated numerically and found to reduce this jitter [60][61]. This can help compensate for the random frequency shifts of the solitons. However these techniques add unwanted complications to the transmission system in that they require active electronic control including clock recovery.

2.4.3 Electro-striction

Another problem in soliton transmission is the acoustic optic effect (or Electro-striction)[62][63][64]. As solitons propagate they send acoustic shock waves transverse to the axis of the fibre into the cladding which results in a frequency shift of the pulses and has no detrimental effect on transmission of the individual pulses. This self-frequency shift is common to all pulses and thus results in equal changes in velocity and ultimately temporal position for all pulses. However as these waves reflect they interact with later arriving pulses, (around 20ns later for fibre with an outer diameter of 125μm) and also causes a frequency shift on the later arriving pulses. It is this effect that is most important as the pulse to pulse interaction is pattern dependent. These random frequency changes result in velocity changes and timing shift at the receiver due to GVD. For the same reasons as for Gordon Haus jitter the effect is reduced at lower dispersions. Electro-striction timing jitter increases quadratically with distance, but is reduced to linear if a filter is included. In long distance transmission systems, this effect is minimal since the operating dispersion is typically low.

2.4.4 Average power limit

While the SNR ratio places a lower limit on the operating power there are a couple of constraints on the maximum power. These are the maximum safe average power within the fibre and the lifetime reliablity characteristics of solid state devices, which are reduced when driven at high powers. A common belief is that solitons require much higher power than NRZ systems since they make use of the non-linearity within the fibre. However solitons require a mark to space ratio of about 1:5 (as will be discussed in the soliton-soliton interactions section of this chapter) whereas the mark to space ratio in an NRZ system is effectively 1:1 as the power in a one occupies the entire bit window. The large mark to space ratio in the soliton

system brings down the average power. However there are other factors such as dispersion and pulse width which also govern the average power of the soliton which must be considered for a fair comparrision. The average power for a soliton can be calculated from Equation 2-81 below. Where P_0 is the peak power of the pulse and T_R is the duration of the bit window. A factor of 2 is included in the denominator to account for the absence of pulses due to the data encoded on to them.

$$P_{av} = R\int_{-T_R/2}^{T_R/2} P_0 \sec h^2\left(\frac{t}{\tau_0}\right)dt$$

Equation 2-81

Performing this integration gives

$$P_{av} = \left[P_0\tau_0 R\tanh\left(\frac{t}{\tau_0}\right)\right]_{-T_R/2}^{T_R/2}$$

Equation 2-82

which evaluates to

$$P_{av} \cong \frac{2P_0\tau_0}{T_R}$$

Equation 2-83

Substituting for P_0 and τ_0 with Equation 2-55 and Equation 2-58 the equation becomes

$$P_{av(sol)} = \frac{N^2\lambda^2 D_2}{2\pi c\gamma\tau_0 T_R}$$

Equation 2-84

For a fixed mark to space ratio m_r, where $T_R = m_r\tau_0$ the equation becomes

$$P_{av(sol)} = \frac{N^2\lambda^2 D_2}{2\pi c\gamma m_r\tau_0^2}$$

Equation 2-85

This equation gives the average power required to support stable pulses for a given dispersion and at a given data rate. The minimium power tolerable for an NRZ system is dictated by the SNR requirement at the receiver which was discussed in the Signal to Noise Ratio section of this chapter. This is given by Equation 2-86 below.

$$P_{av(NRZ)} = 2(SNR)\mu h\nu B(G-1)\frac{L}{L_a}$$

Equation 2-86

Thus for a 10GBit/s system with an amplifier spacing L_a of 50km fibre loss of 0.2dB/km, μ is the inversion factor and B = half the bit rate (5GHz) and the minimum SNR limit at the receiver is required to be 23dB. The minimum average power required for transmission distance L of 10,000km is 0.23mW. For a soliton system operating with a dispersion of 0.2ps/nm km and a mark to space ratio of 1:6 (15ps FWHM pulses). The average power is calculated to be 0.15mW by taking γ to be $2W^{-1}km^{-1}$. This shows that the average power in a soliton system is lower than with an NRZ pattern and well within the range of the power requirements of UK safety standards. However Equation 2-86 shows that for a given mark to space ratio the power increase as a square of the data rate ($1/T_R$). Thus as the drive towards higher data rates continues, this required operating power will dramatically increase and may be of serious concern.

2.4.5 Soliton-soliton interactions

In order to operate at high data rates it is necessary for pulses to be placed close together in time. Unfortunately, a disadvantage of the non-linearity that holds the solitons together is that it also results in an interaction effect. This is as a result of the small finite tails of the soliton that extend into neighbouring solitons. The superposition of these small tails on neighbouring solitons causes them to propagate at different velocities[65]. A pair of solitons at the input to a transmission line can be described by Equation 2-87.

$$u(0,\tau) = \sec h\left(\tau - \frac{T_R/2}{\tau_0}\right) + r\sec h\left(\tau + \frac{T_R/2}{\tau_0}\right)e^{i\theta}$$

Equation 2-87

Where T_R is the intial seperation, r is the relative amplitude and θ is the relative phase. Equation 2-14 can be solved with this equation using the inverse scattering method, which gives an insight to the nature of these interactions. There are several characteristics, which can affect these interactions such as pulse chirp, and higher order non-linearity and higher

order dispersive effect. However, for simplicity these are not discussed here. Numerical simulations and calculations have shown that for equal amplitude (r = 1) and equal phase ($\theta = 0$) the pulses are subject to an attraction force which causes them to collapse into each other[66]. This phenomena has also been demonstrated experimentally[67]. After the collision the solitons emerge intact, but maintain their attraction force and eventually collapse again. The pulses continue to collapse periodically along the fibre with period Z_p define in Equation 2-88 below[67]

$$Z_p = Z_0 \exp\left(\frac{T_R}{2\tau_0}\right)$$

Equation 2-88

For the loss-less case, these pulses will first collapse at a distance $Z_p/2$ after the initial launch point. True data provides a random presence of neighbouring pulses which results in the soliton-soliton interaction randomly distorting the data stream. The interaction between pulses is closely linked to the pulse overlap, which increases as the pulse separation is decreased. This results in a relatively slow temporal shift in the early stages of the collapse, which becomes a more rapid shift as the mark to space ratio decreases. As a result, the majority of the collapse happens over a relatively short distance of the entire collapse distance. To avoid this problem the collapse distance must be kept above twice the system length. Since this collapse distance is a function of pulse width and pulse separation, this can be achieved by increasing the mark to space ratio. For a 10Gbit/s soliton system operating with a dispersion of 0.5ps/nm km and a mark to space ratio of 1:5 the collapse will occur after a distance of 21,000km. However if the mark to space ratio is increased to 1:10 this collapse distance is increased to 432,000km and with a mark to space ratio of 1:20 (5ps pulse) the collapse distance increase to 730Mm. Typically, a mark to space ratio of 1:6 is used. This increases the collapse length sufficiently for any global transmission system for most practical dispersion values. Figure 2-6 shows the evolution of two pulses as they propagate along the fibre.

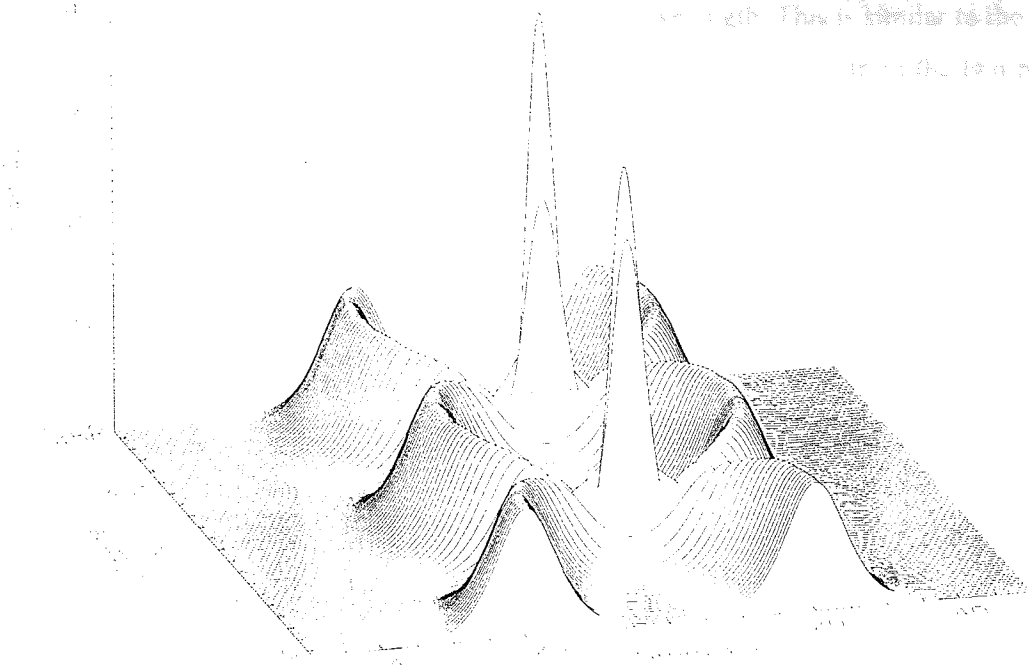

Figure 2-6 Transmission of two solitons with equal amplitude and phase. The solitons periodically collapse along the transmission line due to the attraction force of soliton-soliton interactions.

The soliton-soliton interaction is very sensitive to the relative pulse phase and amplitude. If the relative phase of the pulses is equal to π ($\theta = \pi$ in Equation 2-87), an opposite effect can be observed where the solitons exert repulsive forces on each other. At first this may be seen as a more desirable characteristic. However, the solitons continue to separate at the same rate regardless of there separation in time. This will eventually result in solitons moving from their bit slot into neighbouring slots and introducing errors. Another method is to use a phase difference between neighbouring pulses of $\pi/2$ or $3\pi/2$. With this phase difference the solitons neither attract nor repel. However this state is unstable and any perturbation will cause the phases to shift to one of the extremes previously mentioned. The use of neighbouring solitons with unequal amplitudes (ie r not equal to 1). results in a different phase evolution for the two solitons, which interferes with the efficiency of this interaction. This has been shown numerically[68] and demonstrated experimentally[69][70]. While the solitons still interact periodically their temporal shift is reduced and for only a 10% difference in amplitude the solitons never collapse.

2.4.6 Cross phase modulation

The non-linearity of the fibre can cause a phase modulation of a pulse at one wavelength on another pulse propagating at a different wavelength. This is similar to the SPM effect discussed earlier and is as a result of the superimposed intensities from the two pulses increasing the non-linearity. This effect is referred to as Cross Phase Modulation (XPM). The effect of XPM is an important issue in WDM systems causing solitons from different channels to interact, the effects of which are discussed later in section 2.5.

The field of two different wavelength signals can be written as

$$E(r,t) = \frac{1}{2}\hat{x}\left[E_1 \exp(-i\omega_1 t) + E_2 \exp(-i\omega_2 t)\right] + c.c$$

Equation 2-89

This leads to a change in refractive index given by

$$\Delta n_j \cong n_2\left(\left|E_j\right|^2 + 2\left|E_{3-j}\right|^2\right)$$

Equation 2-90

This equation shows that that the refractive index is a function of the intensity of both fields E_1 and E_2. The refractive index change manifests itself as a non-linear phase shift, which is given by.

$$\Phi_{NL} = \frac{\omega_j^2 Z}{c}\Delta n_j = \frac{\omega_j^2 n_2 Z}{c}\left[\left|E_j\right|^2 + 2\left|E_{3-j}\right|^2\right]$$

Equation 2-91

The first term of this equation is a result of self phase modulation the second term results from the XPM. The factor of 2 in the second term shows that the effect of XPM is twice that of SPM.

2.4.7 Birefringence

Imperfections in the manufacture of fibre result in a deviation from the ideal perfectly cylindrical fibre. These imperfections lead to the generation of two orthogonal polarised modes with slightly different refractive indexes. These two axes are often referred to as the fast and slow axes of the fibre since they have two different propagation velocities. This leads to a polarisation dependent dispersion referred to as polarisation mode dispersion (PMD). PMD can cause serious problems in that it can result in a splitting of the two modes of the light propagating in the fast and slow axis. While current technology allows fibre to be

manufactured with very low PMD, some of the older fibre installed in the ground today has a higher PMD. This is a problem when considering the upgrade to higher data rate NRZ systems which are susceptible to this effect[71]. Solitons however have been found to be more tolerant of PMD than NRZ systems[20][72][73][74][75][76]. This is due to the non-linearity in the fibre, which causes the two solitons in the two different modes to trap each other through XPM such that they propagate together at some average velocity of the fast and slow propagation velocities. Considering here the XPM of two waves of the same frequency propagating in orthogonal polarisation modes. This can be studied using an elliptical polarisation input field given by

$$E(r,t) = \frac{1}{2}\left(\hat{x}E_x + \hat{y}E_y\right)\exp\left(-i\omega_0 t\right) + c.c$$

Equation 2-92

Again this results in a change in the refractive index for each polarisation given by

$$\Delta n_x = n_2\left(\left|E_x\right|^2 + \frac{2}{3}\left|E_y\right|^2\right)$$

Equation 2-93

$$\Delta n_y = n_2\left(\left|E_y\right|^2 + \frac{2}{3}\left|E_x\right|^2\right)$$

Equation 2-94

The XPM induces a non-linear birefringence that causes a change in polarisation state of any elliptical polarised wave. This results in a phenomenon known as non-linear polarisation rotation. The non-linear dependence of the polarisation change results in a greater degree of rotation for higher powers. For a soliton, the peak power will undergo a greater rotation than the lower power tails of the pulse. This effect is utilised in the transmission experiment discussed in Chapter 8 to produce saturable absorption with the aid of a polariser.

2.5 Multiple wavelength channels

While the experimental basis of this thesis is single channel transmission, the importance of WDM cannot be ignored. The future of high bandwidth communication links will require multiple wavelength channels to make full used of the broad spectrum provided by Erbium doped fibre amplifiers. The addition of these extra channels gives rise to problems such as Four Wave Mixing[77] (FWM) and residual frequency shifts from inter-channel pulse

collision. FWM products are frequency components generated during pulse collisions and are as a result of the non-linearity in the fibre. These components are generated at frequencies ω_3 and ω_4 where $\omega_1 + \omega_2 = \omega_3 + \omega_4$, ($\omega_1$ and ω_2 being the frequencies of the WDM channels).

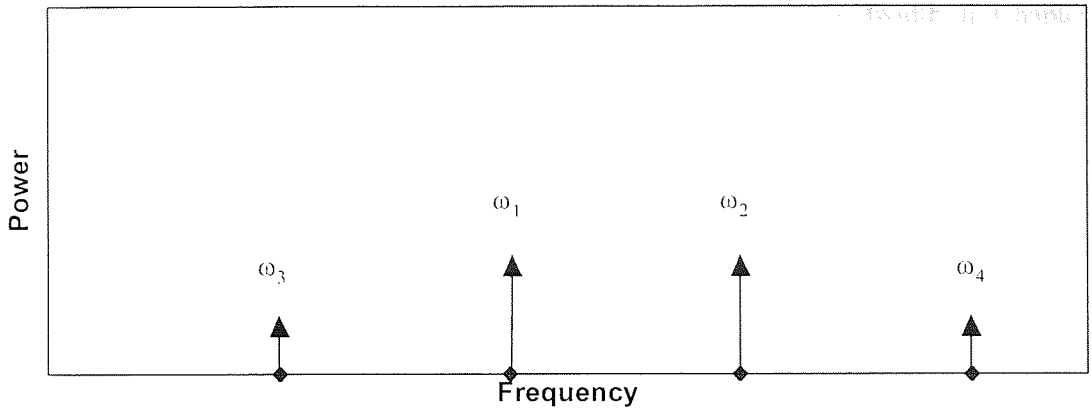

Figure 2-7 FWM Frequency components ω_3 and ω_4 generated through the non-linear mixing between ω_1 and ω_2

For solitons in the lossless transmission case the presence of these FWM components is only temporary, as after the collision the energy in these components is reabsorbed by the soliton. However the perturbation due to loss and amplification in a real system results in these products remaining after the collision[78][79]. The growth of these products with transmission distance and the continuous loss of energy from the soliton to these frequencies can become a problem in WDM systems. Another major problem in WDM soliton systems is the residual frequency shifts occuring through the non-linear soliton-soliton interactions between colliding solitons from different wavelengths. Two solitons propagating at different wavelengths will have different propagation velocities due to the dispersion in the fibre. For the case when the slower pulse leads transmission the two pulses will collide. During this collision these solitons will interact in much the same way as the soliton-soliton interaction in single channel transmission. This interaction through the pulse overlap results in an attraction force between the pulses. In the first half of the collision, this results in an increase in the velocity of the faster moving pulse and a decrease in the velocity of the slower moving pulse. When the pulses emerge in the second half of the collision, the same attraction force returns the pulses to their original velocities. This effect does not pose a serious problem until the effects of loss and amplification are taken into account. The imbalance in power and thus non-linearity in the two halves of the collision can results in a net shift in the frequencies of the pulses[80][81], which through dispersion will result in pulses drifting from their bit slots. Numerical investigations into this effect in a lumped amplifier transmission system has shown

that this effect can be sufficiently minimised by ensuring that the collision takes place over no less than two amplifier spans[82]. This places a limit on the maximum amplifier spacing in the transmission line, and increases the cost of the system by increasing the number of amplifiers required. The collision induced frequency shifts can be reduced by increasing the channel spacing[82][83], however this will limit the efficient use of the available bandwidth. In Chapter 3, a method of overcoming this problem through dispersion management is discussed.

2.6 Summary

In this chapter the NLSE equation has been introduced. This is a mathematical interpretation of the propagation characteristics of the optical fibre. The solution of the NLSE brings about the concept of the soliton, which provides a stable balance between the dispersion and non-linearity. The solution is only found in the anomalous dispersion regime. No such balance is found in the normal regime. Some of the important characteristics that influence the transmission were also discussed with the factors that govern these characteristics. The general findings were that transmission performance is better at lower dispersions, where effects such as electro-striction, Gordon Haus jitter and soliton-soliton interaction are minimal. However the proportional power-dispersion relationship places a limit on the lowest operating dispersion through the Signal to Noise ratio requirements. In order to improve the capability of these systems and overcome some of these characteristics (particularly Gordon Haus Jitter), it is necessary to find a method of relaxing this dispersion-power relationship. The next chapter discusses a technique known as dispersion management, which provides several benefits over a uniform transmission system, one of which changes the dispersion-power dynamics of the soliton.

Chapter 3

Dispersion Management

3.1 Introduction

In the previous chapter, soliton transmission was discussed in terms of uniform dispersion systems, where the dispersion of the fibre is constant throughout the transmission line. However in recent years there has been a lot of interest in transmission systems with varying dispersion throughout the link. In this Chapter some of the aspects of dispersion management are discussed. The technique discussed in section 3.3 is of most interest in this thesis and is the method used in subsequent chapters to overcome the high dispersion of standard fibre at 1.55μm.

3.2 Exponential Dispersion tapering

In section 2.3.3 a linear relationship between the required pulse power and operating dispersion for a stable soliton was introduced. In real systems the effect of loss reduces the power of a pulse with propagation and consequently interferes with the balance between dispersion and non-linearity. The concept of the average soliton can be applied to the launch power of the soliton to solve this problem and maintain the long term stability of the pulse (introduced in section 2.3.5). However a requirement of the average soliton concept is that the amplifier spacing must be less than the soliton period[21]. This may cause a problem when working with short pulses (several ps). Additionally as was discussed in section 2.5 in WDM systems the perturbation of loss and amplification results in the growth of Four Wave Mixing (FWM) products and collision induced frequency shifts. These effects are largely reduced by keeping the amplifier spacing less than half the collision length between channels. However this places a serious constraint on the amplifier spacing.

An alternative method of meeting this balance is through the use of dispersion tapering between amplifiers. By suitably tapering the dispersion exponentially along the fibre, the requirement of the dispersion power relationship in Equation 2-55 can be met continuously along the entire length of the amplifier span. This essentially gives an exponentially falling GVD to match the exponentially falling SPM resulting from loss. It has been shown that this

allows an amplifier spacing greater than the soliton period[84][85][86]. The dispersion tapering effectively suppresses the perturbation on the pulse and reduces the growth of FWM products and the collision induced frequency shifts[82][87]. As a result the corresponding constraints on the channel spacing and amplifier spacing are removed. However the manufacture of such fibre is complex and lossy, and therefore not practical. An alternative less complicated method is to use an approximated stepwise profile[88][89]. Although with this method there is still an interchange between the dominance of SPM and the dominance of GVD, it is reduced compared with that of the average soliton concept in section 2.3.5. Such methods of continuously meeting the balance between SPM and GVD within an amplifier span are not commonly used. Another alternative technique is discussed in the next section where alternating signs of dispersion allow transmission with lower path average dispersion than the conventional soliton. This extends the soliton period while also suppressing the effects of FWM and collision induced frequency shifts[90].

3.3 Dispersion Management

The most common form of dispersion management is that of a two step dispersion map. These maps consist of two lengths of fibre with opposite signs of dispersion, (ie one being in the anomalous ($D_2 > 0$) and one in the normal dispersion regime ($D_2 < 0$)). Although this introduces high dispersion into the transmission line which is known to enhance detrimental effects such as Gordon Haus Jitter and electro-striction, this high dispersion is localised. Over a whole transmission span the dispersion is at some average between the two fibres, and for appropriate selection of fibre it can be almost zero. A schematic of such a dispersion map is shown in Figure 3-1. There are several advantages of such dispersion maps, in particular numerical simulations have shown that the stable powers of the soliton in these dispersion maps are enhanced over the equivalent uniform system with the same path average dispersion[91][92]. Before the reasons for this enhanced power are discussed it is useful to understand the effects the dispersion map has on the pulse as it propagates.

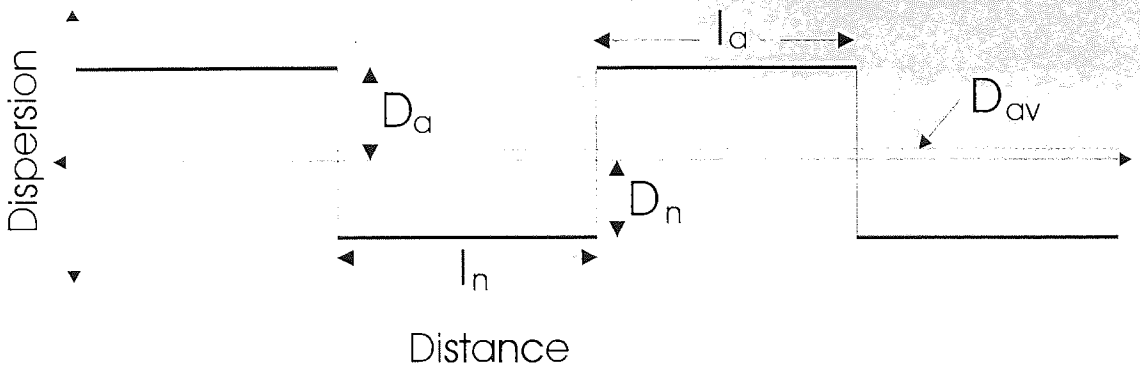

Figure 3-1 A two step dispersion map consisting of a length of fibre l_a with anomalous dispersion D_a, and length of fibre l_n with normal dispersion D_n. Together these give an low average dispersion D_{av} given by Equation 3-1

The schematic in Figure 3-1 shows two periods of a dispersion map, each period has two lengths of fibre L_a and L_n with dispersions D_a and D_n. These combine together to give an average dispersion D_{av}, which can be calculated from Equation 3-1. These maps need not be symmetrical and stable soliton transmission has been demonstrated even with mostly normal dispersion fibre[93].

$$D_{av} = \frac{l_a D_a + l_n D_n}{l_a + l_n}$$

Equation 3-1

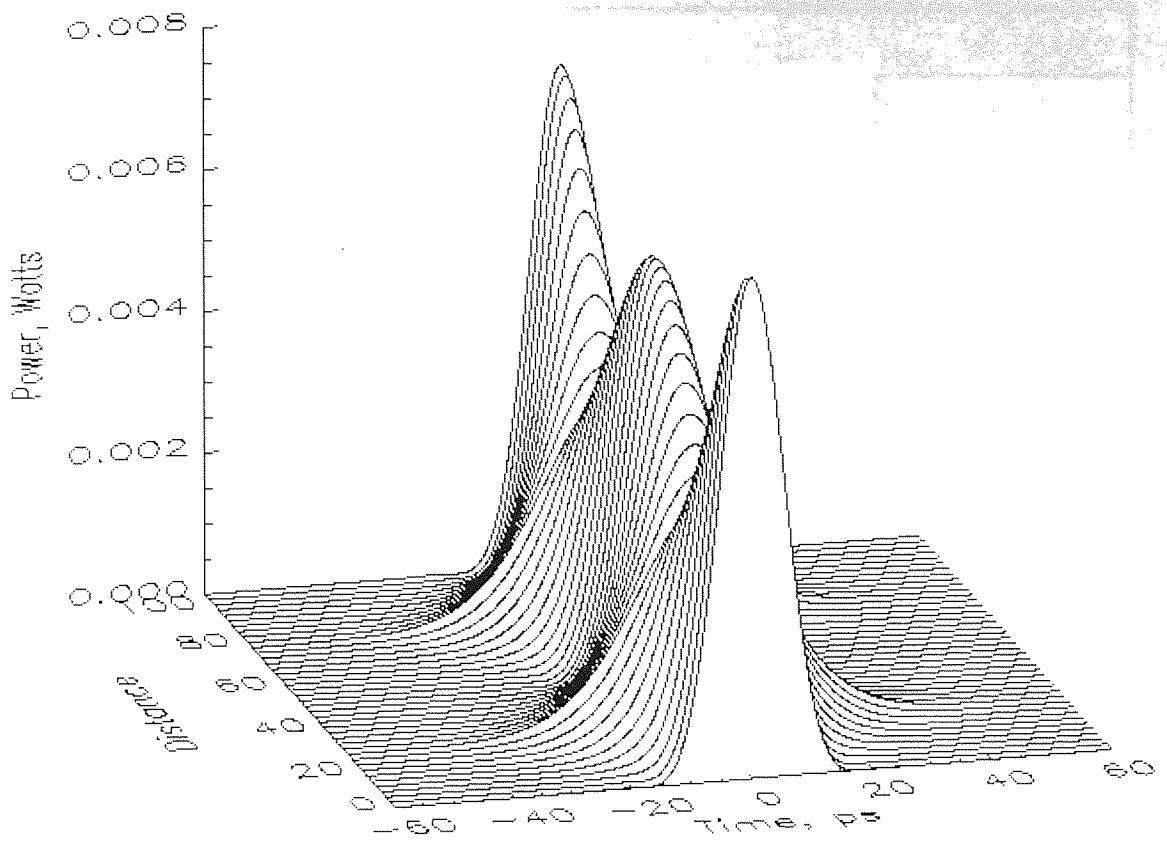

Figure 3-2 3D Plot of a pulse breathing within a dispersion map The minimum pulse width is 12.5ps and the maximum pulse width is 20ps. The length of the amplifier span is 100km with the anomalous and normal dispersion sections having corresponding dispersion of 3.8 and –3.6ps/nm km, and each having a length of 50km.

These dispersion maps give rise to pulse breathing of the propagating solitons. The high local dispersion in each section of the map induces a chirp on the pulse causing it to broaden. The periodic nature of the dispersion induces a periodic oscillation of the chirp as the pulse propagates. Over an entire span the net dispersion is much lower (usually near zero), and is balanced by the non-linearity. Figure 3-2 shows a three dimensional plot of a stable pulse propagating within a dispersion map. While the pulse undergoes a breathing process within each span, over a multiple number of spans the pulse is asymptotically stable

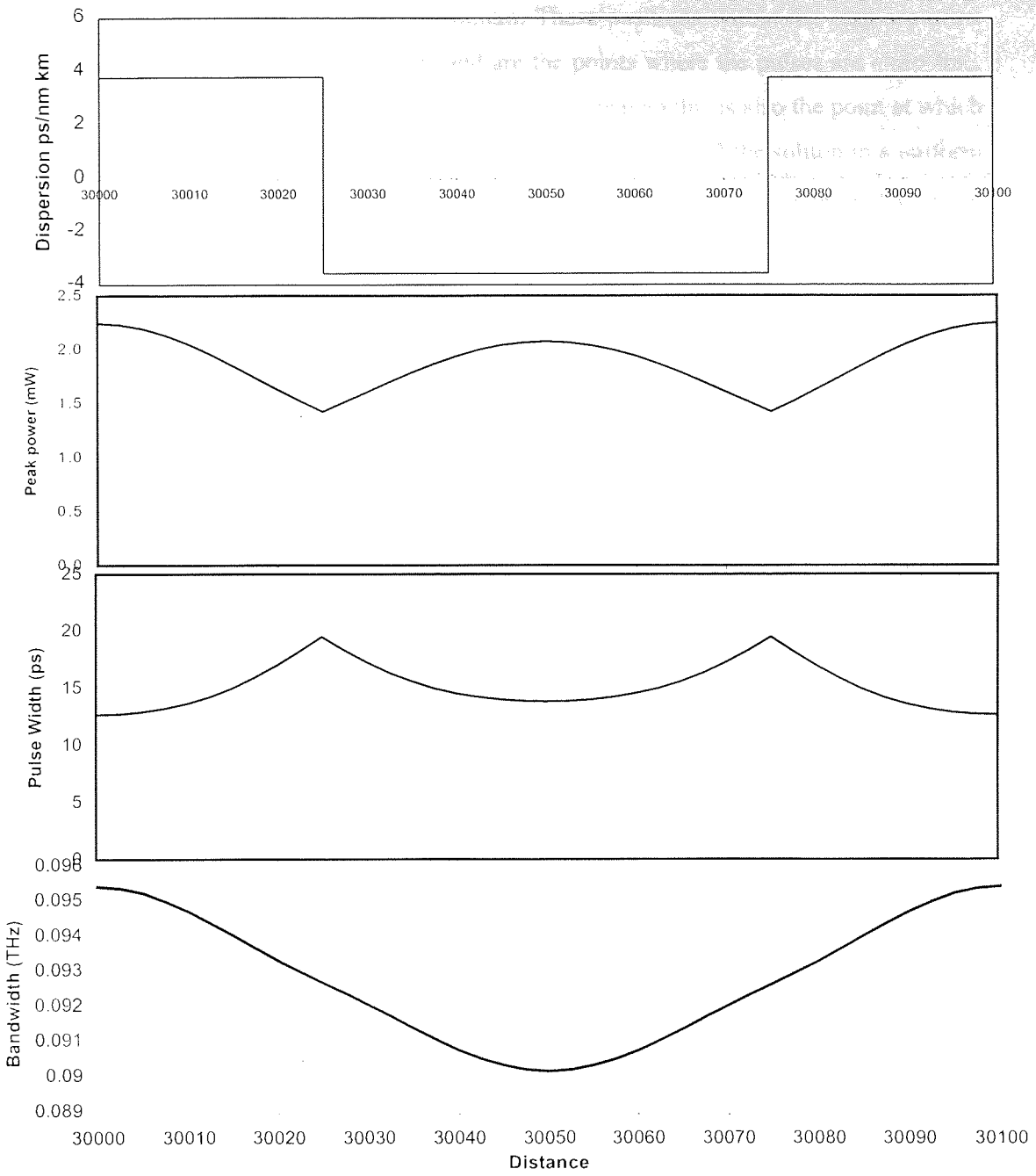

Figure 3-3 (a) 100km Dispersion Map consisting of two sections of 50km with dispersions of 3.8 and -3.6 ps/nm km. The average dispersion of which is 0.1ps/nm km. (b) Peak power of the pulse within the map, the maximum peak powers of 2.25mW corresponding to the mid points of each section (c) the pulse width within the map, the minimum width coincides with the mid point of either section which is referred to as the chirp free or transform limited point. (d) shows the evolution of the pulse bandwidth within the map showing lowest bandwidth in the normal dispersion and greatest bandwidth in the anomalous dispersion.

Figure 3-3 shows statistics of the evolution of the pulse within the dispersion map carried out by Ref[94]. For the ideal dispersion managed soliton with breathing matched to the map, the pulse width is at a maximum at the boundary between fibre sections, since this is the point where the pulses have accumulated the most chirp within the map. At the mid points

of each section the pulse width is at a minimum. These positions within the map are often referred to as the transform limited points and are the points where the pulses are chirp free. As the spectral width does not change much throughout the map this is also the point at which the time bandwidth product is minimum. As it was noted in chapter 2 the soliton in a uniform system is of the shape of a hyperbolic secant and has a time bandwidth product ($\Delta t \times \Delta \nu$) of ~0.32. For a dispersion managed soliton the stable shape of the pulse tends more towards that of a Gaussian shape[92] (which has a transform limited time bandwidth product of around 0.44). Increasing the amount of local dispersion and thus the pulse breathing within the map causes the stable pulse shape to be even more closely matched to that of the Gaussian shape. The simulation in Figure 3-3 was taken for a lossless transmission system. The result of loss affects the non-linearity and results in the transform limited point for the breathing soliton being shifted away from the mid-point of each section of fibre towards the later end of the fibre.

Due to this pulse breathing within these systems it is particularly important where the pulse is launched within the map and the amount of chirp the pulse has when it is launched. In the diagram of the pulse breathing in Figure 3-2 and the corresponding graphs in Figure 3-3, the pulse breathing is ideally matched to the dispersion map. If the pulse breathing were not matched with the map, the pulse would undergo an evolution process that would result in dispersive waves being shed by the pulse as it achieves a breathing cycle matched with the map[91]. This miss match of the launch point and the radiation of dispersive waves has been found to result in a degraded performance of the system[95]. To remove or reduce this radiation of dispersive waves, it must be ensured that the launched pulses have the correct chirp. There are two methods of achieving this, in the first method the pulses are pre-chirped with fibre, a grating or a phase modulator before being launched into the beginning of the first map. The chirp must have the correct sign and magnitude corresponding to the beginning of the map. This method also requires post dispersion compensation at the end of the final dispersion map to remove the remaining chirp. A schematic of this is shown in the Figure 3-4.

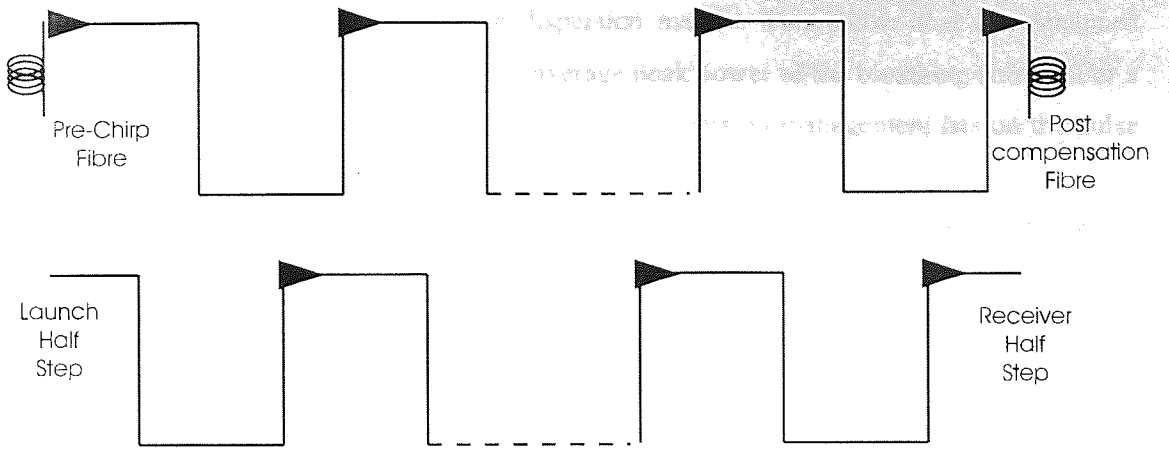

Figure 3-4 Two different techniques used to achieve optimum launch into a dispersion managed system. (a) Using pre and post chirp compensation and (b) launching into a half step section from fibre of the dispersion map. Detection is also carried out after a half step to ensure shortest pulses.

The second method involves selecting the launch point within the map to match the chirp of the pulses. Assuming an initial transform limited pulse this is at a point mid way through either section of fibre. This launch point is achieved by starting the transmission line with a half step of either type of fibre illustrated in Figure 3-4. Other important points to note about the pulse cycle are the peak power and the bandwidth evolution. The evolution of the peak power can be merely explained by the spreading of the pulse energy in time due to the pulse chirp. Figure 3-3 shows the maximum peak powers are at the points where the pulse width is at a minimum and lowest peak powers are at the points where the pulses are most chirped. The evolution of the pulse spectrum shows an increased bandwidth of the spectrum during transmission in the anomalous dispersion fibre and reduced bandwidth in the normal dispersion fibre. This is explained by the fact that in the anomalous section the lower frequencies on the leading edge of the pulse are subject to a downward chirp due to the non-linearity, and the frequencies on the tail of the pulse are subject to an upward chirp due to the non-linearity. These together give an increased pulse bandwidth. In the normal dispersion section the opposite is true where the frequencies on the leading edge of the pulse are the higher frequencies and are subject to a downward chirp, and the lower frequencies on the trailing edge of the pulse are subject to upward chirp. These together give a reduced bandwidth. This bandwidth evolution is closely related to the pulse breathing within the map as greater temporal breathing results in greater spectral breathing.

3.4 Enhanced Soliton Power

It may appear that the power enhancement arises from the reduced average intensity of the pulse due to the pulse breathing within the map. However simulations have shown that the peak power of the dispersion managed soliton is greater than the peak power of the equivalent

uniform soliton at all points within the dispersion map[91]. This shows that the enhanced power can not be explained by the reduced average peak power of the breathing soliton. For a true explanation it is necessary to analyse the effect dispersion management has on the pulse bandwidth.

The effect of dispersion on the broadening of the pulse is dependent on the pulse bandwidth, the greater bandwidth the greater the broadening. In the anomalous dispersion, the bandwidth of the soliton is greater than in the normal dispersion, which results in a greater effective anomalous dispersion. This effective increased dispersion is only as regards to the balance between dispersion and non-linearity of the soliton. (ie it has no bearing on the path average dispersion which effects Gordon Haus jitter, Electro-striction ect). In order to maintain the balance between the non-linearity and the effective dispersion it is necessary to have the enhanced soliton power. The relationship between the enhanced power and dispersion management has been the subject of much research. In order to discuss the relationship here it is useful to define a parameter known as the map strength[96]. This is given in the equation below as S.

$$S = \frac{|\beta_{2a}|l_a + |\beta_{2n}|l_n}{\tau^2_{fwhm}}$$

Equation 3-2

Where β_{2a} and β_{2n} are the dispersions (ps^2/km) of the anomalous and normal sections respectively, l_a and l_n are the corresponding length of the anomalous and normal sections. τ_{fwhm} is the full width half maximum of the pulse at the transform limited point within the map. This map strength determines the degree of pulse breathing within the map, which is closely related to the spectral breathing and the power enhancement factor. The dependence of the map strength on the lengths and dispersions of the fibre sections is as a result of the accumulative dispersion that these sections would induce on the pulse. The dependence on pulse width arises from the relationship with the spectral bandwidth. A larger spectral bandwidth will result in a much greater time domain broadening. A map strength of less than 1 is typically considered to be a weak map, and a map strength above 4 is considered to be strong. Simulation have determined a relationship between the energy enhancement of a pulse and map strength[96], which is given as.

$$\sigma = 1 + 0.7S^2,$$

Equation 3-3

This is valid for map strengths up to 3. For greater values of S the relationship is more complicated and the energy enhancement is also dependent on the ratio between the local dispersion and the normalised average dispersion. The power enhancement aids transmission

in several ways. The greater power in the pulse increases the signal to noise ratio and extends the distance at which this limits error free transmission. This is seen by increasing the S_0 term on the nominator of Equation 2-73 in section 2.4.1. The power enhancement also extends transmission distances beyond the Gordon Haus limits, this is achieved in two ways. Firstly the enhanced power relaxes the constraints of the pulse power dispersion relationship. This allows propagation closer to the zero dispersion and as will be demonstrated later in Chapter 5, for strong dispersion maps propagation on the dispersion zero and normal dispersion is also possible. Equation 2-75 shows that by reducing the dispersion (β_2 term) this timing jitter is reduced. The enhanced soliton energy also makes the central wavelength more resilient to the random frequency shifts caused by the absorption of ASE shown numerically[97][98][99] and experimentally[100][101]. This is due to the greater ratio between signal power to absorbed ASE power. The improvement is seen as increase in the average soliton power term A_0 which appears on the denominator of Equation 2-75, and on the numerator of Equation 2-78. This dispersion management technique is also compatible with soliton control methods such as guiding filters[102] and sliding guiding filters[103].

The dispersion management also has a significant effect on soliton-soliton interactions. For dispersion maps with S less than three, these interactions are reduced[98][104]. This is partly as a result of the change in stable pulse shape from the hyperbolic secant towards a Gaussian shape. The intensity of the tail of a Gaussian pulse is exponential, and therefore much sharper than the tail of a hyperbolic secant. The lower intensities of the overlapping tails of the dispersion managed soliton results in reduced interaction between pulses. Although in dispersion management the pulse breathing periodically expands the pulse to reduce the mark to space ratio, (which for a uniform system is known to increase these interactions). The interaction occurs between the upwardly chirped tail of one pulse and the downwardly chirped tail of the other pulse. As a result the efficiency at which the tails interact is reduced. However when considering strong dispersion managed systems these interactions are increased due to the presence of large pulse overlap. These increased interactions in dispersion management are the subject of the experiment in chapter 6

3.5 Dispersion Management in WDM

Multiple channel collisions in uniform system can have a detrimental effect on WDM transmission. Section 2.5 of chapter 2 discussed the effects of imbalanced pulse collisions from different channels, which causes residual frequency shifts of pulses. Simulations have shown that if the pulse collision was more than 2 times the length of the amplifier span that the effect was minimal. Ensuring this is the case can seriously constrain the maximum amplifier spacing to unpractical lengths. The use of dispersion management has been found to

reduce this problem. Although the presence of high dispersion reduces the pulse collision duration between channels, in dispersion management the high dispersion is beneficial. The low path average dispersion ensures that the frequency shifts have minimal effect on the temporal position of the pulses. The alternating signs of dispersion in the map cause repeated collisions to take place between pulses from different channels[108][106][107][108]. Where in the anomalous dispersion of the map the higher wavelength channel propagates faster than the lower wavelength channel, in the normal dispersion section of the map the opposite is true. Therefore a collision that takes place in the first section will be repeated in reverse in the second section of the map. This collision will also be repeated over several subsequent periods of the map. In effect this extends the distance of the collision between pulses from different channels to multiple amplifier spans and meeting the requirement $L_{collision} > 2L_{amplifier\_span}$ giving reduced net frequency shift. It has also been found that the interaction between chirped solitons is less than that of an unchirped soliton[109]. This benefit of dispersion management on collision induces frequency shifts has also been demonstrated experimentally[110][111][112]. Another benefit with regards to WDM systems is the large local dispersion which is known to break the phase matching condition required for efficient transfer of energy to the FWM components[113][114], reducing the build up of these components.

3.6 Summary

In this chapter many of the benefits of dispersion management have been discussed. The periodic pulse breathing has been found to result in an increased stable pulse power over that of the uniform system. This reduces the limiting effects such as Gordon Haus jitter and Signal to Noise Ratio. The relaxation of the dispersion pulse power relationship allows the dispersion to be reduced further, which also reduces the effects of Gordon Haus jitter. For weak dispersion management it has been found that the soliton-soliton interaction length is increased. However as will be observed in Chapter 6 the soliton-soliton interactions are increased for strong dispersion managed systems. Dispersion management also has many benefits for WDM systems, the repetitive collision between pulses from different channels effectively extends the collision length between pulses to many amplifier spans, This effect suppresses the residual frequency shift associated with imbalanced collisions. The high local dispersion also breaks the phase matching condition and thus reduces the presence of FWM products due to the non-linearity.

Chapter 4

The Recirculating loop experiment

4.1 Introduction

All transmission systems consist of the essential three elements required for communication, which are the transmitter, the transmission medium, and the receiver. In order to simulate a real transmission system in the laboratory each of these elements needs to be reproduced. This chapter explains these three modules and the components used for them in the experiments discussed in the subsequent chapters. The different methods of generating a soliton data source will be discussed followed by a description of the operation of the transmission loop and receiver. The loop corresponds to the transmission medium in which the different fibre configurations and components are tested. At the receiver several methods of quality analysis were performed, these methods will also be discussed in this chapter. Other features of the experiment that will be discussed are the Erbium doped fibre amplifier configurations, the measurement technique for the pulse width and the measurement technique for the average dispersion within the loop.

4.2 The Erbium doped fibre amplifier

The key component in the growth of optical fibre communications was the development of the erbium doped fibre amplifier. This provides broad band amplification in the 1.55μm low loss window, and has opened the way for long distance all optical communication links. The erbium doped fibre amplifier is an integral part of the transmitter, the transmission medium, and the receiver. Important characteristics to consider when designing an erbium doped fibre amplifier are the gain, the output power and the noise figure. These characteristics can be influenced by the erbium doped fibre length, the amplifier configuration, the pump wavelength and the pump power. The pump power can be controlled

at the time of use and offers some flexibility on the gain and output power, but the other characteristics must be selected at design time. The length of the erbium doped fibre effects the amount of pump power that is absorbed, this essentially affects the gain and the maximum output power of the amplifier. The amplifiers operate with lowest noise figure when the pump absorption in the Erbium fibre is saturated. As a result the length of erbium fibre in the amplifier should be optimised to give the required gain when in saturation.

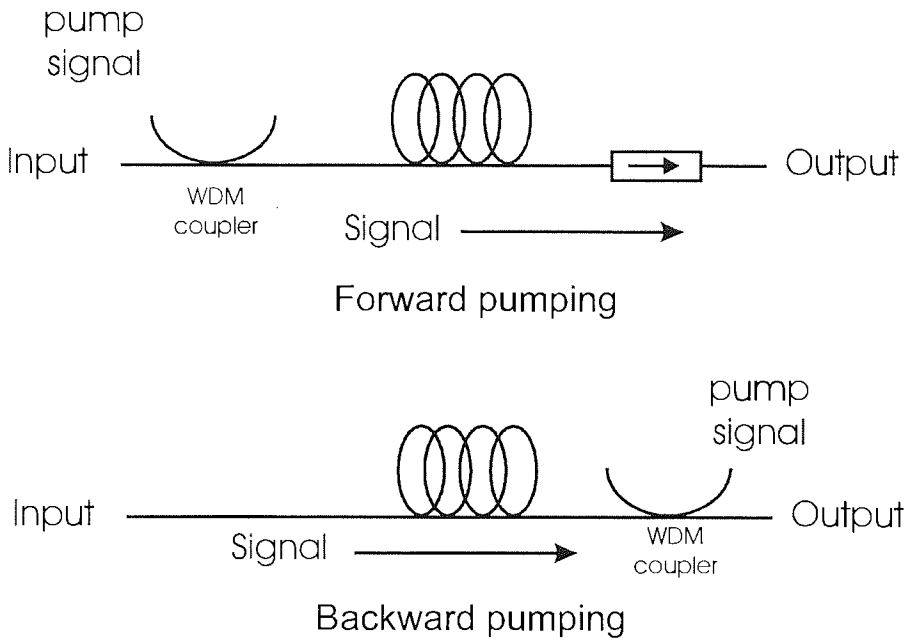

Figure 4-1 schematic showing the co-propagating and counter-propagating pump configurations of the erbium doped fibre amplifiers. Co-propagating pump being with the signal direction, and counter propagating pump being against the signal

The two most basic configuration of an EDFA are co-propagating pump and counter propagating pump. Co-propagating for when pumping in the same direction as the transmitting signal, and counter propagating for when pumping in the opposite direction to the transmitting signal. Co-propagating pump amplifiers have better noise figures than the counter-propagating pump amplifiers. However a greater saturated output power can be achieved with the counter propagating amplifiers. Occasionally two stage amplifiers are used to give low noise figure when requiring high gain for a small signal, the first stage is optimised for lower power amplification and the second stage is optimised to give high saturated output power. The other important factor for consideration when designing an amplifier is pump wavelength. The optimum pump wavelengths for an erbium doped fibre amplifier are at 1480nm and 980nm. Pump diodes at 1480nm are cheaper and more readily available than the 980nm pump diodes, however the noise figures of the 980nm pumped amplifiers are much less than those pumped at 1480nm[115]. In the experiment discussed in the following chapters an EDFA is used to compensate for the loss of the fibre and components within the transmission loop. This amplifier can be used up to many 1000s of times per

transmission. It is therefore imperative that this amplifier has a low noise figure, thus a 980nm-pumped amplifier was used here, which is a cost effective use of the 980 pump diode. The other amplifiers in the receiver and transmitter are only used once during transmission it is therefore not so important that they to have low noise figure, thus 1480nm pumped amplifiers are used here. The general noise figure measured for the amplifier used in the loop was approximately 4dB.

4.3 Pulse width measurement

Knowledge of the pulse width is particularly important when concerned with calculating pulse chirp, mark to space ratio and map strength. The pulse widths used in these experiments vary from 30ps to 5ps. These short pulse widths are beyond the measurement capabilities of the sampling 'scope and photo-diode. Therefore pulse width measurements were carried out using the second harmonic generated from the input intensity I(t) incident on a non-linear crystal. This second harmonic intensity $I_{2nd}(t)$ is given as

$$I_{2nd}(t) \propto \int_{-\infty}^{\infty} I(t)^2 \, dt$$

Equation 4-1

In order to determine the auto-correlation the input pulse stream is split into two paths where one of the paths is delayed by time T relative to the other and recombined into a single beam incident on the non-linear crystal. Assuming that the power is equally split, then the incident intensity can be written as

$$I(t) = \frac{1}{2} I_p(t) + \frac{1}{2} I_p(t - T)$$

Equation 4-2

Where $I_p(t)$ is the intensity profile of the pulse. Substituting this into Equation 4-1, the second harmonic can be written as

$$I_{2nd}(t) \propto \int_{-\infty}^{\infty} \left[\frac{1}{2} I_p(t) + \frac{1}{2} I_p(t - T) \right]^2 dt$$

Equation 4-3

$$\propto \int_{-\infty}^{\infty} I_p(t)^2 + 2 \int_{-\infty}^{\infty} I_p(t) I_p(t - T) dt + \int_{-\infty}^{\infty} I_p(t - T)^2 \, dt$$

Equation 4-4

Using a non-collinear configuration for the two optical paths incident on the crystal, the first and last terms can be removed. This leaves

$$I_{2nd} \propto 2\int_{-\infty}^{\infty} I_p(t) I_p(t-T)dt$$

Equation 4-5

The intensity of this second harmonic with respect to T is the auto-correlation of $I_p(t)$. From the FWHM of I_{2nd} the pulse width can be determined through a conversion factor k, where k = 1.41 for a Gaussian pulse and k = 1.55 for a $Sech^2$ pulse.

4.4 The soliton sources

The initial part of any communications system is the transmitter. For a soliton system this usually consists of a soliton pulse source and a data modulator. The data modulator is typically a Mach Zehnder $LiNbO_3$ modulator. To simulate the randomness of true data in the laboratory the modulator is usually driven with a pseudo random bit stream (PRBS) generated by a pattern generator. There are many methods for generating solitons, each method has it own characteristics. For commercial systems the characteristics of long term and short term stability, and device durability are of great importance. Any changes in wavelength (particularly when considering WDM systems), pulse output power and pulse width will have an effect on the performance of the transmission system. The deviation in wavelength in a WDM system can also increase the effects such as DWDM cross talk with neighbouring channels and thus degrade the system performance. Any significant changes in pulse width can have an effect on soliton-soliton interactions and the power dynamics of the pulses during transmission. For commercial systems, sources should have a long-term stability in terms of 10s of years. This long term stability can be provided by integrated solid state devices such as DFBs. In the laboratory experiments however such long-term stability is comparatively less important. Stability is only required for the duration it takes to complete experiments, this is typically in terms of hours, however it is important that the sources can be consistent from one experiment to another for comparative purposes. Thus the source characteristics must be repeatable. In the laboratory experiments flexibility is a great asset. The ability to tune characteristics such as the wavelength of the source allows versatility within experiments. This flexibility can be provided by devices such as mode locked erbium fibre ring lasers and external cavity mode locked lasers. The operation of these devices however is more complex, and the stability is less than that of the solid state devices.

There are many other characteristics to consider in a soliton source such as extinction ratio, pulse chirp and timing jitter. The maximum amount of timing jitter tolerable at the

receiver for a 10Gbit/s transmission system is around 6ps, for a 40Gbit/s soliton system this falls to 1.5ps. Consequently an initial rms timing jitter of 1ps will contribute 17% and 67% of the total tolerable timing jitter of the 10Gbit/s and 40Gbit/s systems respectively. The chirp on a pulse source can also have a negative effect on transmission in both uniform and dispersion managed systems. In a uniform dispersion system, a chirped pulse will shed off dispersive waves as it propagates to form a chirp free soliton[116]. For dispersion managed systems it is important that pulses are launched with the correct chirp relative to the launch position within the dispersion map. This prevents the release of dispersive waves as the soliton achieves the stable breathing matched to the dispersion map (as seen in Chapter 3). These dispersive waves can form a pedestal, which can be amplified with distance (creating a noise floor). The degree of pulse breathing within the map is also affected by the pulse width. The pulse width required for a 10Gbit system is 20ps, to give a mark to space ratio of 1:5. Broader pulse widths can increase the soliton-soliton interactions through increased pulse overlap. In dispersion managed systems the pulse width also affects the map strength of the system, which effects the power enhancement of the pulses.

The sources used in the subsequent experiments are individually discussed here. These sources include a fibre ring laser, a gain switched DFB, a Tuneable laser combined with an EAM (Electro Absorption Modulator), an integrated DFB and EAM, and a jitter suppressed (through signal feedback) gain switched DFB. Each method has advantages and disadvantages, which will also be discussed.

4.4.1 Fibre ring laser

Fibre lasers have long been used as a method of producing soliton pulses, they offer flexibility in operating wavelength and have a good extinction ratio. However this is at the expense of long term stability and simplicity. The long lengths of fibre needed to propagate the solitons in the cavity are prone to drifts due to environmental changes, making them unpractical for commercial systems. The fibre laser described in this chapter was used to produce a pulse rate of 10GHz. Figure 4-2 shows a schematic of the fibre laser. The gain medium was provided by a 980nm pump diode and 33m of erbium doped fibre in much the same way as a Erbium doped fibre amplifier. The 980nm pump power is pumped into the erbium fibre via a 980/1550 WDM coupler. At the other end of the Erbium fibre another WDM coupler is used to couple out the remaining 980nm pump signal. The Fabry Perot bandpass filter provided tuneability of the lasing wavelength within the cavity. Two isolators were placed within the ring laser to prevent any counter-propagating light travelling around the loop. The active mode locking was provided by the Mach Zehnder $LiNbO_3$ modulator. This was driven with an RF signal from a frequency synthesiser. The frequency of the RF drive signal is set to a harmonic of the fundamental frequency of the laser cavity to achieve

mode locking. The mode locking must also be optimised by optimising the polarisation controller, the RF power, and the DC bias to the $LiNbO_3$ modulator. The 80/20 coupler was required to couple out some of the of the recirculating pulses within the cavity. The main problem with a fibre laser is stability, small drifts in fibre length as a result of environmental temperature changes cause a change in the mode frequencies of the cavity. If the mode frequency used for mode locking drifts to far from the frequency of the RF signal the laser will cease to mode lock. This can limit the stability of the laser down to minutes.

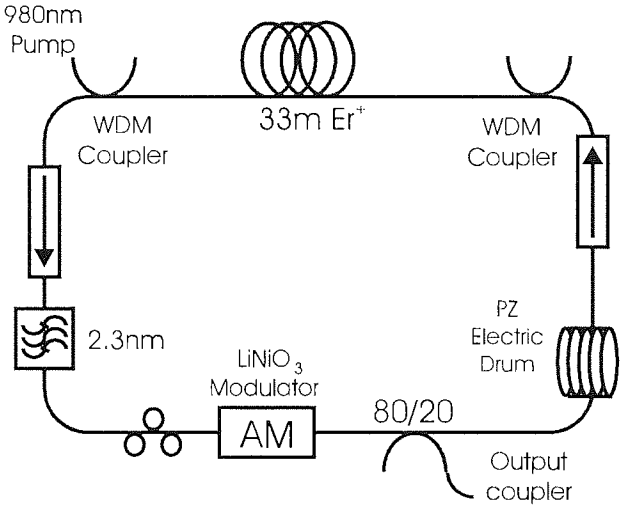

Figure 4-2 the fibre ring laser, showing the gain medium, the filter and the $LiNbO_3$ modulator used for active mode locking. Also included in the laser is a piezo electric drum for controlling the cavity length, and a polarisation controller to optimise polarisation with the cavity.

In order to increase the stability, a mechanism for compensating for the cavity length changes was used. This was done with the aid of a piezo electric drum. By wrapping a portion of fibre around the drum and including it as part of the cavity in ring laser, a small degree of cavity length control can be achieved. Applying an electric voltage to the piezo electric drum causes it to expand, stretching the fibre wrapped around the drum and increases the cavity length. To provide control for the piezo electric drum, a 90/10 coupler was placed at the output of the fibre laser. The 10% was fed into a 10GHz photo diode the output of which was mixed with the drive frequency for the modulator using a 10GHz mixer to produce an error signal. The error signal was fed into a control box that controls the voltage to the piezo electric drum. Any small cavity length changes which results in a small frequency change of the output from the fibre laser will result in a mis-match of the input frequencies to the mixer, which would produce an error signal. The error signal would cause the control box, to adjust the cavity length by changing the voltage applied to the piezo electric drum. This mechanism provides a greater degree of stability, which enables the laser to remain mode locked for several hours before the cavity length drift exceed that that can be compensated for by the mechanism. At which time the fibre ring laser must be optimised and re-locked at the new mode frequency. This is sufficient for laboratory experiment but by no means practical for a

real transmission system. An additional method of increasing stability is to add temperature control to the fibre within the cavity. This reduces cavity drifts over a longer period of time. However this technique was not applied in this fibre laser. The main advantage of a fibre laser as a source is wavelength tuneability. The wavelength of operation could be tuned over most of the erbium bandwidth 1530-1560nm, enabling the operating wavelength to be tuned to different operating dispersions or regimes without the need for reconfiguring the fibre in the loop. This makes some experiment less labour intensive. The output power of this fibre laser was typically between 0 and 1dBm. The majority of the fibre within the cavity was standard fibre which has a high dispersion, and unfortunately prevented the fibre laser from supporting true solitons. This meant that the pulse width was governed by the $LiNbO_3$ modulator and not the propagation power in the cavity. The typical pulse width of the source varied between 17 and 22ps and the spectral width was found to be ~0.22nm (gives a time bandwidth product of 0.55).

4.4.2 Gain switch DFB

In commercial systems factors such as stability, reliability and durability are very important in a pulse source. These qualities can be provided by solid state devices. In particular DFB sources offer a viable solution, and are preferred to unstable lasers such as fibre ring lasers and external cavity mode locked lasers. These devices are also compact and only require simple temperature control. A big disadvantage with the gain switched DFB is the large amount of chirp present on the output pulses which must be compensated. The DFB is also essentially fixed in wavelength (apart from a small degree of tuneability through temperature control). The DFB used in the subsequent chapter was suitable for 10GHz pulse generation and had an operating wavelength of 1555nm. The output power vs electrical current response is shown in Figure 4-3.

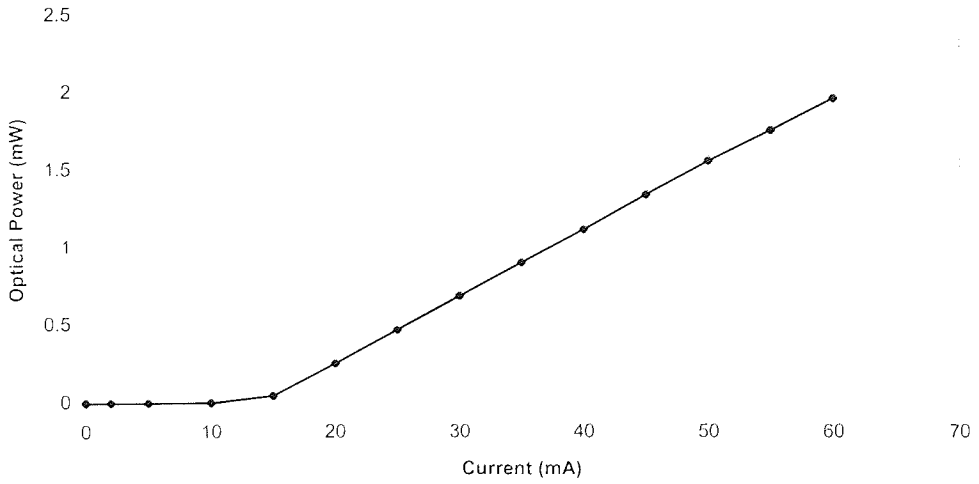

Figure 4-3 Optical output power vs bias current for the DFB

The electrical drive for this device was provided by a bias 'T'. The DC bias is applied to the bias 'T' such that the DFB current was set above the threshold, for this DFB this was around 35mA. The 10GHz RF signal from the frequency synthesiser is applied to the RF input of the bias 'T' with a power of 11dBm. This Gain switches the DFB on and off periodically at a rate of 10GHz producing 45ps pulses. These pulses were compressed down to 20ps with 92ps/nm km of dispersion compensating fibre. The spectral bandwidth of the source was 0.35nm, which gives a time bandwidth product of 0.89. This shows that there is still a degree of chirp on these pulses.

4.4.3 Jitter suppressed gain switched DFB

The jitter suppressed gain switched DFB utilises optical signal feed back into the DFB cavity to reduce the pulse timing jitter. The schematic of the setup is shown in Figure 4-5. The operation of the DFB itself is much the same way as the gain switched DFB described in section 4.3.2. The output power vs electrical current is shown in Figure 4-4.

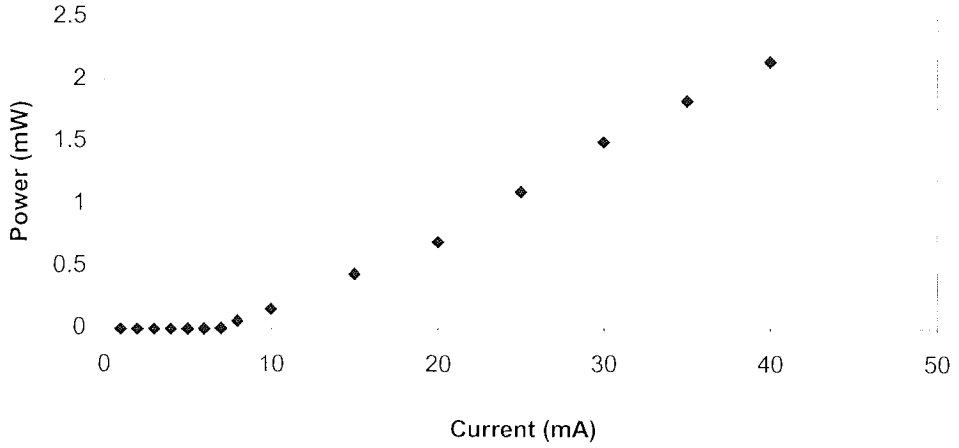

Figure 4-4 Electrical bias current vs output power of the jitter suppressed DFB.

A bias 'T' is connected to the input of the DFB and the DC bias set above the threshold, which is 35mA. A 10GHz RF voltage is applied to the AC input of the bias'T', which gain switches the DFB to produce pulses with a 15ps FWHM width. The spectral output of the DFB had a 3dB bandwidth of 0.6nm, giving a time bandwidth product of 1.1.

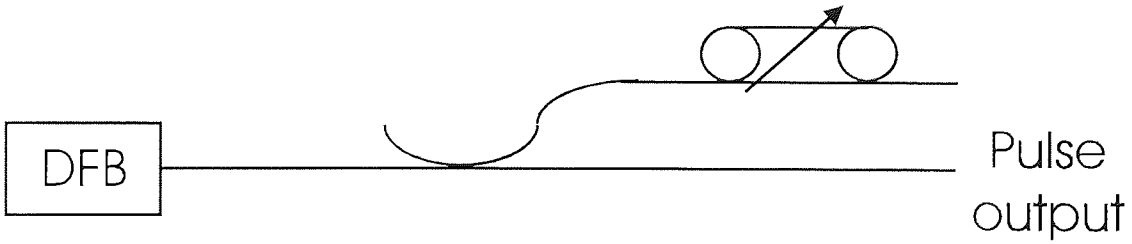

Figure 4-5 Schematic of jitter suppressed feed back gain switched DFB. The output of the DFB is split into two arms. One of which supplies the output pulse stream, the other forms the feedback cavity.

These pulses can be compressed down to achieve chirp free pulses with a time bandwidth product of 0.37 using dispersion compensating fibre. The graph shown in Figure 4-6 shows pulse width vs degree dispersion compensation. The minimum pulse width was found to be 5ps, requiring -25ps/nm of dispersion compensation.

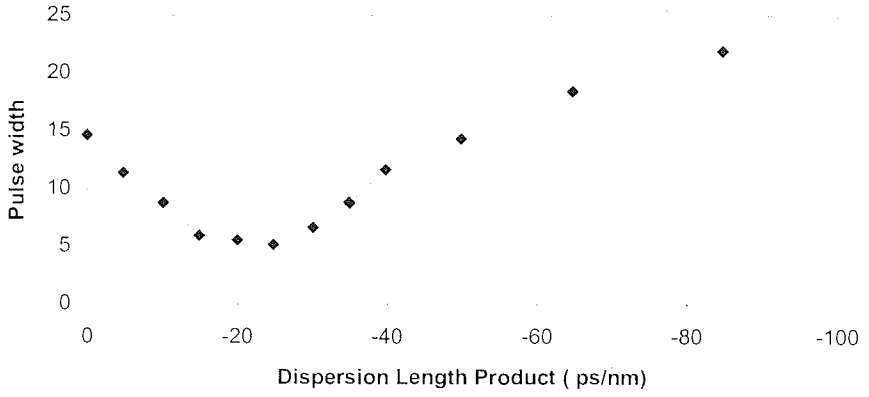

Figure 4-6 pulse width (FWHM) after various amounts of dispersion compensation (dispersion length product). The minimum pulse widths is 5ps requiring –25ps/nm km of dispersion compensation.

The jitter suppression of the DFB is provided by the optical feed back system. A coupler placed at the output of the DFB splits the pulse power. One of the arms of the coupler provides the output for the pulses. The other arm is for the feed back mechanism, and contains a variable reflector which reflects the pulses back into the DFB. The gain switching of the DFB is then seeded on the pulses fed back into the cavity. This reduces the timing jitter that results from the spontaneous emission noise floor below the threshold. The power in the fed back signal should be large enough to raise a coherent wave above the spontaneous emission noise floor but low enough so as not to be above the threshold level of the DFB. The fibre stretcher in the feed back mechanism is used to ensure that the gain switching and the feed back pulses are synchronised.

4.4.4 TL+EAM and integrated DFB + EAM

A useful method of generating pulses is with the combination of a tuneable laser and an EAM (Electro Absorption Modulator). Combined together these create a stable source that is also tuneable in wavelength. The Tuneable laser provides the CW light at the required wavelength, and the EAM is used to carve the pulses from the CW light. The EAM response to DC bias is shown in Figure 4-7.

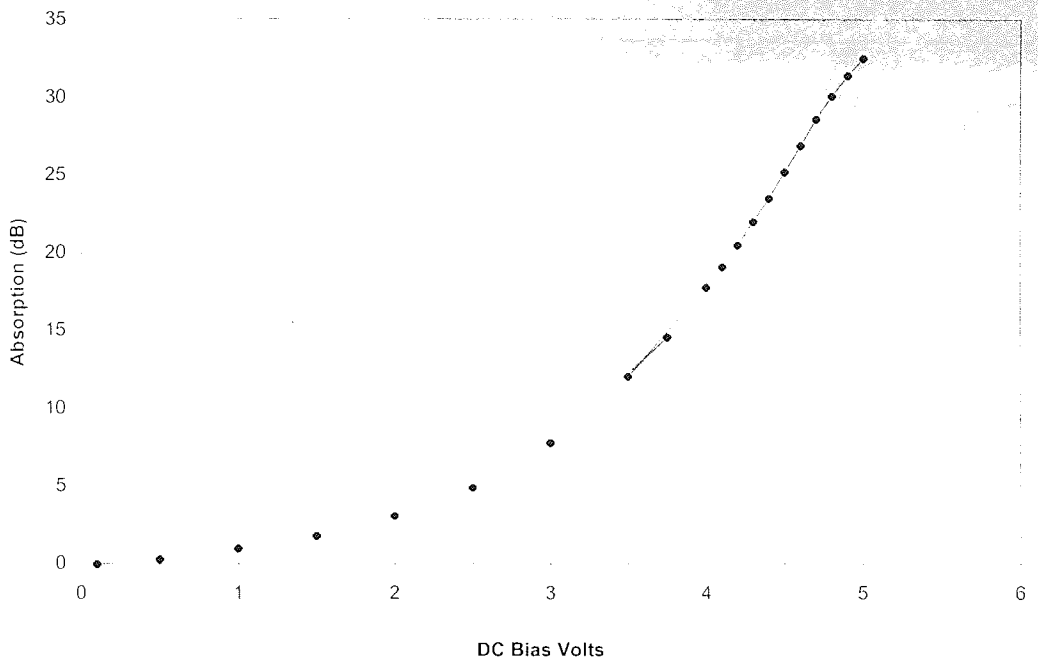

Figure 4-7 Absorption of the Electro Absorption Modulator with DC bias voltage.

The EAM provides a high speed electrically controllable optical absorption switch. A bias 'T' configuration is used in much the same way as the DFBs discussed previously. The bias voltage is applied to the bias 'T' so as to set it into high absorption, for this EAM the bias was typically 3.5V. A 10GHz RF electrical signal with 12dBm of power was applied to the ac input of the bias 'T'. This drives the EAM between the high and low absorption states periodically to generate a temporal pass window for the CW light to pass through. This generates pulses with a FWHM of 20ps and a time bandwidth product of 0.57. This chirp is removed by passing the pulses through normal dispersion fibre. The graph in Figure 4-8 shows pulse widths recorded using an auto-correlator after the pulses are subject to various amount of dispersion compensation. The pulse width compresses down to a full width half maximum of 13ps, at this pulse width the time bandwidth product is found to be 0.37, which is close to transform limited. This technique of pulse generation can be applied to multiple wavelengths to generate a WDM source.

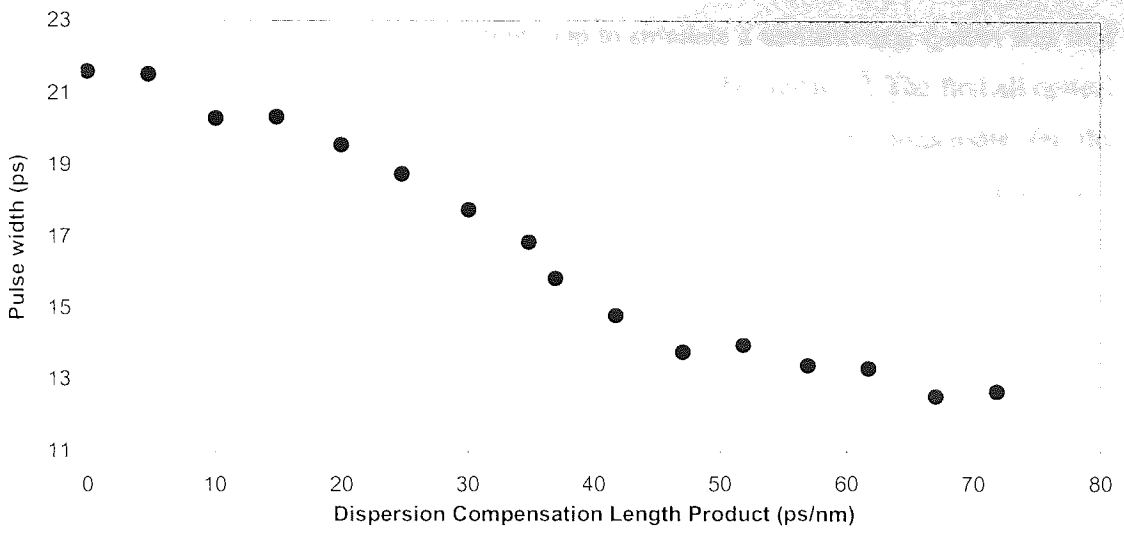

Figure 4-8 pulse width vs dispersion compensation (dispersion length product). The uncompensated pulse width being 22ps. 70ps/nm of compensation (normal dispersion) for dispersion was required to generate chirp free pulses of around 13ps.

A similar device that was used as a soliton source was a combined integrated DFB and EAM (as a single chip), with DFB bias current, the EAM bias and the RF connections are all integrated onto the chip. The drive current for the DFB section was 44mA and the bias voltage for the EAM section was 1.1V. The 10GHz RF power used was 15dBm. This gives output pulses with a FWHM of 30ps, and a spectral bandwidth of 0.11nm. For which the time bandwidth product is 0.41. The wavelength of operation was 1550nm. Due to the DFB this device is fixed in wavelength. The other major problem with this device was that the EAM had a poor extinction ratio (having manufactures specifications of 12dB). However such integrated devices are much more stable than the combined discrete CW Laser and EAM, since there is no external fibre which can be prone to polarisation drifts.

4.5 The recirculating loop

The experiments reviewed in the subsequent chapters were all conducted using a transmission loop. A transmission loop can act as a long distance transmission medium. The loop can be used to propagate a signal over a distance of a multiple number of round trips of the loop, thereby enabling transmission over many thousands of kms without the need for thousands of km of optical fibre. A typical transmission loop consists of only a few amplifier spans of fibre (between 1 and 4) although some loops contain many more. These spans are formed to provide an enclosed loop. The fact that only a few amplifier spans are present in the loop makes it easier to reconfigure for the testing of different components and fibre configurations. These transmission loops are also only a fraction of the cost of a full

transmission system, requiring only a fraction of the fibre and a fraction of the components (ie EDFA and filters). The use of a recirculating loop to simulate a transmission system was first carried out using an electronic repeater system to regenerate the signal[117]. The first all optical transmission systems tested in a loop used Raman amplification to compensate for the loss[118]. Since the development of EDFAs the use of transmission loops to investigate a transmission systems performance has become common. Transmission loops are seen as one of the most convenient methods for testing new ideas and components for long distance transmission[119]. The disadvantage of a recirculating loop is that the components and fibre used within the loop are used a many number of times periodically through propagation. Such periodicity is uncharacteristic of a real transmission system. In a real transmission system the components used will have different characteristics through out the transmission link. The fibres used will also not be as periodic. Amplifier spans may vary along the transmission path in both dispersion and length. These factors can lead to a deviation between the maximum error free transmission distance achieved in a transmission loop and the maximum distance of error free transmission in an equivalent full transmission system. The effect is more pronounced in a single amplifier span, where every span is exactly the same. This periodicity can be reduced by increasing the number of amplifier spans within the loop. Short loops may also result in the over use of some components, ie in a single span loop it may be necessary to include essential component in every amplifier span that would normally only be required every Nth amplifier span, such components include isolators, filters, and couplers. These components contribute to extra loss within the loop, which essentially requires extra gain and introduces extra noise.

The transmission loop experiments discussed in the following chapters were all carried out using a single span loop (single amplifier span). The loop consisted of the fibre applicable to one amplifier span plus the extra components required in a transmission loop. A band-pass filter is included in the loop to filter out the ASE generated from the amplifier. An isolator is located before the coupler within the loop to prevent ASE co-propagating around the loop from either the loop amplifier or from an external amplifier through the output coupler. It is important that effects such as polarisation dependent loss and polarisation dependent dispersion are minimal in the components within the loop, as these would inhibit transmission. A common problem of EDFAs is that of hole burning[120] in a specific polarisation, which degrades transmission[121]. The loop fibre is split into two sections either side of the launch and detection coupler with the amplifier in the middle as shown in Figure 4-9. By controlling the distribution of fibre between these two sections the launch and detection point can be moved within the amplifier span. The distribution of fibre around the launch coupler is usually chosen so as to launch the transform limited pulses into the transform limited point within the dispersion map, yielding a better transmission performance.

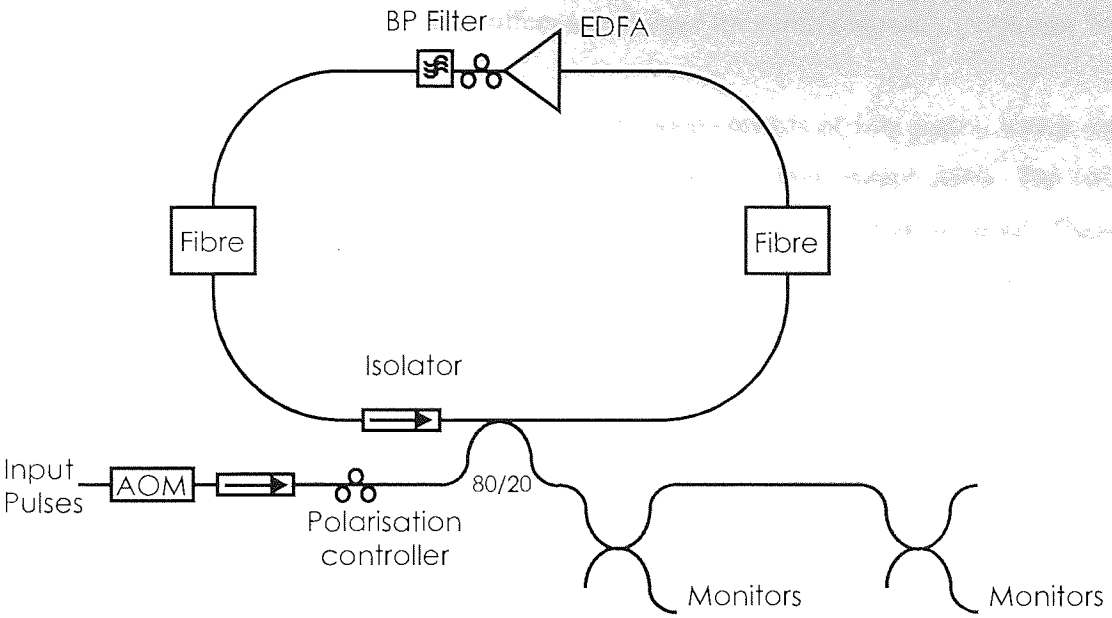

Figure 4-9 Schematic of a single span transmission loop. The fibre is split into two section, the first section is the half step into the amplifier span. The 80/20 coupler providing both the launch point into the loop and the detection point.

The source signal is launched into the loop via the input coupler. The choice of this coupler is of particular importance since it leads to a trade off between launch power into the loop and transmission loss within the loop during transmission. While a 50/50 coupler will provide only 3dB input loss through the coupler, it will also result in a 3dB loss each round trip of the loop. A 70/30 coupler however (30% launched into the loop) will result in a 5.2dB loss launching through the coupler, but only a 1.55dB loss each recirculation. Higher loss in the coupler can cause power transients during recirculation that occur as a result of the low launch power into the loop, which in turn increases the amount of noise released by the loop amplifier. In the former case the greater loss from the coupler in the loop requires greater gain, which also results in increased noise from the amplifier. The final choice of coupler was an 80/20 ratio with the 20% being launched into the loop giving a 7dB loss when launching into the loop and 80% of the power being maintained within the loop during transmission. This results in only a 1dB loss through the coupler each round trip of the loop. The optical signal is launched into the coupler via an AOM (Acousto Optic Modulator) which provides high extinction (greater than 60dB) and fast switching speeds (0.2μs). The high extinction is required to reduce unwanted signal continuously leaking into the launch coupler as the transmitting signal propagates around the loop. The sharp switching edges are required to ensure the loop is efficiently filled, leaving no gaps without overfilling the loop. The loss of the AOM used was 6dB, this further adds to the problems of the launch power into the loop. The loop EDFA compensates for the loss of the entire loop and controls the transmission power. Increasing or decreasing the pump power in the EDFA gives an increased or decreased

saturated output power. This mechanism offers a technique for controlling and optimising the transmission power within the loop.

The process of transmitting a signal around the loop consists of five stages, which are controlled by two delay generators. Each delay generator has three output states. The two delay generators are linked in a chain to form six states of which only five are used. These states are A, B, C and D, E, F. During state A the AOM is opened to allow pulses to be injected into the loop, this should be open for no longer than the fill time of the loop. Over filling the loop will cause the injecting stream to be superimposed on the already recirculating contents of the loop. In the majority of the experiment in this thesis, the length of the loop is around 38km, which corresponds to a fill time of 180μs. The pulses are propagated around the loop during state B, which is set to be a multiple number of the recirculation times plus a further 30μs. The 30μs is required to allow the clock to lock and data synchronisation of the BERTS (Bit Error Test Set). This 30μs wait cuts short the measurement window, at state C, which sets both the sampling 'scope and the BERTS to carry out measurements. The duration of these measurements is set to be slightly short of the remainder of the recirculation. The last few μs of the recirculation are discarded due to the response of the AOM at the end of the launch state (A). At the end of states C the second delay generator is triggered, which turns off the pump power to the amplifier within the loop. This changes the amplifier from amplification to attenuation, which attenuates and essentially removes the propagating signal from the loop. The duration of state E allows the re-pumping of the amplifier. State F is not used and is set to a small value at the end of which, state A of the first delay generator is triggered to repeat the transmission. These states are labelled in Figure 4-10, with output states of A,B and D.

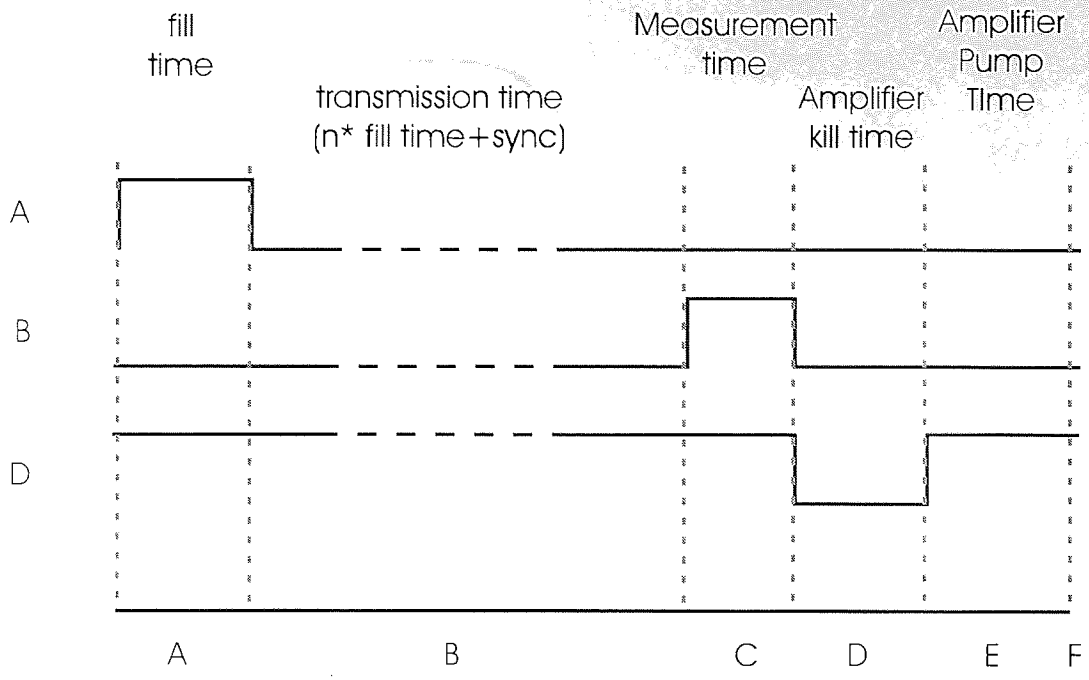

Figure 4-10 State diagram of loop transmission showing the five stages to perform transmission. The filling the loop, propagation of the signal, measurement time, amplifier kill time and the amplifier re-pump time.

4.6 Dispersion measurement through mode frequency

When carrying out the transmission experiments it is particularly important that the dispersion characteristics of the fibre contained within the loop are known accurately. It is sometimes the case that a source is required to operate with a dispersion to the accuracy of a tenth of a ps/nm km. The accuracy of measuring the lengths of individual fibres and their individual dispersion make it impossible to calculate the exact dispersion of the combined fibre within the loop. Therefore a method is used for which the dispersion and combined dispersion slope can be measured while the fibre is in the loop.

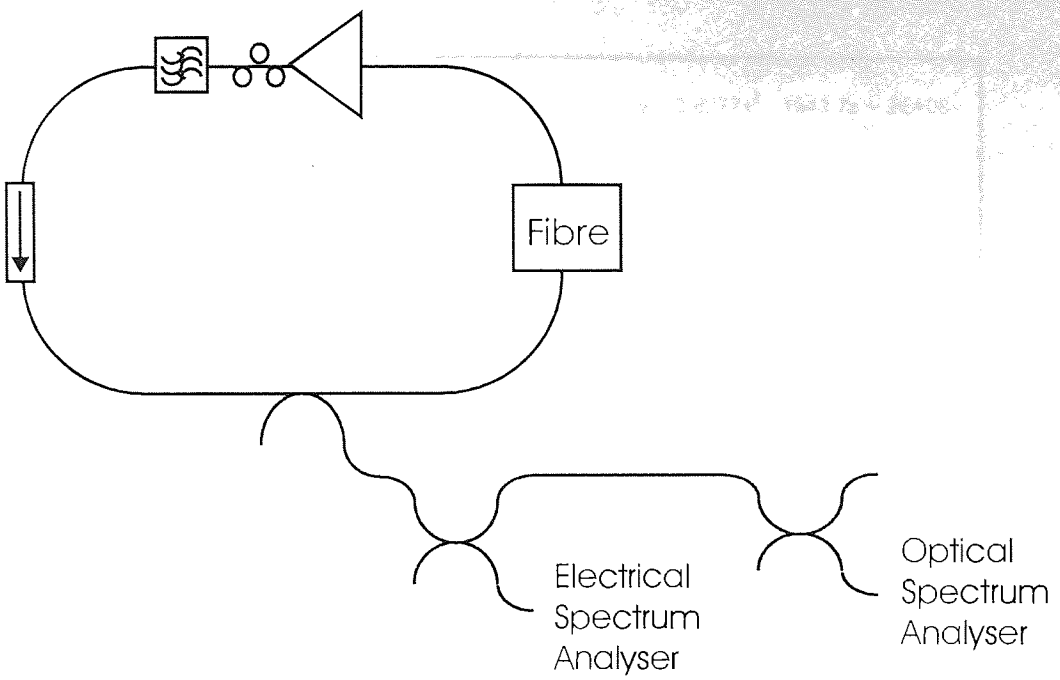

Figure 4-11 Cavity ring laser used to measure the dispersion of the fibre, the essential components being the filter and the amplifier and the output coupler.

The two vital components required within the loop to make the dispersion measurements are the amplifier and a tuneable band pass filter. The amplifier provides the gain medium to ensure that lasing occurs within the loop. The wavelength at which the cavity lases is determined by the wavelength of the band pass filter. As with any lasing cavity, frequency modes are generated, these can be observed on an electrical spectrum analyser at the output of the loop. The period of the fundamental mode of this cavity is equal to the round trip time of the loop. The variation in wavelength will cause this round trip time to change slightly due to the dispersion (ps/nm km) which in turn shifts the frequency of the mode. It is from this variation of the round trip time with wavelength that the dispersion and dispersion slope can be determined. Measuring the shift of the fundamental frequency allows the dispersion to be measured. This fundamental mode is typically a few kHz (for a 38km loop this is 5.3kHz). The variation in frequency of the fundamental mode is very small and therefore difficult to measure, however this frequency change can be measured at a one of the high frequency modes. It is often sufficient to measure the mode frequency at around 10GHz. At these frequency the mode shift with wavelength are magnified by the mode number. At 10GHz this is a magnification of around $2x10^6$. From a plot of modes frequency with wavelength, the changes in the fundamental mode with wavelength can be determined very accurately. Plotting the inverse of this fundamental mode reveals the round trip time with wavelength. Provided that the dispersion measurement is made across the dispersion zero the plot should show a minimum turning point (which corresponds to the dispersion zero) as in Figure 4-12.

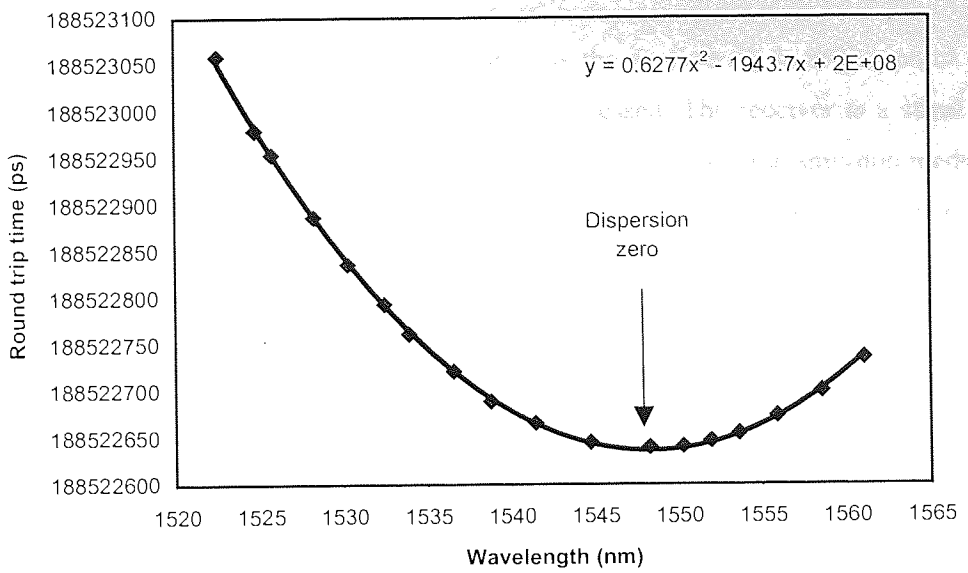

Figure 4-12 Measurement of round trip time with wavelength. The dispersion zero is the turning point of the curve. A dispersion-wavelength equation can be acquired by differentiating a parabolic fit to this curve.

From a 2nd order polynomial equation of best-fit the dispersion zero can be determined. Differentiating this equation and dividing by the loop lengths reveals the average dispersion equation in terms of ps/nm km. A plot of such an equation is shown in Figure 4-13.

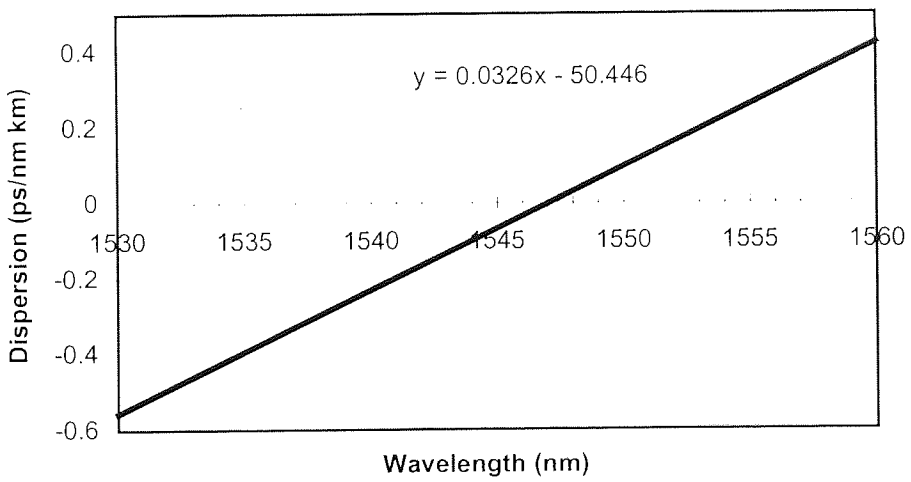

Figure 4-13 A plot of dispersion vs wavelength, which was extracted from the equation for the curve fit shown in Figure 4-12. The equation of this line also reveals the dispersion slope.

The equation reveals the dispersion slope, and setting y equal to 0 and solving for x gives the dispersion zero wavelength.

4.7 The Receiver

The final section of the transmission system is the receiver. It is at this point in the system that the transmission performance should be assessed. The receiver is a stand alone section having no other links to the transmitter other than through the transmission medium. It is therefore required to provide its own data rate synchronisation, this can be extracted from the transmitted signal through a clock recovery system. In this section, the methods for determining the performance of a transmission system, i.e. timing jitter measurements, Q-value measurements and bit error rate measurements are discussed.

4.7.1 The clock recovery

An important feature of any remote receiver is its ability to recover and maintain accurately the data rate transmitted from the source. Two commonly used techniques to recover the data rate are through the use of a high Q filter or through a Phase Lock Loop (PLL). The high Q filters are essentially very narrow band selective filters, which can be used to extract the data frequency from the transmitted signal. These devices are useful when using optical time division multiplexing, since they can be used to extract the data rate of one of the individual channels, aiding the de-multiplexing process. However in this thesis it is the PLL that was used to provided clock recovery, and is illustrated in Figure 4-14.

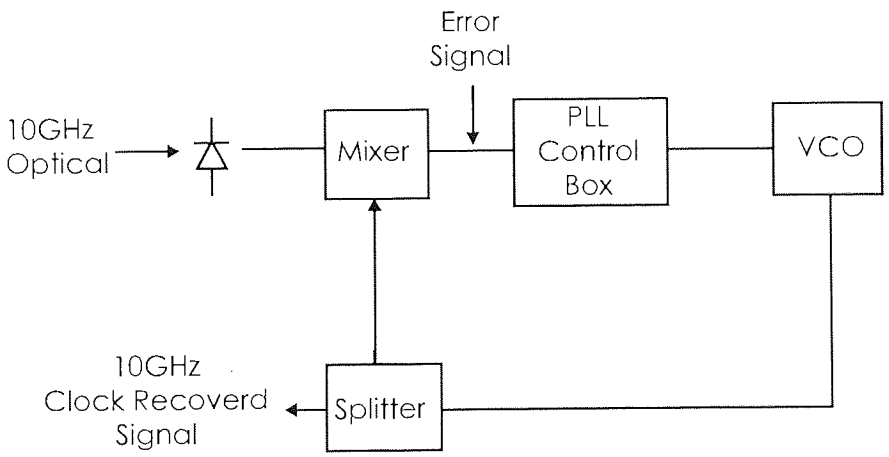

Figure 4-14 The clock recovery Phase Lock Loop system. The PLL locks onto the 10GHz component of the received signal. The VCO of the PLL generates the trigger signal for the sampling' scope and BERTS.

10% of the received signal is converted into an electrical signal via a 10GHz photo-diode and electrical amplifier. This signal is mixed with the output signal of the VCO (voltage-controlled oscillator), which generates a signal with output frequency equal to the error in VCO frequency (relative to the incoming data rate). This is fed into a control box, which provides the voltage control for the VCO. The gain characteristics and RC time constant can be adjusted on the control box to optimise this clock recovery. The output of the

VCO was split twice to provide three outputs one of which was for the mixer, and the two others supplied the trigger for the sampling 'scope and BERTS.

The measurement process is all synchronised off state C of the 1st delay generator. This controls an Electro absorption switch, which is inserted between the PLL and the sampling scope. This blocks the trigger signal for all states except C. By doing this all sample measurements taken on the sampling-scope correspond to the selected transmission distance. The C output of the delay generator also controls the measurement window of the BERTS, and for this reason the first 30μs of the measured recirculation are discarded to allow the BERTS to synchronise the received PRBS pattern with its own internally generated PRBS pattern. Once the synchronisation has been achieved error rate measurements can be taken.

4.7.2 Sampling 'scope measurements

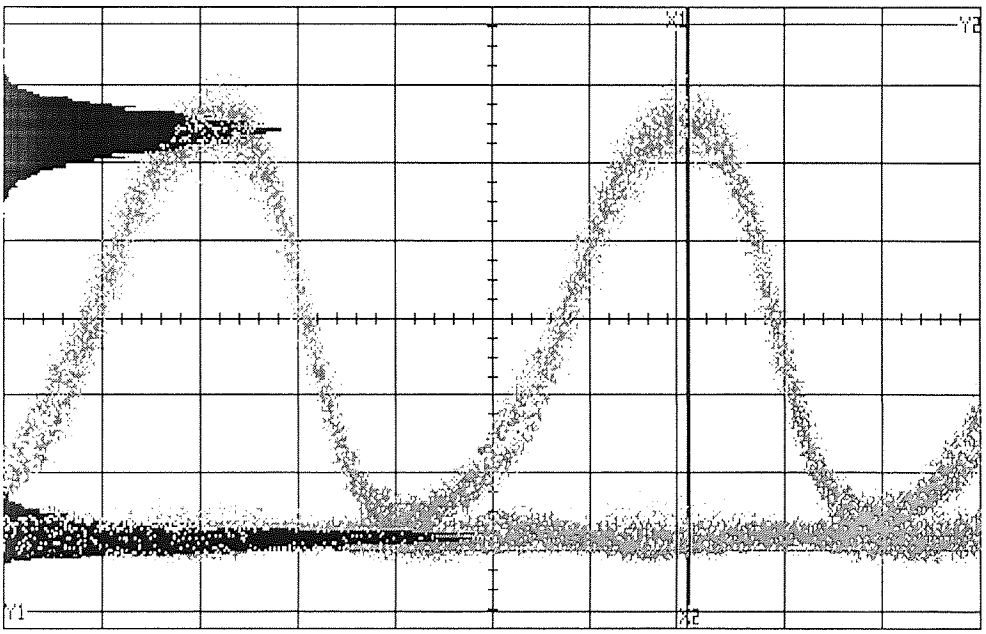

Figure 4-15 Example a Q value measurement of a pulse eye. The Histogram on the left is constructed from the window at the centre of the eye on the right. Statistical information such as mean value and standard deviation are extracted from the two peaks in the histogram.

The sampling 'scope plots sampled voltages taken across a specified period. This requires a trigger as a reference point within the bit window. The sampled voltage levels are recorded at different delay times from this reference point, building up a image of the waveform to produce traces such as eye diagrams. Statistical information about the pulse can also be gathered from the sampling 'scope, namely rms timing jitter and voltage histograms taken over a specific time window within the waveform. The mean value and standard deviation of the voltages corresponding to the 1's and for the 0's can give an indication of the expected error rate. Figure 4-15 shows a sampling 'scope trace taken for a Q value measurement. The position of the window should be placed at the peak of the pulse, and the

window should be kept small so as to restrict the measurement to the peak of the pulse. On the far left of the oscilloscope there is a histogram plot of the distributed voltage samples recorded. The distribution of samples shows two peaks. The top peak corresponds to a received pulse (a one), the bottom peak corresponds to the absence of a pulse (a zero).

By collecting statistical information about the mean value and standard deviation of these two peaks the Q value can be calculated[122].

$$Q = \frac{\mu_1 - \mu_0}{\sigma_1 + \sigma_0}$$

Equation 4-6

Where μ_1 is mean value of the top peak, μ_0 is the mean value of the bottom peak. σ_1 and σ_0 are the standard deviations of the top and bottom peaks respectively. Equation 4-7 can be used to estimate the error rate from the calculated Q value.

$$BER = \frac{1}{\sqrt{2\pi}} \frac{\exp\left(-Q^2/2\right)}{Q}$$

Equation 4-8

Figure 4-16 shows a plot of bit error rate against Q-value.

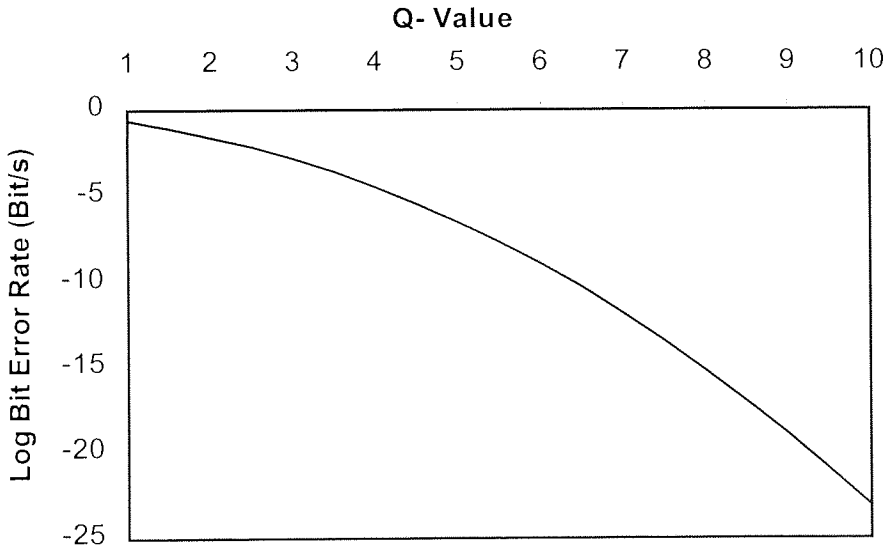

Figure 4-16 A plot of equation 4.2 shows Q value vs Error rate. For a value of Q equal to 6, the error rate is estimated at 10^{-9}.

An error rate of 10^{-9} is deemed acceptable and error free for research purposes. From Figure 4-16 it can be seen that this corresponds to a value of Q of 6, any value lower than this is not considered acceptable.

The timing jitter measurements are taken in a similar way to the voltage statistics acquired for the Q value. This time the measurement window is horizontal and placed at half

the amplitude of the pulse. Any sampling points appearing in this voltage window are recorded in the histogram at the bottom of the trace. The voltage window should be small so as to keep the measurement around the same voltage (typically around half the peak). The trace shows an example of a jitter measurement taken for a pulse stream, the two peaks represent the leading edge and the trailing edge of the pulses. The standard deviation of these peaks is rms timing jitter.

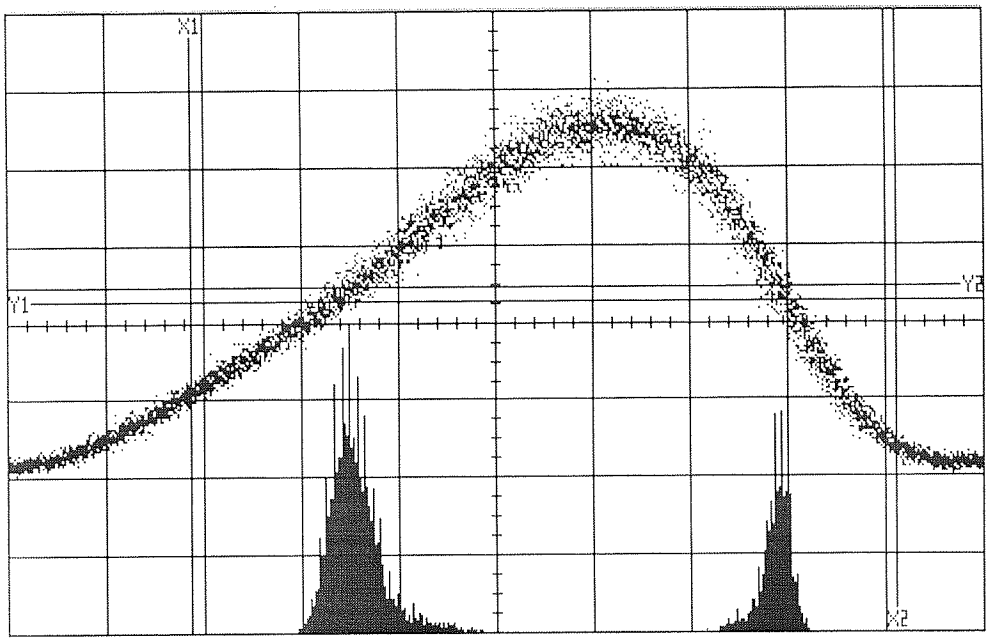

Figure 4-17 sampling 'scope trace showing measurement of the timing jitter of a pulse stream. The histogram shown at the bottom was extract from the samples occurring within the voltage window placed at half the amplitude of the pulse.

4.7.3 Bit Error Rate Measurements

While the sampling 'scope provides good analysis of the system, it is ultimately the error rate measurements that are used to evaluate the performance. Error rate measurements are performed using a BERTS. One of the advantages of the BERTS over the sampling 'scope is that it gives instantaneous feed back on the error rate of the system, which allows adjustments to be made to the components within the transmission loop with continuous instant feedback. The BERTS requires a 10GHz trigger signal provided by the clock recovery to provide a time reference for the arriving pulses. From this reference point the delay time on the BERTS can be controlled to allow the bit sampling to be taken at any point within the bit slot of the data stream. For optimal error rate this sampling point needs to be set to the middle of the eye. The BERTS also provides control over the threshold voltage to distinguish between 1's and 0's. Any voltage sampled by the test set above this level is recorded as a '1' any value sampled below this point is recorded as a '0'. During transmission this can be optimised to reduce the errors. The BERTS is operated in burst mode. Burst mode allows

control over the intervals over which the BERTS will sample error rates. This is controlled by the Stanford delay generators and corresponds to transition from state C in Figure 4-10. Measurements were carried out once the transmission distance has been reached. It is important that the measurement window does not straddle the following recirculation as this would cause a discontinuity in the PRBS stream which would result in the test set loosing synchronised for the remainder of the measurement window and therefore recording invalid errors.

The duration it takes to carry out error measurements using a recirculating loop is much longer than in a straight-line experiment. This is due to the long duration in each transmission where no measurements are taken while the signal propagates around the loop to the required distance. For example, the typical length of the loop is 38km, which gives a single recirculation time of 184μs. To transmit these pulses for 100 recirculations the full transmission cycle including fill time, kill time (time to remove signal from loop), transmission time and re-pump time would take around 19.0ms. The sample window for this loop length will be 150μs. Thus it would take 19ms to acquire 150μs of transmission. For a 10Gbt/s data stream this measurement duration corresponds to 150Mbits. In order to achieve a bit error rate of 10^{-9}, 10^{+9} bits must be sampled. This requires transmission to be performed ~700 times, which would take more than 13 seconds to complete. This duration multiples up with the distance of transmission, and for a distance of 1,000 recirculation the duration is 10 times as long. The same latency is also seen with the sampling 'scope in which sampled waveforms take longer to acquire when operating at longer transmission distances. The problem can be reduced by using a longer transmission loop as this will allow more bits per transmission cycle. The longer loop will also enable a greater proportion of the PRBS pattern to be included in a single transmission (38km will only store 0.07% of a 2^{31}-1 PRBS pattern at 10Gbit/s). A common technique for presenting the maximum error free transmission distance is to plot error rates vs distance on a log error rate vs distance graph. This forms a straight line, which crosses the 10^{-9} point at the maximum error free distance.

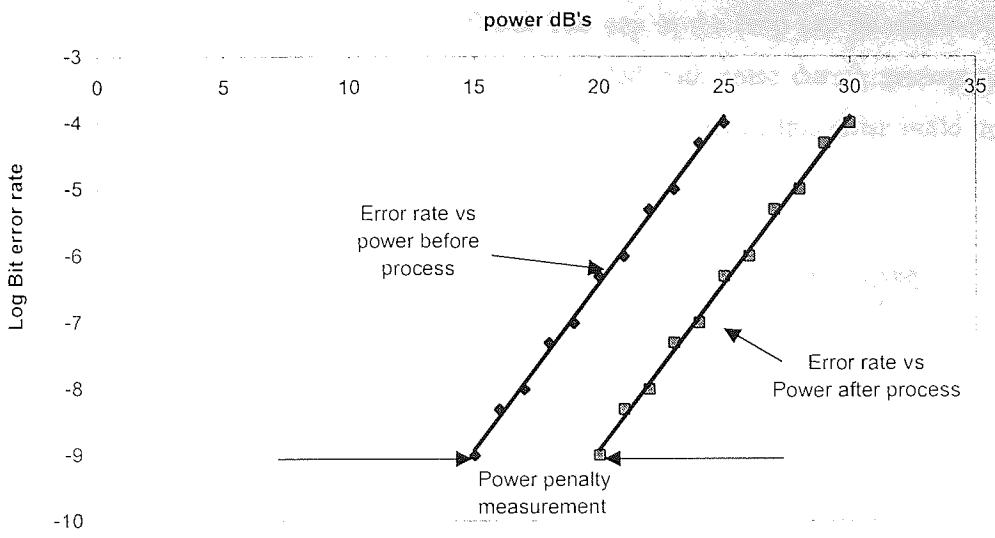

Figure 4-18 An example power penalty measurement. Two straight lines of bit error rate vs power, The error rates taken after transmission show a displacement along the power axis. This power is taken to be the power penalty.

Power penalty measurements can also be used to determine performance. The power penalty is measured by taking a log plot of the bit error rate vs power (in decibels) before a signal is processed (transmitted) and the error rate vs power after processing. These are recorded on a log bit error rate vs power (in decibels). Any extra noise on the signal will result in displacement along the power axis, this is taken to be the power displacement (As illustrated in Figure 4-18).

4.7.4 The Monitors

The 20% continuous output from the loop is split using two optical couplers, the first is a 70/30 with the 70% being split by a 90/10 coupler, of which the 90% is fed to the receiver. This gives two remaining other outputs from the loop, these are be used to provide two simultaneous monitoring points. Three instruments were used for monitoring, these were the photo diode, the electrical spectrum analyser and the optical spectrum analyser and are discussed in this section.

The Photo diode is used to determine the power recirculating around the loop. The measurement is taken from the 30% output of the first coupler. Due to the gating of the amplifier and the initial power launch into the loop, the power from the loop 30% output was variant with time. It was therefore necessary to use an oscilloscope to allow the voltage output from the photo diode to be recorded at an instant during transmission. The power measured can then be equated back to the average power in the loop and ultimately the average pulse power during propagation. By under filling the loop it is also possible to monitor the noise

floor during transmission. Figure 4-19 below shows a trace taken from the oscilloscope with the loop 10μs short of being completely filled. The gap in the loop can be observed during each recirculation. In this graph the gap is slowly filled with noise during propagation. The components in the transmission system can be optimised to reduce this noise build up in this power gap and improve transmission.

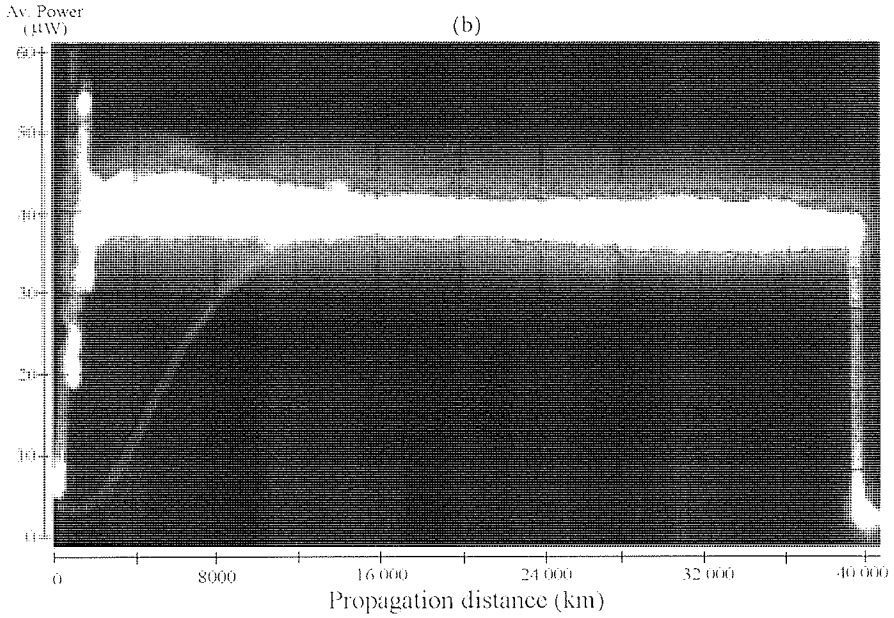

Figure 4-19 Trace taken from the slow photo diode showing the pulse power with propagation and the baseline noise.

The electrical spectrum analyser can be used to observe the presence of a particular frequency component in the signal during transmission. This was typically done using the 10% output from the second coupler. The frequency span of the electrical spectrum analyser is set to zero and the centre frequency set to the frequency of interest (typically the data rate). The sweep time determines the duration over which the trace is taken and a trigger signal from the Stanford delay generator ensures the recording of the trace is synchronised with transmission. If the trace shows the component falling with distance, then there is a deterioration in the signal during propagation. Figure 4-20 shows an electrical spectrum analyser trace taken for a sustained 10GHz signal propagating within the loop.

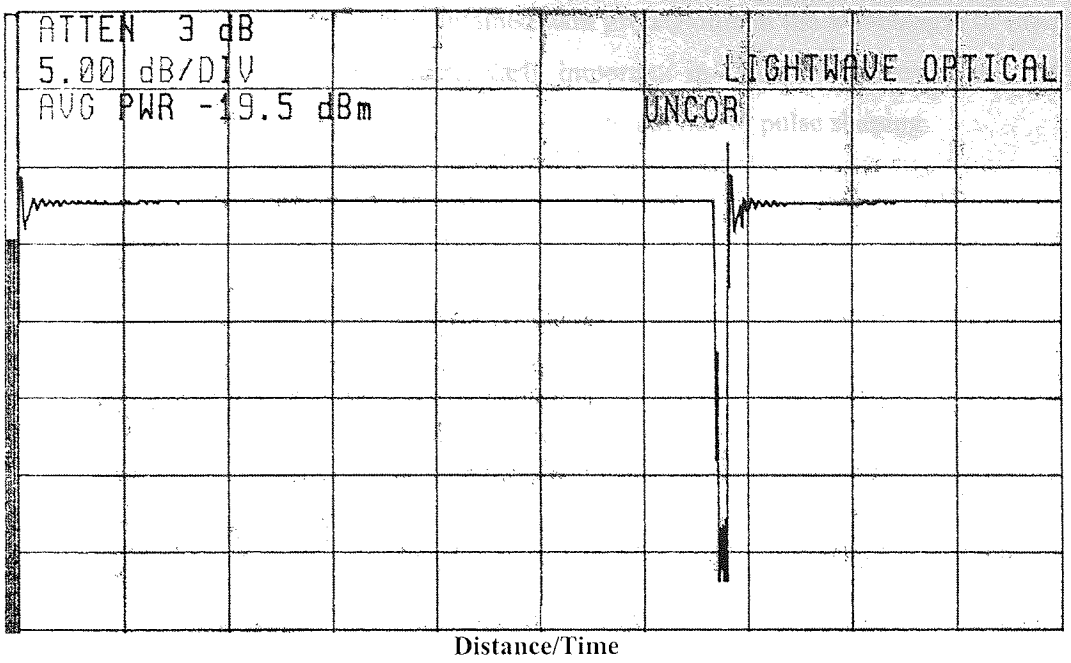

Figure 4-20 Trace take from the electrical spectrum analyser showing the 10GHz component propagating within the transmission loop. This trace shows good transmission of the 10GHz component.

The optical spectrum analyser can also be used in the same way as the electrical spectrum analyser to analyse wavelength components present during transmission. The wavelength span should be to zero and the central wavelength set to the wavelength of interest. The Stanford delay generator provided synchronisation with the transmission cycle of the loop. The sweep time determines the duration (distance) over which the wavelength is monitored. Below is a graph showing such a trace taken from the spectrum analyser.

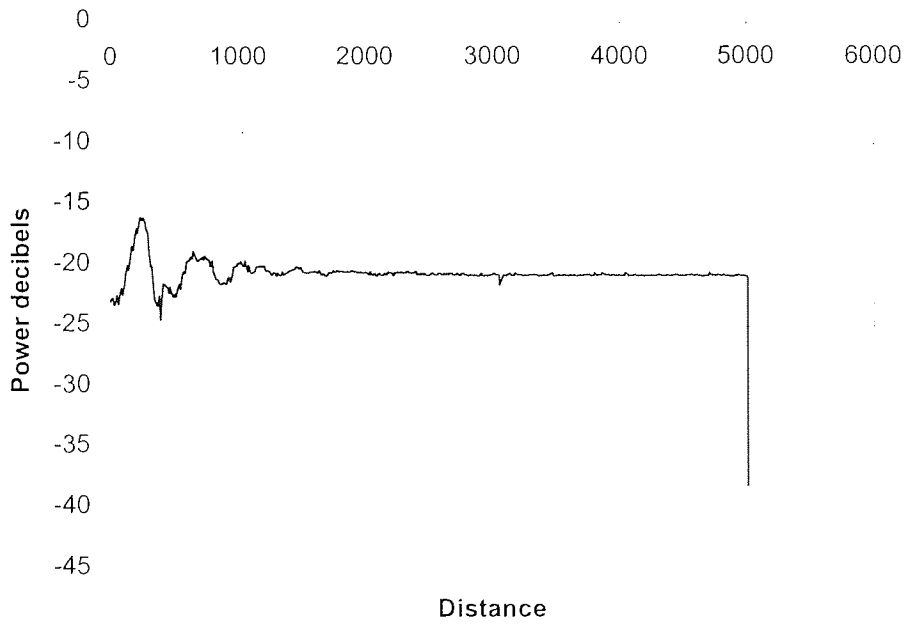

Figure 4-21 Power Measurement from the 10% output of the recirculating loop at a single wavelength using an optical spectrum analyser. After the initial power fluctuations due to low launch power, the power at this wavelength steadies out.

This shows a constant power maintained with propagation at the wavelength of interest within the loop. This technique is particularly important in Chapter 7 where it is used to monitor the changes in the spectral width of a pulse stream due to pulse shaping.

4.8 Summary

In this chapter the three modules of the communications system were discussed. Different methods of creating a pulse stream were discussed along with their advantages and disadvantages. The use of an optical loop as a means of transmitting a signal over long distances was also discussed. The main methods of analysing the quality of the received signal were described, such as Q-value measurements timing jitter measurements and power penalty measurements. Also mentioned in this chapter were the configuration aspects of the EDFAs and the dispersion measurement technique for the fibre within the loop.

Chapter 5

Transmission of a 10Gbit/s pattern using various average dispersions

5.1 Introduction – The power dispersion relationship

As explained in chapter 2, one of the major limitations in a soliton transmission system is Gordon Haus jitter. This is a scattering of arrival times of pulses through group velocity dispersion (GVD) due to the minute random wavelength shifts. These random wavelength shifts are as a result of the Amplifier Spontaneous Emission (ASE) generated by the amplifiers being absorbed by the soliton. One method of reducing this jitter is to operate at lower dispersions. However the problem in a uniform soliton system is that the pulse power is proportional to the dispersion, and reducing the dispersion requires the soliton power to be reduced. In order to provide adequate signal to noise ratio at the receiver there is a lower limit on the transmission power of the soliton, which places a lower limit on the operating dispersion. This ultimately places a Gordon Haus jitter limit on the maximum achievable error free distance. The introduction of dispersion management has provided a solution to this problem.

One of the major benefits behind dispersion managed systems is the enhanced stable pulse power compared with that of a uniform system. This enhanced power is as a result of the spectral breathing that takes place within the dispersion map. As explained in Chapter 3, this increases the dispersive effect of the anomalous section of the dispersion map on the soliton. Therefore an enhanced power soliton is required in order to maintain the balance between the dispersion and non-linearity. This enhanced power can extend transmission distances beyond the Gordon Haus jitter limit of the conventional soliton system. This is achieved in two ways, firstly the enhanced power gives the solitons more resilience to the

frequency shifts from the absorbed ASE. Secondly, the enhanced power also allows transmission closer to the dispersion zero without the problem of the Signal to Noise Ratio. This lower dispersion reduces the temporal walk off of the solitons due to the small frequency shifts. The dispersive term (β_2) is seen in the nominator of the Gordon Haus jitter equation in Equation 5-1. It can be seen that as β_2 tends to zero the Gordon Haus jitter also tends to zero.

$$\left\langle t_N^2 \right\rangle = \frac{2\pi n_2 N_{sp} |\beta_2| hc(G-1)L^3}{9\tau_0 \lambda^2 A_{eff} L_a \Lambda_0^2}$$

Equation 5-1

In Chapter 3, a parameter known as the map strength (S) was introduced. Investigations have determined a relationship between this map strength, the pulse power and the average dispersion[96]. It has been found that the dispersion management results in partial de-coupling between pulse power and the dispersion[123], giving stable pulse powers that are less variant over a dispersion range. This property of dispersion management is beneficial to WDM systems since it reduces the power variation between channels near dispersion zero. Increasing the map strength increases this de-coupling effect giving a flatter response. For large map strengths it has also been found that propagation on the dispersion zero and into the normal dispersion is also possible. This was first shown numerically by Nijhof *et al*[127] and subsequently confirmed by Ref [125] [126][127].

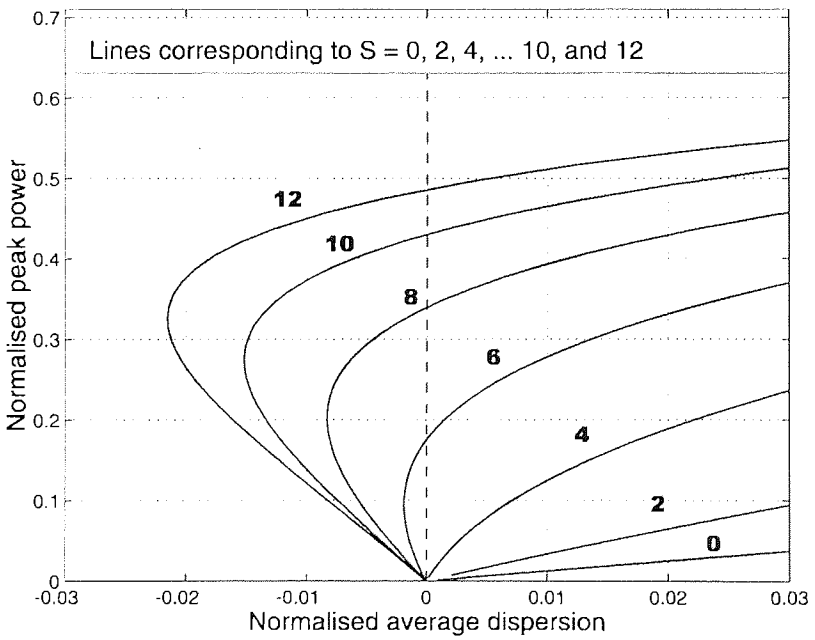

Figure 5-1 Normalised peak power vs Normalised average dispersion for different map strengths of a symmetric dispersion map[128]. (S=0 represent a uniform system). The graph shows that for values of S greater than four that the curve penetrates into the normal dispersion. Increasing the map strength allows propagation further into the normal regime.

The results[128] shown in Figure 5-1 show the relationship between a normalised stable pulse power and Normalised average dispersion, plotted for several values of map strengths

(S equal to 0,2,4...10 and 12). S=0 represents a uniform system where the stable power and dispersion can be seen to be linearly related and meet at the origin. For stronger maps the stable power is increased as the theory suggests and the degree of variation in power with dispersion range is reduced. For a map strength of S greater than 4 the stable pulse power curves penetrate into the normal dispersion before crossing into the anomalous regime. This stable transmission in the normal regime contradicts many of the early beliefs that solitons systems could only operate in the anomalous regime. A physical interpretation of this Normal propagation was explained by J. H. Nijhof[129]. The stable balance between dispersion and non-linearity in the normal dispersion is explained by the same spectral breathing that gives rise to the enhanced soliton power. The broader spectrum in the anomalous section of the map, gives an increased effective anomalous dispersion on the soliton. In the normal dispersion section the narrower spectrum reduces the effect of the dispersion. As a result the soliton is subject to an effective anomalous dispersion, even though the actual average dispersion is normal. To summarise, the increased effective anomalous dispersion resulting from dispersion management can also shift the effective dispersion from the normal into the anomalous. Asymmetry within the dispersion map has an additional influence on this power dispersion relationship. Further simulation results, relating the normalised peak power to the normalised average dispersion using two asymmetric maps are shown along with the symmetric map in Figure 5-2[130]. These are labelled (a), (b) and (c). Map (a) was predominately Normal dispersion with a Normal to Anomalous length ratio of 10:1. Graph (b) was the symmetric map as in Figure 5-1 and map (c) was the predominately anomalous dispersion map with a Normal to Anomalous length ratio of 1:10. By contrasting these graphs it can be seen that propagation can be achieved further into the normal dispersion regime when the map contains predominately anomalous dispersive fibre. Using a map with predominantly normal dispersion fibre restricts this propagation in the normal dispersion.

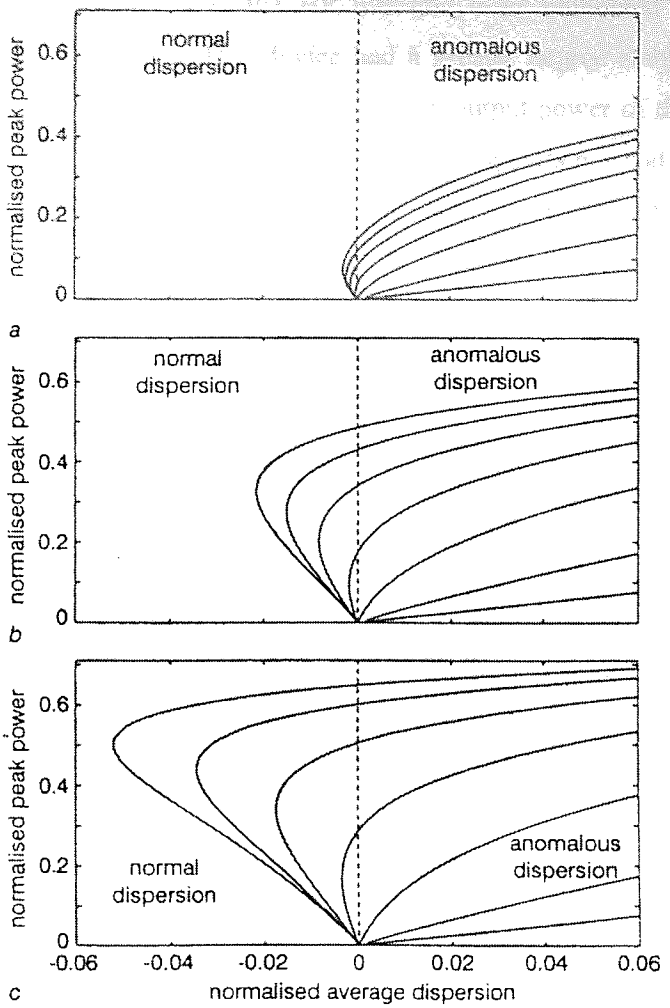

Figure 5-2 A comparison of stable propagation powers against dispersion for three dispersion maps carried out by[130]. (a) corresponds to a dispersion map with a 10:1 normal to dispersion length ratio, (b) corresponds to the symmetric dispersion map and (c) corresponds to the a dispersion map with 70% of the fibre being anomalous dispersion with a 1:10 normal to dispersion length ratio.

The focus of this experiment is to investigate the dispersion tolerance with stable transmission on the zero and into the normal dispersion regime using a strong dispersion managed system, the dispersion map used was also applicable to the upgrade problem of standard fibre. With around 80% of the fibre being standard fibre and the remaining 20% being dispersion compensating fibre. This provides an asymmetric map more closely related to that in Figure 5-2 (c), which further promotes propagation in the normal regime.

In order to achieve transmission at various average dispersions, two different methods were used. The first method takes advantage of the dispersion slope of the fibre. By tuning the wavelength of transmission, different path average dispersions can be obtained. The disadvantage of this method is that it introduces the wavelength dependent effects that may be present in the EDFAs and the pulse source, which may influence the final results. Two sources were used for this method. The first was the fibre laser, this has the disadvantage of being unstable and can be inconsistent with regards to the pulse width from one transmission

to another. The second source was the HP tuneable laser combined with the Electro-Absorption Modulator (TLEAM). This device had a greater degree stability than the fibre laser, and was consistent with the pulse width. The low output power of this device however meant that extra amplification was required, thus introducing extra noise at the source.

The second experimental method was carried out using two fixed wavelength devices. The First being the gain switched DFB and the second being Erricson Integrated DFB and Electro-absorption modulator. In order to vary the average dispersion for the fixed wavelengths of the source, the lengths of fibre in the map were altered. This method avoids the wavelength dependence of source and the EDFA, but will introduce small changes in the map strength.

5.2 Dispersion tolerance through varying the operating wavelength

The dispersion map used in this experiment is illustrated in Figure 5-3. The total length of the map, which is equal to the length of one amplifier span, was 38.8km. The first section of the map consisted of 32.0km of the standard fibre with a dispersion of around 17ps/(nm km). The second section contains the dispersion-compensating module with a length of 6.8km and a dispersion of around –76ps/(nm km).

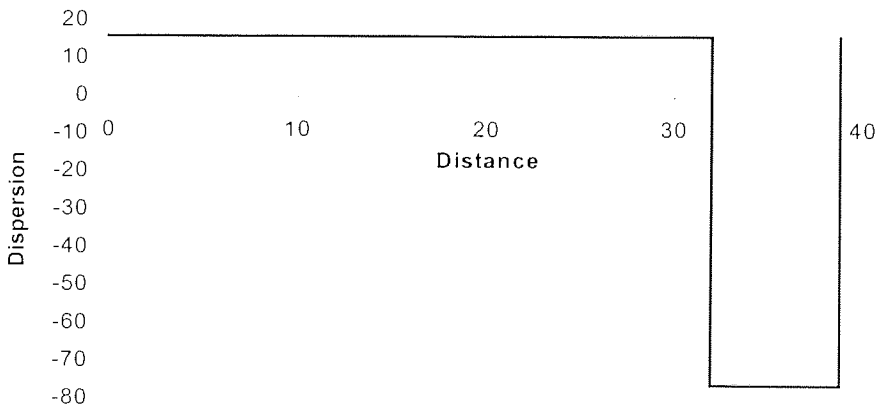

Figure 5-3 Dispersion map containing 32km of standard fibre with a dispersion of 17ps/nm km, and 6.8km of dispersion compensating fibre with a dispersion of –76ps/nm km.

The average dispersion characteristics of the map were measured using the dispersion measurement technique described in section 4.6. The zero dispersion and dispersion slope were measured to be 1546.5nm and 0.03ps/(nm km)^2 respectively. These wavelength dispersion characteristics are shown in Figure 5-4

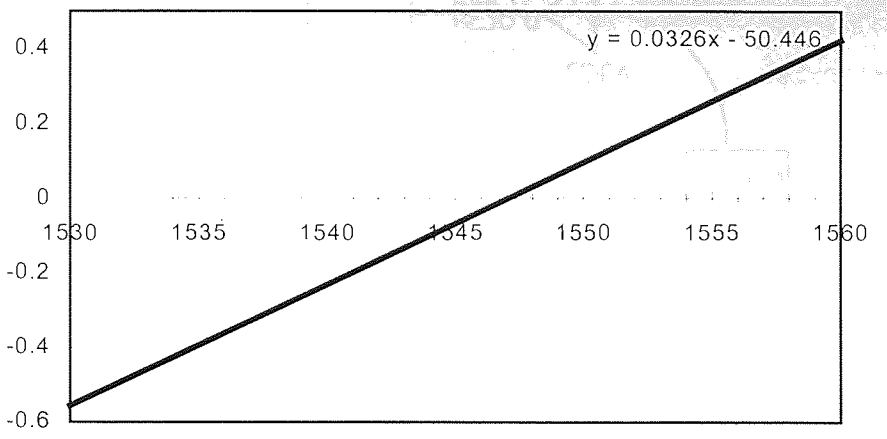

Figure 5-4 Dispersion measurement for loop set up containing 32.0km of stndard fibre and 6.8km of DCF. The disperison zero is at 1546.5nm and the slope 0.03ps^2/nm km.

This dispersion map was setup in the recirculating loop (described in Chapter 4) and is shown in Figure 5-5. The loop consisted of a single amplifier span with the AOM used to gate the pulses into loop via an 80/20 coupler. The coupler is configured such that only 20% of the power into the coupler is launced into the loop, this correspondinds to a 6dB loss. Consequently only 20% of the power in the loop is released each recirculation, corresponding to a 1dB loss each round trip. This 20% output was split by a 70/30 coupler, with the 70% being split again by a 90/10 coupler. The 30% output was used to monitor the optical power within the loop and the 10% used to monitor the 10GHz frequency component using the electrical spectrum analyser. The remaining 90% output was fed to the receiver, which consisted of clock recover phase lock loop (PLL) circuit, and a bit error rate test set (BERTS) or sampling 'scope. The clock recovery provided the clock reference for the BERTS and sampling 'scope, and required 10% of the receiver power. Therefore another 90/10 coupler was required at the receiver. The position of the launch coupler was located 19.2km into the standard fibre section of the map. The remaining 12.8km of the standard fibre acted as a half-step to provide an optimum launch point for transform limited pulses. The total loss of one round trip of the loop was 14.9dB, which was compensated for by the loop EDFA. The EDFA was located at the boundary between the 12.8km half-step and the dispersion compensating module. This amplifier had a noise figure of around 4dB. The total loss of the standard fibre was 6.5dB, approximately 0.2dB/km. The total loss of the dispersion compensating module was 4.2dB, including the extra splice loss of splicing from standard fibre to disperison compensating fibre. The band pass filter had a 3dB bandwidth of 2.3nm and an insertion loss of 2.2dB. Its purpose was to suppress the ASE generated by the amplifier and reduce the Gordon Haus Jitter. The isolator and the launch coupler make up the remaining 2dB of loss in the loop. The polarisation controllers were used to optimise the polarisation within the loop.

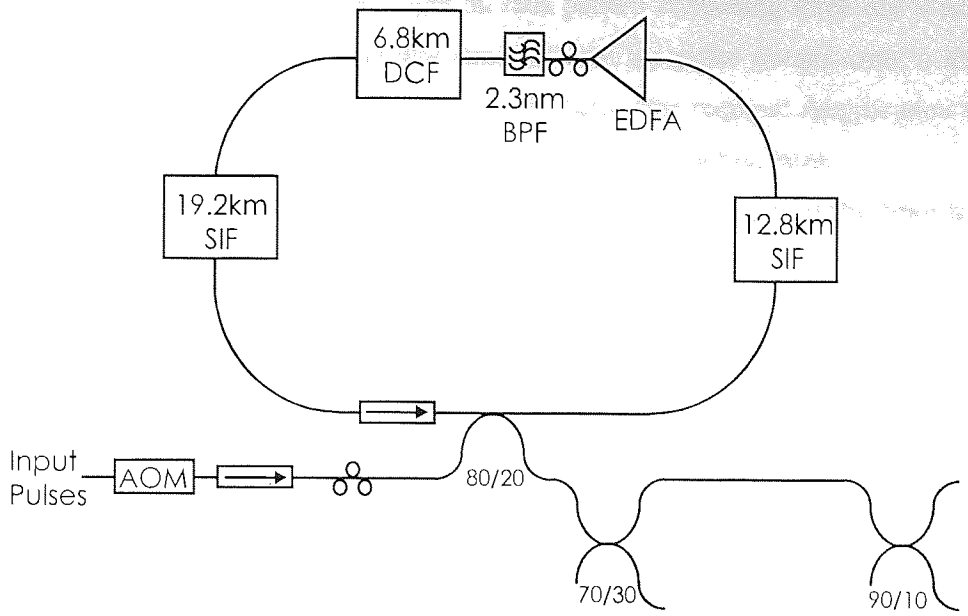

Figure 5-5 Loop set up containing 32 km of SIF and 6.8 km of DCF. The standard fibre was split into two sections of 12.8km and 19.2km, allowing a launch point midway through the standard fibre. The signal was launched into the loop via the 80/20 coupler. A 70/30 coupler split the 20% output from the loop, and 90/10 coupler split the 70% output of the 70/30 coupler to provided two monitoring points. The 2.3nm band pass filter after the amplifier provided ASE suppression.

The source used for the first set of transmission results was the 10GHz fibre-ring laser described in Chapter 4 section 4.4.1. The pulse stream from this source was inconsistent and unstable with widths varying from 17 to 22ps between experimental results. The spectral bandwidth was 0.22nm, giving a time bandwidth product for the source of around 0.55. This indicates that there was a small degree of chirp present on the pulses from the source, which means the launch point is not at the optimum as would have been desired (this source is not a true soliton fibre ring laser and therefore produces chirped pulses). While it is difficult to say what pulse widths would have evolved to during transmission, if the spectrum is maintained a transform limited pulse width would have had a full width half maximum of 15ps. For the dispersion map used, this would give a map strength of around 6.5. With such a strong dispersion map there is a significant amount of pulse breathing, which as will be shown in Chapter 6 dramatically increases the soliton-soliton interactions. In this dispersion map this is to the extent that they have become the limiting factor in error free transmission. While these interactions can be suppressed to some extent (Also discussed in Chapter 6), the purpose of this experiment is to show stable soliton transmission with various average dispersions. It is therefore merely enough to suppress these interactions by using a fixed 10Gbit/s pattern for transmission. The pattern chosen was set to give mark to space ratio large enough to suppress these interactions. This is done by keeping mark to space ratio of greater than 10:1 which is achieved by having at least one zero slot between pulses (200ps separation). Although this restriction makes this effectively a 5Gbit/s data pattern, it still comes under the same detection window constraints as a 10Gbit/s data pattern since pulses must remain in the 10Gbit/s time

slot. The pattern used was a repeated eight-bit data pattern containing three one's and five zero's set-up as '01010001'. The data was encoded onto the pulse stream using a lithium-Niobate modulator. The modulator used was slightly below the required specification with a 3dB-frequency response of 6GHz also contributing to a poor extinction ratio.

The various dispersions were achieved by tuning the wavelength of the fibre laser in accordance with the measured dispersion shown in Figure 5-4. Table 5-1 shows the dispersions of operation used for transmission with the corresponding wavelengths.

Wavelength	1541.9	1542.5	1543.6	1545.3	1546.6	1547.0	1548.1	1550.0	1552.0	1553.5	1555.0	1557.2
Dispersion	-0.14	-0.12	-0.09	-0.04	0.00	0.01	0.05	0.10	0.16	0.21	0.25	0.32

Table 5-1 This table shows the dispersion for the selected wavelengths of operation. The selected wavelengths span 15nm.

For this range of dispersions the soliton period was calculated and found never to be less than 170km, and therefore always satisfying the criteria that the amplifier span is much less than the soliton period ($L_a < 8Z_0/10$). Transmission was optimised to achieve maximum error free distance at each wavelength. These distances were recorded for each wavelength along with the average power. The results of which are shown in Figure 5-6 and Figure 5-7 respectively.

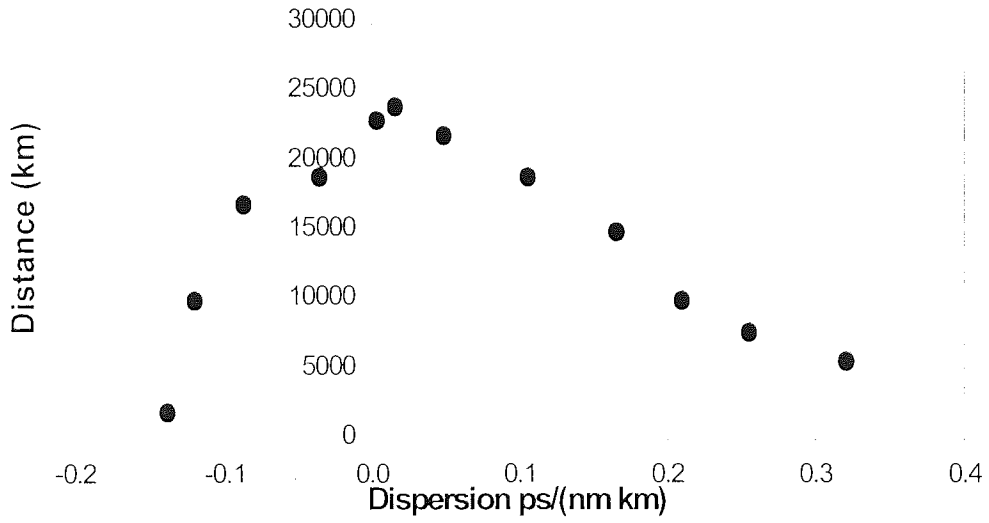

Figure 5-6 Dispersion vs maximum error free distance for the Fibre laser. The maximum distance of transmission peaks at 0.05ps/nm km with a distance of 24000km. The graph shows significant propagation in the normal dispersion regime.

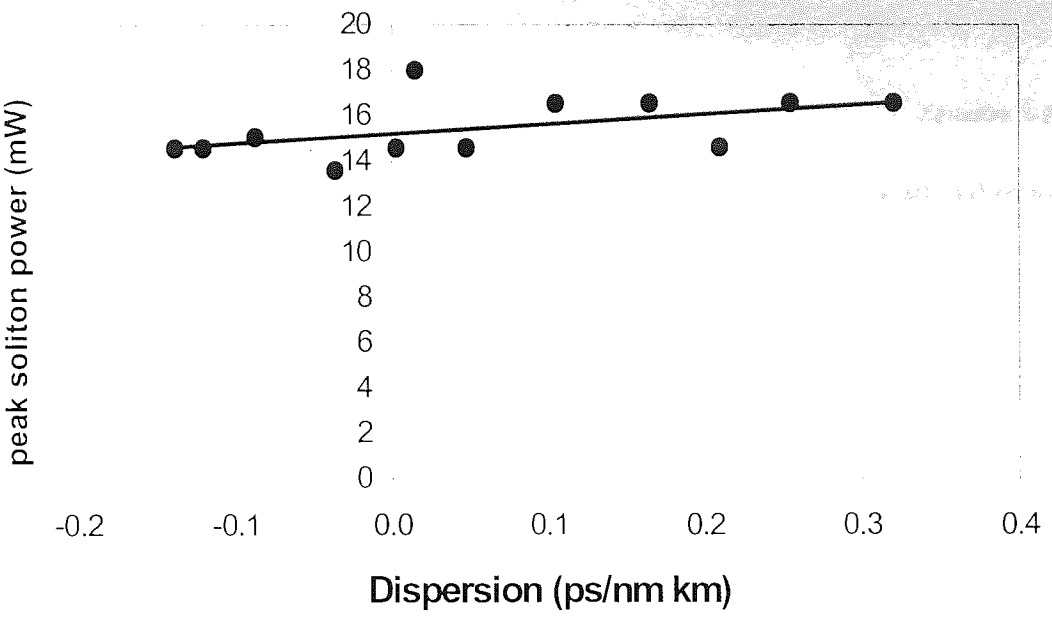

Figure 5-7 Average power vs operating dispersion. The results show an almost constant power across the dispersion range as predicted for a strong dispersion managed system.

It can be observed in Figure 5-6 that stable propagation was achieved both on the dispersion zero and into the normal regime. The significance of this result can be understood when calculating the expected pulse broadening if the non-linearity were not cancelling out the effects of dispersion. Distances of over 10,000km were achieved at a dispersion of –0.1ps/(nm km), (this corresponds to 3nm in to the normal dispersion). For a system where stability were not achieved and dispersion left to act alone, the pulses would broaden to 250ps. Easily in excess of what would be required to cause errors through intersymbol interference. However in this set-up no such effect could be observed, confirming that actual stable pulse propagation had been achieved in the Normal regime. The powers used for transmission are also of particular interest. Figure 5-7 shows the pulse power vs dispersion corresponding to the transmission results shown in Figure 5-6. The stable power measurements remain almost constant over the dispersion range. With the average peak pulse powers between 14 and 18mW extending to the dispersion zero and into the normal regime. This coincides well with the theory that indicates for strong maps that there is a de-coupling between the average dispersion and pulse power. The maximum distance of transmission falls off quicker into the normal dispersion regime than into the anomalous. For dispersions greater than 0.16ps/nm km, the results show the maximum transmission distances falling off as a function of D_2 (as would be expected from a Gordon Haus jitter limited transmission). The maximum distance of transmission for a dispersion of 0.16ps/nm km was found to be 15,000km. The maximum tolerable timing jitter for an error rate of less than 10^{-9} is given by

$$\left\langle t_N^2 \right\rangle \leq \left(\frac{t_w}{6.1} \right)^2$$

Equation 5-2

Where $2t_w$, the time window the pulses are expected to arrive within, is typically taken to be one third of the bit window (In this case 30ps). Therefore

$$\left\langle t_N^2 \right\rangle \leq \left(\frac{15}{6.1} \right)^2$$

$$\left\langle t_N^2 \right\rangle \leq 6\,ps$$

The Gordon Haus Jitter for an unfiltered system

$$\left\langle t_N^2 \right\rangle = \frac{2\pi m_2 N_{sp} |\beta_2| hc(G-1)L^3}{9\tau_0 \lambda^2 A_{eff} L_a \Lambda_0^2}$$

Equation 5-3

where the values used for this calculation are

n_2	=	$2x10^{-20}$
N_{sp}	=	2
λ	=	$1550x10^{-9}$ (m)
L_a	=	$38x10^3$ (m)
H	=	$6.67x10^{-34}$
C	=	$3x10^8$ (m)
A_{eff}	=	$50x10^{-12}$ (m^2)
τ_0	=	$\tau_{fwhm}/1.763 = 8.5x10^{-12}$
G	=	$10^{14.9/10} = 31$
D_2	=	0.16ps/nm km = $0.16x10^{-6}$ (s/m^2)

$$\beta_2 = -\frac{\lambda^2}{2\pi c} D_2 = \frac{\left(1550x10^{-9}\right)^2}{2\pi x 3x10^8} 0.16x10^{-6} = 2.03x10^{-28}$$

$$\Lambda_0^2 = \frac{G\ln(G)}{G-1} = 3.55$$

Thus the Gordon Haus Jitter at distance L= 15,000 is found to be

$$\left\langle t_N^2 \right\rangle = \frac{2\pi \cdot 2 \cdot \left(2.03x10^{-28}\right) \cdot 2x10^{-20} \cdot 6.67x10^{-34} \cdot 3x10^8 \cdot (31-1)}{9 \cdot 8.5x10^{-12} \cdot \left(1550x10^{-9}\right)^2 \cdot 50x10^{-12} \cdot 38.8x10^3 \cdot 3.55} \cdot (15x10^6)^3 = 8.17x10^{-22}$$

It is also necessary to include the reduction factor for the Gordon Haus jitter due to the filter, which is given as

$$f(x)=\frac{3}{2}\frac{1}{x^3}\left[2x-3+4\exp(-x)-\exp(-2x)\right]$$

Where x is given as

$$x=4\delta Z=\frac{4L}{3\left(2\pi\Delta\lambda_f\tau_0\right)^2 L_a}=\frac{4\cdot 15x10^6}{3\cdot\left(2\pi\cdot 2.87x10^{11}\cdot 8.5x10^{-12}\right)^2\cdot 38.8x10^3}=2.19$$

Where $\Delta\lambda_f$ is the bandwidth of the filter and is given as

$$\Delta\lambda_f=\frac{c}{\lambda^2}\Delta\lambda=\frac{3x10^8}{\left(1550x10^{-9}\right)^2}2.x10^{-9}=2.87x10^{11}$$

Thus the value of $\boldsymbol{f(x)}$ for a given distance L=15,000km is

$$f(x)=\frac{3}{2}\cdot\frac{1}{(2.19)^3}\left[2\cdot 2.19-3+4\exp(-2.19)-\exp(-2\cdot 2.19)\right]=0.26$$

The power enhancement must also be taken into account, for the purposes of experimental analysis this can be treated as a multiplying factor to the Λ_0^2 term seen on the denominator of Equation 5-3. The average peak power of the soliton in a uniform system is given as

$$P_0=\frac{|\beta_2|}{\gamma\tau_0^2}=\frac{2.03x10^{-28}}{1.5x10^{-3}\cdot\left(8.5x10^{-12}\right)^2}=1.87mW$$

Where γ is taken to be $1.5W^{-1}km^{-1}$. The average peak power in the experiment was found to be 16mW. This gives a power enhancement of 8.5. Therefore the full Gordon Haus jitter calculation for a distance L=15,000km is given as

$$\left\langle t_N^2\right\rangle_{GHJ-filtered}=\left\langle t_N^2\right\rangle_{GHJ}.f(x).\frac{1}{power\_enhancement}=8.17x10^{-22}\cdot 0.26\cdot\frac{1}{8.5}=2.499x10^{-23}$$

$$r.m.s\_jitter=\sqrt{2.499x10^{-23}}=5ps$$

This falls slightly short of the 6ps limit for error free transmission. The non-ideal launching conditions for the soliton pulses are likely to have increased the amount of jitter accumulated on the pulse stream. Below 0.016ps/nm km of dispersion the maximum error free distances reach a peak, with a transmission distance of 24,000km. Here the limiting factor is believed to be the Signal to Noise Ratio. The Signal to Noise ratio (introduced in chapter 2) for a transmission system can be calculated from

$$SNR=\frac{S_0}{4N_a(G-1)\mu h\upsilon\Delta\nu}$$

Where for a bit error rate of less than 10^{-9} the SNR_{dB} must be greater than 21.6dB. μ is the inversion factor, G is the gain of the amplifier υ is the frequency of the signal, N_a is the

number of amplifiers, Δυ is the bandwidth of the signal and So is the average output power of the amplifier. This evaluates to

$$SNR = 10^{\frac{21.6}{20}} = 12$$

Taking Δv to be the bandwidth of the signal, which for 0.22nm corresponds to 27.5GHz, and taking v to be the signal frequency, which is $1.9\text{x}10^{14}$Hz. The average power out of the amplifier is (S_0) 6.6mW

μ	=	2
h	=	$6.67\text{x}10^{-34}$
S_0	=	6.6mW
N_a	=	L_a/L

Substituting in for N_a and rearranging for L the equation becomes

$$L = \frac{L_a \cdot S_0}{4N_a(G-1)\mu h\nu \cdot \Delta\nu \cdot SNR}$$

This evalutates to

$$L = \frac{38.8x10^{3} \cdot 6.6x10^{-3}}{4 \cdot (31-1) \cdot 2 \cdot 6.67x10^{-34} \cdot 1.9x10^{14} \cdot 27.5x10^{9} \cdot 12}$$

$$L = 25{,}500km$$

This calculation compares well with the maximum error free distance achieved experimentally.

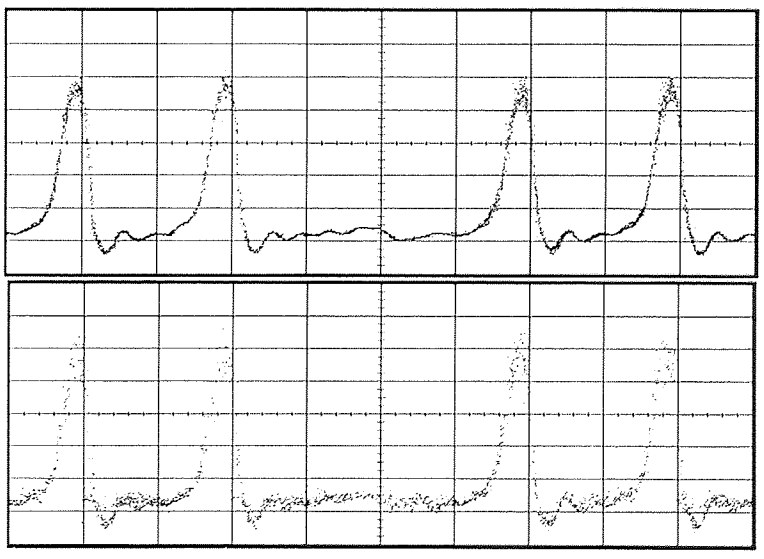

Figure 5-8 Two eye diagrams showing (a) The back to back waveform of a 01010001 pattern and (b) The waveform pattern after 20,000km taken at 0.01ps/(nm km).

Using the sampling 'scope, two sampled waveform patterns were taken and are shown in Figure 5-8. These were taken by triggering on a fixed point within the pattern and show a sampled state of the pattern after transmission over 20,000km compared with the back to back

waveform. These were taken at the optimum dispersion of 0.01ps/(nm km). It can be seen from the peaks of the pulses that there is a build up of amplitude jitter from the noise released by the amplifier.

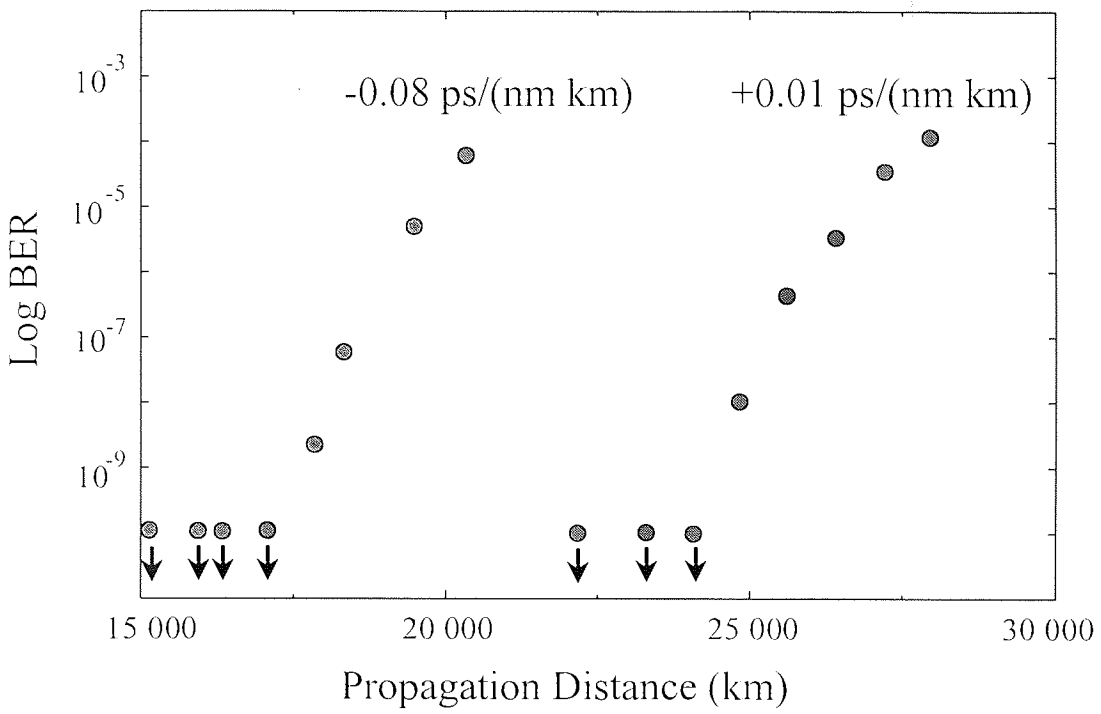

Figure 5-9 Results of error rate vs distance taken at optmium dispersion 0.01ps/(nm km) showing maximum transmission distance of 24,000km. The maxium distance of 15,000km is also shown at a dispersion of –0.08ps/nm km.

Figure 5-9 shows transmission vs error rate taken at the optimum dispersion of 0.01ps/(nm km). Error rates vs distance were also taken in the normal dispersion with a dispersion of -0.08ps/(nm km), where the maximum distance achieved was 15,000km. At this dispersion and distance without the balance with non-linearity, the pulse width would be expected to broaden to more than 250ps, which is sufficient to cause inter-symbol interference.

The experiment was repeated for the Tuneable Laser and Electro-absorption modulator. This device gives a pulse width of around 22ps and has a spectrum of 0.25nm and thus a time bandwidth product of 0.63. This again is not the optimum for the launch point used. With this spectral bandwidth the pulses should compress down to around 13ps, giving a map strength of 9. This source is tuneable over the entire erbium bandwidth. The portion of standard fibre in this dispersion map was slightly less at 31.85km this resulted in a small shift in the dispersion zero to 1549nm, but dispersion slope remains approximately at 0.03ps^2/nm km. These dispersion characteristics are shown in Figure 5-10.

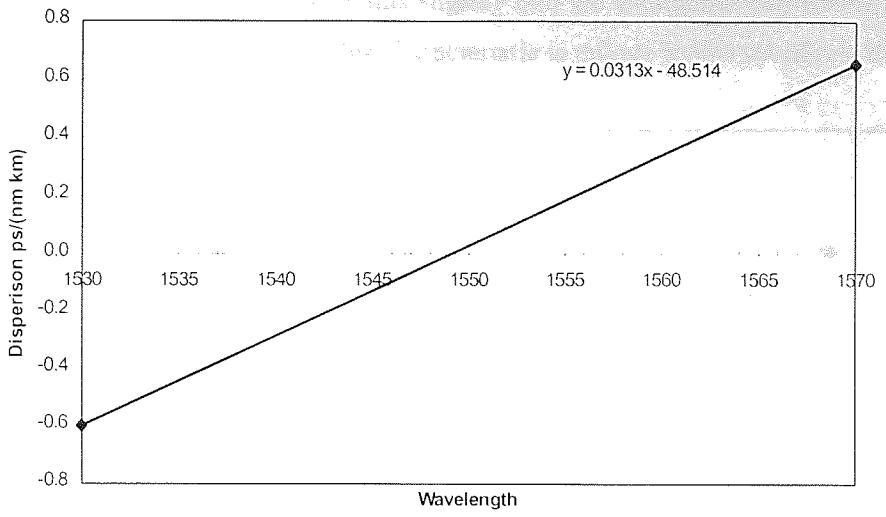

Figure 5-10 Dispersion characteristics for loop used for Tuneable Laser and Electro-Absorption Modulator.

The Tuneable Laser was tuned to different wavelengths and transmission optimised to achieve the maximum error free distance, the results of which are shown in Figure 5-11, with the power characteristics of these transmission results shown in Figure 5-12.

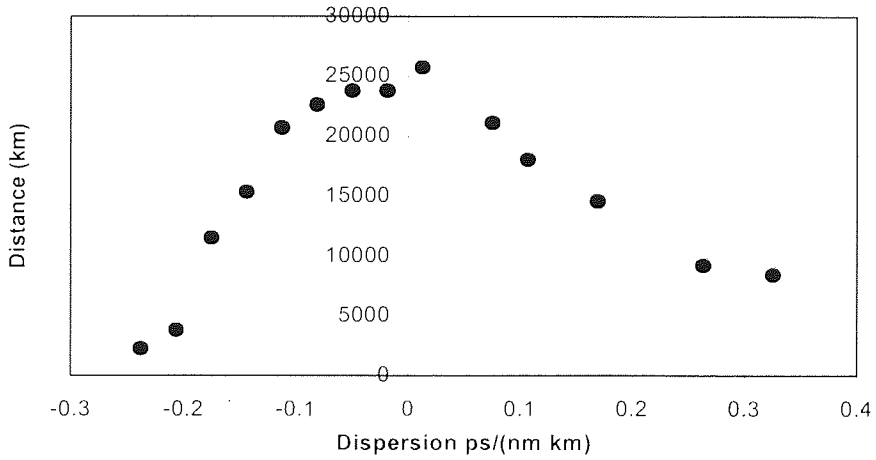

Figure 5-11 Maximum error free distances vs dispersion for the combined Tuneable Laser and Electro-Absorption Modulator. The maximum error free distance is at around 0.01ps/nm km.

The maximum distance with respect to dispersion compares well with the fibre laser results. The optimum transmission is achieved when the dispersion is slightly anomalous (around 0.01ps/nm km). However there is a sharper fall off in maximum transmission distance in the anomalous than in the normal dispersion regime. Figure 5-12 shows the average peak power with dispersion. The trend of these results differs slightly from those measured when using the fibre laser, propagation distance being maintained further into the normal dispersion than the anomalous. The reason for this may be due to some of the results

not being optimised, particularly the results slightly into the anomalous dispersion. As will be seen with the next two pulse sources this characteristic is unique to this set of results.

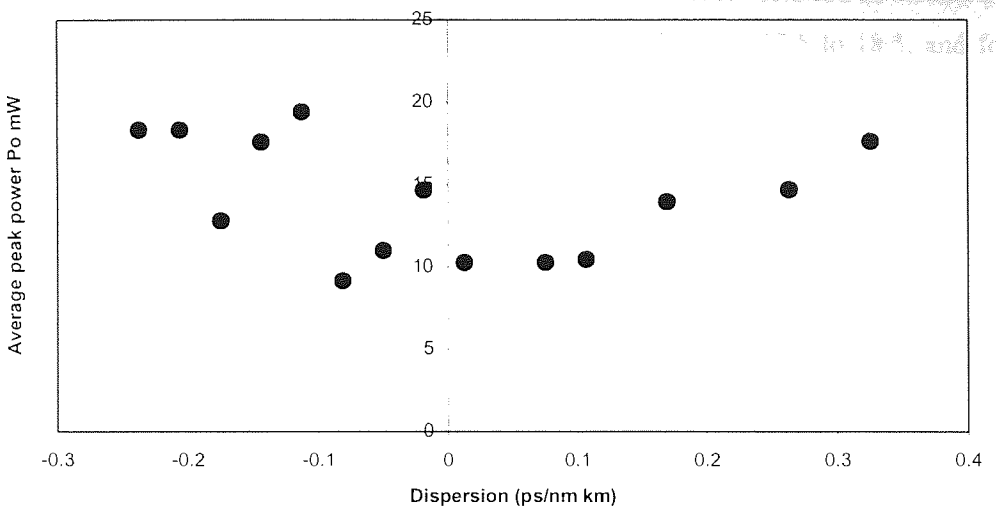

Figure 5-12 Average power during transmission against average dispersion when using the Tuneable Laser and Electro-absorption as modulator the source.

5.3 Dispersion analysis by varying the proportions of fibre in the loop

The previous results were obtained by tuning the wavelength of the source to achieve the various average dispersions. With this technique any wavelength dependence characteristics of the system, either in the source the EDFA gain or SNR could have an influence on these results. For this reason the experiment was repeated, this time removing the wavelength dependence by using two devices of fixed wavelength, these were the gain switched DFB at 1555nm and the integrated DFB and EAM at 1550nm, (discussed in Chapter 4). As with the two previous devices, there was chirp present on the pulse streams from devices making the launch point not ideal. The DFB had a pulse width of 20ps with a spectrum of 0.33nm, giving a time bandwidth product of 0.87. For the spectral bandwidth the pulses should compress down to a pulse width of 9ps. The Erricson DFB and EAM has a pulse width of 30ps, and a spectral width of 0.11nm, which gives a time bandwidth product of 0.41. This would correspond to a transform limited pulse width of 25ps.

In order to vary the average dispersion, the loop was setup as shown in Figure 5-13. The standard fibre length was 30.5km and made up of two sections of 12.8km and 17.7km. The 12.8km length providing a half step into the standard fibre section of the dispersion map. Extra lengths of standard fibre were inserted after the 17.7km section in order to vary the average dispersion. The same DCF module was used as with the previous results. These extra

lengths were 300m, 400m, 500m, 600m, 800m, 1000m, 1200m and 1700m. This results in a map length ranging from 37.3km to 39km. The average dispersion vs fibre length is shown in Figure 5-14 for both the DFB and integrated DFB and EAM. This variation in standard fibre length gave a map strength variation for the gain switched DFB of 17.8 to 18.3, and for the DFB and integrated EAM a map strength variation of 2.3 to 2.4.

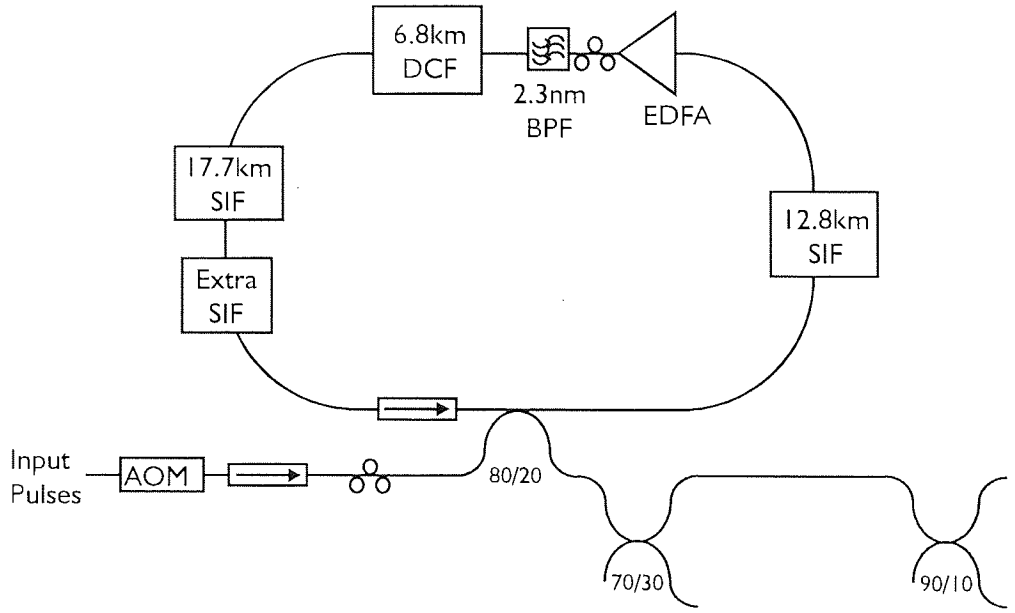

Figure 5-13 Diagram showing loop setup similar to the last section. The second section of standard fibre is reduced to 17.7km. This allows the average dispersion to be varied from 0.3ps/nm km in the normal up to 0.5ps/nm km in the anomalous.

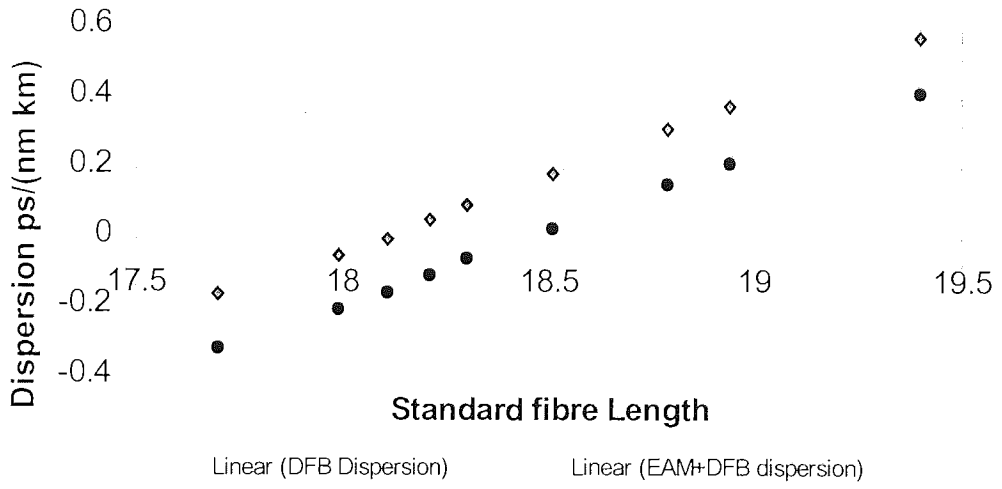

Figure 5-14 Average dispersion vs the length of the extra standard fibre length inserted into the loop shown in Figure 5-13. The dotted line shows the average dispersion for the DFB. The continuous line shows the average dispersion for the DFM and integrated EAM.

As with the experimental results taken with the fibre laser, transmission distance was optimised through the amplifier power and polarisation state at each wavelength. The results for these two devices are shown in Figure 5-15. These results compare well with those

measured when using the fibre laser, the maximum transmission distances fall off quicker in the normal dispersion regime than in the anomalous. The best performance for both devices was achieved with slightly anomalous dispersion with distances approaching 30,000km. This is greater than that for the fibre laser, Tuneable Laser and Electro-Absorption Modulator. The reason for the poor performance with Electro-Absorption modulator and fibre laser in the previous section is thought to be due to the quality of the pulse source.

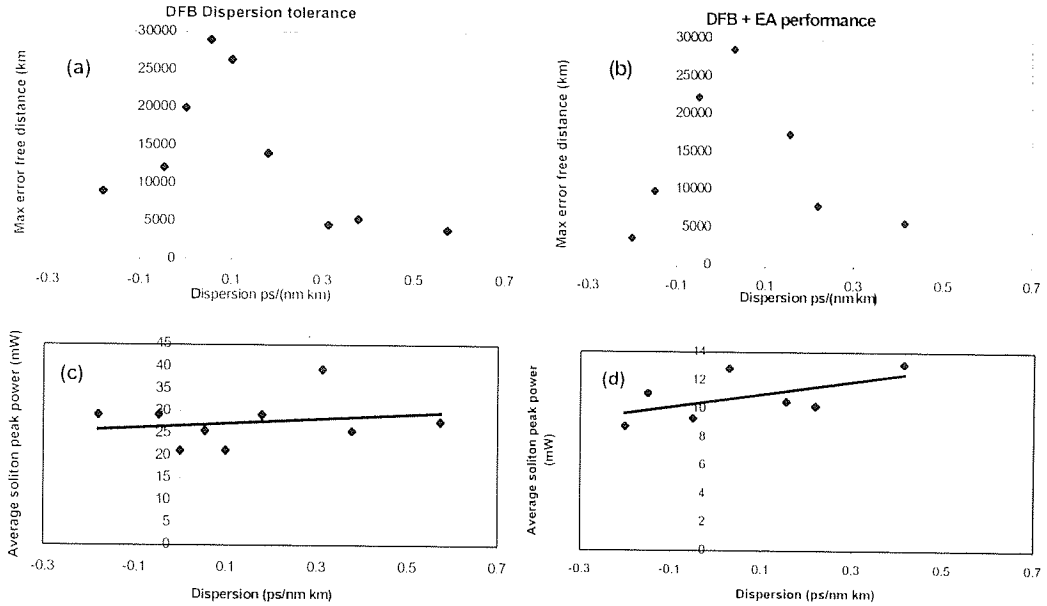

Figure 5-15 Maximum error free distances vs dispersion for the Gain switched DFB Graph (a) and Integrated DFB and EA modulator Graph (b). Graphs (c) and (d) show the corresponding average peak powers of the pulse of the pulses. Both graphs show stable finite powers extending into the normal dispersion.

Graph (a) shows a point in the normal with a dispersion of –0.18ps/nm km at 9000km. For an non-balanced pulse with this dispersion the pulse would have broadened to a FWHM 534ps.

$$Pulsewidth = \sqrt{\tau_{fwhm}^{\ 2} + \tau_{dispersion}^{\ 2}}$$

Where $\tau_{dispersion}$ is the pulse broadening due to the dispersion and is given as

$$\tau_{dispersion} = D_2 \cdot \Delta\lambda \cdot L = 0.18 \cdot 0.33 \cdot 9000 = 534 ps$$

This gives an expected pulse width of

$$Pulsewidth = \sqrt{10^2 + 534^2} = 534 ps$$

This pulse width is in excess of that that would be required to cause errors through intersymbol interference between neighbouring pulses, and it can therefore be concluded that a stable regime has been found.

Analysis of transmission of integrated DFB and EAM also shows propagation in the normal. However the map strength for this source (with a pulse width of 25ps when transform

limited) was 2.4. This is less than the map strength of 4 that simulations predict is required for stable propagation in the normal dispersion. Analysis of the results show that the expected broadening of the pulse is significantly less than that expected for the DFB. The particular point taken for this analysis was the result at a dispersion –0.15ps/nm km with a distance of over 10,000km The $\tau_{dispersion}$ for the pulse is given as

$$\tau_{dispersion} = D_2 \cdot \Delta\lambda \cdot L = 0.15 \cdot 0.11 \cdot 10000 = 165 ps$$

This gives a pulse expected pulse width of

$$Pulsewidth = \sqrt{25^2 + 165^2} = 167 ps$$

This result is less convincing than the previous results, the contribution of the spectral breathing (to give increased effective anomalous dispersion) and the possible error in measured dispersion may yield a shorter expected pulse width than that calculated above (possibly short enough so as not to cause intersymbol interference). For such broad pulses with narrow spectra it is necessary to transmit error free over greater distances to conclude that stable transmission in the normal dispersion has been achieved.

5.4 Conclusions

This experiment has demonstrated the transmission of stable pulses, with a finite power using a strong dispersion map around and below the dispersion zero. The optimum dispersion was slightly anomalous at around 0.02 to 0.05ps/nm km. The sources used in this experiment were not optimised with respect to the chirp and the launch point within the map. Despite this significant propagation in the normal dispersion was observed. The map used in our experiment was asymmetric containing mainly anomalous dispersion. Simulations have shown that such a map is more effective in supporting stable solitons further into normal dispersion, than a map containing mainly normal dispersion fibre[130]. The results clearly show that its possible transmit stable pulses over 10,000km in a dispersion range from -0.1ps/nm km to 0.2ps/nm km. With the dispersion slope used in this experiment this dispersion range corresponds to around 10nm. With greater dispersion slope compensation this range could easily be extended across the erbium bandwidth. The pattern used in this system only gives an indication of the transmission limitations due to Gordon Haus jitter and noise, and was chosen such that pulses were separated by at least 200ps. This was so as to avoid the soliton-soliton interaction effect, which is greatly increased in a strong dispersion managed system. The next chapter demonstrates these increased interactions between strong dispersion managed solitons, and a technique for reducing them by suitable optimisation of the position of the amplifier within the map.

Chapter 6 Soliton-soliton interactions in a dispersion managed system

6.1 Introduction

The main advantage of dispersion management is the enhanced pulse power resulting from the pulse breathing which occurs within the dispersion map. The enhanced power extends the maximum transmission distances beyond the Gordon-Haus jitter limit of the uniform system. This is due to the greater signal to noise (amplifier spontaneous emission (ASE)) ratio at the output of the amplifiers. The dispersion management also relaxes the constraints of the dispersion-power relationship present in a uniform system, allowing transmission closer to or at the dispersion zero, which also reduces Gordon Haus jitter. Research has shown that for strong dispersion maps propagation into the normal dispersion regime may also be achieved as was discussed in Chapter 5. The chapter discussed and demonstrated both of these benefits with enhanced propagation powers, propagation at zero dispersion and into the normal dispersion regimes. Transmission beyond the Gordon Haus limit of a uniform system was also achieved. However little attention was paid to the limitations of soliton-soliton interactions. The focus of this chapter is the problem of soliton-soliton interactions, and how they effect transmission in a strong dispersion managed system.

Soliton-soliton interactions are a non-linear interaction effect that results from the small but finite energy present in the tails of the soliton. The effect of the interaction is dependent on several factors such as relative pulse amplitude and pulse phase and most notably the mark to space ratio. The effect of the super positioning of the tails from neighbouring pulses results in a small wavelength shift which causes the soliton to move from its temporal position. For the classical case of two solitons propagating with the same phase and amplitude there will be an attraction force which will pull the pulses together such that they will eventually collapse. This effect is not detrimental to the system, provided the entire system length is less than half the soliton collapse distance. For a uniform system the collapse distance for two solitons

propagating in a loss-less medium is given by Equation 6-1, where Z_C is the collapse distance, Z_0 is the soliton period, T_R is the initial pulse separation and τ_0 is related to the Full Width Half Maximum (FWHM) pulse width by Equation 2-58. This equation relates the pulse separation and pulse width (Mark to space ratio) to the collapse distance. Increasing the separation or decreasing the pulse width will extend the collapse distance (i.e. the collapse distance is extended when using a larger mark to space ratio). The problem is largely overcome by using a mark to space ratio of greater than 1:5.

$$Z_c = \frac{Z_0}{2}\exp\left(\frac{T_R}{2\tau_0}\right)$$

Equation 6-1

In dispersion managed systems, soliton-soliton interactions behave differently, this is due to the pulse breathing that occurs within the dispersion map. Simulations have shown that for weak dispersion managed systems this interaction effect is actually reduced[98]. The small amount of breathing which occurs within the map causes a de-phasing between neighbouring pulse tails and therefore a reduction in the interaction effect. In strong dispersion managed systems however a large amount of pulse breathing takes place, to such an extent that there is considerable overlap between neighbouring pulses. It is this overlapping that causes an increase in interaction between pulses[131]. The interaction effect increases further with the strength of the map as this causes greater breathing. Figure 6-1 shows simulation results showing how the collision length varies with map strength. The pulses used had FWHM of 20ps and were separated by 100ps, they were launched into a map consisting of normal and anomalous sections of fibre, each of length 100km. The results show that the interaction length increases with map strength up to a strength of 1.5, but beyond this point the interaction length decreases such that it will eventually fall below that for the uniform system of 64Mm.

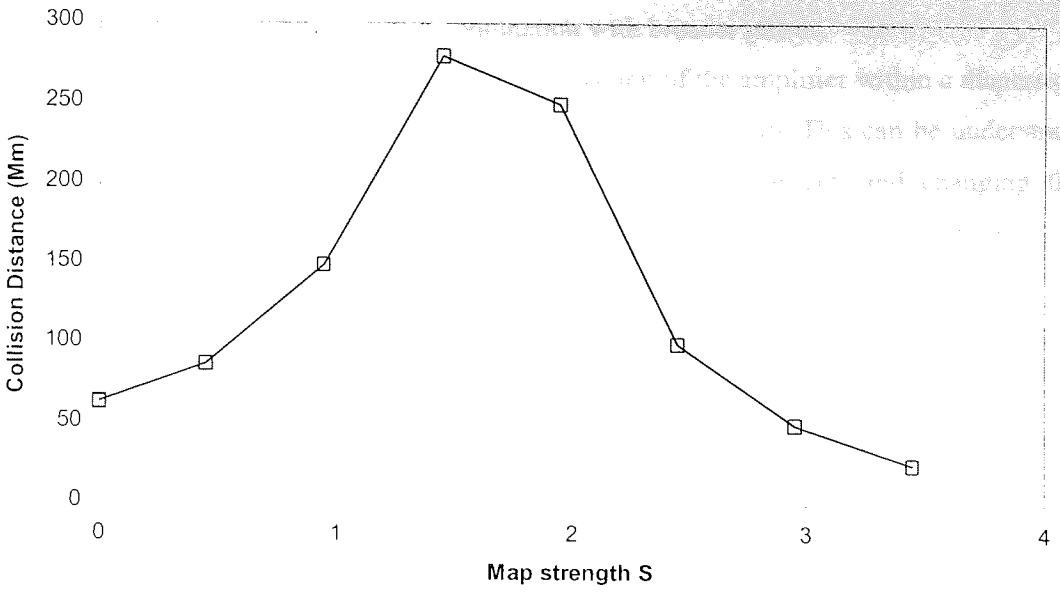

Figure 6-1 Map strength against collision distance due to soliton interactions. These results were taken for a two step map consisting of anomalous and normal sections of 100km. The pulse width of the pulses used was 20ps. The strength of the map was increased by increase the dispersion of the two section of fibre[98].

As with the previous chapter this experiment aims to demonstrate the feasibility of transmitting 10Gbit/s over standard fibre. The use of standard fibre for operation in the 1.55μm window for a dispersion managed systems or in the upgrade of currently installed systems, will bring about large map depths. Therefore these soliton-soliton interactions are an important factor for consideration. In order to extend transmission distances over standard fibre this problem needs to be addressed and a method of reducing the interactions investigated. The dispersion map used in this chapter was similar to that used in chapter 5, with the map strength such that soliton-soliton interactions have become the limiting factor in error free transmission. The experiment will demonstrate these increased soliton-soliton interactions in a strong dispersion managed system, while also showing a technique for reducing them through amplifier placement within the map.

6.1.1 Reducing soliton-soliton interactions

While in a uniform system the soliton-soliton interactions can be reduced by using a shorter pulse width (which will increase the mark to space ratio) this does not hold true for a dispersion managed system as a shorter pulse width would result in greater map strength. This in turn would cause greater breathing within the map and thus greater interactions between pulses. The alternative is to reduce the map strength by using broader transform limited pulses, which would have a narrower spectrum and therefore be subject to less pulse

breathing within the map. However in this chapter we present another technique of reducing the interactions, which could be used in conjunction with broader pulses.

Numerical simulations have shown that the position of the amplifier within a dispersion map has a significant effect on the soliton-soliton interaction length. This can be understood from the fact that soliton-soliton interactions are a non-linear effect, and changing the amplifier position within the map, changes where the majority of non-linear interactions takes place. The amplifier position can be optimised such that the pulse power dynamics within the map give reduced non-linearity along the sections of large pulse overlap. Recent simulations have shown that for a two-step symmetrical dispersion map the optimum positions for the amplifier lie near the mid-point of either section of fibre[135]. In this experiment the dispersion map contains predominately standard fibre compensated for by high negative dispersion compensating fibre (DCF), and thus giving an asymmetric map. The pulse breathing dynamics within these asymmetric maps are different from those of symmetric maps, this will have an effect on the optimum amplifier position. Some simulations were carried out to investigate these interactions with amplifier position within such an asymmetric map[133]. These were carried out using the variational method. This analysis technique differs from practical systems in that the launched pulses are perfectly matched in power and chirp to the dispersion map, this ensures that the pulses do not radiate dispersive waves. In a practical system this ideal condition is difficult to achieve.

The map used consisted of 6.8km of dispersion compensating fibre (-76ps/nm km) followed by 31km of standard fibre (16ps/nm km) giving a total length of 37.8km. The pulses used had a FWHM of 20ps, giving a map strength of 3. The amplifiers used in this system were noiseless, thus removing the limitations of SNR and Gordon Haus jitter. The remaining limitation on maximum transmission distance was soliton-soliton interactions, which were recorded against amplifier position within the map, these results are shown in shown in Figure 6-2.

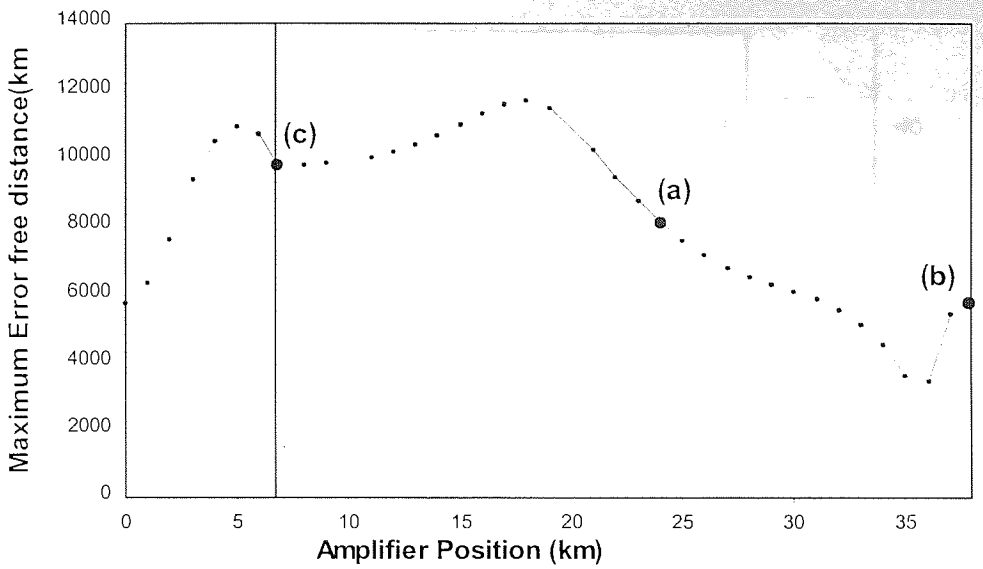

Figure 6-2 Maximum transmission distance with amplifier position for a 10GBit/s system[133]. The first 6.8km of the graph correspond to dispersion compensating fibre with a dispersion of –76ps/nm km. The remaining 31km corresponds to the standard fibre with a dispersion of 16ps/nm km. The three points labelled (a) at 8200km, (b) at 5800km and (c) at 9,800km correspond to amplifier position used in the experiment.

The first 6.8km of the graph represent the amplifier positions within the dispersion compensating fibre, the remaining 31km represent the standard fibre positions. The results indicate that the position of the amplifier within the map plays an important part in transmission. While distances of 12,000km can be achieved with the amplifier in the optimum position, placing the amplifier at the worst position reduces the maximum distances to less than 4,000km. As with the simulations for the symmetric map the results indicate that the optimum amplifier positions within the map correlates closely with the local pulse width. The optimum positions lie close to the transform limited points. These are the positions in which higher powers are more acceptable, since this is where there is the least pulse overlap. In this chapter the position of the amplifier and its effect on maximum transmission distance within a recirculating loop has been investigated. It will be confirmed that the soliton-soliton interactions are indeed greater in strong dispersion managed systems and that they are also strongly dependent on the amplifier position within the map.

6.2 The Transmission loop configuration

The dispersion map used in the experiment was 38.1km long and was similar to the map used for the simulations shown in Figure 6-2. The map contained 31.3km of standard fibre with a dispersion of 16.5ps/(nm km) which was compensated for by 6.8km of dispersion compensating fibre (DCF) with a dispersion of -76ps/(nm km). This dispersion map is illustrated in Figure 6-3.

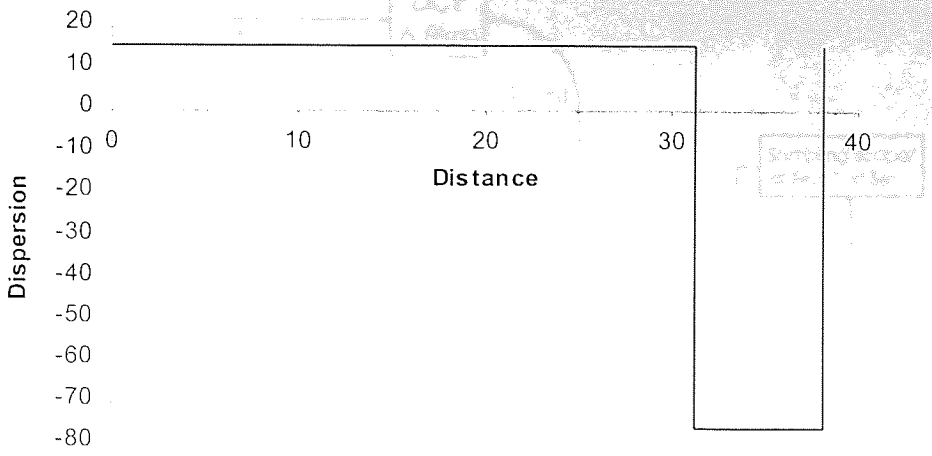

Figure 6-3 Dispersion map with 31.3km of standard fibre 16ps/(nm km) and 6.8km of dispersion compensating fibre -76ps/(nm km)

The map was put together in a single span re-circulating loop as shown in the schematic in Figure 6-4. The standard fibre was split into two sections of 13.6km and 17.7km. This enabled the 80/20 launch/detector coupler to be placed close to the transform limited point within the map, and provided an optimum launch point for transform limited pulses. The coupler was orientated such that only 20% of the input power into the coupler was launched into the loop, but this in turn means that only 20% of the power in the loop was lossed through the coupler each recirculation. This corresponds to an extra loss of 1dB within the loop. The output power from the loop was split by a 70/30 coupler, with the 30% output providing a power monitor for the signal in the loop. The remaining 70% output was split again by a 90/10 coupler, the 10% tap was used to monitor the 10GHz frequency component in the signal during transmission with the electrical spectrum analyser as explained in section 4.7.4. The 90% output was amplified through an Erbium Doped Fibre Amplifier (EDFA) before being split by another 90/10 coupler. The 10% provided the signal for the clock recovery and the remaining 90% was fed directly into the lightwave converter of the reciever. The clock recovery consisted of a 10GHz photodiode and phase lock loop.

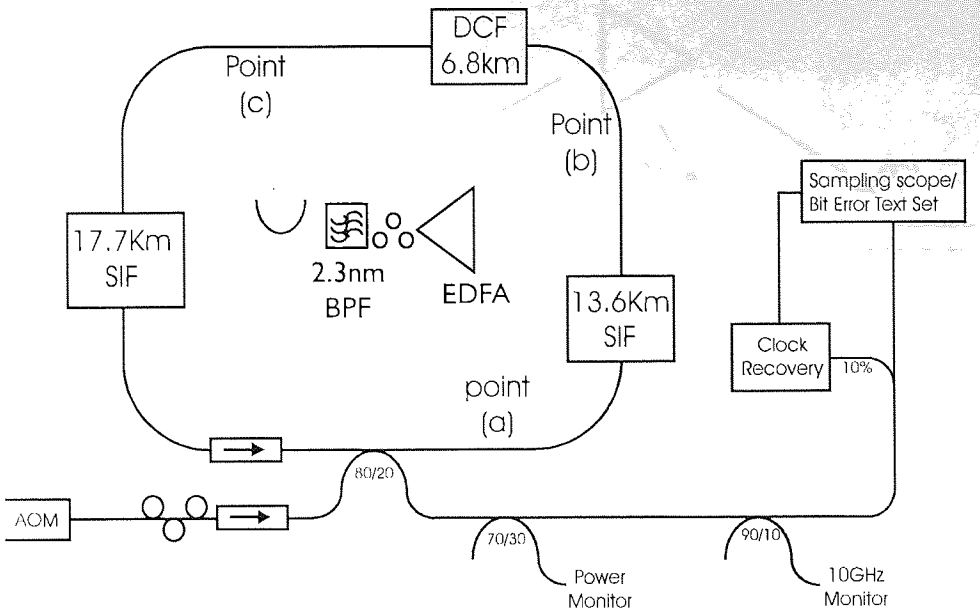

Figure 6-4 The transmission experiment set up, with 31.3km of standard fibre compensated for by 6.8km of dispersion compensation fibre. The three different amplifier positions within the loop are Label (a) Midway through the amplifier (b) Before the DCF and (c) after the DCF. Tha amplifier insert is shown within the rectangle. Included with the amplifier is a Band Pass filter to filter out the ASE, and a polarisation controller to control the polarisation in the loop.

The loss of the entire loop was measured to be 14.9dB. The standard fibre had a total loss of 6.5dB and the loss of the dispersion compensating fibre (DCF) including excess splice losses was 4.2dB. The entire loss of the loop was compensated for by the EDFA, which had a noise figure of about 4dB when in saturation. For the experiment the amplifier was located at three different points within the map; (a) 17.7km into the standard fibre, (b) before the DCF and (c) after the DCF. These points are illustrated in the loop diagram in Figure 6-4. The DCF was a sealed module and could not be accessed, so this meant that an amplifier position midway through the DCF was not practical. These three positions within the map are illustrated more clearly in Figure 6-5. A Fabry Perot band pass filter was placed immediately after the amplifier. This had a 3dB bandwidth of 2.3nm and an insertion loss of 2.2dB. Its purpose was to reduce the ASE generated by the loop amplifier. A 5% coupler was placed after the filter giving an extra loss of 0.3dB, this gave access to another monitoring point within the loop. The remaining 0.7dB of loss was accounted for by the isolator before the coupler.

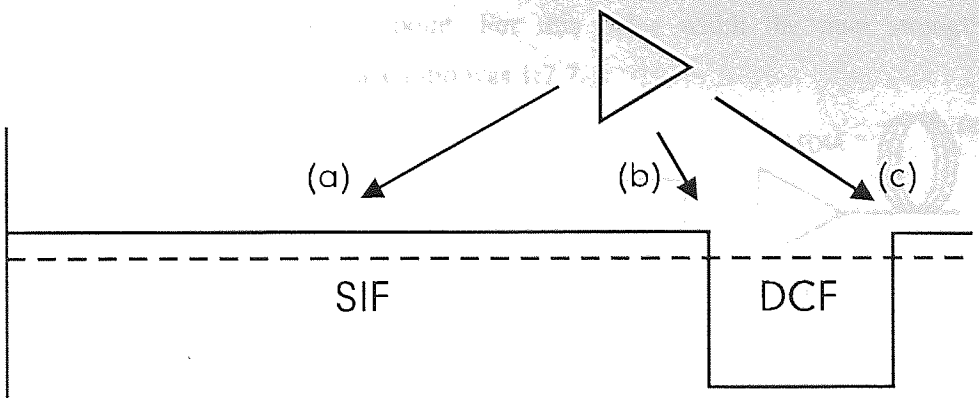

Figure 6-5 A schematic showing the three amplifier positions, (a) midway through the SIF, (b) before DCF, (c) immediately after DCF.

The dispersion characteristics were measured using the technique discussed in chapter 4 and are shown in Figure 6-6. The dispersion zero was found to be at 1549.8nm, and the dispersion slope found to be 0.03ps/(nm^2 km).

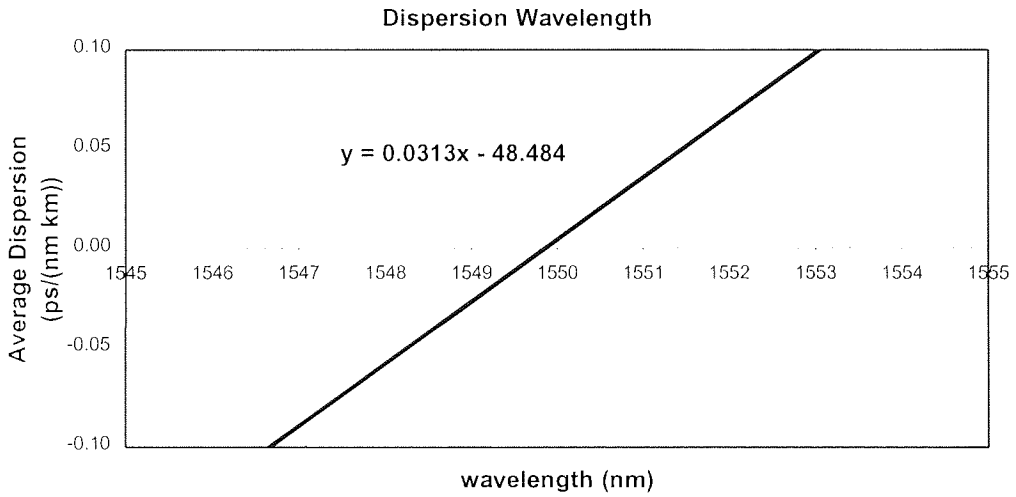

Figure 6-6 Dispersion vs wavelength measurement for fibre in the loop. The Dispersion zero located at 1549.8nm and the dispersion slope ~0.03ps/(nm km).

The Tuneable Laser and Electro Absorption Modulator (EAM) provided the pulse source. This source is both stable and tuneable in wavelength. The Tuneable laser wavelength was set to 1551nm and the output was fed directly into the Electro-absorption modulator (EAM). At this wavelength the average dispersion of the loop was 0.04ps/nm km. The EAM was driven with an RF signal at 10GHz, producing pulses with a FWHM of 20ps. These were then amplified before a 10Gbit/s 2^{31}-1 pseudo random bit stream (PRBS) pattern was encoded on to the them using a $LiNbO_3$ Mach-Zehnder modulator. The pulses were then amplified again before being compressed using dispersion compensating fibre with a total dispersion of -72ps/nm. The pulses compressed to a full width half maximum of 13ps, giving a time-bandwidth product of 0.37, which shows that the source was transform-limited and ideal for

launching at the transform limited point. For this pulse width the map strength was approximately 8, and the mark to space ratio was 1:7.7.

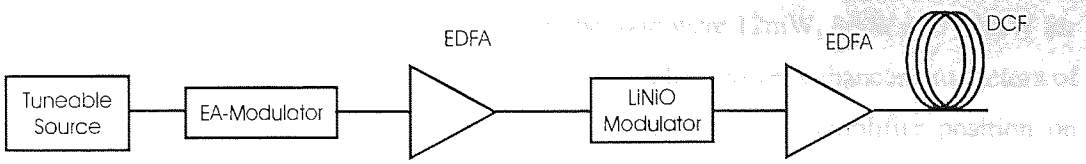

Figure 6-7 Tuneable Laser and EA Modulator combined to give 13ps pulse source

The pulses were gated into the loop via the Acousto Optic Modulator (AOM). The bit error test set was gated such that error rate measurements were taken once pattern synchronisation had been achieved at the appropriate recirculation of the loop. The propagating signal in the loop was terminated by terminating the amplifier within the loop, after which the amplifier is re-pumped and propagation repeated. For each of the three amplifier positions, the input, and loop polarisation controllers and the loop amplifier pump power were optimised using the 10% output to the electrical spectrum analyser and the Bit Error rate Test Set as performance monitors. Once the maximum distances with bit error rates of less than 10^{-9} had been achieved, bit error rates vs distance were taken.

6.3 The transmission results

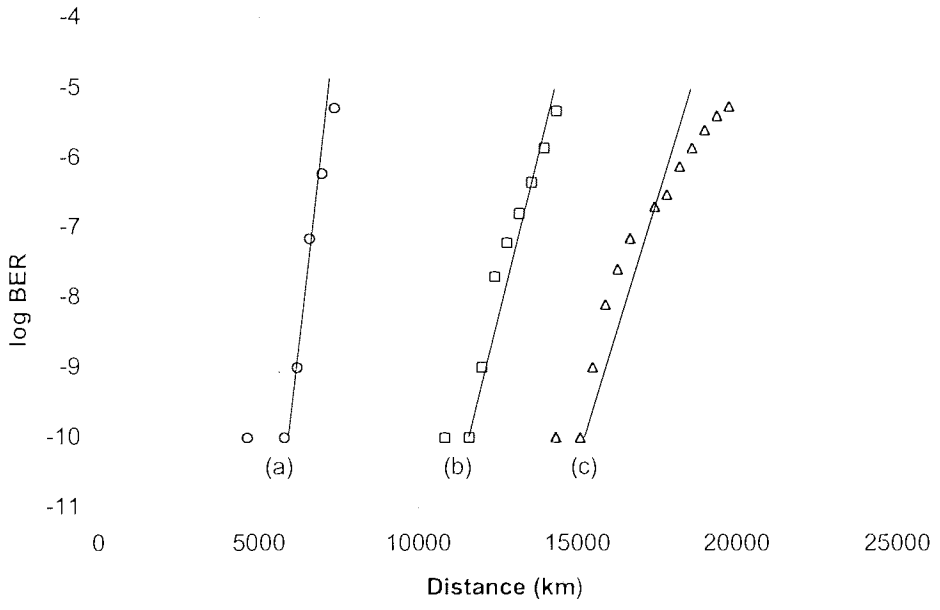

Figure 6-8 Error rates vs distance for three configurations labelled in Figure 6-5. (a) maximum distance of 6,200km, (b) maximum distance of 12,000km and (c) maximum distance of 16,500km

Figure 6-8 shows the error rates vs distance for each of the three positions. For position (a) with the amplifier placed 17.7km into the standard fibre, error free transmission could only be achieved as far as 6,200km. In positions (b) and particulary (c) where the

amplifier is placed at the boundary's between the SIF and DCF. Transmission faired significantly better with distances of 12,000km and 16,500km respectively. The optimum average peak pulse powers for transmission within the loop were 12mW, 8mW and 15mW for positions (a), (b) and (c) respectively. This gives corresponding power enhancement factors of 9, 6 and 12. These results clearly indicate a strong dependence of amplifier position on maximum error free transmssion distance. The optimum of the three amplifier positions was position (c) immediately after the DCF, this is a suitable position as regards to the installation of new and the upgrade of old links, as this allows the amplifier to be inserted at the boundary between fibres.

These results do not comply well with the simulation results shown in Figure 6-2, which shows the maximum transmission distances for similar positions (a), (b) and (c) are at 8,200km, 5,800 and 9,800km respectively. While both simulation and experimental results agree that positioning the amplifier immediately after the DCF (position (c)) would achieve the greater of the error free distances, the simulations also indicate that placing the amplifier 17.7km into the standard fibre (position (a)) should yield better performance than the amplifier position before the DCF (position (b)), this contradicts the results acquired experimentally where in fact position (a) only reached half the distance of position (b). The reason for this is probably down to a combination of several factors. Firstly the map strength in the loop experiment was more than twice that of the simulations. Also a variational method was used to perform the simulations, which ensures that pulses are launched with ideal power and ideal chirp. In the experiment the launched chirp and pulse power were always of the same from amplifier position to amplifier position. The fibre losses and the non-linearity (effective core area) were considered equal for both fibres in the simulations, where as in the experiment the DCF had a smaller core and thus higher non-linearity and higher loss than the standard fibre. These differences may have contributed to a change in shape of the graph shown in Figure 6-2. The greater non-linearity in the DCF may result in a sharper tail off of maximum transmission distance when the position of the amplifier moves beyond the optimum position (Mid-point) of the standard fibre. This could result in position (a) performing worse than position (b) as was found experimentally. This also suggests that there may be a more optimum position at an earlier point within the standard fibre.

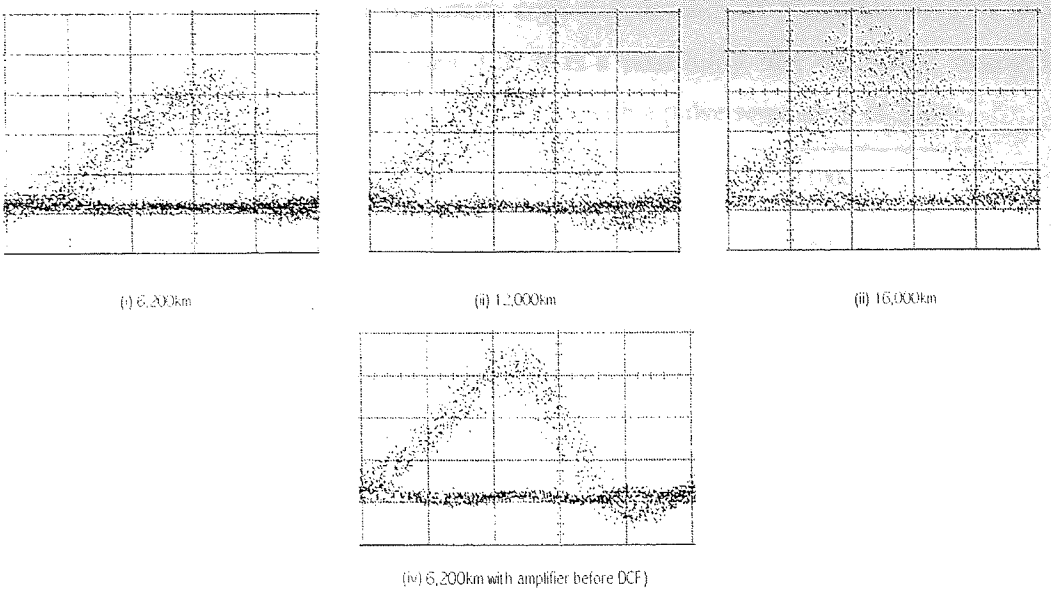

Figure 6-9 Four eyes for a 2^{31}-1 PRBS, three of which are shown at the maximum error free distances for the three configurations that were used for the results in Figure 6-8. (i) within the SF taken at 6,200km. (ii) before the DCF, taken at 12,000km and (iii) after the DCF taken at 16,000km. The bottom eye, (iv) was taken with the amplifier placed before the DCF at 6,200km.

In Figure 6-9 there are four eye diagrams taken for a 2^{31}-1 PRBS pattern. The first three show transmission up to the maximum error free distance for all three configurations, with (i), (ii) and (iii) corresponding to configurations (a), (b) and (c). An important aspect of the eyes to be noted is that there is relatively no noise in the zeros. All the errors appear to result from pulse jitter, which is resulting from either amplitude noise or timing jitter. The waveform shown in Figure 6-9 (i) is of particular interest in that a much greater jitter appears on the trailing edge of the pulse than on the leading edge. This is observed as the eye closes from the trailing edge of the pulse. The waveform in (iv) taken at the same distance as (i) but this time using configuration (b) shows no such extensive timing jitters. This indicates that moving the amplifier has reduced this effect.

To further confirm that this amplifier dependence was due to the interactions some further error rate measurements were taken using two simple 6-bit data patterns (i) 010100 and (ii) 011000. This will allow the comparison of two different pulse separations. As with the 2^{31}-1 PRBS pattern transmission was optimised to achieve maximum error free distance with each of the three amplifier positions. These results are shown in the table in Figure 6-10. For position (a) using pattern (ii) the maximum achievable error free distance was 8,100km which is much shorter than the 20,000km achieved using configurations (b) and (c). Using pattern (i) all the configurations had error free distances of or in excess of 30,000km. This pattern dependency is a good indication that the limitation is down to soliton-soliton interactions. The fact that error free distances using (b) and (c) are extended with pattern (i) suggests that while the interactions are reduced in configurations (a) and (b), they are still the

limiting factor. For pattern (i) the maximum error free distance of 30,000km in (a) is shorter than the 35,000km achieved by (b) and (c). It is a possibility that the strong interactions present in this set-up are still having an effect even with a pulse separation of 200ps.

Configuration	(i) 010100	(ii) 011000
(a)	30,000km	8100km
(b)	35,000km	20,000km
(c)	35,000km	20,000km

Figure 6-10 A Table showing maximum distances of error free transmission. Using two different 6-bit patterns. Three different amplifier positions were used. (a) midway through the standard fibre, (b) before the DCF, and (c) after the DCF

To investigate the effects taking place during transmission and further confirm that the problem is down to soliton-soliton interactions, the sampling 'scope was used to observe the waveform characteristics during transmission. By using a simple short pattern it is possible to set the trigger threshold on the sampling 'scope to a fixed point within the pattern. This allows monitoring of the waveforms and any changes that occurred during propagation. The loop set-up used was the same as that for configuration (b), with the amplifier immediately before the DCF. The 5% tap output after the amplifier and filter provided a monitor point at the maximum chirp point before the DCF. The pattern used was 01100101, this pattern includes two neighbouring pulse and two pulses separated by a zero for comparative purposes. The resulting waveforms are shown in Figure 6-11.

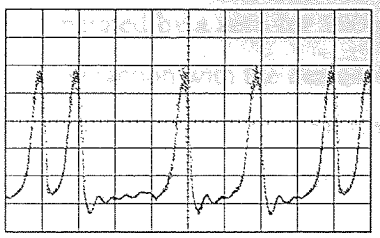

(i) Back to Back waveform

Transform limited point

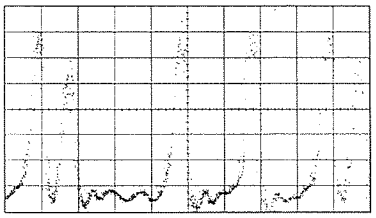

(ii) 4000km

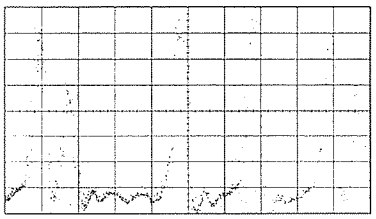

(iv) 8000km

Boundary point (before DCF)

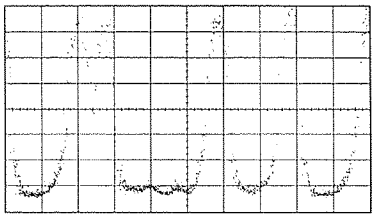

(iii) 4000km

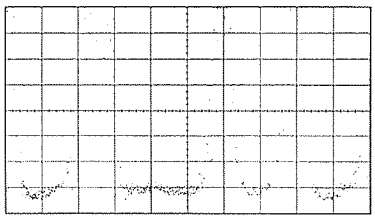

(v) 8000km

Figure 6-11 Five sampled waveforms taken with configuration (ii) to show the interaction effect. Waveform (i) shows the waveform before transmission. The subsequent waveforms, (ii) and (iii) show transmission after 4000km at the transform-limited point and after the DCF receptively. (iv) and (v) are the correspond waveforms at 8000km.

Waveform (i) corresponds to the back to back output and provides a reference for the initial waveform shape, (ii) and (iii) show transmission after 4000km at the transform limited point and the output of the amplifier (before the DCF) respectively, (iv) and (v) are the corresponding waveforms taken after 8000km. It can clearly be observed that through transmission the pattern is subject to some distortion, which has been imposed on the two pulses placed in the neighbouring bit slots shown in the left of the traces. The distortion manifests itself in a change in amplitude between the pulses. The leading pulse maintains its original amplitude while for the trailing pulse the amplitude decreases. Waveform (ii) shows the drop in amplitude after 4000km, (iv) taken at 8000km shows that the waveform deteriorates further with distance. The reason for this distortion, and not the standard soliton-soliton interaction collapse is not clear but it is thought to be due to pulse overlap at the boundaries, which is observed in (iii) and (v). After 4000km, the two neighbouring pulses shown in (iii) have significant pulse overlap at the boundary between the DCF and standard fibre. At 8000km this is much worse with the pulse overlapping to the extent that it becomes difficult to differentiate between the two pulses. The fact that no such distortions can be

observed for the pulses that are separated by a zero (or 200ps) supports the theory that these distortions can only be due to the interaction with the nearest neighbouring pulses.

Using configuration (a), which has the poorest transmission performance with a 2^{31}-1 PRBS pattern, a further comparison of the interaction between two neighbouring solitons was carried out using two different separation distances. This time the patterns used were both 14-bits long and consisted of only two pulses. The first pattern used a pulse separation of 100ps (in neighbouring bit slots). The second pattern used a pulse separated of 200ps (separated by a zero). The 14-bit length of the pattern ensures that no other pulses are having any significant effect. These patterns were propagated in the loop and the polarisation controllers were optimised to achieve maximum error free transmission distance. Three waveform measurements were taken at three different distances, 2300km, 4200km & 7300km and are shown in Figure 6-12. The same effect that was present in the previous pattern can be observed, only this time it is more pronounced. The waveforms on the right show the progressive change in pulse amplitude of the trailing pulse using 100ps separation over distance. After 7300km the trailing pulse can be seen to have almost totally collapsed. The pulse waveforms for the pulses separated by 200ps show no signs of such distortions. The fall in amplitude of the trailing pulse explains the closure of the eye taking place from the trailing edge of the pulse shown in Figure 6-9 (a).

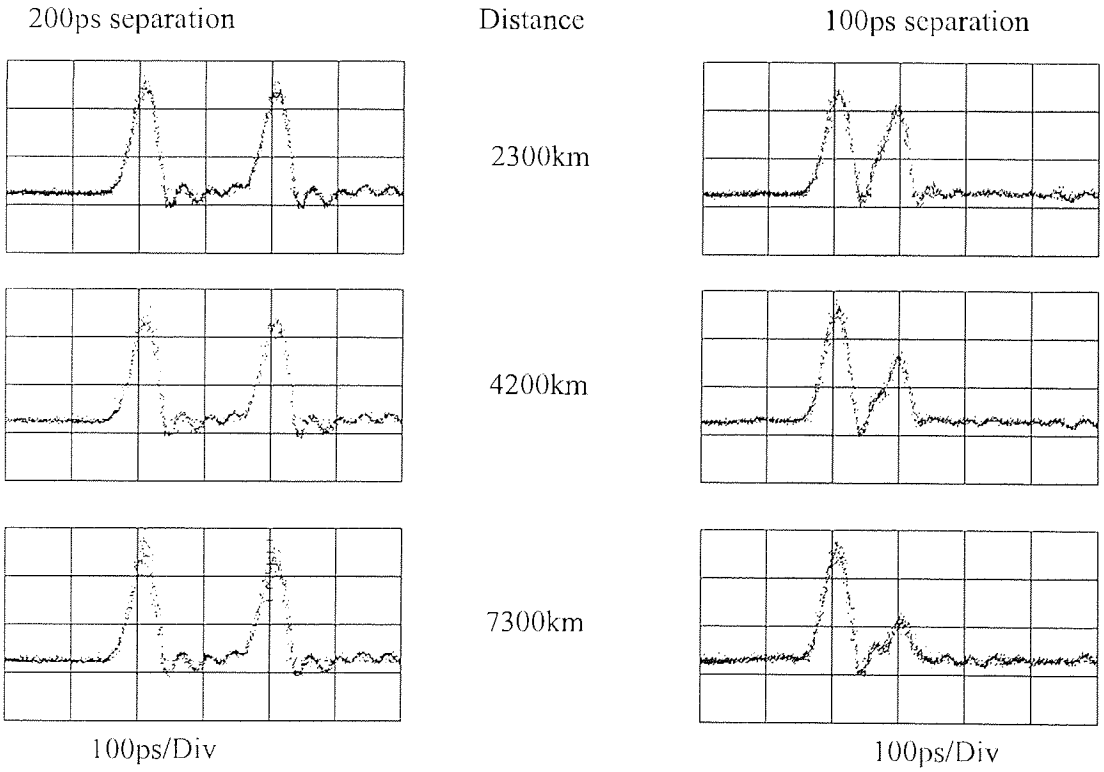

Figure 6-12 Waveforms at distances of 2,300km, 4,200km & 7,300km. The two patterns used were 14-bit in length consisting of 2 pulses. On the left the pulses have a separation of 200ps, on the right the pulse separation is 100ps.

In chapter 5, at the same average dispersion the average peak pulse power within the loop was 15mW. In this chapter the peak pulse power for all three cases were calculated to be 12mW, 8mW and 15mW for (a) (b) and (c). In the case of (a) and (b) the power is slightly lower, this is probably due to the need to reduce the non-linearity to minimise the soliton-soltion interactions. Figure 6-13 shows three sets of waveforms showing the transmission of two pulses seperated by 100ps over 2000km using three different power peak powers. The amplifier configuration used was the same as (b). Waveforms (a), (c) and (e) using peak pulse power of 15mV, 24mV and 40mV were taken at the transform limited point. (b), (d) and (f) show the respective waveform taken at the output of the amplifier which is at the boundary before the DCF. For waveforms (a) and (b) with peak powers of 15mW, (a) shows only a small distortion of the waveform at the transform limited point, and (b) shows only a small amount of pulse overlap. Comparing these with (c) and (d) the corresponding traces with a peak power of 24mW, it can be observed that there is a greater distortion and pulse overlap at higher powers. This effect is more pronounced when operating at pulse peak powers of 40mW. These results are evidence that this distortion is non-linear dependent.

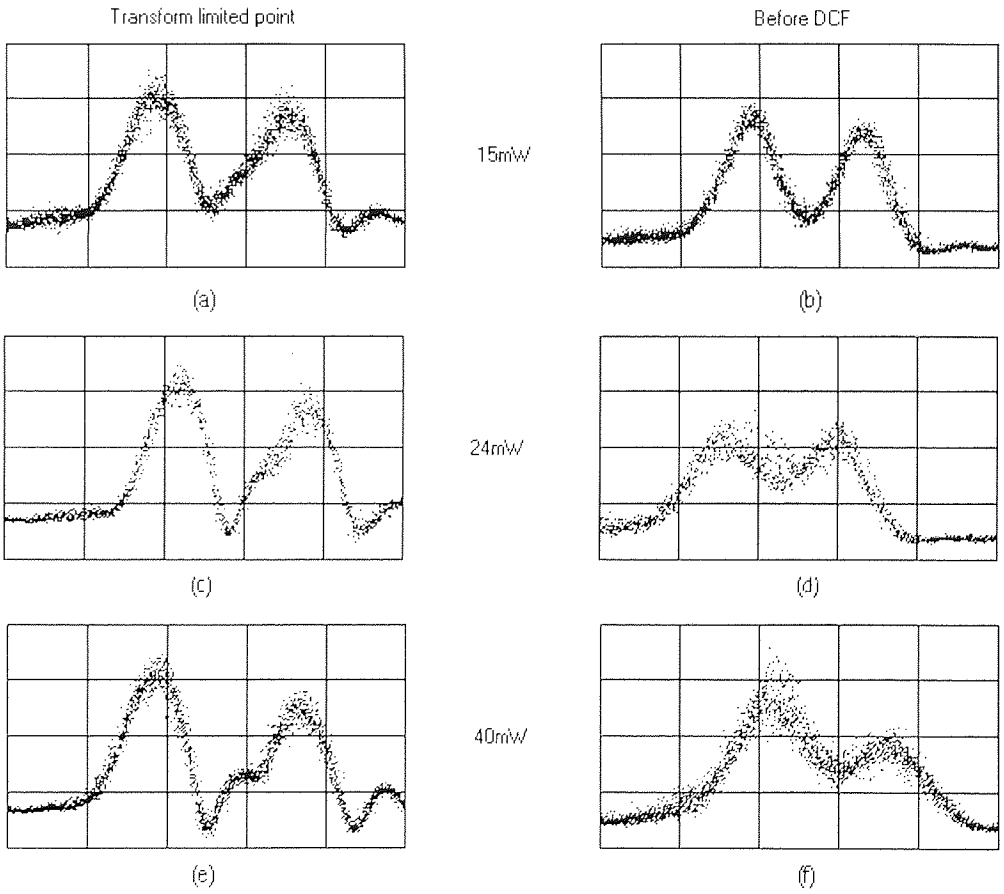

Figure 6-13 Three waveform patterns taken after 2000km of propagation using configuration (b). The three waveforms correspond to three different peak pulse powers (Powers calculated at the output from the amplifier). (a) and (b) correspond to a peak pulse power of 15mV, taken at the transform limited point and before the DCF respectively. (c) and (d) are the two respective points with a peak pulse power of 24mV. The remaining graphs (e) and (f) correspond to a peak power of 40mV.

6.4 Conclusions

In this chapter it has been shown that soliton-soliton interactions are the limiting factor in error free transmission when using strong dispersion maps. This effect is significantly increased over that of a uniform system. The effect manifests itself in a pulse amplitude distortion, which increases with distance, eventually causing the eye to close. It has also been shown that the position of the amplifier within the dispersion map plays a significant role in reducing these effects. Locating the amplifier in the wrong position within the map can reduce the maximum transmission distance significantly. The optimum of the tested positions in the experiment lay immediately after the DCF. This is suitable for both the upgrade of currently installed, and the installation of new systems, since the DCF and EDFA can be inserted at the same points within the transmission line. However this position may not be the actual optimum point within the map. The simulation results indicate that the optimum positions lie half way through the normal and anomalous fibre sections where the pulse width is minimum. The poor performance achieved experimentally when the amplifier was placed within the standard fibre can be explained by considering several factors. Firstly the amplifier position in the experiment was not half way but two thirds of the way into the standard fibre. The simulations indicate that there is a fairly rapid fall off in transmission distance when the amplifier position is moved beyond the half way point of the section of standard fibre. This fall off may be sharper when factors such as the extra non-linearity and loss of the DCF are taken into account in the simulations. The greater map strength may also play a part in the shape of this graph. More amplifier positions within the map need to be investigated in order to determine the optimum position, particularly at points less than and up to half way through the standard fibre. Investigating the optimum point within the DCF is also of particular interest since the option to insert the amplifier and DCF at the same point is more desirable and practical for the installation of a transmission system. It has also been shown in the experiment that these interactions are power dependent and can be reduced by operating with lower pulse powers as would be expected for a non-linear effect. It must also be noted that the experiment has demonstrated transmission of a 10Gbit/s 2^{31}-1 PRBS data pattern over a maximum distance of 16,500km, using 80% standard fibre. This is the furthest distance reported over standard fibre using any modulation format. This distance is well in excess of the distance required for any trans-oceanic transmission system, but such transmission distances do indicate that the system is robust, and that it is feasible to use either greater amplifier spans or even move up to higher data rates. With the maximum distances still falling short of both the Gordon Haus jitter and the SNR limit, the limiting factor in this system still appears to be soliton-soliton interactions. For a more optimised system it may be a benefit to use broader pulses, which would weaken the map and thus reduces the

interactions. Doing this in conjunction with optimising the amplifier position within the map should yield a more optimum transmission system. The other benefit of this system is that the large dispersions present in the map lends the system to wavelength division multiplexing, since high local dispersions have been known to reduce the effects of Four Wave Mixing and residual frequency shifts that arise from power imbalanced collisions.

Chapter 7

Non-linear polarisation rotation

7.1 Introduction

Saturable absorbers have long been utilised in passively mode-locked lasers to generate ultra short pulses[134][135][136]. The basic principle of operation of a saturable absorber is to provide higher absorption for low power signals and lower absorption for higher power signals, thereby discriminating the low power signals that pass through the device. By placing these devices periodically along the transmission line this low power discrimination can be utilised to reduce the build up of the base line noise in the zero slots as a result of the Amplifier Spontaneous Emission (ASE) generated by the amplifiers. This can increase error free transmission distances significantly[137][138]. Dispersive waves released by imperfectly launched pulses, (which can increase the interaction between pulses[139][140]) can also be suppressed using these devices[141]. The pulse shaping provided by these devices is as a result of the higher absorption imposed on the lower intensities of the trailing and leading edges. For the use of saturable absorbers in a soliton transmission system there are two important characteristics that must be considered, these are the switching power and the switching time. The switching power is the input power required to drive the saturable absorber into the low loss regime. This switching power must be less than the peak pulse powers propagating in the fibre. The peak pulse power at the output stage of an amplifier in a transmission line is typically in the range of a few milliwatts. Therefore a suitable saturable absorber will have a switching power no greater than this. The switching time is the saturable absorbers response time to a change in input. For the generation of ultra short pulses the response time can be slightly different for leading and trailing edge of the pulses (rise and fall times). On the trailing edge of the pulse the response time, which is sometimes referred to as the recovery time must be short enough to at least follow the trailing edge of the pulse. On the leading edge however a slightly slower response will aid pulse narrowing, since it will suppress more of the leading edge of the pulse.

Currently switching speeds of quantum well saturable absorbers fall short of those required for 10-30ps pulses. This factor along with switching power required make these devices unsuitable for practical systems, research however is ongoing to improve the characteristic of these devices. For experimental purposes there are some alternative techniques for producing saturable absorption. An imbalanced non-linear optical loop mirror can be used, which gives a non-linear output response to the input power[142][143]. However these loop mirrors require either long length of fibre or high pulse powers to utilise the non-linear phase shifts required for switching. The method used in this chapter utilises a polarisation dependent loss element and the non-linear polarisation rotation characteristic of the transmission fibre to provide saturable absorption. This technique has previously been used to demonstrate long distance transmission of a 76MHz pulse stream[144]. Here this technique is used to achieve error free transmission of 10Gbit/s 2^{31}-1 PRBS pattern over 200,000km.

7.1.1 Non-linear polarisation rotation

Imperfections in the structure of optical fibre result in a deviation from the ideal cylindrical geometry, this leads to a variation of the propagation coefficient with polarisation state. The variation can be resolved into two orthogonal propagation modes of the fibre. Due to the different propagation velocities of these modes they are commonly referred to as the fast and slow axis. A signal launched into the fibre can be resolved into two components propagating in these two axes. The effect of Cross-Phase-Modulation (XPM) causes the two components to interact through a non-linear refractive index change that the two modes induce on each other. A given field **E** propagating in the fibre can be resolved into these two components, these are labelled $\mathbf{E}_x$ and $\mathbf{E}_y$ and are defined in equations 7-3 and 7-4 below.

$$E_x = E\cos(\theta)$$

Equation 7-1

$$E_y = E\sin(\theta)$$

Equation 7-2

Where θ is the angle of launch relative to the x axis.

The non-linear refractive index change resulting from these components is given in Equation 7-3 and Equation 7-4 below.

$$\Delta n_x = n_2\left(\left|E_x\right|^2 + \frac{2}{3}\left|E_y\right|^2\right)$$

Equation 7-3

$$\Delta n_y = n_2\left(\left|E_y\right|^2 + \frac{2}{3}\left|E_x\right|^2\right)$$

Equation 7-4

Where $\Delta\mathbf{n}_x$ and $\Delta\mathbf{n}_y$ are the respective refractive index changes in the fast and slow axis, and $\mathbf{n}_2$ is the coefficient of the refractive index. These non-linear refractive index changes which are generated by these components are in effect a non-linear birefringence. As mentioned in section 1.6 it can be shown that a birefringence can cause a polarisation rotation of the light through propagation[111]. Which in this case is referred to as non-linear polarisation rotation. The non-linear dependence of this birefringence results in the higher intensities of light undergoing a greater degree of polarisation rotation than the lower intensities giving an intensity dependent polarisation rotation of the soliton[145][146]. For a given fixed field strength $\mathbf{E}$ the rate of polarisation rotation is also dependent on fields $\mathbf{E}_x$ and $\mathbf{E}_y$ and can therefore be controlled by the angle at which the light is launched into the fibre. It is this intensity dependence of non-linear polarisation rotation that is used to discriminate lower intensities of a field.

7.1.2 Saturable absorption

The non-linear polarisation rotation leads to power dependent polarisation rotation where high powers have a greater degree of rotation than the lower powers. Placing a polarisation dependent element in the transmission line gives an intensity dependent output response[147]. A polarisation controller can be used to align the polarisation of the pulses in the fibre such that the higher power signals are aligned with the low loss axis of the Polarisation Dependent Loss (PDL) element. The low power noise has not undergone the same degree of rotation and is therefore not aligned with the low loss axis and is subject to a greater loss. Repeatedly subjecting the noise to this extra loss with transmission can not only prevent the build up, but also remove the presence of noise. As will be seen later in this chapter, the extra loss required for the noise in the high loss axis is only in the order of a couple of decibels. Placing these devices periodically along the transmission line can reduce the build up of baseline noise released from the amplifiers. Since the non-linear response time is in the order of Femto seconds, the response time of the saturable absorber can be considered near instantaneous for the pico second pulses used in this experiment. In this chapter periodic

saturable absorption is utilised to demonstrate error free propagation of data over very long distances while at the same time generating short pulses.

7.2 Long distance transmission with periodic saturable absorption

A Tuneable Laser (TL) and an Electro-Absorption Modulator (EAM) provided the pulse source for this experiment. The wavelength of the laser was set to 1542.4nm and the output fed directly into the EAM. The EAM was driven with a 10GHz RF signal. This modulates the CW light to give pulses with a FWHM of 20ps.

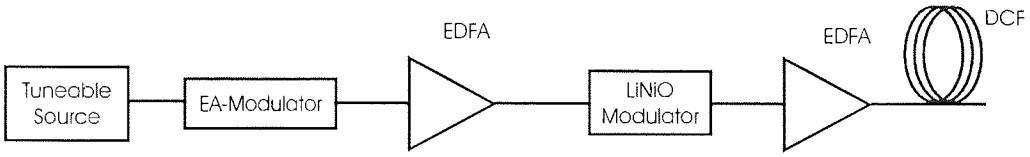

Figure 7-1 The tunable laser provides the light source for the EAM which modulates the light to generate pulses. The pulses are then amplified before data is encoded on to them with a $LiNbO_3$ modulator. The pulses are then amplified again before being compressed down to chirp free pulses with a FWHM of 13ps.

The pulses were amplified using an Erbium doped fibre amplifier (EDFA) before a 2^{31}-1 PRBS data pattern was encoded on to them using a 10GHz $LiNbO_3$ Mach-Zehnder modulator. The pulses were then amplified again before being linearly compressed with dispersion compensating fibre with a total compensation of –72ps/nm. This produces transform-limited pulses with a FWHM of 13ps and a spectral width of 0.25nm giving a time bandwidth product of 0.37. The configuration of the source is shown in Figure 7-1.

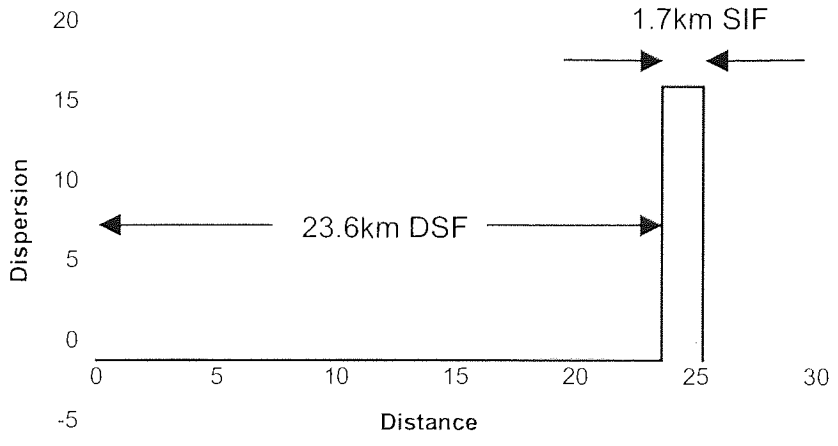

Figure 7-2 Dispersion map consisting of 23.6km of Dispersion shifted fibre with a dispersion of –1 ps/nm km followed by 1.7km of Standard fibre with a dispersion of 15.6ps/nm km).

The amplifier span of the loop in this experiment was relatively short compared with the experiments in Chapters 5 and 6 with a total length of 25.3km. The map used was

asymmetric, consisting of mostly normal dispersion fibre as illustrated in Figure 7-2. The normal dispersion section consisted of 23.6km of dispersion shifted fibre with a dispersion zero of 1557nm. At 1542.4nm (source wavelength) this had a dispersion of –1.05ps/(nm km). This normal dispersion was compensated for by 1.7km of standard fibre, which had a dispersion of around 15.6ps/(nm km) at the source wavelength.

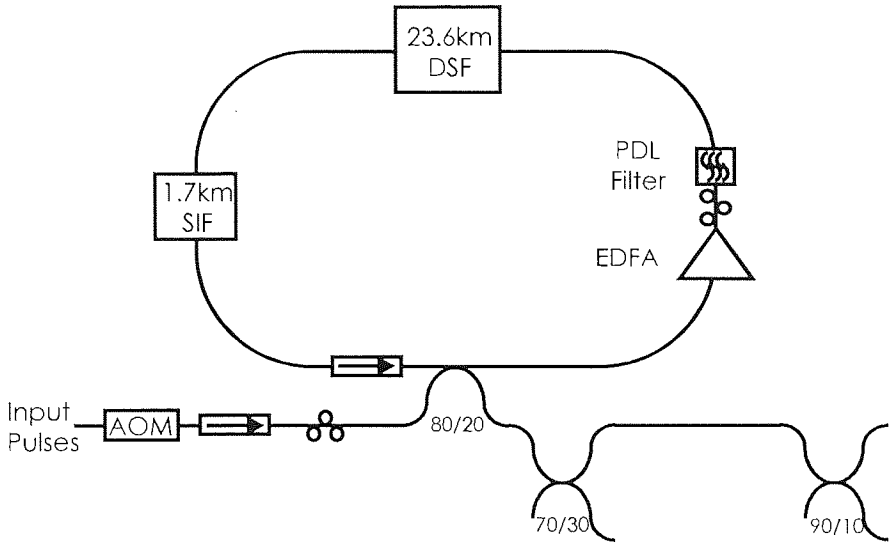

Figure 7-3 Transmission Loop set-up with 23.6km of DSF with a dispersion of –1.05ps/nm km which is compensated for by 1.7km of SIF with a dispersion of 15.6ps/nm km, giving a result amplifier span of 25.3km. The filter placed after the amplifier had a polarisation dependent loss, this was used with the non-linear polarisation to discriminate low power signal. The wavelength characterisation of this filter is shown in Figure 7-5.

The map was set-up in the loop as shown in Figure 7-3. The amplifier, which had a noise figure of around 4dB was placed immediately after the standard fibre, this compensates for the 10.7dB loss of the loop. A filter was placed after the amplifier, which provided the polarisation dependent loss for the saturable absorber as well as filtering the ASE. The bandwidth of the filter was 2nm with a minimum loss of 2.2dB. In order to control the polarisation within the loop and essentially at the input to the filter, a polarisation controller was located immediately before the filter. An 80/20 launch and detect coupler was placed between the amplifier and the standard fibre within the map, this gives a loss of 1dB for each recirculation and a 7dB launch loss into the loop. The position of this coupler is not at the transform-limited point within the map, but at the boundary where pulses are broadest. Ideally the coupler should be positioned at one of the chirp free points near the mid point of either the DSF or SIF sections. However such is the pulse shaping that takes place in this experiment, and the long distances of transmission, this is not detrimental. The detection point within this map is also not as important since the breathing of the pulses is not significant to cause intersymbol interference at the receiver. The launch polarisation into the loop was controlled by another polarisation controller which was located immediately after the Acousto Optic Modulator (AOM). The losses of the DSF and standard fibre sections were 6.3dB and 0.5dB

respectively, with the remaining 0.7dB of loss accounted for by the isolator placed before the launch and detect coupler. The output from the launch/detect coupler was split by a 70/30 coupler, the 30% output was used as a power monitor through a slow photo-diode (125MHz). The 70% output was split again by a 90/10 coupler, with the 10% being fed into the electrical spectrum analyser. This provided a monitor for the 10GHz signal component present in the signal during transmission, which gives a reference to the stability of the pulses within the loop. The remaining 90% output from this coupler was amplified before being fed into the receiver, which consisted of a Phase Lock Loop (PLL) and a lightwave converter. The PLL was used to recover the clock signal for the Bit Error Test Set (BERTS) and sampling 'scope, this required a 10% split of the receiver power via a coupler. The remaining 90% was fed into the lightwave converter to provide the electrical signal for the BERTS and the sampling 'scope.

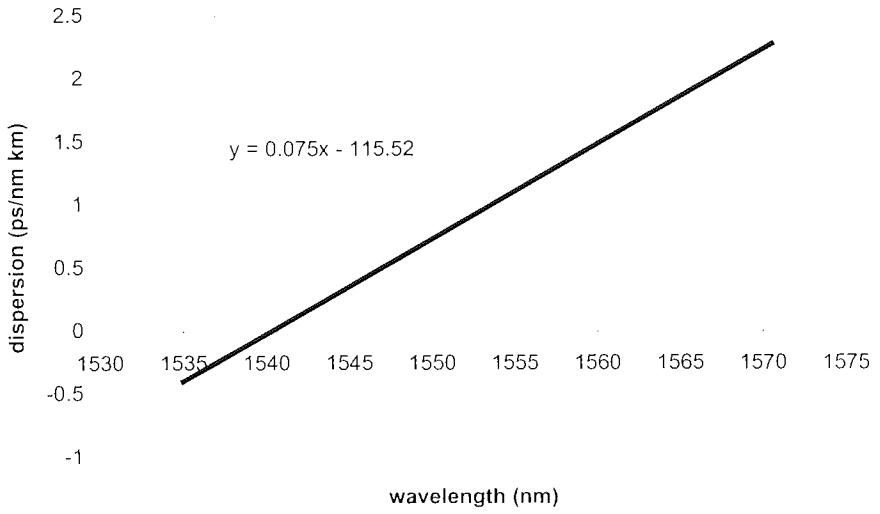

Figure 7-4 Dispersion vs wavelength measurements, showing the dispersion zero at 1541nm and the dispersion slope to be 0.075ps/(nm^2 km)

Figure 7-4 shows the measured average dispersion within the loop, with the dispersion zero at 1541nm, and a dispersion slope of 0.075ps/(nm km). The measurement technique used for this measurement is described in Chapter 4 section 4.6. At the operating wavelength this gives a path average dispersion of 0.1ps/nm km. A wavelength dependent characterisation of the filter is shown in Figure 7-5. Graph (a) shows the PDL, graph (b) shows the Normalised output power of the filter, giving a bandwidth of 2nm. The measurements were carried out using a polarisation state analyser. The peak of the filter pass band was set to the wavelength used for transmission (1542.4nm), and the wavelength of the tuneable laser was tuned from 1540 to 1550 in steps of 0.1nm. At each wavelength the difference between the maximum and minimum loss through polarisation (PDL) was recorded and plotted on the graph. The PDL

varied between 6dB and 0.2dB over the measured region, with the polarisation dependent loss at the wavelength of operation being between 0.2 and 1.4dB.

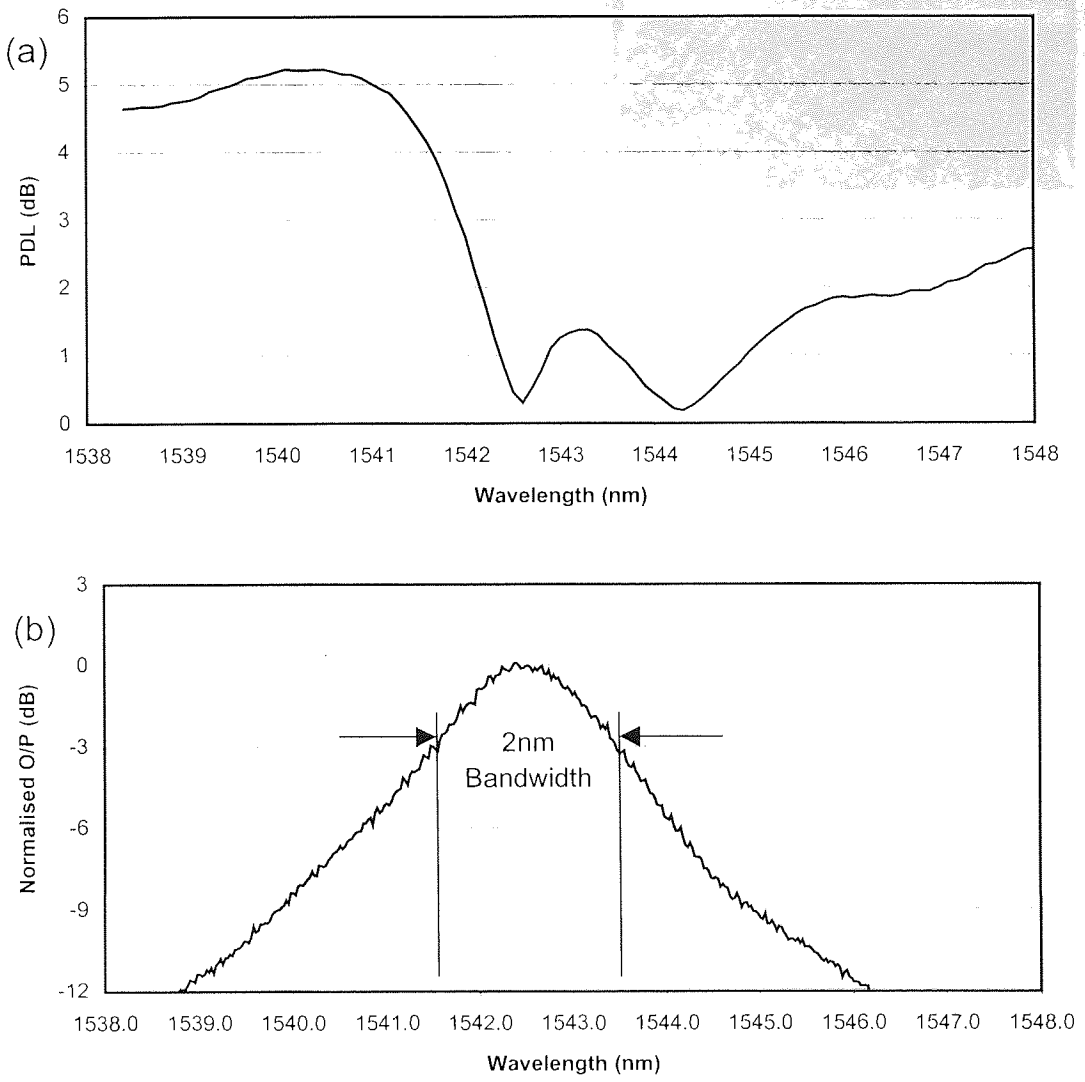

Figure 7-5 Characteristics of the polarisation dependent loss filter. The polarisation dependent loss of filter is shown as a function of wavelength in (a). while (b) shows the loss profile of the filter with a 3dB bandwidth of 2nm.

The pulses were gated into the loop via the launch/detector coupler using an AOM (Acoustic Optic Modulator). The gating time of the AOM was set to be 10μs less than the entire fill time of the loop and thus leaving a gap in the recirculating power in the loop. It was then possible to monitor the noise floor through the gap in the power using the slow photo diode. The polarisation controller within the loop, and the polarisation controller at the input to the loop were optimised while monitoring the bit error rate on the BERTS, the electrical spectrum analyser and the noise floor from the slow photo diode. At the optimum polarisation the signal is subject to less loss than the noise and thus the noise floor remains suppressed.

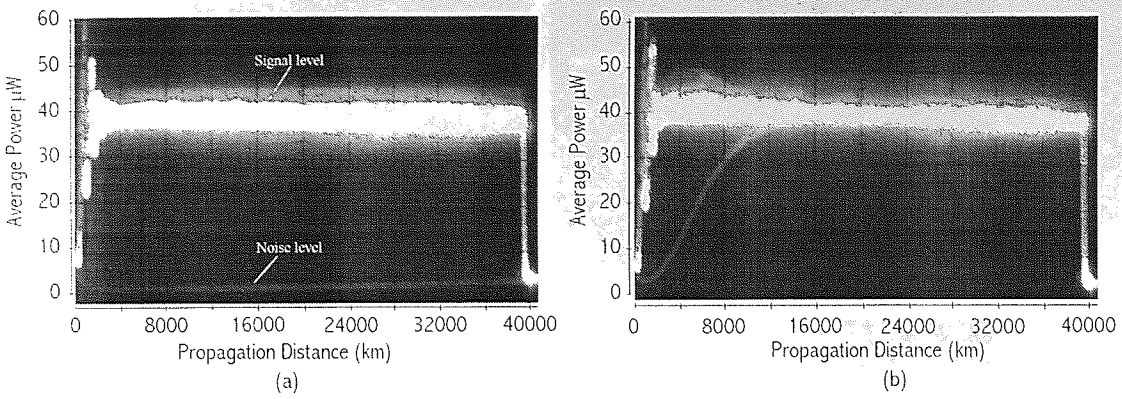

Figure 7-6 Two oscilloscope traces show the loop output power with propagation. The loop was not entirely filled, this enabled the monitoring of the base line/ noise level. Graph (b) shows the baseline level quickly increasing until it reaches the signal level. Graph (a) for the optimised polarisation and shows the base line noise suppressed totally across the 40,000km span.

Figure 7-6 shows two traces taken from the oscilloscope for the slow photo-diode. The power gap in seen as a faint line below the signal power. The trace without optimised polarisation is shown in (b) with the base-line noise level quickly rising until after 8000km where it has completely filled the gap in the loop. With this polarisation state in the loop it is likely that the PDL of the filter does more to restrict transmission than to aid it, since the polarisation may be such that it results in more loss for the signal than the noise. Trace (a) shows the diode output when the polarisation controllers were optimised and the noise floor suppressed. It can clearly be seen that in (a) the noise level is suppressed for the full 40,000km. This suppression can also be observed well in excess of this distance. By interrupting the delay generators that control the loop timings such that the loop remains permanently in recirculation (transmission mode), it is possible to observe such noise floor suppression for several minutes. Figure 7-7 shows four traces taken from the oscilloscope of the power gap at different times. The times that the traces were recorded were, immediately after the initial launch, after 2 minutes of recirculations, after 6 minutes of recirculations and after 7 minutes of recirculations. These traces show the gap in the loop remained suppressed for up to 6 minutes, at which time it was then filled by noise from the amplifier shown on trace (d). The total transmission time that the noise floor remains suppressed for can vary from seconds to minutes, the duration of which is dependent on fine polarisation settings within the loop.

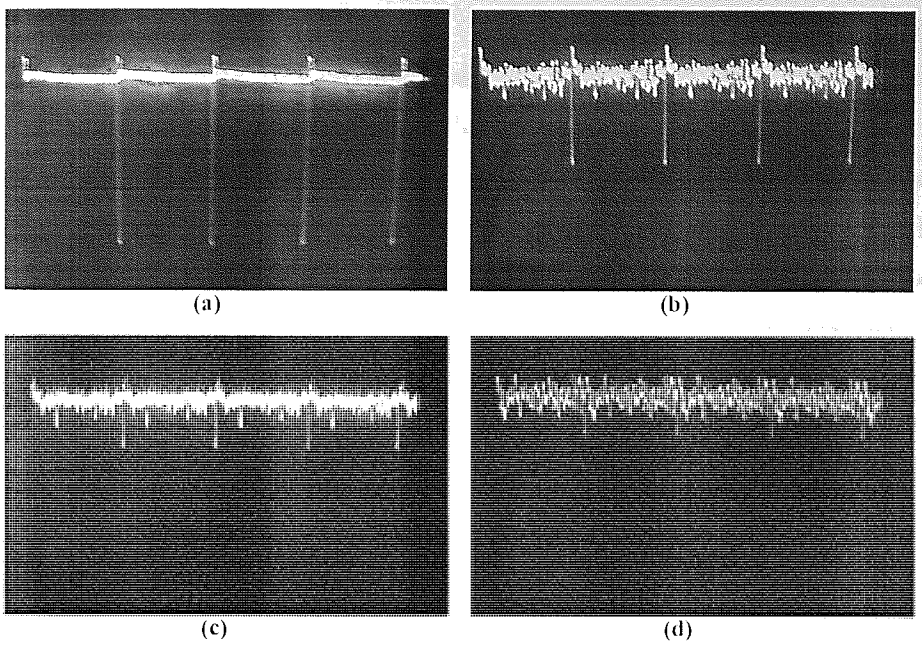

Figure 7-7 Four traces from the oscilloscope of the output from the slow photodiode which show the suppression of the noise floor when signal is left to propagate around the loop for long periods of time. Trace (a) was captured after 0mins, (b) 2mins, (c) 6mins and (d) after 7mins.

Using the BERTS the maximum distance of transmission that could be achieved with a bit error rate of less than 10^{-9} was found to be 200,000km. Transmission at such distance makes taking measurements difficult. It takes over 1100 transmission cycles to read 10^{+9} bits using a 90μs measurement window. At these transmission distances it also takes over one second to complete a transmission cycle. This corresponds to twenty minutes to record error rates of less than 10^{-9}. Nevertheless the experiment remained stable for a period long enough to record these error rates. This shows that in the laboratory this system is stable despite the high polarisation sensitivity. During the recording of some of the results the system had been found to remain stable for up to an hour.

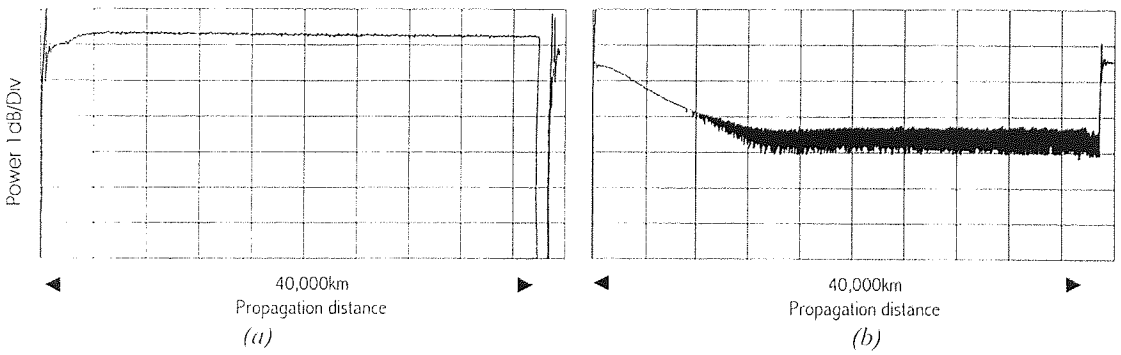

Figure 7-8 Two electrical spectrum analyser traces showing the 10GHz component with transmission for both optimised and non-optimised polarisation states. (a) is the optimised and (b) is the non-optimised state.

Figure 7-8 shows two traces taken of the 10GHz signal component using the electrical spectrum analyser from the 10% monitor. Trace (a) is for the case when the polarisation in the loop was optimised and (b) for when the polarisation was not optimised. When the polarisation was optimised the 10GHz signal component was sustained with transmission. Where as for the case when the polarisation was not optimised as in that shown in Figure 7-6 (b), the 10GHz component level was found to fall quickly into the noise with transmission indicating that the pulses have been attenuated. Figure 7-8 shows two eye diagrams taken before transmission and after 20,000km of transmission, these are labelled (a) and (b) respectively. The eye in (b) shows no indication of degradation after 20,000km when comparing with (a). However in the base of the eye there is an increased ringing effect (Oscillations) from the photo-diode indicating that some pulse shortening has taken place.

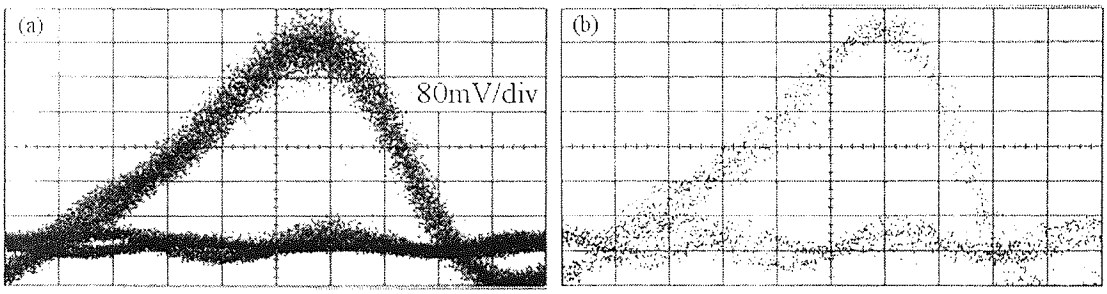

Figure 7-9 An eye diagram taken after 20,000km in (b) shows little timing jitter is observed compared to the Back to Back eye shown in (a).

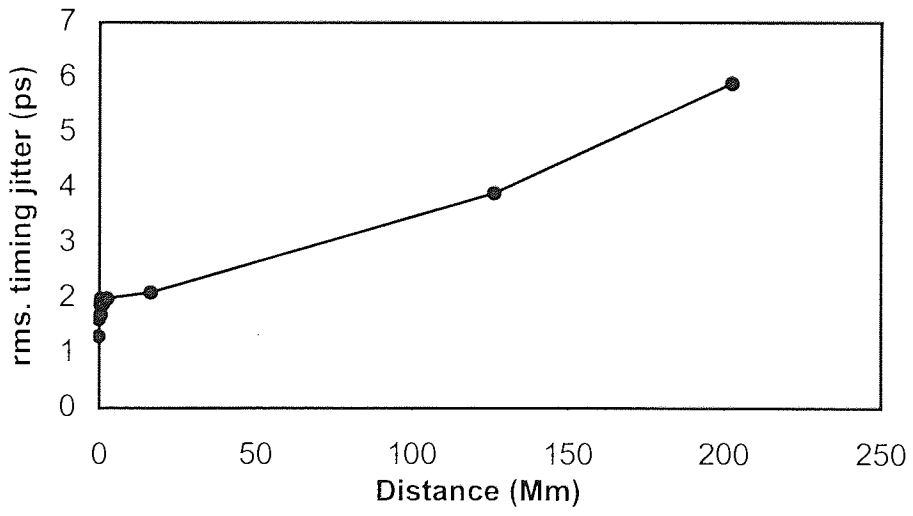

Figure 7-10 Timing jitter measurements recorded using the sampling 'scope at several distances of transmission up to 200,000km. The timing jitter at 200,000km coincides with the maximum tolerable jitter of a 10Gbit/s system are the maximum error free distance recorded on the BERTS

To analyse the degradation of the eye with distance statistical information about the timing jitter and Q-value measurements were taken using the sampling 'scope. These results are shown in Figure 7-10 and Figure 7-11. The timing jitter measurements were found to co-inside well with the maximum distance of error free transmission found using the BERTS, with jitter measurements found to be below 6ps up until 200,000km of transmission. This confirms that the system is jitter limited and that noise build up has been suppressed due to the saturable absorption mechanism. It must be noted that the timing jitter before transmission is 1.3ps, over the first 1000km there is a sharp rise to 2ps. This is as a result of the initial evolution of the pulses.

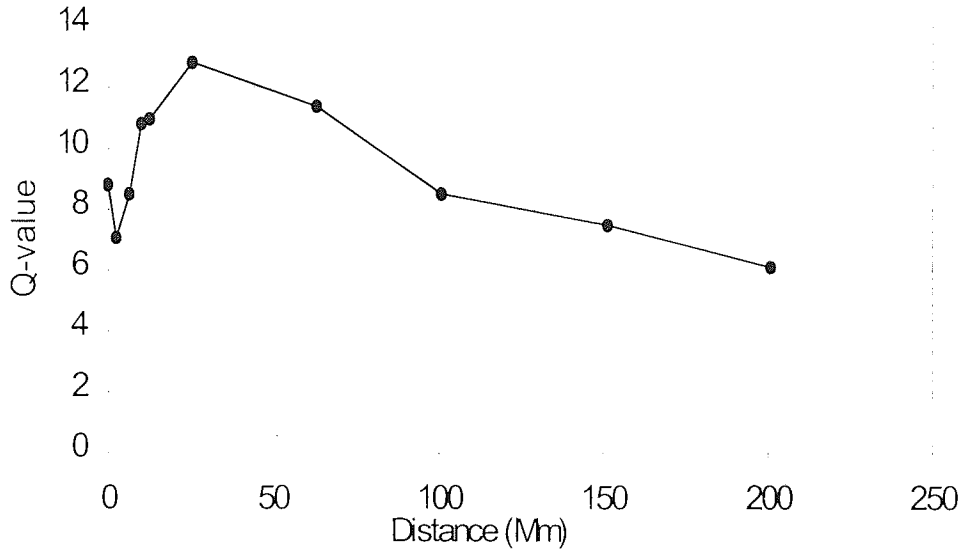

Figure 7-11 Q Values vs distance. The initial value of Q at launch was 9. After transmission of 25,000km this increases to 13 as the signal noise is removed. The Q-value decreases slowly with distance to 6 after 200,000km, which is the minimum tolerable value of Q for an error free system. This agrees well with the maximum error free distance recorded on the BERTS and the maximum distance due to jitter in Figure 7-10.

The Q value measurements show the initial Q value at the launch point to be 9. After transmission over 2500km there was an initial drop in the Q-value to 7, beyond this point the Q-value is actually increased to a maximum value of 13, at 25,000km. After which the Q-value falls slowly with distance to 6 at 200,000km of transmission. This is the minimum value of Q for a bit error rate of less than 10^{-9}, and therefore agrees with the maximum error free distances found from the timing jitter and BERTS measurements.

This error free distance is a substantial increase on the maximum error free distances achieved in the previous chapters. To understand the reasons for the low timing jitter and the initial evolutions shown in the Q-value, further investigations were carried out. These investigates were to determine the pulse width and spectrum changes during transmission. For

analysis of the spectrum with transmission, two traces were taken at different wavelengths using the 10% output. These were recorded at two different wavelengths, with the wavelength span of the optical spectrum analyser set to zero. This method was discussed in section 4.7.4. The traces are shown in Figure 7-12. At the central wavelength of 1542.4nm the spectral power increases due to the slightly lower launch power, this then steadies out after 200km of transmission. At 1542nm (0.4nm off the centre) there is initially no spectral power present in the signal. Then after 120km energy is generated at this wavelength. The reason for the generation of this new frequency component can be put down to the pulse shaping from the saturable absorber. The broadening of the spectrum indicates that the pulse width has been reduced. After 240km of transmission the power level at this wavelengths stables out. Therefore the majority of the evolution of the pulses must be taking place within the first 10 recirculations. Beyond this distance there is still noise reduction taking place, which is observed in the increases in Q value up until 25,000km of transmission.

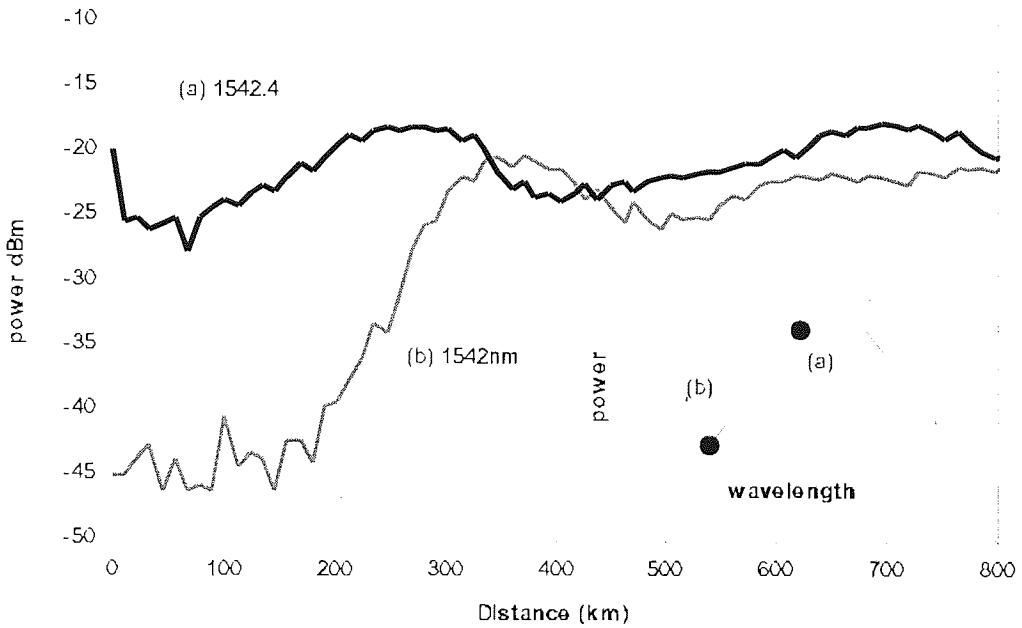

Figure 7-12 The spectral power component at two different wavelengths within the signal spectrum. Trace (a) shows the wavelength with distance at 1542.4nm, while Trace (b) shows the power at 1542nm with distance. The insert in the bottom right shows these two wavelengths on the spectrum of the launched signal. Trace (a) being a point near the peak of the spectrum and Trace (b) being at the edge of the launched spectrum. The generation of energy at 1542nm during transmission indicates a broadening of the spectrum.

Due to these long distances of propagation it is possible to record spectral traces of the signal during transmission using the optical spectrum analyser. This is done over many thousands of recirculations and is valid provided there is very little spectral change over the recirculations of measurement. This enabled the spectral width of the transmitted signal to be determined. Figure 7-13 shows the spectral trace taken at the input, and during transmission.

The input spectrum shown in trace (a) has a 3dB bandwidth of 0.25nm. Clearly in (b) there is a dramatic increase in spectral bandwidth, with the 3dB bandwidth expanding by more than four times to 1.1nm.

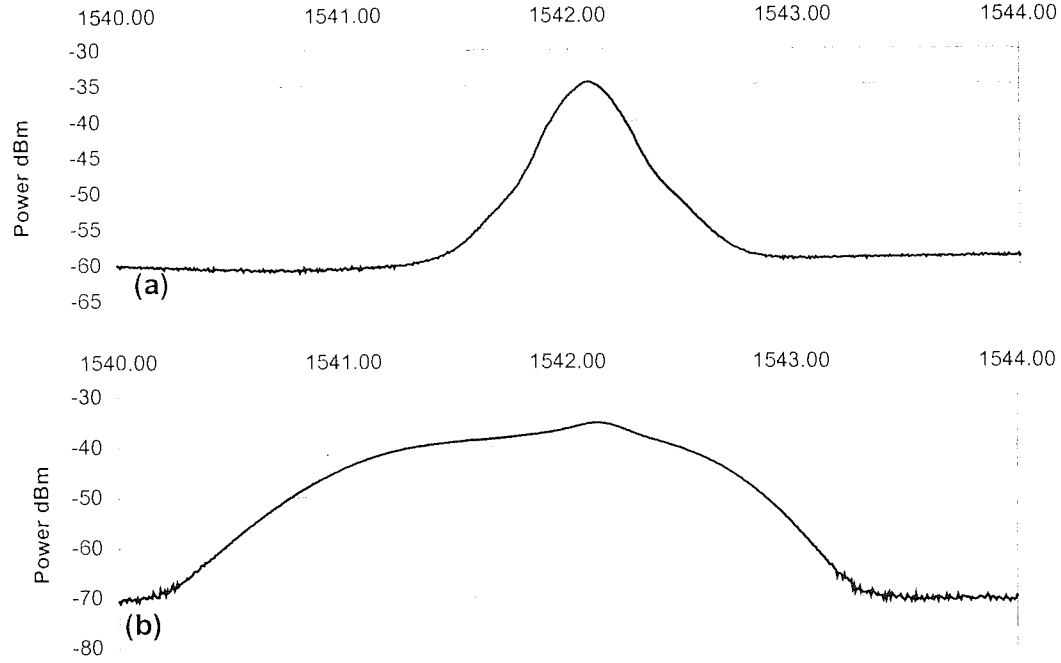

Figure 7-13 Optical spectra of the source and the signal after transmission. The input spectrum has a 3dB bandwidth of 0.25nm. After transmission this expands too 1.1nm, this happen as a result of the pulse shaping within the saturable absorber. This is also shown by the generation of new spectral components in Figure 7-12.

Applying the same principle for recording spectral traces shown in Figure 7-13 with the autocorrelator, (i.e. assuming that once the pulses are stable they will maintain there width and shape) it is possible to take autocorrelations during transmission from the output signal of the loop. The assumption that the initial pulse width and the evolution period have very little influences on the final autocorrelation, is valid, since the settling down period is only 250km, slightly more than 0.1% of the entire transmission distance of 200,000km. Two autocorrelations are shown in Figure 7-14, (a) is the autocorrelation taken from the source before transmission and (b) is the autocorrelation during transmission.

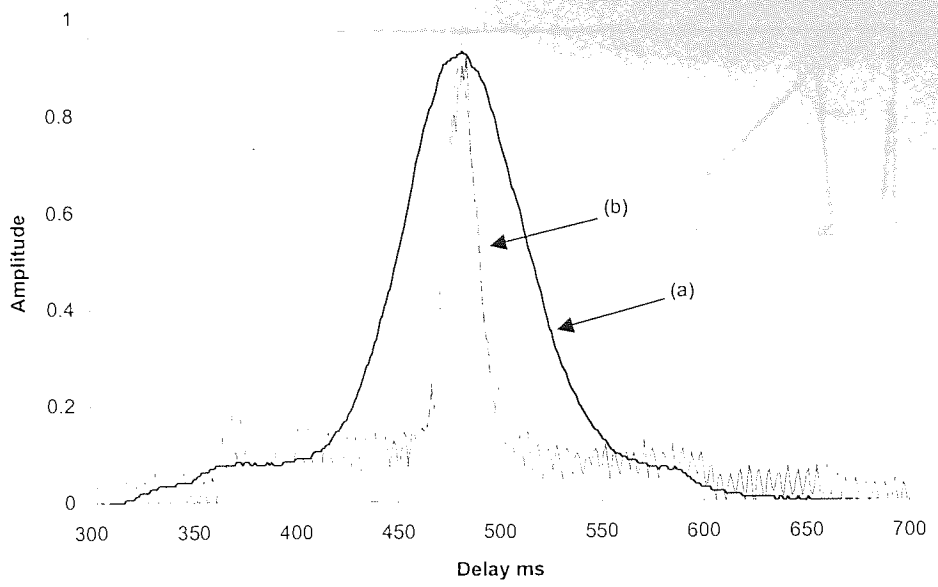

Figure 7-14 Auto correlation's of the source and the transmitting signal. The curve fit to the input autocorrelation show a pulse width of 23ps. The same fit to the auto correlation after transmission shows a pulse width of 6.5ps.

Autocorrelation (b) corresponds to a 6.5ps pulse width, this is a considerable pulse shortening on the launched 23ps pulse width. These results coincide well with simulation carried out by Govan *et al*[148] which also show similar pulse shaping from a similar system. The autocorrelation shown in Figure 7-14(b) was taken at the end of the standard fibre within the map, and is thus the pulse width at one of the broadest points. To determine the minimum pulse width the 1.7km section of standard fibre was replaced by two sections of 600m and 1.1km. This made it possible to take autocorrelations at two different points within the standard fibre using a 5% coupler. These results are shown in Figure 7-15 along with corresponding simulation results provided by Ref [149].

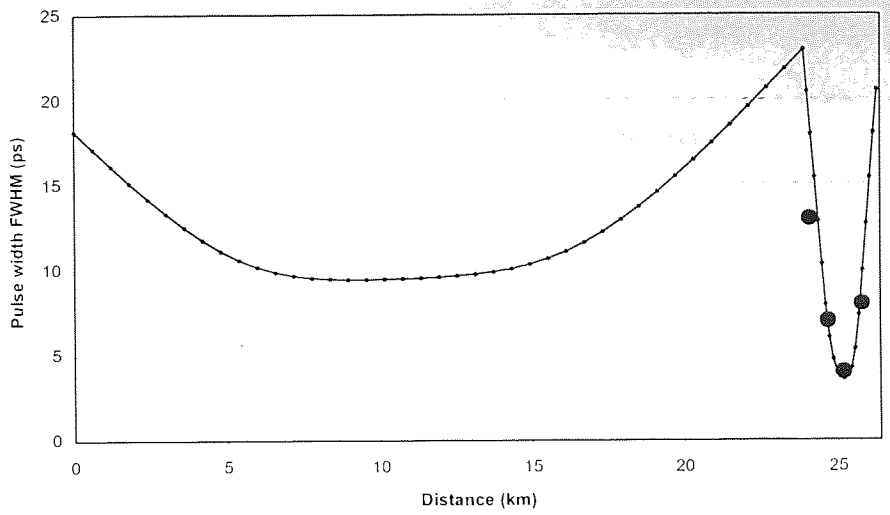

Figure 7-15 Experimental and simulation pulse widths vs position within the dispersion map. The four black circles correspond to the experimental points and the small dots correspond to the simulation results. The first 23.6km of the graph correspond to the DSF and the remaining 1.7km the SIF.

A point within the dispersion-shifted fibre could not be obtained since the DSF was wound on a single drum. The simulation results show a good agreement with the experimental points within the standard fibre. The minimum pulse width within the map was found to be 4ps. For the given spectrum of 1.1nm this corresponds to a time bandwidth product of 0.55, which is significantly higher than the time bandwidth product of the uniform hyperbolic secant soliton of 0.31 and the Gaussian 0.44 of the dispersion managed system. This is as a result of the sharper pulse tails due to the pulse shaping in the saturable absorber. The increase in spectral width results in a 1:2 ratio with the filter bandwidth, giving strong wavelength guiding of the pulses. Together with the power enhancement factor these are the reasons the maximum distances of error free transmission are greatly increased. The benefits of strong wavelength guiding can be seen when calculating the Gordon Haus jitter. Below are calculations for the Gordon Haus jitter of this system at 500,000km.

From section 2.4.2 the Gordon Haus Jitter is taken to be

$$\left\langle t_N^2 \right\rangle = \frac{2\pi n_2 N_{sp} |\beta_2| hc(G-1)L^3}{9\tau_0 \lambda^2 A_{eff} L_a \Lambda_0^2}$$

Equation 7-5

Where the values used for the calculation are

n_2 = 2×10^{-20}

N_{sp} = 2

λ = 1550×10^{-9} (m)

L_a = 25.3×10^3 (m)

h	=	$6.67\text{x}10^{-34}$
C	=	$3\text{x}10^{8}$ (m)
A_{eff}	=	$50\text{x}10^{-12}$ (m^2)
τ_0	=	$\tau_{fwhm}/1.763 = 4\text{x}10^{-12}/1.763 = 2.27\text{x}10^{-12}$ (s)
G	=	$10^{10.7/10} = 11.75$
D_2	=	0.1ps/nm km $= 0.1\text{x}10^{-6}$ (s/m^2)

$$\beta_2 = -\frac{\lambda^2}{2\pi c} D_2 = \frac{\left(1550x10^{-9}\right)^2}{2\pi x 3x10^8} 0.1x10^{-6} = 1.27x10^{-28}$$

$$\Lambda_0^2 = \frac{G\ln(G)}{G-1} = 2.69$$

Thus the Gordon Haus Jitter at distance L= 500,000 is found to be

$$\left\langle t_N^2 \right\rangle = \frac{2\pi \cdot 2 \cdot \left(1.27x10^{-28}\right) \cdot 2x10^{-20} \cdot 6.67x10^{-34} \cdot 3x10^8 \cdot (31-1)}{9 \cdot 2.27x10^{-12} \cdot \left(1550x10^{-9}\right)^2 \cdot 50x10^{-12} \cdot 25.3x10^3 \cdot 2.69} \cdot (500x10^6)^3 = 1.43x10^{-16}$$

The reduction factor for the Gordon Haus jitter due to the inline filtering is given as

$$f(x) = \frac{3}{2}\frac{1}{x^3}\left[2x - 3 + 4\exp(-x) - \exp(-2x)\right]$$

Where x is given as

$$x = 4\delta Z = \frac{4L}{3\left(2\pi\Delta\lambda_f \tau_0\right)^2 L_a} = \frac{4 \cdot 500x10^6}{3 \cdot \left(2\pi \cdot 2.5x10^{11} \cdot 2.27x10^{-12}\right)^2 \cdot 25.3x10^3} = 2072$$

Where $\Delta\lambda_f$ is the bandwidth of the filter and is given as

$$\Delta\lambda_f = \frac{c}{\lambda^2}\Delta\lambda = \frac{3x10^8}{\left(1550x10^{-9}\right)^2} 2x10^{-9} = 2.5x10^{11}$$

Thus the value of $f(x)$ for a given distance L=500,000km is

$$f(x) = \frac{3}{2} \cdot \frac{1}{(2072)^3}\left[2 \cdot 2072 - 3 + 4\exp(-2072) - \exp(-2 \cdot 2072)\right] = 7x10^{-7}$$

The power enhancement must also be taken into account, which can be treated as a multiplying factor on the Λ_0^2 term seen on the denominator of Equation 7-5. The average peak power at this dispersion for a soliton in a uniform system is given as

$$P_0 = \frac{|\beta_2|}{\gamma\tau_0^2} = \frac{1.27x10^{-28}}{1.5x10^{-3} \cdot \left(2.27x10^{-12}\right)^2} = 16mW$$

Where γ is taken to be $1.5W^{-1}km^{-1}$. The average peak power in the experiment was found to be 58mW, giving a power enhancement of 3.6. Therefore the full Gordon Haus jitter calculated for a distance L=500,000km is given as

$$\left\langle t_N^2 \right\rangle_{GHJ-filterd} = \left\langle t_N^2 \right\rangle_{GHJ} . f(x). \frac{1}{power\_enhancement} = 1.43x10^{-16} \cdot 7x10^{-7} \cdot \frac{1}{3.6} = 2.78x10^{-23}$$

$$r.m.s\_jitter = \sqrt{2.78x10^{-23}} = 5.3ps$$

This is a much greater distance than that achieved experimentally. The reasons such error free distances are not observed in this experiment may be partly due to the initial evolution that takes place after launching the pulses. In Figure 7-10 this evolution period can be seen to raise the jitter up to 2ps within the first 1000km. Additionally an inaccuracy in the measurement in the bandwidth of the filter (due to the polarisation dependence) will also have a significant effect on the Gordon Haus jitter.

In a conventional soliton systems where no saturable absorption mechanism is used, this filtering would be too narrow and would inducing too much extra loss on the signal, this in turn would require greater amplification and limit the maximum transmission distance through noise. The optimum filter bandwidth for a typical soliton system is around ten times the signal spectrum. However in this case it is the saturable absorption effect that suppresses the noise, which allows very narrow filtering of the signal.

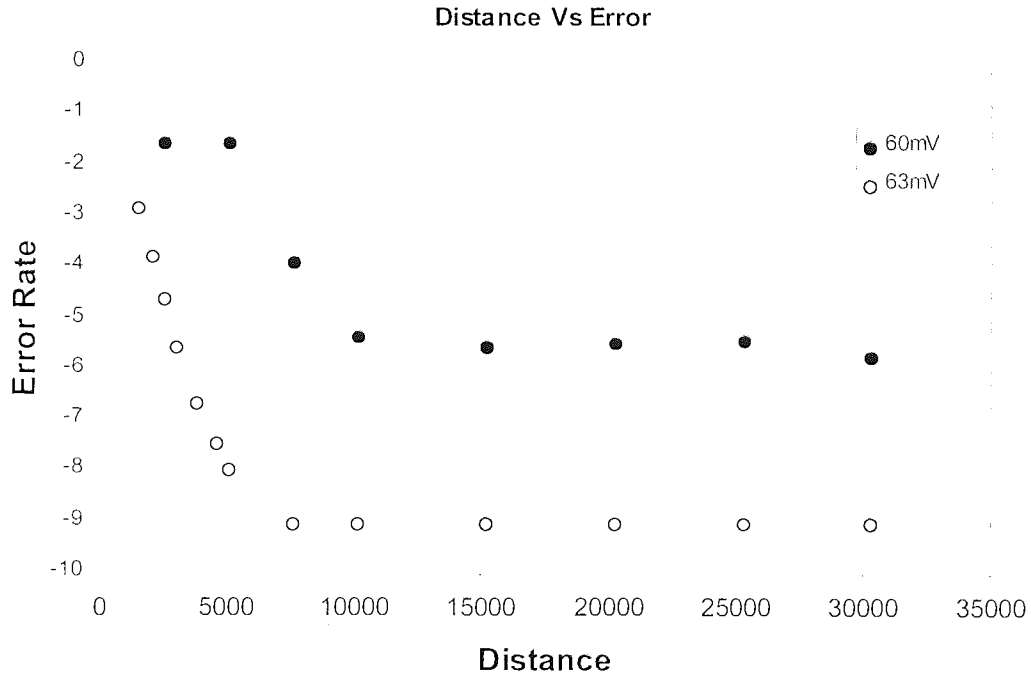

Figure 7-16 Error rates vs distance for fixed threshold voltage taken at two different voltage levels close to the base line, 60mV and 63mV. Error rates are clearly suppressed with transmission indicating that the base line noise is being suppressed.

The suppression of noise with transmission that is observed in Figure 7-6 can also be observed from the Bit Error Rates results shown in Figure 7-16. For this set of results the

propagation distance was set to 30,000km and the polarisation controllers optimised for error free transmission and suppressed baseline noise. The voltage threshold level of the BERTS was set to the base of the eye so that it gave error rates just on 10^{-9}. Using this threshold level error rates against distance were taken from 1500km up to 30,000km. The results show errors due the noise floor that is present over the first 8,000km being reduced through transmission. The same effect is observed for a lower threshold of 60mV, where the initial high error rates are reduced until after the first 10,000km where the error rate remains at $5x10^{-5}$. In effect the eye is improved during transmission. Figure 7-17 confirms this with two eye diagrams, taken before and after 50,000km of transmission. The source was not fully optimised and had a large amount of noise in the baseline. After transmission it can be seen that the noise in the base of the pulses has been removed. At this distance the BERTS showed that error free transmission had been achieved and the 2^{31}-1 PRBS pattern maintained.

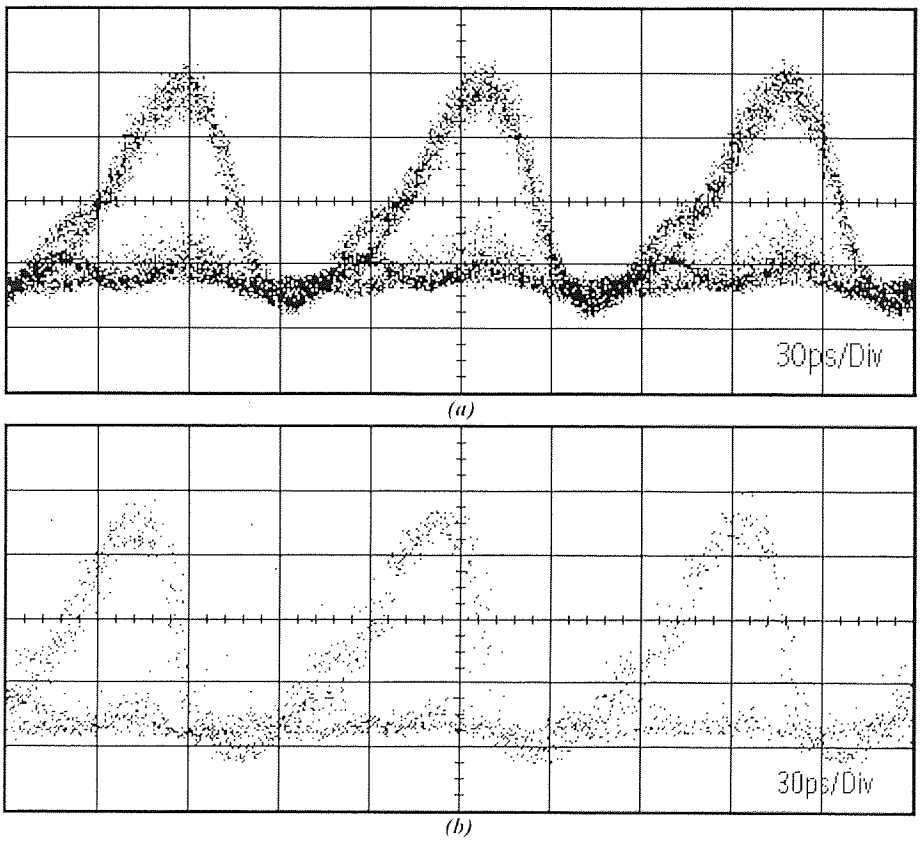

Figure 7-17 Two eye diagrams taken, (a) at the source and (b) after transmission over 50,000km. (a) The amplitude jitter present in the base of the eye indicates the presence of noise in the zeros. (b) shows no sign of noise present in the zeros after 50,000km of transmission indicating that the noise has been removed.

The improvement of the signal is further illustrated in the power penalty measurement shown in Figure 7-18. This consists of two power vs bit error rate measurements, one taken at the back to back output from the source and one after 30,000km of transmission. The graph shows that there is a 1.5dB power penalty improvement through transmission, as opposed to the power penalty loss associated with signal degradation.

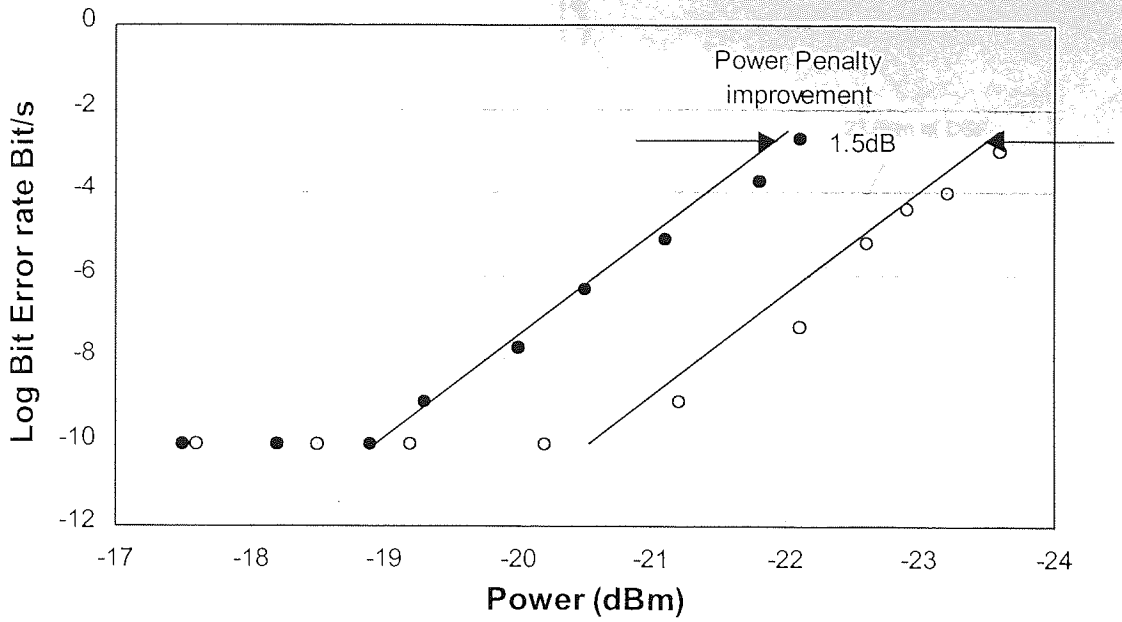

Figure 7-18 power vs error rate measurements at the B-B point (circles) and after 20,000km of transmission (filled circles). The results show a 1.5dB power penalty benefit after transmission.

The following section discusses attempts to repeat the saturable absorption though non-linear polarisation rotation with variations on the set up used in the previous section. This will further aid the understanding of the essential characteristics required for the successful operation of this system. This investigation is targeted at two aspects of the system, the first being the dispersion map and the second being the PDL element.

7.2.1 Investigation of the dispersion map

In order to determine the role of the map in this system, several other dispersion maps were tested to see if the same baseline suppression could be observed as that shown in the photo-diode in Figure 7-6 (a). In total five dispersion maps were tested and are shown in Figure 7-19. This includes the original dispersion map labelled (a). The map labelled (b) contained the same 23.6km of DSF but the amount of SIF was reduced to 1.2km. In map (c) the standard fibre was reduced to 800m. These alterations to the map shifted the dispersion zero to 1545.2nm and 1549.3nm respectively, the wavelength of the source and filter pass band were shifted to 1546.5nm and 1550.3nm accordingly. This changed the respective dispersions of the DSF and SIF to 0.8ps/(nm km) and 15.8ps/(nm km) for (b) and 0.5ps/(nm km) and 16.1ps/(nm km) for (c). Map (d) was a uniform map of 36km in length and had a dispersion zero of 1543.3nm to maintain the wavelength of operation and the same average dispersion.

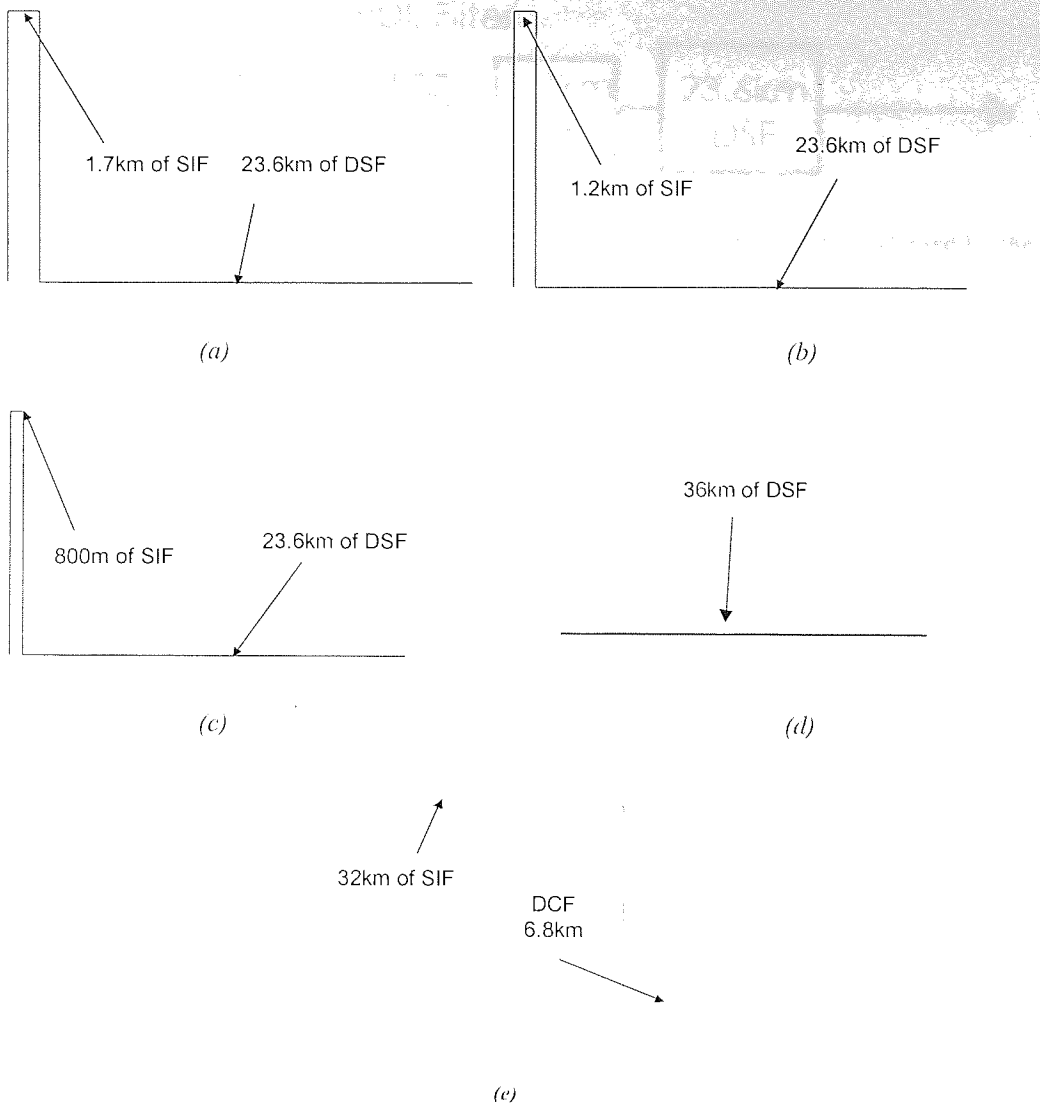

Figure 7-19 Five dispersion maps tested for transmission with saturable absorption. Map (a) is the original map with 23.6km of DSF and 1.7km of SIF. Map (b) is 23.6km of DSF with 1.2km of SIF. Map (c) 23.6km of DSF and 0.8km of SIF. Map (d) shows a unform dispersion map with a disperison of 0.1ps/nm km) and length . Map (e) contains 32km of SIF and 6.8km of DCF.

Using maps (a) and (b), the successful suppression of baseline noise was achieved by optimising the polarisation controller at the input and polarisation controller within the loop. However in (c) and (d) suppression of the baseline could not be achieved, which indicates that the dispersion map plays an important role in enabling the pulse switching to occur, and that the strength of the map is also important. It may be that the switching is possible in maps (a) and (b) because of the power enhancement provided by the dispersion management. In the weaker maps the power of the soliton may not be sufficient to give saturable absorption. Map (a) was also tested in reverse such that the amplifier and filter were before the SIF as shown in Figure 7-20. Attempts to suppress the baseline noise during propagation with this configuration proved successful, indicating that the sign of the chirp at the PDL filter is not important.

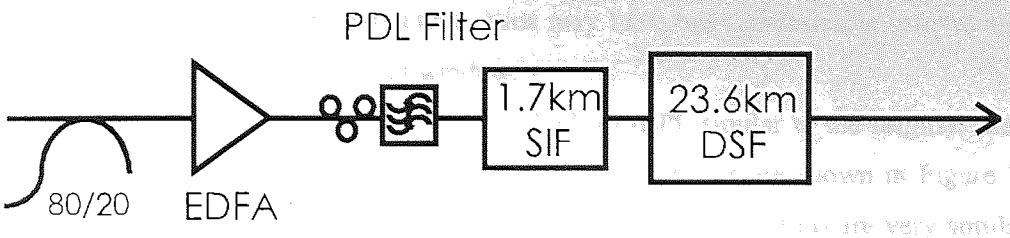

Figure 7-20 The dispersion map reversed such that the 1.7km of standard fibre is followed by the 23.6km of DSF, and the PDL filter is placed immediately before the Standard fibre.

The final map shown in Figure 7-19 (e) consisted of 32km of standard fibre compensated for by 6.8km of DCF, this is similar to the maps used in Chapters 5 and Chapter 6. The filter and amplifier were located at boundary after the standard fibre. The same attempts to utilise the saturable absorption in this system maps were made, but found to be unsuccessful. This may be due to the large map strength that would be produced as a result of the short 4ps pulses. The large map strength would cause large pulse breathing to take place within the map, which may results in stable peak pulse powers that are far too low for switching to occur at the boundary between fibres.

From these tests on different dispersion maps, it appears that the system requires a degree of dispersion management to support saturable absorption. However it is not clear how much dispersion management the system can tolerate. For strong dispersion maps it may be necessary to relocate the polarisation dependent loss element away from the boundary point in the map and towards the transform limited point.

7.2.2 Investigation of the Polarisation dependent loss element

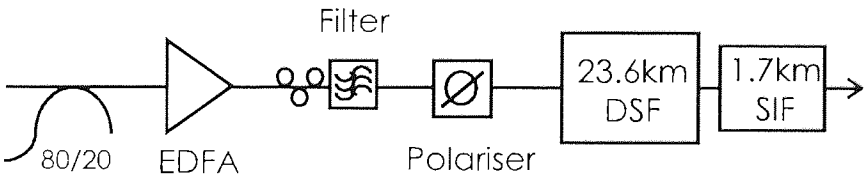

Figure 7-21 The configuration of the NPR experiment using a polariser as the polarisation discriminating element. The extinction ratio between the high and low loss axis is 30dB. A filter with a bandwidth of 2.4nm was placed after the polariser to provide the same wavelength guiding as with the original filter.

To investigate the importance of the characteristics of the polarisation dependent loss element, three other PDL elements were tested using the original dispersion map. The first of which was a polariser, this had a 30dB ratio extinction between the high and low loss axis, which is much greater than the 1.4dB found with the originally element. This was positioned in the span immediately after a bulk Fabry Perot band pass filter (FP-BPF, as shown in the diagram in Figure 7-21. The filter had a 3dB bandwidth of 2.4nm and was used to provide the spectral filtering present in the original PDL element. The PDL of this filter was very low so as to avoid any interference with the PDL of the polariser. Attempts to transmit using this set

up were unsuccessful. The high extinction ratios may have been undesirable, providing too much loss and a very narrow switching window.

The other two elements tested were both bulk FP-BPF similar to the original used in the previous section. The PDL characteristics of these two filters are shown in Figure 7-22 along with their loss wavelength characteristics. The characteristics of (a) are very similar to the original filter used in the previous section, with the same bandwidth of 2nm and a similar PDL curve. The characteristics of filter (b) are different in that it has a narrower bandwidth and a different wavelength dependence of the PDL. The filters were inserted into the original map containing 23.6km of DSF and 1.7km of SIF as a direct replacement for the original filter. The same attempts to achieve a suppressed base line by optimising the polarisation were made.

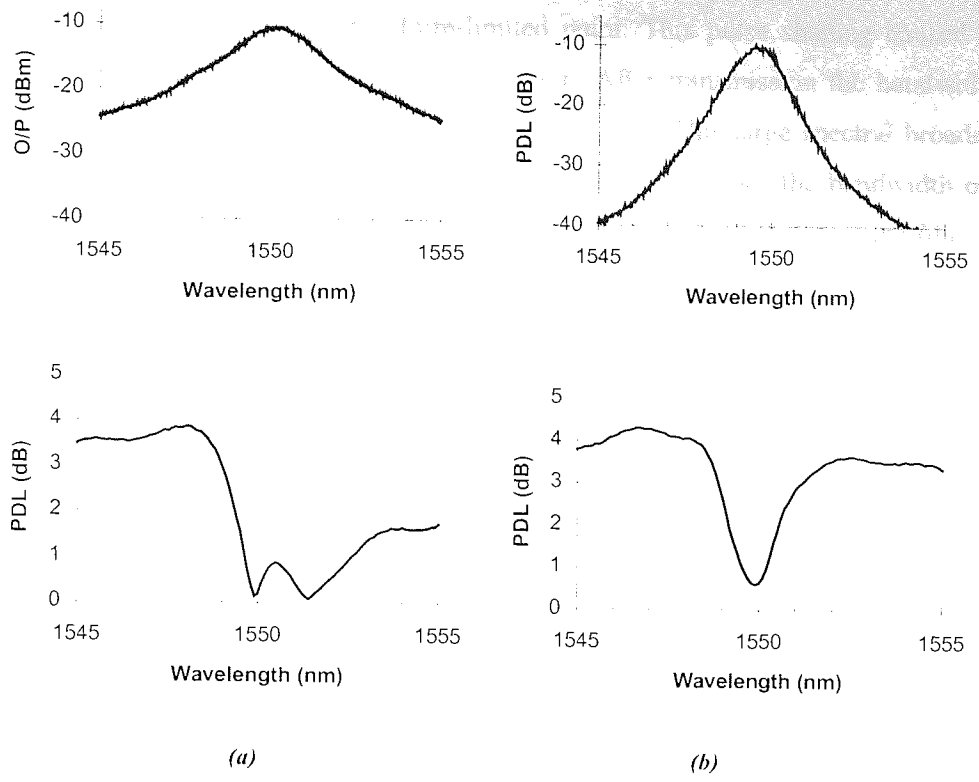

Figure 7-22 The characterisation of the two filters tested in this section. The top graphs show the loss spectra and the bottom graphs show PDL vs wavelength. Filter (a) is much like the filter used in the previous section except that the bandwidth is measured at 2.4nm. Filter (b) had a bandwidth of 1.2nm and a different PDL wavelength curve.

The first filter was found to be successful in providing saturable absorption, however suppression with the second filter was not successful. This is may be due to either the narrow bandwidth of the filter or an essential difference in the PDL characteristics. Exactly which of these characteristics prevented saturable absorption has not been determined. The restriction on the available devices with specific characteristics prevents a full investigation into the device requirements for this system. Further information about how the loss of the device varies with polarisation state may give further insight into the optimum and most desirable characteristics.

7.3 Conclusions

This chapter has demonstrated the transmission of short pulses over ultra long distances with the aid of saturable absorption. The saturable absorption was achieved through the combination of non-linear polarisation rotation within the fibre, and the PDL provided by a Fabry Perot band pass filter. The PDL of the filter over the spectrum of the pulse was between 0.2 and 1.4dB. This small PDL provided sufficient discrimination between the signal and noise to give a suppressed baseline with transmission. In the first 250km there was a

evolution period in which the pulse shaping took place. The pulse shaping reduces the pulse width to a FWHM of 4ps at the transform-limited point. This pulse shaping caused large spectral broadening to take place during transmission. After transmission the bandwidth of signal had expanded by more than a factor of four to 1.1nm. This large spectral broadening meant that the bandwidth of the filter which was originally ten times the bandwidth of the launch signal was only twice the bandwidth of the transmitting signal, therefore the filter gave very strong guiding of the soliton wavelength. With such high guiding present in the system the Gordon Haus jitter limit was extended to 200,000km. During the initial evolution period there was an increase in the timing jitter which continued up to 25,000km. This evolution period may be suppressed by launching pulses that are more closely matched to those found in transmission. This would require generating pulses with FWHM of 4ps and matching the chirp to the map by either pre-chirping or launching at the transform-limited point within the map. Despite the small accumulative dispersions within the map, the short pulses result in a map strength as high as 4.4.

Variations on the original configuration were tested and the failure to achieve saturable absorption with several of these configurations indicated that the system requirements for operation were stringent. While positioning the filter at either of the boundary points showed successful saturable absorption, attempts to achieve saturable absorption with any significant deviation from the original map proved unsuccessful. Saturable absorption could not be achieved in the case of the uniform map and the map with 800m of SIF, but was achieved using when the map strength was increased by using 1.2km and 1.7km of SIF. This indicates that the dispersion management plays an important role in this system. The enhanced powers produced by the map may have aided the pulse switching through the saturable absorber. The attempts to transmit using the SF - DCF dispersion map however proved unsuccessful. This may be due to the large map strength (~90) that would result from the generation of 4ps pulses. Such very high map strengths would result in large pulse breathing within the map and give broad pulses at the boundary point where the saturable absorption was set to take place. As a result these broader pulses will have a lower peak power and will overlap and inhibit the operation of the saturable absorber mechanism. A possible area for further research into this system would be to investigate different positions for the filter, either mid way through the SF or DCF. At these positions the pulses may have sufficient peak power to enable switching. The same investigation could also apply to the original system with 23.6km of SIF and 1.7km of SIF. The experiment showed that a filter with specific characteristics can be used to provide successful saturable absorption. What these specific characteristics are that are required to support saturable absorption is not fully known. A more rigorous characterisation of the polarisation dependent loss of the filter is required. The variation of loss of the filter with respect to the polarisation, and how this varies with wavelength over the spectrum of the

pulse may give further insight into its function. This could then be compared with other filters with polarisation dependent loss and the polariser. An in depth study of these characteristics may enable the development of such device for operation with different pulse widths and different dispersion maps.

This technique for saturable absorption used in this chapter would be impractical for a real communication system. The polarisation dependence of the saturable absorber is undesirable, since an inline control mechanism would be required to ensure that polarisations are maintained along the transmission line. The development of discrete quantum well devices would be an important step to realising saturable absorption practically. Currently the switching powers and response times are insufficient for practical use. These large distances achieved in this system are far in excess of what is required for any global communications system. This combined with the short pulse widths opens up the possibility of transmit data rates as high as 40Gbit/s over distances much greater than 10,000km. The long periods of error free transmission within the loop may also make such systems viable for the application of optical data storage.

Chapter 8

40Gbit/s soliton transmission

8.1 Introduction

With the ever-increasing demand for greater network bandwidth, a considerable amount of interest has been focused on increasing the data rate of single channel (single wavelength) transmission. Operating at data rates of 40Gbit/s has been the focus of much research[150][151][152]. The operation at higher data rates potentially opens the way for greater spectral efficiency. The greater data rates per channel would essentially mean fewer channels, which would reduce the spectral redundancy associated with the channel spacings. The general aim is to move towards fewer channels at higher data rates, with the ultimate spectrally efficient system having a single channel with a data rate such that the spectrum occupies the entire available bandwidth. The use of less channels will reduce the number of transmitters and receivers and lower the cost and complexity of managing such a high data rate system. For example a 320Gbit/s transmission system would require 32 channels operating at 10Gbit/s. When operating these channels at 40Gbit/s only 8 channels are required, this will give a considerable saving on system management. The operation of transmission links at higher data rates using less channels can also provide better network compatibility, utilising various optical processing techniques such as add and drop multiplexers[153][154]. The major disadvantage of these higher data rates is that the shorter bit window results in a system that has less tolerance to timing jitter. Therefore these higher data rate transmission systems will generally have a shorter maximum error free distance.

The direct generation of a 40Gbit pattern poses many difficulties, the essential electronics components required to support data rates of 40Gbit/s directly, are either currently not available or are expensive. An alternative technique of generating a 40Gbit/s pulse stream with data is to use Optical Time Division Multiplexing (OTDM). This is a technique compatible only with RZ format and is achieved by interleaving pulse streams from separate

data channels before transmission. For this technique it is essential that pulses widths are significantly shorter than their initial bit interval such that they don't overlap when they are superimposed with other pulse streams. For experimental purposes this interleaving of channels can be implemented using an imbalanced Mach Zehnder interferometer. This consists of an optical coupler which splits the power equally into two separate paths, one of these path is longer than the other such that the bit slots are offset by half a bit window. The signal is recombined at the other end of the interferometer and a data rate at twice that of the input is produced. A variable delay controller in one of the arms can be used to fine tune the temporal position of the interleaving channels. This technique can be cascaded to produce even higher data rates provided the extinction ratio of the source is sufficient. The difficulties arise however at the receiver where these channels need to be de-multiplexed. A technique that has been the subject of much research in OTDM has been to switch pulses from these channels using a SOA-NOLM (semi-conductor optical amplifier-non-linear optical loop mirror). However stability can be a problem in such techniques. A more practical method is to use an Electro-Absorption Modulator (EAM) to create a switching window that will allow only one of the channels to pass through. This is a solid state device, which makes it more suitable for real transmission systems, and is the method used in this experiment.

Recent work has shown that it is possible to transmit data rates of 40Gbit/s (2 x 20 Gbit/s) over 8,700km without active control[152][155][156]. This was achieved using an optimised dispersion map. Distances of over 10,000km were achieved by orthogonally polarising neighbouring channels using the same dispersion map. However this dispersion map, which was optimised for a single channel, had a low map strength (less than 1) and was made up of fibres with low dispersion. Although these low local dispersions have proved effective in single channel transmission, the same distances of transmission can not be expected of multiple wavelength systems. The effect of FWM and collision induced frequency shifts can have a detrimental effect as was discussed in section 3.5. This chapter has explored experimentally the limitation of transmission of single channel 40Gbit/s pulses over standard fibre. While the transmission over standard fibre of a single channel cannot be expected to achieve the transmission distances as far as 8700km, it is known that the large local dispersions will reduce the parasitic effects of FWM and collision induced frequency shifts in WDM systems. Standard fibre also makes up a large proportion of the fibre installed in the ground today, thus this experiment will also determine the feasibility of upgrading these standard fibre(1.3μm systems) system to 40Gbit/s, and the potential for 40Gbit/s WDM systems.

A major problem that arises when moving up to 40Gbit/s, is that very short pulses are required (~5ps) to allow the interleaving of the channels. These short pulses result in a very large map strength in the presence of the high dispersion of standard fibre, and are thus

subject to large pulse breathing. Chapter 6 discussed the detrimental effects of pulse overlap on soliton-soliton interactions at 10Gbit/s. With the experiment in this chapter, this effect is expected to be more pronounced.

Recent experimental work has demonstrated that with the aid of mid span spectral inversion as dispersion compensation, distances of 186km have been demonstrated in a field trial[157] and 434km in the laboratory[158]. However numerical simulations have suggested that it is possible to transmit over 2000km of standard fibre using dispersion management[159]. This technique is entirely passive and is the method used in this chapter which will demonstrate experimentally the transmission of 40Gbit/s OTDM (4 x 10 Gbit/s 2^{31}-1 PRBS) data using RZ pulses over 1000km of standard fibre.

8.2 40GBit/s Multiplexing and De-multiplexing

The pulse source for this experiment was provided by a jitter suppressed gain switched DFB laser. This had an operating wavelength of 1557nm and provided a 10GHz pulse stream with a pulse width of 15ps FWHM (Full Width Half Maximum), the bandwidth was measured to be 0.5nm, the entire source is illustrated in Figure 8-1. The pulse stream was amplified and a 2^{31}-1 PRBS data pattern encoded onto it with a $LiNbO_3$ Mach-Zehnder modulator. The pulses were then multiplexed up to 40Gbit/s with two cascaded Mach-Zehnder interleavers. In the first Mach-Zehnder interleaver the pulses were split into two paths with a 50/50 coupler, one of the paths being longer than the other such that when they are recombined in the second 50/50 coupler the bits were 50ps out of phase. This generates a 20Gbit/s data stream at the output of the coupler. One of the output ports of this coupler supplies the pulse stream to the input of the second Mach-Zehnder interleaver. Unfortunately the power from the other output is discarded thereby incurring a 3dB power loss. In the second Mach-Zehnder interleaver, the 20Gbit/s stream is split again by another 50/50 coupler, when they are recombined the 50ps bit slots are 25ps out of phase, this produces the final 40Gbit/s data stream. Again one of the outputs of the second Mach Zehnder interferometer is discarded, thus another 3dB power loss is incurred on the pulse stream. This gives an entire loss of 6dB for the Multiplexer. The delay between the interleaved pulse streams is sufficient to provide de-correlation between the 10Gbit/s 2^{31}–1 PRBS patterns of the four channels. The pulses were then amplified before being compressed down to 5ps using 25ps/nm of dispersion compensation. This gives a 40Gbit/s data stream with a mark to space ratio of 1:5. In each stage of the multiplexer, a fibre stretcher is present, which can be used to fine tune the temporal positions of each channel. In the other arm there is a polarisation controller to allow the polarisation alignment of all the channels. A possible technique to aid the de-multiplexing process of these channels is to either, miss align one of the channels temporally within its bit slot or use unequal soliton

amplitudes[160][161]. This results in a stronger 10GHz component in the pulse stream, which can be locked to with a 10GHz Phase Lock Loop circuit and can be used to drive the 10GHz EAM, however this adds complexity to the system. In this experiment a different technique for clock recovery is used where the 10GHz signal is recovered at the output of the de-multiplexer. This means that control over the channel selection at the receiver is not possible. It is therefore essential that the polarisation and temporal alignment of the separate channels is equal to avoid any channel selection bias. Two techniques were applied to achieve this state at the output of the MUX (Multiplexer). The first method used the electrical spectrum analyser, this is polarisation insensitive and therefore ideal for aligning the channel spacing independently of the polarisation state. The highest frequency that could be monitored using the electrical spectrum analyser was 22GHz. This is too low to monitor the strength of the 40GHz component of the multiplexed signal, but is sufficient to monitor the two residual frequency components present at 10GHz and 20GHz, These components result from non-perfectly aligned channel spacing. The channel spacing were aligned to reduce these components through the delay controllers present in each stage of the multiplexer. This technique must be performed with no data on the pulse stream, since the presence of data generates many other frequency components making it difficult to observe the 10GHz and 20GHz components.

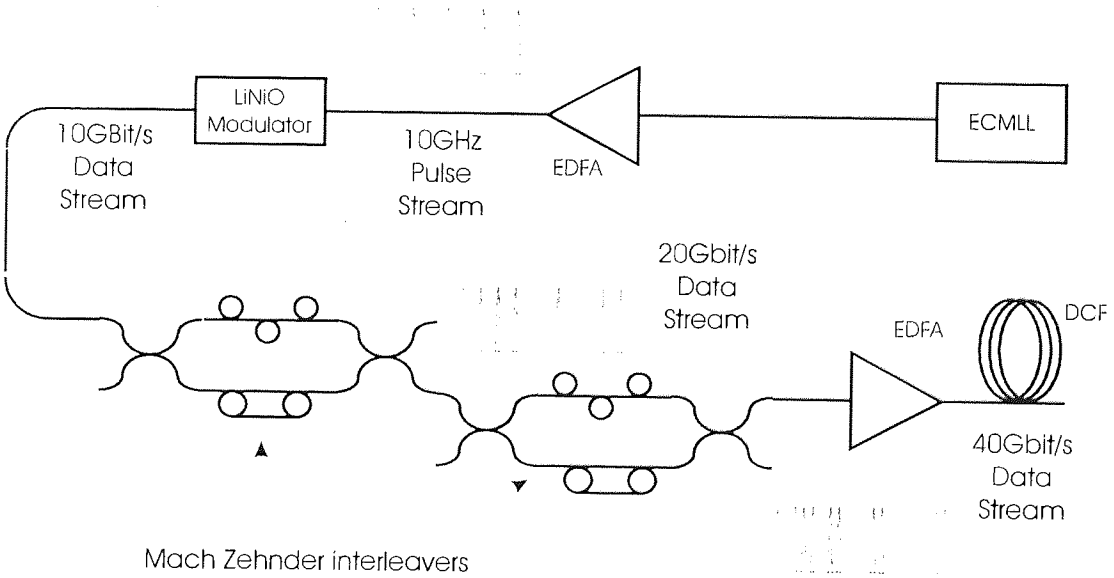

Figure 8-1 The 40Gbit/s data source. A 10GBit/s data stream is generated by Jitter suppressed gain switched DFB and 10GHz $LiNbO_3$ modulator. Conversion up to 40Gbit/s is achieved through two Mach-Zehnder interleavers.

To align the polarisation of the channels an autocorrelator was used. It is the polarisation dependence of the autocorrelator, that is essentially used to align the channels. Through the closely spaced channels at the input to the autocorrelator it is possible to observe cross-correlations. These cross-correlations appear as peaks either side of the central autocorrelation peak. For the case when the channels are not all aligned with the

autocorrelator, the peaks of the cross-correlations are lower than the autocorrelation. Such an autocorrelation trace is shown in Figure 8-2 (a).

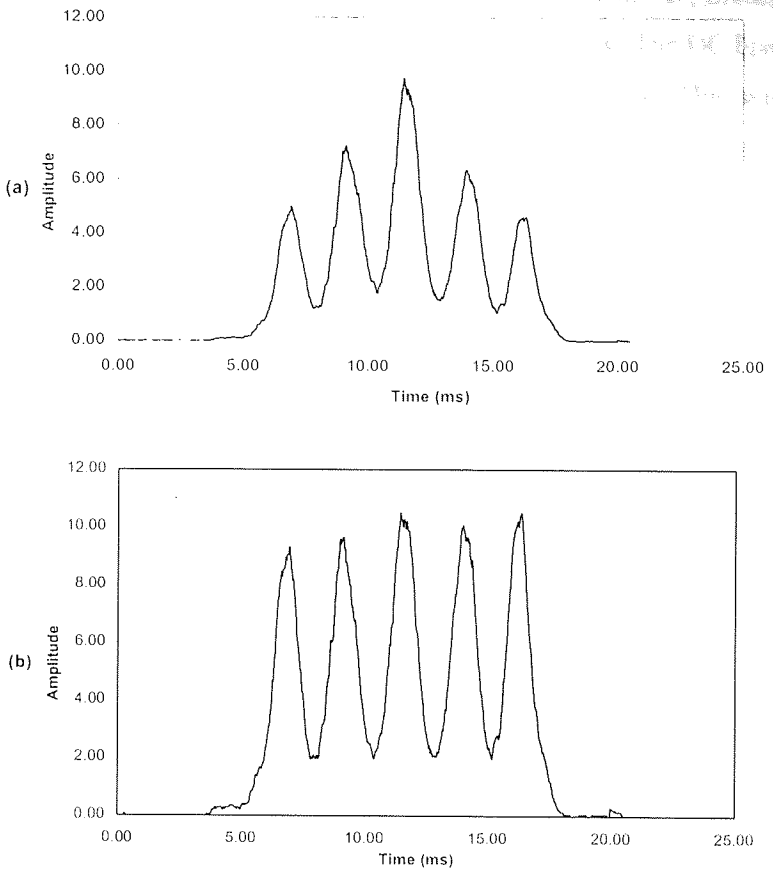

Figure 8-2 Autocorrelations of the 40Gbit/s pulse stream. (a) has channels in multiple polarisations, showing peaks of different amplitudes. The central peak represents the autocorrelation while the outer peaks represent cross-correlations with neighbouring pulses. Graph (b) shows a pulse stream of single polaristion, where cross-correlations peaks match the autocorrelation peaks

To align the channels the polarisation controllers in the two stages of the multiplexer need to be set such that all of the cross-correlation peaks on the autocorrelator are at the same height as the central peak. These peaks should also remain equal in amplitude regardless of any polarisation change at the input to the autocorrelator. This being the case, the cross-correlations will be equal to the autocorrelations, indicating that the channels are polarisation aligned. An autocorrelation trace taken from a polarisation aligned 40Gbit/s source is shown in the graph in Figure 8-2 (b). Again the polarisation optimisation needs to be performed on a pulse stream (no data) since the frequent absence of neighbouring pulses will effect the amplitude of the cross-correlation peaks in the trace.

In order to recover a 10Gbit/s data stream the 40Gbit/s pulse stream needed to be de-multiplexed. This was done with the aid of an Electro Absorption Modulator. The system is illustrated in Figure 8-3. The response of the 10GHz EAM is such that at zero voltage bias, the optical path through the EAM is low loss, and increasing the voltage increases the

absorption. In order to generate a switching window a bias 'T' was connected to the electrical input of the EAM and a DC bias applied. This DC bias sets the EAM into the high loss region, and applying an RF signal with sufficient power to the bias 'T', drives the EAM into the low loss region periodically to produce the switching window. The DC bias setting on the EAM can be used to control the width of the switching window. This window width is optimised during the propagation experiment and must be such that it will only allow one of the 10Gbit/s channels to pass through.

The recovery of the 10GHz RF component that was used to modulate the EAM was performed by a 10GHz clock recovery system. This was placed after the EAM so that it can lock onto the 10Gbit/s de-multiplexed channel. An electrical phase controller was placed between the Voltage Controlled Oscillator (of the PLL) and the EAM, which must be set so that the phase relative to the clock recovery will allow pulses to pass through the centre of the switching window. Then provided that the free running frequency of the PLL is close enough to the 10GHz component of the 10GBit/s streams, the PLL system will lock onto one of these channels. There was no control over which of the channels was selected by the de-multiplexer, but it was assumed to be a random selection from one transmission to another. This is the reason for the emphasis on the timing and polarisation alignments of the OTDM channels.

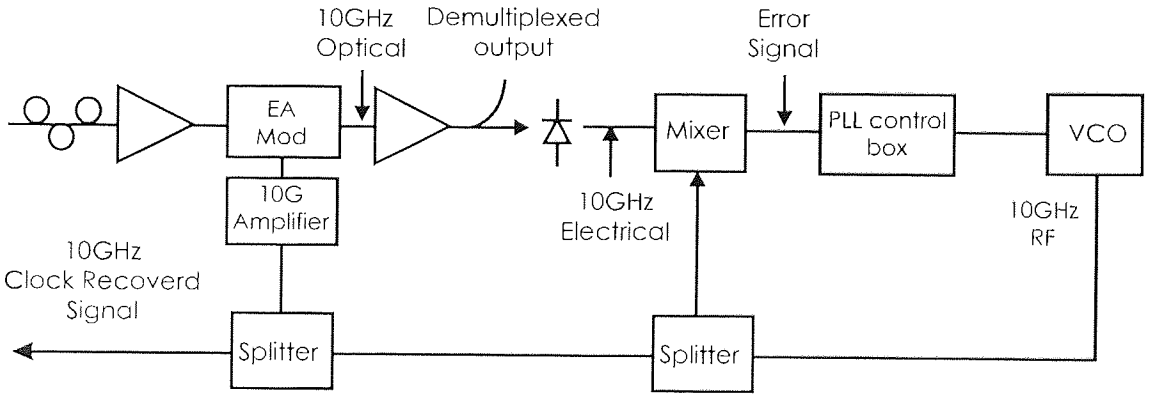

Figure 8-3 Simultaneous clock recovery and 40Gbit/s to 10Gbit/s de-multipex. The clock recovery is performed after the Electro-absorption modulator using a 10GHz phase lock loop. The demultiplexed 90% output is fed to the sampling 'scope and bit error test set.

Due to the presence of some polarisation sensitivity in the de-multiplexer a polarisation controller was placed at the input to allow optimisation during propagation. The output of the VCO was split three times providing the 10GHz electrical signal for the mixer in the PLL, the amplifier at the input to the EAM and the trigger signal for the Bit Error Test Set and sampling 'scope. Figure 8-4 shows three sets of eyes taken using a 20GHz photodiode on the sampling oscilloscope. (a) represents the direct output from the data source at 10Gbit/s, (b) the pulses after they are multiplexed up to 40Gbit/s. This traces show pulses of equal spacing

and equal amplitude, indicating that a good 40Gbit/s pulse data stream has been achieved, which is essentially preventing any channel selection bias occurring in the de-multiplexer. Trace (c) of the de-multiplexed 10Gbit/s channel shows no presence of any of the other channels reaching the receiver. The limited response of the photo-diode hides the true mark to space ratio, which at this point is 1:20. The small oscillations present on the tail of the pulses is due to the frequency characteristics of the photodiode and is a characteristic of both the source and de-multiplexed eyes alike.

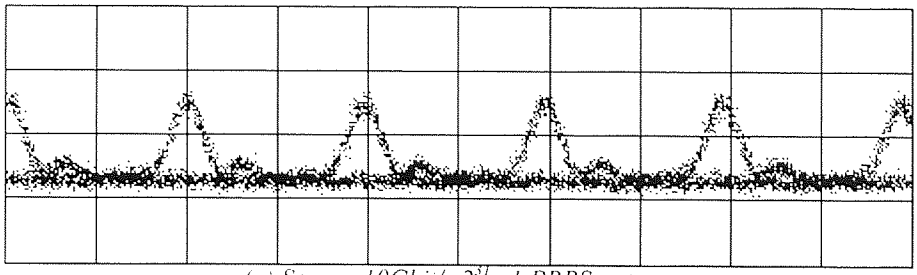

(a) Source 10Gbit/s $2^{31}-1$ PRBS pattern

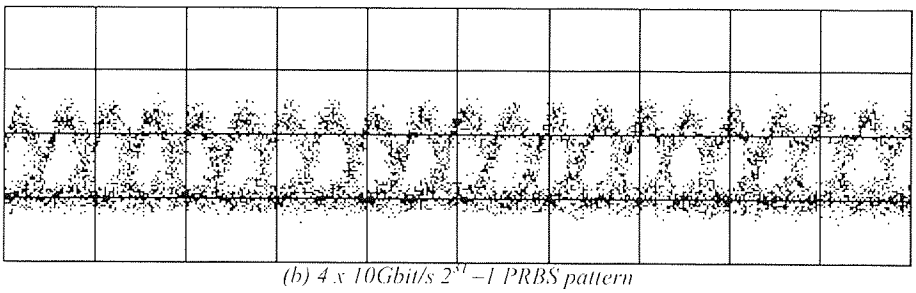

(b) 4 x 10Gbit/s $2^{31}-1$ PRBS pattern

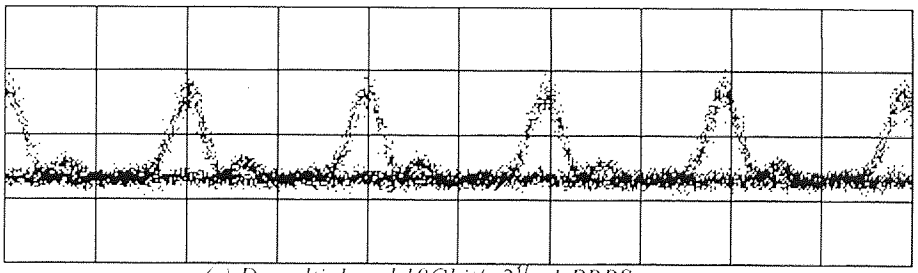

(c) Demultiplexed 10Gbit/s $2^{31}-1$ PRBS pattern

Figure 8-4 Three eyes showing the pulses before multiplexing 10Gbit/s, (a) before multiplexing, (b) after being multiplexed up to 40Gbit/s (4 x 10Gbit/s $2^{31}-1$ PRBS). The final trace (c) is taken after the de-multiplexer and shows one of the de-multiplexed 10Gbit/s channels.

8.3 40Gbit/s transmission

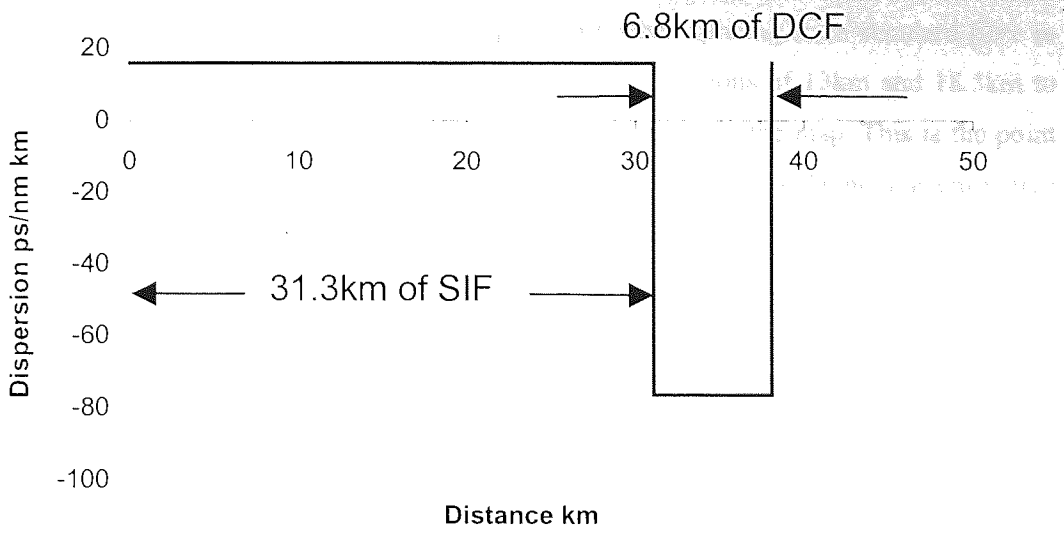

Figure 8-5 The dispersion map consisting of 31.3km of standard fibre with a dispersion of 16.5ps/nm km and 6.8km of DCF with a dispersion of –75.6ps/nm km giving a total length 38.1km.

The dispersion map used was 38.1km in length and consisted of 31.3km of standard fibre. At the wavelength of operation this had dispersion of 16.5ps/nm km. The remaining 6.8km consisted of dispersion compensating fibre with a dispersion of –75.6ps/nm km, producing a dispersion map as illustrated in Figure 8-5.

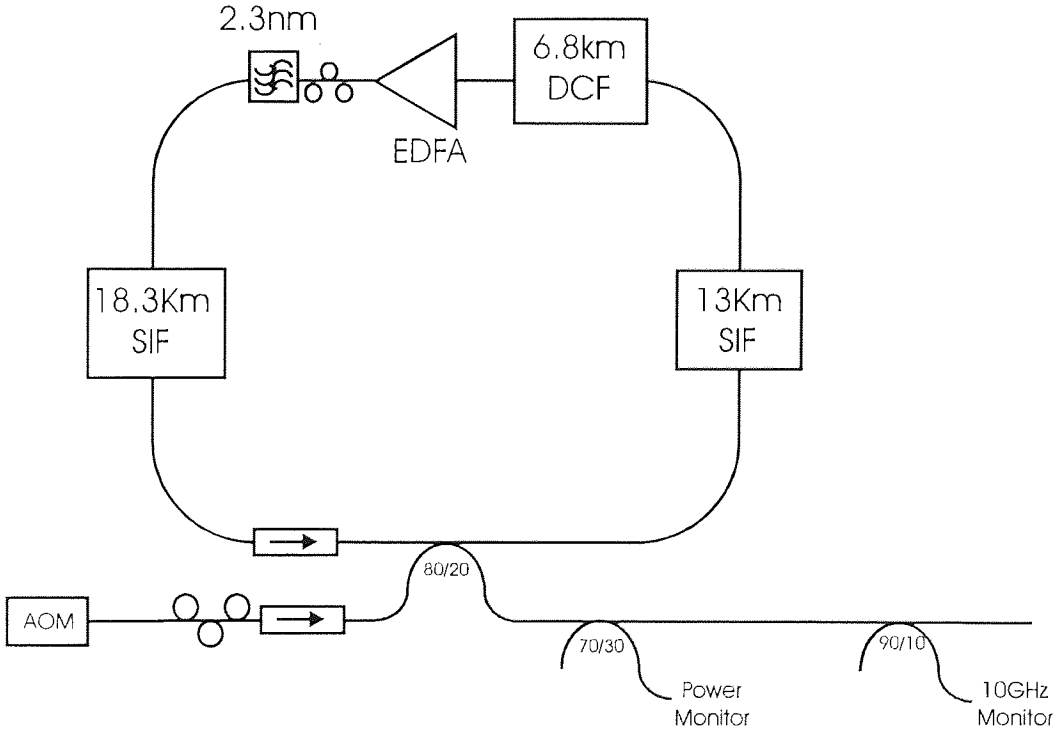

Figure 8-6 The experimental setup, containing 31.3km of SIF of which 13km was a half step and 6.8km of DCF. The Erbium doped amplifier compensates for 15.3dB loss of the loop. The 2.3nm filter provided a degree of wavelength guiding.

The fibre was set-up within the loop as shown in Figure 8-6. The total round trip loss was measured to be 15.3dB with the standard fibre contributed to 6.8dB of the loss. The DCF had a total loss of 4.2dB including the extra splice loss when splicing from standard fibre to DCF and vice versa. The standard fibre was split into two sections of 13km and 18.3km to provided a launch point close to the transform limited point within the map. This is the point where the pulses are at their minimum width and therefore ideal for launching chirp free pulses. The 80/20 launch/detect coupler provided 20% launch power into the loop and 20% power released from the loop (1dB loss) each round trip. This released power was split by a 70/30 coupler, of which the 70% output was split again by a 90/10 coupler. The 90% was fed through an Erbium Doped Fibre Amplifier (EDFA) before being fed into the de-multiplexer. Due to power constraints of the EAM this EDFA was set to give an output power no greater than 1dBm. The remaining 10% and 30% outputs provided monitoring points during transmission. The loop EDFA, which compensated for the entire loss of the loop (with a gain of 15.3dB), was positioned at the end of the SIF. A 2.3nm filter, a polarisation controller and 5% coupler were placed at the output of the EDFA. The broad spectrum of the source meant that the signal bandwidth relative to the filter bandwidth was 1:5 which is relatively low (typical the ratio is 1:10). This means that the filter provided some degree of wavelength guiding which is known to reduce Gordon Haus Jitter. The isolator before the coupler accounted for the remaining 0.7dB loss of the loop. Its purpose was to prevent any counter-propagating ASE travelling around the loop. The isolator at the output of the AOM also prevented any reflections from the AOM travelling into the loop. The dispersion zero was measured and found to be at 1556nm. The DCF provided a partial slope compensation for the standard fibre resulting in a combine dispersion slope of $0.03ps^2/(nm\ km)^2$. This gives a dispersion of 0.03ps/(nm km) at the wavelength of operation.

The pulses were gated into the loop through the launch coupler using the AOM and were propagated around the loop until the required distance of transmission had been reached. A further 30μs was allowed before the BERTS and sampling 'scope were set to take measurements for the remaining duration of recirculation. The extra 30μs is to allow the BERTS to synchronise its internal pattern with that received from the loop. In order to repeat this transmission and take more samples, the propagating signal within the loop was removed by terminating the amplifier within the loop. The amplifier is then re-pumped to allow the transmission to be repeated. The polarisation controllers at the input to and within the loop were optimised for maximum error free propagation. The de-multiplexer was optimised through a polarisation controller on its input and through the width of the switching window controlled by the EAM DC bias.

8.3.1 Transmission over 1000km of standard fibre

Error rate measurements were recorded using the bit error test set at the output of the de-multiplexer. These error rate measurements were recorded after various transmission distances and are shown in Figure 8-7.

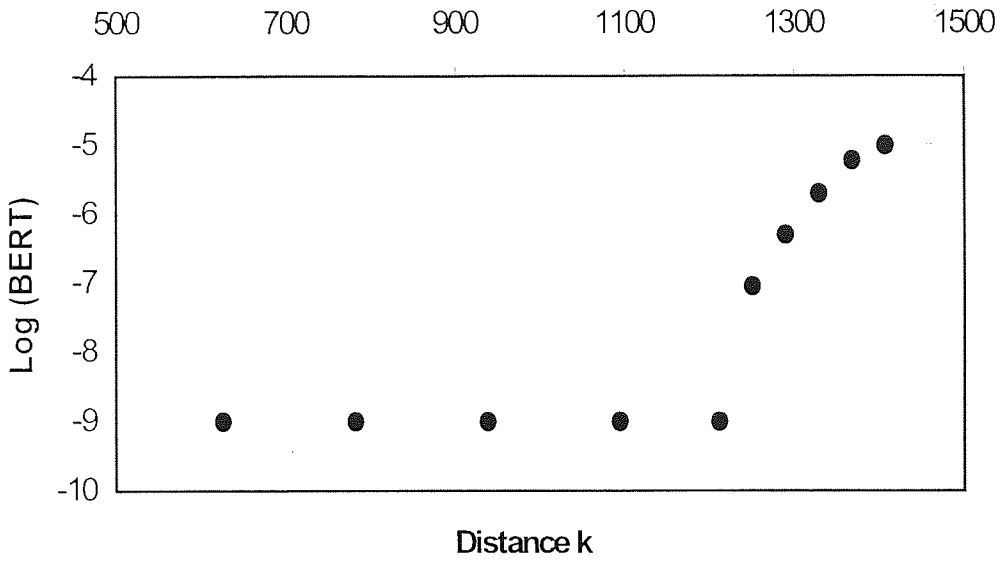

Figure 8-7 bit error rates vs distance for the 40Gbit/s (4x10Gbit/s 2^{31}-1 PRBS) showing a maximum distance of 1,220km for error free transmission.

The results show the maximum distance of error free transmission to be 1,200km. Taking into account the portion of DCF in the loop, this corresponds to 1,000km of standard fibre. The average peak pulse power during transmission was found to be 8.8mW. Comparing this with the average peak power of the equivalent uniform system, which would be 4.2mW, shows that the power enhancement factor is 2 for this system. This is lower than would typically be required for a strong dispersion managed system. However stable transmission was achieved over 1254 dispersion lengths showing that a new stable regime between the dispersion and non-linearity has been found. Due to the limitations of the amplifier power within the loop it may not have been possible to operate at the expected higher powers required for the power enhanced dispersion managed system. The optimised switching window for the de-multiplexer was found to be between 12 and 17ps. This was optimised to be wide enough to allow sufficient power through, but narrow enough to provide extinction of the neighbouring channels.

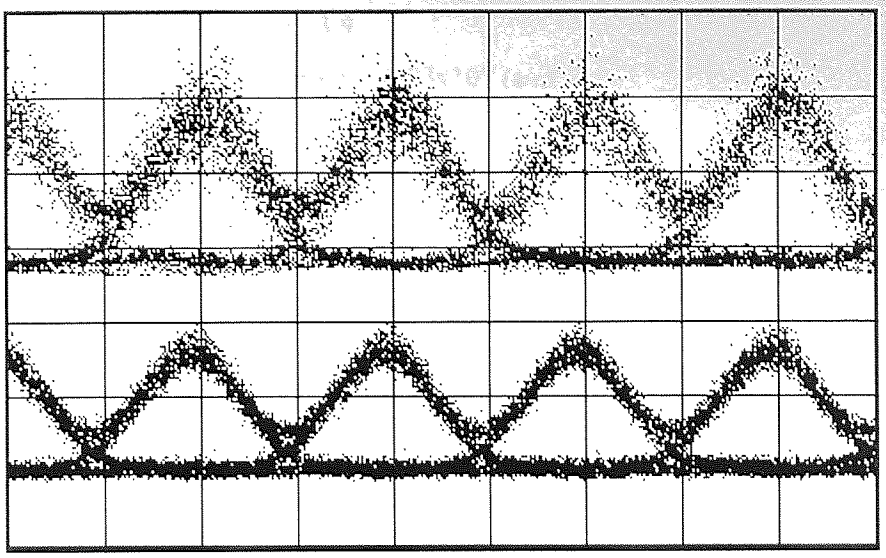

Figure 8-8 Two eye diagrams. Taken after 1220km of transmission and taken at the back to back point out of the de-multiplexer.

Figure 8-8 Shows two eye diagrams taken at the output of the de-multiplexer after a transmission distance of 1,200km (the maximum error free distance) and at the output of the de-multiplexed before transmission. The eye diagram after transmission shows an open eye still present after 1,200km. The lack of noise present in the base of the eye indicates that the system is not limited by noise. However there is a large degree of jitter present on the pulses, which is the limiting factor of this system. Whether the jitter present in the eye is due to timing jitter or amplitude jitter on the pulses is not clear from this eye diagram, since it is taken from the output of the de-multiplexer.

Taking the maximum tolerable timing jitter is 1.5ps, and the Gordon Haus Jitter for an unfiltered system to be

$$\left\langle t_N^2 \right\rangle = \frac{2\pi n_2 N_{sp} |\beta_2| hc(G-1)L^3}{9\tau_0 \lambda^2 A_{eff} L_a \Lambda_0^2}$$

Equation 8-1

where the values used for this calculation are

n_2	=	2×10^{-20}
N_{sp}	=	2
λ	=	1550×10^{-9} (m)
L_a	=	38.1×10^{3} (m)
H	=	6.67×10^{-34}
C	=	3×10^{8} (m)
A_{eff}	=	50×10^{-12} (m^2)
τ_0	=	$\tau_{fwhm}/1.763 = 2.8\times10^{-12}$

$G = 10^{15.3/10} = 33.9$

$D_2 = 0.03\text{ps/nm km} = 0.03\text{x}10^{-6}\ (\text{s/m}^2)$

$$\beta_2 = -\frac{\lambda^2}{2\pi c} D_2 = \frac{\left(1550x10^{-9}\right)^2}{2\pi x 3x10^8} 0.03x10^{-6} = 3.8x10^{-29}$$

$$\Lambda_0^2 = \frac{G\ln(G)}{G-1} = 3.57$$

Thus at a distance of 15,000km t_N^2 is found to be

$$\left\langle t_N^2 \right\rangle = \frac{2\pi \cdot 2 \cdot \left(3.8x10^{-29}\right) \cdot 2x10^{-20} \cdot 6.67x10^{-34} \cdot 3x10^8 \cdot (33.9-1)}{9 \cdot 2.8x10^{-12} \cdot \left(1550x10^{-9}\right)^2 \cdot 50x10^{-12} \cdot 38.1x10^3 \cdot 3.57} \cdot (15x10^6)^3 = 5.2x10^{-22}$$

It is also necessary to include the reduction factor for the Gordon Haus jitter due to the filter, which is given as

$$f(x) = \frac{3}{2}\frac{1}{x^3}\left[2x - 3 + 4\exp(-x) - \exp(-2x)\right]$$

Where x is given as

$$x = 4\delta Z = \frac{4L}{3\left(2\pi\Delta\lambda_f \tau_0\right)^2 L_a} = \frac{4 \cdot 15x10^6}{3 \cdot \left(2\pi \cdot 2.87x10^{11} \cdot 2.8x10^{-12}\right)^2 \cdot 38.1x10^3} = 20.6$$

Where $\Delta\lambda_f$ is the bandwidth of the filter and is given as

$$\Delta\lambda_f = \frac{c}{\lambda^2}\Delta\lambda = \frac{3x10^8}{\left(1550x10^{-9}\right)^2} 2.3x10^{-9} = 2.87x10^{11}$$

The value of $f(x)$ for a given distance L=15,000km is

$$f(x) = \frac{3}{2} \cdot \frac{1}{(20.6)^3}\left[2 \cdot 20.6 - 3 + 4\exp(-20.6) - \exp(-2 \cdot 20.6)\right] = 7x10^{-3}$$

The power enhancement must also be taken into account, which is seen as a multiplying factor of the Λ_0^2 term seen on the denominator of Equation 8-1. The average peak power of the soliton in a uniform system is given as

$$P_0 = \frac{|\beta_2|}{\gamma\tau_0^2} = \frac{3.8x10^{-29}}{1.5x10^{-3} \cdot \left(2.8x10^{-12}\right)^2} = 3.2mW$$

Where γ is taken to be $1.5\text{W}^{-1}\text{km}^{-1}$. The average peak power in the experiment was found to be 8.8mW, which gives a power enhancement of 2.75. Therefore the full Gordon Haus jitter calculation for this distance is

$$\left\langle t_N^2 \right\rangle_{GHJ-filterd} = \left\langle t_N^2 \right\rangle_{GHJ} \cdot f(x) \cdot \frac{1}{power\_enhancement} = 5.2x10^{-22} \cdot 7x10^{-3} \cdot \frac{1}{2.75} = 1.34x10^{-24}$$

$$r.m.s\_jitter = \sqrt{1.34x10^{-24}} = 1.1ps$$

Therefore it can be concluded that at 1,200km Gordon Haus Jitter is not the limiting factor. The limit of the Signal to Noise ratio for this system can be calculated from

$$SNR = \frac{S_0}{4N_a(G-1)\mu h \upsilon \Delta v}$$

Where for a bit error rate of less than 10^{-9} the SNR_{dB} must be greater than 21.6dB. This evaluates to

$$SNR = 10^{\frac{21.6}{20}} = 12$$

Taking Δv to be the bandwidth of the signal, which for 0.5nm corresponds to 62GHz, and taking v to be the signal frequency, which is 1.9×10^{14}Hz. The average power out of the amplifier is (S_0) 3.2mW

μ = 2

h = 6.67×10^{-34}

S_0 = 3.2mW

N_a = L_a/L

Substituting in for N_a and rearranging for L the equation becomes

$$L = \frac{L_a \cdot S_0}{4N_a(G-1)\mu h\nu \cdot \Delta v \cdot SNR}$$

This evalutates to

$$L = \frac{38.1x10^3 \cdot 3.2x10^{-3}}{4 \cdot (33.9-1) \cdot 2 \cdot 6.67x10^{-34} \cdot 1.9x10^{14} \cdot 62x10^9 \cdot 12}$$

$$L = 4{,}575km$$

This indicates that the signal to noise ratio is not the limiting factor. Again this distance is in excess of that achieved in the experiment. However such is the strength of this map that other effects such as soliton-soliton interaction due to pulse breathing may be having an effect on the pulses such as those observed in chapter 6, and are probably the limiting factor.

8.3.2 Investigation of launch the position

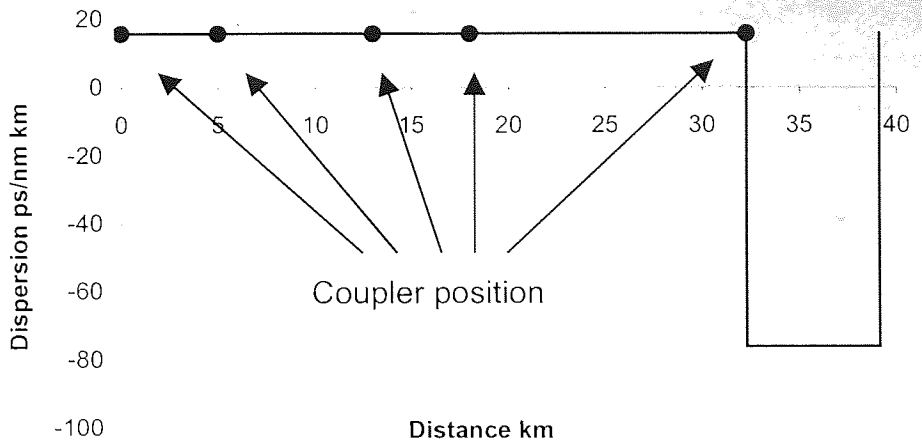

Figure 8-9 The different positions of the loop (launch and detection) coupler within the SIF. The distances were 0km, 5km, 13km, 18km, and at the end of the SIF.

When using a dispersion map the effect of launching at the incorrect launch point results in dispersive waves being irradiated by the pulses. This happens as the solitons evolve to achieve the balanced pulse breathing within the map that is normally associated with the stable dispersion managed solitons. In this section the position of the launch-detect coupler is investigated to show that an optimum launch point lies near the mid point of the standard fibre section. The position of the launch detect coupler was moved to several different points within the standard fibre, these were 0km (beginning of standard fibre), 5km, 13km, 18km and at the boundary point after the standard fibre. These points are shown in Figure 8-9. For each position the system was optimised for maximum error free transmission and the distance recorded. The results are shown in the graph in Figure 8-10.

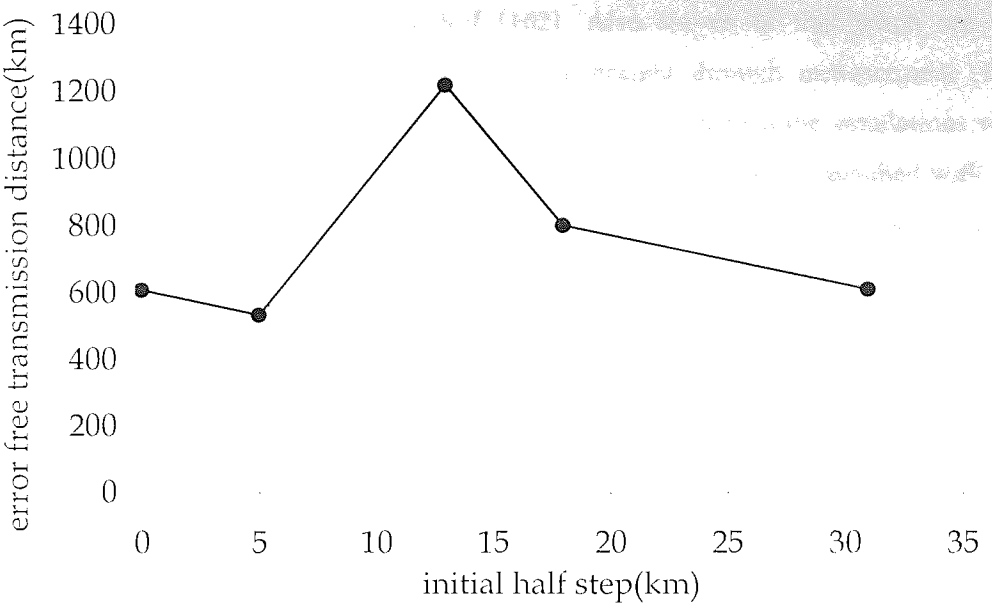

Figure 8-10 Maximum distance of transmission vs launch/detection point within the standard fibre. The Maximum distance peaks near the mid-point .

The optimum launch point is found to be close to the mid-point of the SIF (the transform limited point), as would be expected from a dispersion managed soliton like system. The maximum error free distance was recorded at 1,200km of transmission. Moving the launch and detect point away from the transform-limited point within the standard fibre results in a reduction of the maximum error free transmission distance. This shows that although the pulse powers are lower than would normally be expected of a dispersion managed system, non-linearity still plays a part in these pulses.

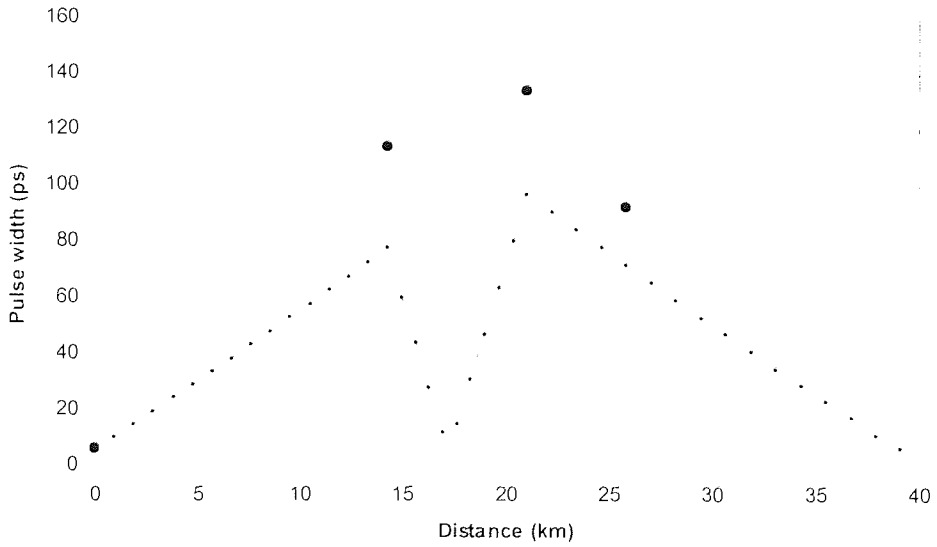

Figure 8-11 Simulations of pulse width vs position within the dispersion map. The black circles represent the measured pulse widths from a straight through transmission

The graph in Figure 8-11 shows simulations of the FWHM pulse width with position within the dispersion map provided by Ref [162]. Also shown in this graph are the experimentally recorded pulse widths, taken from a straight through measurement (first recirculation of the loop). This shows that the pulse widths greater than the simulations with FWHM as broad as 135ps. These were taken for ideally launched pulses, launched with the chirp matched to launch point within the map, and shows the importance of the detection position within the map. The two minimum pulse width positions can be observed near the mid-point of the SIF and near the mid-point of the DCF. De-multiplexing at a point away from these transform limited locations would result in broader pulses at the receiver. The further away from these points the receiver is located the broader the pulses will be. This would result in a penalty at the receiver due to intersymbol interference. At the boundary points within the map the pulse have broaden to a FWHM greater 125ps. Thus the FWHM of the pulses can span as many as five bit slots. The peak powers at these points will also be reduced since the energy is spread over a longer period of time.

8.4 Conclusions

The experiment in this chapter has successfully demonstrated the error free transmission of a 40Gbit/s data stream, which consisted of four 10Gbit/s channels encoded with a 2^{31}-1 PRBS pattern and multiplexed up to give a 40Gbit OTDM data stream. The polarisations of all four channels were aligned to give single polarisation transmission and therefore not utilising the advantages of polarisation multiplexing. The maximum distance of transmission achieved was 1,200km, which corresponds to 1,000km of standard fibre. This is the furthest distance of transmission over standard fibre at 40Gbit/s to date, and is a sufficient distance for any terrestrial point to point link. The technique used to overcome the large dispersion was entirely passive requiring no in-line active control. The high local dispersions in this system are particularly attractive for WDM transmission, since it is known that high local dispersion reduces the detrimental effects of FWM and residual frequency shifts due to the power variant inter channel pulse collisions. The use of these higher data rates and less WDM channels may give rise to greater spectral efficiency by reducing the redundancy associated with the channel separation. Less WDM channels will also be an advantage when concerned with the complexity and cost of system management. The average pulse powers used in transmission was twice that required in the equivalent uniform soliton system. This is not the power enhancement that would normally be expected from a very strong dispersion managed system. Never the less pulses were shown to be stable over 1254 dispersion lengths, and therefore concluding that a new stable operating regime has been found in this very strong map. The maximum distance of transmission falls short of the limit calculated for the

GH jitter and also falls short of that calculated for the SNR. The limitation of this system is therefore thought to be down to the pulse interaction (possibly through XPM) that occurs when pulses overlap during the breathing cycle. The large amount of breathing (greater than 100ps) results in the overlap between pulses spanning more than four bit slots. The fact that the system shows no sign of noise limitation leads to the conclusion that there is scope for increasing the amplifier span. This would reduce the number of amplifiers that would be required for installation in a system and thus lower the cost.

Chapter 9

Conclusion

Prior to the experimental chapters of this thesis, the concept of soliton transmission was introduced. Chapter 3 introduced dispersion management and the benefits applicable to both single channel and WDM transmission and Chapter 4 discussed the experimental techniques applied to chapters 5, 6, 7 and 8. The majority of the experiments in this thesis were focused on soliton transmission over standard fibre at 1.55μm. Standard fibre has the advantage of being simple to manufacture compared with the more complex fibre type such as dispersion shifted fibre (DSF) and large effective area fibre (LEAF). This promotes standard fibre as a cost-effective medium for transmission. The high dispersion at 1.55μm was compensated for by lumped dispersion compensating fibre, creating a two step dispersion map. While these experiments demonstrate the viability of upgrading currently installed 1.3μm systems to higher data rates, there are several desirable characteristics that also promote standard fibre systems as viable for the future installation of transmission links. Although such standard fibre systems are not the optimum systems for maximum transmission of a single channel system, there are several other benefits that lend these systems to WDM transmission. Chapter 5 of this thesis demonstrated the de-coupling between path average dispersion and the soliton pulse power, giving near constant pulse powers across a range of dispersions. The map strengths used in this experiment were sufficiently high enough to give stable pulse powers on the dispersion zero and into the normal dispersion regime. This near constant soliton power with respect to dispersion is very desirable for WDM systems, since it reduces the power variance between channels near dispersion zero. The dispersion compensating fibre used in this experiment also provided partial dispersion slope compensation of the standard fibre. The resultant slope was found to be 0.03ps/nm km. With this slope error free propagation over 10,000km was observed over a range of 10nm (from –0.1ps/nm km to 0.2ps/nm km) using a simple fixed 10GBit/s data pattern, beyond this range of dispersions the transmission was limited to less than 10,000km by Gordon Haus Jitter. With a greater degree of slope compensation the wavelength range can be greatly increased to extend over the erbium bandwidth. The limiting effects of Four Wave Mixing (FWM) and collision induced frequency shifts in WDM systems are also significantly reduced in strong dispersion managed systems. The high local dispersion prevents the phase matching condition required to generate

efficient for FWM components. The large alternating signs of dispersion cause repeated collision to take place between pulses from different channels. This has been shown to have the positive effect of reducing the collision induced frequency shifts.

An unfortunate consequence of the large pulse breathing that takes place within these strong dispersion maps is the increased soliton-soliton interactions. Chapter 6 investigated this effect and demonstrated that in the particular system used that soliton-soliton interactions were the limiting factor in error free transmission. The effect manifests itself as a pulse distortion due to the overlap between breathing solitons. This chapter also addressed this problem and demonstrated that these interactions can be suppressed to a degree by optimising the amplifier position within the dispersion map. Conveniently the optimum position of the amplifier was found to be at the boundary after the dispersion compensating module. This position is ideal for the upgrade of old standard fibre systems, since the DCF and amplifier can be inserted as one module periodically along the transmission line. This position also reduces the complexity of installing new transmission systems. The maximum distance of error free transmission with a 2^{31}-1 PRBS pattern was 16,500km, which is the greatest distance achieved over standard using any modulation format. This distance is in excess of that that would be required for a Trans-oceanic system, thus showing that there is a degree of robustness of this system that there is potential for greater amplifier spans or higher data rates. The conclusion from these two experimental chapters is that standard fibre offers a viable medium for which to transmit dispersion managed solitons over transoceanic distances at 10GBit/s. The strong dispersion management will ensure that the parasitic effects of WDM transmission are kept to a minimum.

Despite the greater margin of error with soliton transmission over linear RZ and NRZ systems, their remains a significant opposition to soliton format. This is due to the greater spectral width of solitons compared with RZ and NRZ formats, which in turn requires greater channel spacing and less efficient use of the available bandwidth. The important factor that may eventually bring about the application of solitons in commercial systems is the problem of non-linearity. RZ and NRZ are linear formats and must avoid the non-linearity of the fibre by limiting the power in the transmission line. The development of new erbium band (at 1460nm-1520nm and 1570nm-1610nm) continues to extend the available bandwidths and increase the number of channels that can be supported. However due to the effects of XPM there will be a limit on the maximum power in the transmission line, and the addition of extra channels will require the power in each individual channel to be reduced. Eventually the limit of signal to noise ratio will prevent the power being reduced any further, and place a limit on the maximum number of channels that can be used. It is in this situation that solitons may have major advantage. Soliton, unlike linear RZ and NRZ do not suffer the same penalty of non-linearity. Provided that the FWM and collision induced frequency shifts are suppressed

by dispersion management, soliton from different channels can collide and emerge without any detrimental effects. This will enable the power in each individual channel to be independent of the total number of channels in the system. Until this limitation has been reached, the spectral efficiency of solitons will continue to be a limiting factor.

Improvement of this spectral efficiency may by achieved by operating systems with few channels at high data rates. Chapter 8 of this these focussed on the error free transmission of 40GBit/s data stream (4x10Gbit/s OTDM 2^{31}-1 PRBS pattern) using the same standard fibre system used in Chapter 5 and Chapter 6. The maximum transmission distance achieved was 1220km or 1000km of standard fibre. This is the greatest transmission distance to date over standard fibre at 40Gbit/s, and is sufficient for any terrestrial point to point link. The map strength calculated for this system was very large, however the power enhancement factor was approximately 2. This is considerably less than would be expected from a strong dispersion managed system, nevertheless the pulses showed stable transmission over many dispersion lengths concluding that a new stable regime had been found between dispersion and non-linearity. The large map strength resulted in a large pulse breathing within the map. At the broadest within the map the pulse widths were measured to be 135ps. Comparing this with the bit window of 25ps shows that the detection point within the map is crucial in avoiding intersymbol interference. As with the 10Gbit/s system this system should also support WDM at this data rate with only a small penalty due to FWM and collision induced frequency shifts. The smaller number of channels required compared with a 10GBit/s system should reduce the spectral redundancy due to channel spacing. The reduced number of channel will also simplify the management of such systems.

Chapter 7 investigated a novel technique of saturable absorption in a dispersion managed soliton system. The majority of the fibre in this experiment was dispersion shifted, and therefore not directly relevant to the standard fibre systems discussed previously. The saturable absorption was achieved though the action of non-linear polarisation rotation and a polarisation dependent loss element. The polarisation dependence of this technique makes it inappropriate for a practical transmission system, however it is used here as proof of principle. The maximum error free transmission distance achieved with this technique at 10GBit/s was 200,000km, which far in excess of any other distance achieved without inline control. This ultra long distance is due to the guiding effect of the filter reducing the Gordon Haus jitter, and the noise suppression of the saturable absorption. The saturable absorption also provided pulse shaping and the suppression of dispersive waves. The pulse widths generated in this system were 4ps at the transform-limited point, giving a mark to space ratio of 1:25. The spectral width of the solitons during transmission was 1.1nm, giving a time bandwidth product of 0.55. This is not only greater then the 0.32 associated with the uniform system but is also greater than the 0.44 associated with the Gaussian pulse. This greater time

bandwidth product indicates a poor spectral efficiency compared with the uniform and dispersion managed soliton. However the distances achieved at 10GBit/s were far in excess of what is required for any global transmission link. With this mark to space ratio and low jitter, the prospect of transmission at 40GBit/s over distances of greater than 20,000km is feasible. Saturable absorbers have shown improved transmission in simulation and experiments alike. However the practical realisation of these systems will depend on the development of suitable high-speed low switching power quantum well saturable absorbers, To provide polarisation independent saturable absorption. The application of these devices could be also extended to WDM transmission systems with the aid of a WDM coupler to separate channels prior to saturable absorption.

References

[1] John M. Senior. Optical Fiber Communications, Principles and practice (second edition) Chapter 2 pp61 Prentice hall (1992)

[2] Govind P.Agrawal, Nonlinear Fiber Optics (Second Edition) Chapter 1 pp3-4 Academic Press (1995)

[3] John M. Senior. Optical Fiber Communications, Principles and practice (second edition) Chapter 3 pp91 Prentice hall (1992)

[4] T. Miya, Y. Teramuna, Y. Hosaka and T. Miyashita, Ultra low-loss single-mode fibre at 1.55μm. ELECTRONICS LETTERS Vol 15, No 4 pp106-108, (1979)

[5] Govind P.Agrawal, Nonlinear Fiber Optics (Second Edition) Chapter 1 section 1.2.3 p7 Academic Press (1995)

[6] John M. Senior. Optical Fiber Communications, Principles and practice (second edition) Chapter 2 pp67 Prentice hall (1992)

[7] John M. Senior. Optical Fiber Communications, Principles and practice (second edition) Chapter 2 pp65 Prentice hall (1992)

[8] L. B. Jeunhomme, Single-Mode fiber Optics, Marcel Dekker Inc.,1983.

[9] John M. Senior. Optical Fiber Communications, Principles and practice (second edition) Chapter 3 pp131 Prentice hall (1992)

[10] Govind P.Agrawal, Nonlinear Fiber Optics (Second Edition) Chapter 1 pp15-17 Academic Press (1995).

[11] Govind P.Agrawal, Nonlinear Fiber Optics (Second Edition) Chapter 1 section 1.2.4 p13 Academic Press (1995)

[12] E. Desurvire, J.r. Simpson and P. C. Becker. High gain erbium-doped traveling-wave amplifier. OPTICS LETTERS, VOL. 12, NO. 11 pp888-890 (1987)

[13] B. Clesca, D. Bayart, L. Hamon, J. L. Beylat, C. Coeurjolly, and L. Berthelon, Over 25-nm, 16-Wavelength-multiplexed signal amplification through fluoride-based fiber-amplifier cascade. ELECTRONICS LETTERS, Vol 30,No 7, pp586 (1994)

[14] Ju Han Lee, Uh-Chan, and Namkyoo, Improvement of 1.57~1.61μm Amplification Efficiency by Recycling Wasted Backward ASE through the Unpumped EDF Section. Technical digest of Optical fibre conference, San Diego (1999)

[15] J. Kani and M. Jinno. Wideband and flat-gain optical amplification from 1460 to 1510nm by serial combination of thulium-doped fluoride fibre amplifier and raman fibre amplifier. ELECTRONICS LETTERS, Vol 35, No 12, pp1004-1006 (1999)

[16] A. M. Vensarkar, J. R. Pedrazzani, J. B. Judkins, P. J. Lemaire, N. S. Bergano, and C. R. Davidson, OPTICS LETTERS Vol 21, pp336 (1996)

[17] P. C. Becker, N. A. Olsson, and J. R. Simpson. Erbium-Doped Fiber Amplifiers (Fundamentals and Technology), Academic Press, San Diego, pp59-60 (1999)

[18] F. Matera and M. Settembre. Comparison of the performance of optically amplified transmission systems. IEEE JOURNAL OF LIGHTWAVE TECHNOLOGY, Vol 14, No 1, pp1-12 (1996)

[19] M. Nakazawa, E. Yamada, H. Kubota, Y. Yamamota, and A. Sahara. Numerical and experimental comparison of soliton, RZ Pulse and NRZ pulses under two step dispersion allocation. ELECTRONICS LETTERS, Vol 33, No 17, pp1480-1482 (1997)

[20] L.F. Mollenauer, K. Smith and J. P. Gordon Resistance of soliton to the effects of polerization dispersion in optical fibres. OPTICS LETTERS, VOL. 14, NO. 21 (1989)

[21] F. M. Knox, W Forysiak and N. J. Doran. 10-Gbit/s Soliton Communication Systems Over Standard Fiber at 1.55μm and the Use of Dispersion Compensation. JOURNAL OF LIGHTWAVE TECHNOLOGY, Vol 13, No 10, pp1955-1962(1995)

[22] W. Forysiak and N. J. Doran. Reduction of Gordon-Haus jitter in soliton transmission systems by optical phase conjugation. JOURNAL OF LIGHTWAVE TECHNOLOGY. Vol 13, No 5, pp850-855 (1995)

[23] S. Watanabe, T. Naito, and T. Chikama. Compensation of chromatic dispersion in a single mode fibre by optical phase conjugation. IEEE PHOTONICS TECHNOLOGY LETTERS, Vol 5, No 1, pp92-95 (1993)

[24] M. F. C. Stephens, D. Nesset, K. A. Williams, R. V. Penty, I. H. White, and M. J. Fice. Dispersion compensation at 40Gbit/s over 100 km of standard fibre via mid-span spectral inversion in semiconductor optical amplifier with integrated pump laser ELECTRONICS LETTERS, Vol.35, No.16, pp.1359-1361 (1999)

[25] X. P. Zhang, B. F. Jorgensen. Maximum transmission distance for a 10 Gbit/s signal transmission over nondispersion shifted fibre using mid-span spectral inversion. ELECTRONICS LETTERS, Vol.32, No.8, pp.752-754 (1996)

[26] J. A. R. Williams, L. A. Everall, I. Bennion and N. J. Doran. Fibers Bragg Grating Fabrication for dispersion compensation. IEEE PHOTONICS TECHNOLOGY LETTERS, Vol 8, No 9, pp1187-1189 (1996)

[27] B. J. Eggleton,T. Stephens, P. A. Krug, G. Dhosi, Z. Brodzeli and F. Ouellette. Dispersion compensation using a fibre grating in transmission. ELECTRONICS LETTERS, Vol 21, No 7, pp1610-1611 (1996)

[28] B. Gisin and N. Gisin. Transmission gratings for chromatic dispersion compensation. OPTICS LETTERS, Vol 21, No 9, pp686-688 (1996)

[29] E. Yamada, H. Kubota, T. Yamamoto, A. Sahara, M. Nakazawa 10Gbit/s, 10600km, dispersion-allocated soliton transmission using conventional 1.3um singlemode fibres ELECTRONICS LETTERS, Vol.33, No.7, pp.602-603 (1997)

[30] R. J. Nuyyts, Y. K. Park and P. Gallion Performance improvement of 10Gbit/s standard Fiber Transmission Systems by Using the SPM Effect in the dispersion Compensating Fiber. IEEE PHOTONICS TECHNOLOGY LETTERS, Vol 8, No 10, pp1406-1408 (1996)

[31] P. Harper, F. M. Knox, D. S. Govan, P. N. Kean, I. Bennion, and N. J. Doran. Long distance 10Gbit/s soliton transmission over standard fibre with periodic dispersions compensation. NOC'97, Core and ATM Networks pp18-24, (1997)

[32] E. Yamada, H. Kubota, T. Yamamoto, A. Sahara and M. Nakazawa. 10Gbit/s, 10600km, dispersion-allocated soliton transmission using conventional 1.3μm single mode fibres. ELECTRONICS LETTERS, Vol 33, No 7, pp602-603 (1997)

[33] Govind P.Agrawal, Nonlinear Fiber Optics (Second Edition) Chapter 2 pp28-42 Academic Press (1995)

[34] C. S. Gardener, J. M. Green, M. D. Kruskal and R.M. Miura. Method for solving the Kortweg-de Vries equation. Phys. Rev. Lett, Vol 19, No 19, pp1095- (1967)

[35] V. E. Zakarov and A. B. Shabat. Exact theory of two dimensional self-focusing and one-dimensional self-modulation of wave in nonlinear media. Sov. Phys. JEPT, Vol34, No 1, pp62-69, (1972)

[36] Govind P.Agrawal, Nonlinear Fiber Optics (Second Edition) Chapter 2 section 2.3.2 p44 Academic Press (1995)

[37] A. Hasegawa and Y. Kodama. Guiding-center soliton in optical fibers. OPTICS LETTERS, Vol 15, No 24, pp1443-1445 (1990)

[38] K. J. Blow and N. J. Doran, Average soliton dynamics and the operation of soliton Systems with Lumped Amplifiers. IEEEPHOTONICS TECHNOLOGY LETTERS Vol 3, No 4 pp369 (1991)

[39] L. F. Mollenauer, S. G. Evangelides, and H. A. Haus. Long-Distance Soliton Propagation Using Lumped Amplifiers and Dispersion Shifted Fiber. JOURNAL OF LIGHTWAVE TECHNOLOGY, Vol 9, No 2, pp194-197 (1991)

[40] N. J. Doran, W. Forysiak, F. M. Knox and I. Bennion. Optimizing transmission capacity: long distance terrestrial applications Phil. Trans. R. Soc. Lond. A (1996) 354 pp679-694

[41] N. J. Smith, K. J. Blow, and I. Andonovic. Sideband generation through perturbation to the average sloiton model. IEEE JOURNAL OF LIGHT WAVE TECHNOLOGY, Vol 10, No 10, pp1329-1333 (1992)

[42] A. Yariv. Signal-to-noise considerations in fiber links with periodic or distributed amplification. OPTICS LETTERS, Vol 15, No 19, pp1064-1066 (1990)

[43] J. P. Gordon and H. A. Haus. Random walk of coherently amplified solitons in optical fiber transmission. OPTICS LETTERS, Vol 11 No 1o, pp665-667 (1986)

[44] D. Marcuse. An Alternative Derivation of the Gordon-Haus Effect. JOURNAL OF LIGHTWAVE TECHNOLOGY. Vol 10, No 2 pp273-278 (1992)

[45] D. Marcuse. Calculation of Bit error Prpoabaility for a light wave System with Optical Amplifiers and Post-Detection Gaussian Noise. JOURNAL OF LIGHTWAVE TECHNOLOGY, Vol 9, No 4, pp505-513 (1991)

[46] Y. Kodama and A. Hasegawa. Generation of asymptotically stable optical solitons and suppression of the Gordon-Haus effect. OPTICS LETTERS, Vol, No 1 pp31-33 (1992)

[47] A. Mecozzi, J. D. Moores, H. A. Haus and Y. Lai. Soliton transmission control. OPTICS LETTERS, Vol 16, No 23. pp1841-1843 (1991)

[48] D. Marcuse. Simulations to demonstrate reduction of the Gordon-Haus effect. OPTICS LETTERS, Vol 17, No 1 pp34-36 (1992)

[49] L. F. Mollenauer, J. P. Gordon and S. G. Evangelides. The sliding-frequency guiding filter: An improved form of soliton jitter control. OPTICS LETTERS, Vol 17, No 22, pp1575-1577 (1992)

[50] E. A. Golovchenko, A. N. Pilipetskii and C. R. Menyuk. Soliton propagation with up and down sliding frequency guiding filters. OPTICS LETTERS, Vol 20, No 6, pp539-541 (1995)

[51] A. Mecozzi, M. Midrio and M Romagnoli. Timing jitter in soliton transmission with sliding filters. OPTICS LETTERS, Vol 21, No 6, pp402-404 (1996)

[52] F. Favre, D. Le Guen and M. L. Moulinard. Robustness of 20Gbit/s 63km span 6Mm sliding controlled soliton transmission. ELECTRONICS LETTERS, Vol 31, No 18, pp1600-1601 1995)

[53] S. Kawai. K. Iwatsuki and S. Nishi. Demonstration of error free optical soliton transmission over 30 000km at 10Gbit/s with signal frequency sliding technique. ELECTRONICS LETTERS, Vol 31, No 17, pp1463-1464 (1995)

[54] G. Aubin, T. Montalant, J. Moulu, B. Nortier, F. Pirio and J. B. Thomine. Demonstration of soliton transmission at 10Gbit/s up to 27Mm using signal frequency sliding technique. ELECTRONICS LETTERS, Vol 31, No 1, pp52-53 (1995)

[55] D. LeGuen, F. Favre, R. Boittin, J. Debeau, F. Devaux, M. Henry, C. Thebault and T. Georges. Demonstration of sliding-filter-controlled soltion tranmission at 20Gbit/s over 14Mm. ELECTRONICS LETTERS, Vol 31, No 4, pp301-302 (1995)

[56] J. C. Dung, S. Chi, and S. Wen. Reduction of soliton propagation by zigzag sliding frequency guiding filters. Vol 20, No 18, pp339-341 (1996)

[57] H. P. Yuen. Reduction of quantum fluctuation and suppression of the Gordon-Haus effect with phase-sensitive linear amplifiers. OPTICS LETTERS, Vol 17, No 1, pp73-pp75 (1992)

[58] A. Mecozzi, W. L. Kath, P. Kumar and C. G. Goedde. Long-term storage of a soliton bit stream by use of phase-sensitive amplification. OPTICS LETTERS, Vol 19, No 24, pp (1994)

[59] M. Nakazawa, K. Suzuki, E. Yamada, H. Kubota, Y. Kimura, M. Takaya Experimental Demonstration of Soliton Data-Transmission Over Unlimited Distances With Soliton Control in Time And Frequency Domains, ELECTRONICS LETTERS, Vol.29, No.9, pp.729-730 (1993)

[60] N. J. Smith and W. J. Firth. Suppression of soliton interactions by periodic phase modulation. OPTICS LETTERS, Vol 19, No 1, pp16-pp18 (1994)

[61] N. J. Smith and N. J. Doran. Evaluating the Capacity of Phase Modulator-Controlled Long-Haul soliton Transmission. Optical Fiber Technology 1, pp218-235 (1995)

[62] E. M. Dianov, A. V. Luchnikov, A. N. Pilipetskii and A. N. Starodumov. Electrostriction mechanism of soliton interaction in optical fibers. OPTICS LETTERS, Vol 15, No 6 pp314-316 (1990)

[63] A. N. Pilipetskii and C. R. Menyuk. Acoustic effect and correlated errors in soliton information transmission. OPTICS LETTERS, Vol 21, No 2, pp119-121 (1996)

[64] Y. Jaouen, Laurent du Mouza and Guy Debarge Electrostriction-induced acoustic effect in ultralong-distance soliton transmission systems. OPTICS LETTERS, VOL. 23, NO. 15 (1998)

[65] J. P. Gordon. Interaction forces among solitons in optical fibers. OPTICS LETTERS, Vol 8, No 11, pp596-598 (1983)

[66] Govind P.Agrawal, Nonlinear Fiber Optics (Second Edition) Chapter 5 pp170-172 Academic Press (1995)

[67] F. M. Mitschke and L. F. Mollenauer. Experimental observation of interaction forces between solitons in optical fibers. OPTICS LETTERS, Vol 12, No 5 pp355-357 (1987)

[68] C. Desem and P. L. Chu. Soliton interaction in the presence of loss and periodic amplification in optical fibers OPTICS LETTERS, Vol 12, No 5 pp349-351 (1987)

[69] M. Suzuki, N. Edagawa, H. Taga, H. Tanaka, S. Yamamoto and S. Akiba. Feasibility demonstration of 20Gbit/s single channel soliton transmission over 11500km using alternating-amplitude solitons ELECTRONICS LETTERS, Vol 30, No 13, pp1083-1084 (1994)

[70] M. Suzuki, N. Edagawa, H. Taga, H. Tanaka, S. Yamamoto, S. Akiba. 10Gbit/s, Over 12200km Soliton Data Transmission with Alternating-Amplitude Solitons. IEEE PHOTONICS TECHNOLOGY LETTERS, Vol 6, No 6, pp757-759 (1994)

[71] H. Bulow. Operation of digital optical transmission system with minimal degradation due to polarisation mode dispersion. Electronics letters Vol 31, No 3, pp214-215 (1995).

[72] L. Pierre and J. P. Thiery. Comparison of resistance to polarisation mode dispersion of NRZ and phase-shaped binary transmission formats at 10Gbit/s. ELECTRONICS LETTERS, Vol 33, No 5, pp402-403 (1997)

[73] L.F. Mollenauer, K. Smith and J. P. Gordon Resistance of soliton to the effects of polerization dispersion in optical fibres. OPTICS LETTERS, VOL. 14, NO. 21 (1989)

[74] C. R. Menyuk, OPTICS LETTERS, Stability in birefringent optical fibers. I: Equal propagation amplitudes Vol 12 pp614-616 (1987)

[75] M. N. Islam. C. D. Poole, and J. P. Gordon, Soliton trapping in birefringent optical fibers. OPTICS LETTERS. Vol 14, No 8, pp1011 (1989).

[76] L. F. Mollenauer, and K. Smith, Demonstration of soliton transmission over more than 4000km in fibre with loss periodically compensated for by Raman gain OPTICS LETTERS, Vol 13, pp675-(1998)

[77] Govind P.Agrawal, Nonlinear Fiber Optics (Second Edition) Chapter 10 Academic Press San Diego (1995)

[78] M. J. Ablowitz, G. Biondini, S. Chakravarty, R. B. Jenkins and J. R. Sauer. Four-wave mixing in wavelength-division-multiplexed soltion systems: damping and amplification. OPTICS LETTERS, Vol 21, No 20, pp1646-1648 (1996)

[79] A. Yu and M. J. O'Mahony. Effect of four-wave mixing on amplified multiwavelength transmission systems. ELECTRONICS LETTERS, Vol 30, No 11, pp 876-878 (1994)

[80] L. F. Mollenauer, J. P. Gordon, and M. N. Islam. Soliton propagation in long fibers with periodically compensated loss. IEEE JOURNAL OF QUANTUM ELECTRONICS, Vol 22, pp157-173 (1986)

[81] P. A. Andrekson, N. A. Olsson, P. C. Becker, J. R. Simpson, T. Tanbun-ek, R. A. Logan, and K. W. Wecht. Observation of multi-wavelength soliton collisions in optical systems with fiber amplifiers. APPLIED PHYSICS LETTERS, Vol.57, No 17 pp1715-1717 (1990)

[82] L. F. Mollenauer, S. G. Evangelides, and J. P. Gordon. Wavelength division multiplexing with solitons in ultra long distance transmission using lumped amplifier. IEEE JOURNAL OF LIGHTWAVE TECHNOLOGY, Vol 9, No 3 pp362-367 (1991)

[83] P. A. Andrekson, N. A. Olsson, J. R. Simpson, T. Tanbun-ek, R. A. Logan, P. C. Backer, K. W. Wecht. Soliton Collision interaction force dependence on wavelength separation in fibre amplifier based systems. ELECTRONICS LETTERS Vol. 26, No. 18, pp1499-1501 (1990)

[84] D. J. Richardson, R. P. Chamberlin, L. Dong and D. N. Payne. High quality soliton loss-compensated 38km dispersion-decreasing fibre. ELECTRONICS LETTERS, Vol 31, No 19, pp1681—1682 (1995)

[85] K. Tajima. Compensation of solitons broadening in non-linear optical fibers with loss. OPTICS LETTERS, Vol 12, No 1, pp54-56

[86] R. J. Essiambre and G. J. Agrawal. Ultra-high-bit rate soliton communication systems using dispersion-decreasing fibers and parametric amplifiers. OPTICS LETTERS, Vol 21, No 2, pp116-118 (1996)

[87] M. L. Dennis, W. I. Kaechele, L. Goldberg, T. F. Carruthers, and I. N. Duling. Wavelength-division multiplexing of adiabatic solitons for repeaterless transmission. ELECTRONICS LETTERS Vol 35, No 12, pp1003-1004 (1999)

[88] W. Forysiak, F. M. Knox and N. J. Doran. Stepwise Dispersion Profiling of Periodically Amplified Soliton Systems. JOURNAL OF LIGHTWAVE TECHNOLOGY. Vol 12, No 8, pp1330-1337 (1994)

[89] W Forysiak, F M Knox, and N J Doran, "Average soliton propagation in periodically amplified systems with stepwise dispersion profiled fibre", Opt. Lett. 19 (3), pp. 174-176 (1994)

[90] A. Hasegawa and S. Kumar. Reduction of collision-induced time jitters in dispersion-managed soliton transmission systems. OPTICS LETTERS, Vol 21, No 1, pp39-41

[91] N. J. Smith, N. J. Doran, F. M. Knox and W. Forysiak. Energy scaling characteristics of solitons in strongly dispersion managed fibers. OPTICS LETTERS, Vol 21. No 24, pp1981-1983 (1996)

[92] N. J. Smith, F. M. Knox, N. J. Doran, K. J. Blow and I. Bennion. Enhanced power solitons in optical fibres with periodic dispersion management. ELECTRONICS LETTERS, Vol 32, No 1 pp54-55 (1996)

[93] J. M. Jacob, E. A. Golovchenko, A. N. Pilipetskii, G. M. Carter and C. R. Menyuk. Experimental Demonstration of Soliton Transmission Over 28Mm Using Mostly Nornal Dispersion Fiber. IEEE PHOTONICS TECHNOLOGY LETTERS, Vol 9, No 1, pp130-132 (1997)

[94] L. J. Richardson. Private communication

[95] P Harper, F M Knox, D S Govan, P N Kean, I Bennion, and N J Doran, "Long distance 10Gbit/s soliton transmission over standard fibre with periodic dispersion compensation", European Conference on Networks and Optical Communications, Antwerp, Belgium, pp. 18-24 (1998)

[96] J. H. B. Nijhof, N. J. Doran and W, Froysiak. Energy enhancement of dispersion managed solitons for strong dispersion maps. Conference on Optical Fibre Communications (OFC'98), Techn Digest, San Jose, USA, ThC4 (Feb 1998)

[97] N. J. Smith, W. Forysiak and N. J. Doran. Reduced Gordon-Haus jitter due to enhanced power solitons in strongly dispersion managed systems. ELECTRONICS LETTERS, Vol 32, No 22, pp2085-2086 (1996).

[98] N. J. Smith, N. J. Doran, W. Forysiak and F. M. Knox. Soliton Transmission Using Periodic Dispersion Compensation. JOURNAL OF LIGHTWAVE TECHNOLOGY, Vol 15, No 10, pp1808-1822 (1997)

[99] T Okamawari, A Maruta and Y Kodama. Analysis of Gordon-Haus Jitter in a dispersion-compensated optical transmission system. OPTICS LETTERS, Vol 23, No 9, pp694-696 (1998)

[100] M. Suzuki, I. Morita, N. Edagawa, S. Yamamoto, H. Taga and S Akiba. Reduction of Gordon Haus timing jitter by periodic dispersion compensation in soliton transmission. ELECTRONICS LETTERS, Vol 31, No 23, pp2027-2029 (1995)

[101] G. M. Carter, J. M. Jacob and C. R. Menyuk. Timing-jitter reduction for a dispersion-managed soliton system: experimental evidence. OPTICS LETTERS, Vol 22, No 8, pp513-515 (1997)

[102] L. F. Mollenauer, P. V. Mamyshev and J. P. Gordon. Effect of guiding filters on the behavior of dispersion-managed solitons. OPTICS LETTERS, Vol 24, No 4, pp220-222 (1999)

[103] B. P. Luce. Power enhancement with super-Gaussian sliding-frequency guiding filters. OPTICS LETTERS, Vol 23, No 10, pp765-767 (1998)

[104] S. Wabnitz. Stabilization of sliding-filtered soliton wavelength division multiplexing transmissions by dispersion-compensating fibres. OPTICS LETTERS, Vol 21, No 9 pp638-640. (1996)

[105] A. Hasegawa, S. Kumar, and Y. Kodama, OPTICS LETTERS Vol 32, no xx, pp39- (1996) Check this refference? To see if it is about reduced jitter(due to collisions) through dispersion management.

[106] J. F. L. Devaney, W. Forysiak, A. M. Niculae, and N. J. Doran. soliton collisions in dispersion-managed wavelength-division-multiplexed systems. OPTICS LETERS, Vol 22 No 22, pp1695-1697 (1997)

[107] A. M. Niculae, W. Forysiak, A. J. Gloag, J. H. B. Nijhof, and N. J. Doran. Soliton collisions with wavelength-division multiplexed systems with strong dispersion management, OPTICS LETTERS, Vol 23, No 17, pp1354-1356 (1998)

[108] S. Wabnitz Wavelength Division Multiplexing of Dispersion managed solitons.. European Conference on Optical Communicatons, Madrid Volume 1, pp83-84 (1998)

[109] T. Hirooka and A. Hasegawa. Chirped soliton interaction in strongly dispersion-managed wavelength-division-multiplexing systems. OPTICS LETTERS, Vol. 23, No. 10, pp768-770 (1998)

[110] M. Suzuki, I. Monrita, N. Edagawa, S. Yamamoto, and S. Akiba. 20Gbit/s-based soliton WDM transmission over transoceanic distances using periodic compensation of dispersion and its slope. ELECTRONICS LETTERS, Vol. 33, No. 8, pp691-692 (1997)

[111] F. Favre, D. Le Guen, M. L. Moulinard, M. Hnery, and T. Georges. 320Gbit/s soliton WDM transmission over 1300k with 100km dispersion compensated spans of standard fibre. Vol 33, No 25, pp 2135-2136 (1997)

[112] D. Le. Guen, A. O'Hare, S. Del. Burgo, D. Grot, F. Favre, and T. Georges. Narrowband 640Gbit/s DWDM transmission over 1200km of standard fibre with 100km – 12dB amplifier spans ELECTRONICS LETTERS Vol, 32, pp471-473, (1996)

[113] C. Kurtzke, suppression of fibre non-linearities by appropriate dispersion management. IEEE PHOTONICS TECHNOLOGY LETTERS, Vol 5, No xx, pp1250-1253 (1993)

[114] R. W. Tkach, A. R. Chraplyvy, F. Forgheiri, A. H. Gnauck, and R. M. Derosier. 4-Photon mixing and high speed WDM systems. JOURNAL OF LIGHTWAVE TECHNOLOGY. Vol 13, pp841-849 (1995)

[115] P. C. Becker, N. A. Olsson, and J. R. Simpson. Erbium-Doped Fiber Amplifiers (Fundamentals and Technology), Academic Press, San Diego, pp67 (1999)

[116] C. Desem, and P. L. Chu. Effect of chirping on solution propagation in single-mode optical fibers. OPTICAL LETTERS, Vol 11, No 4, pp248-250 (1986)

[117] T. Tanifuji and M. Ikeda. Pulse circulation measurement of transmission characteristics in long optical fibres. OPTICS LETTERS, Vol 16, No 8 (1977)

[118] L. F. Mollenauer and K. Smith. Demonstration of soliton transmission over 4000km in fiber with loss periodically compensated by Raman gain. OPTICS LETTERS, Vol 13, No 8, pp675-677 (1988)

[119] N. S. Bergano, Circulating loop Transmission Experiments for the study of long-haul Transmission Systems Using Erbium-Doped Fiber amplifiers. JOURNAL OF LIGHTWAVE TECHNOLOGY, Vol 13, No 5, pp879-888 (1995)

[120] M. G. Taylor. Observation of New Polarization Dependence Effect in long Haul Optically Amplified System. IEEE PHOTONICS TECHNOLOGY LETTERS, Vol 5, No 10, pp1244-1246 (1993)

[121] E. Lichtmann. Performance degradation due to polarisation dependent gain and loss in lightwave systems with optical amplifiers. ELECTRONICS LETTERS, Vol 29, No 22, pp 1971-1972 (1993)

[122] Gerd Keiser, Optical Communications Second Edition, Mc Graw Hill, pp286

[123] J. H. B. Nijhof, N. J. Doran, W. Forysiak and A. Berntson. Energy enhancement of dispersion-managed solitons and WDM. ELECTRONICS LETTERS, Vol 34 No 5, pp481-482 (1998)

[124] J. H. B. Nijhof. N. J. Doran, W. Forysiak and F. M. Knox. Stable soliton-like Propagation in dispersion managed systems with net anomalous, zero and normal dispersion. ELECTRONICS LETTERS, Vol 33, No 20, pp1726-1727 (1997)

[125] J. N. Kutz. S. G. Evangelides, Jr. Dispersion-managed breathers with average normal disperision. OPTICS LETTERS, Vol 23, No 9, pp685-687 (1998)

[126] V. S. Grigoryan and C. R. Menyuk. Dispersion-managed solitons at normal average dispersion. OPTICS LETTERS, Vol 23, No 8, pp609-611 (1998)

[127] S. K. Turitsyn, E. G. Shapiro. Dispersion-managed solitons in optical amplifier transmission systems with zero average dispersion, OPTICS LETTERS, Vol 23, No 9, pp682-684 (1998)

[128] J. H. Nijhof, Private communication

[129] J. H. B. Nijhof, W. Forysiak and N. J. Doran. Dispersion-managed soltions in the normal dispersion regime: A physical interpretation. OPTICS LETTERS, Vol 23, No 21, pp1674-1676 (1998)

[130] A. Berntson, D. Anderson, N. J. Doran, W. Forysiak and J. H. B. Nijhof, Power dependence and accessible bandwidth for dispersion-managed solitons in asymmetric dispersion maps. ELECTRONICS LEETERS, Vol 34, No 21, pp2054-2056 (1998)

[131] T. Yu, E. A. Golovchenko, A. N. Pilipetskii and C. R. Menyuk. Dispersion-Managed soliton interactions in optical fibers. OPTICS LETTERS, Vol 22, No 11, pp793-795 (1997)

[132] M. Matsumoto. Analysis of interaction between stretched pulses propagating in dispersion managed fibers. IEEE PHOTONICS TECHNOLOGY LETTERS. Vol 10, No 3, pp373-375 (1998)

[133] A M Niculae, W Forysiak, and N J Doran. Optimal amplifier location in strong dispersion-managed soliton systems, Conference on Lasers and Electro-Optics (CLEO'99), Technical Digest, pp236 (1999)

[134] W. Sibbett and J. R. Taylor. Passive mode-locking in green-yellow using saturable absorber dasbti. IEEE JOURNAL OF QUANTUM ELECTRONICS, Vol 18 No 12, pp1994-1996 (1982)

[135] T. Varghese. Passive mode-locking of a coumarin dye-laser from 505-520nm using doci as the saturable absorber. OPTICAL COMMUNICATIONS, Vol 44, No 5, pp353-356 (1983)

[136] D. J. Harter, Y. B. Band, and E. P. Ippen. Theroy of mode-locked lasers containing a reverse saturable absorber. JOURNAL OF QUANTUM ELECTRONICS, Vol 21, No 8, pp1219-1228 (1985)

[137] S. Bennett, and A. J. Seeds. Error free soliton transmission over trans-oceanic (>8000km) distances using fast saturable absorber and dispersion decreasing fibre. Technical digest of Optical fibre conference, San Diego (1999)

[138] O. Audouin, E. Pallise, E. Desurvire, and E. Maunand. Use of fast in-line saturable absorbers in wavelength-division-multiplexed soliton systems. IEEE PHTONICS TECHNOLOGY LETTERS, Vol 10, No 6 pp828-829 (1992)

[139] K. Smith and L. F. Mollenauer. Experimental observation of soliton interaction over long fibre paths: discovery of a long range interaction. OPTICS LETTERS, Vol 14, No 22, pp1284-1286 (1989)

[140] M. Romagnoli, L. Socci, M. Midrio, P. Franco, T. Georges. Long-range soliton interactions in dispersion-managed links. OPTICS LETTERS, Vol 23, No 15, pp1182-1184 (1998)

[141] R. J. Essiambre and G. P. Agrawal. Control of soliton-soliton and soliton dispersive wave interactions in high bit-rate communication systems. ELECTRONICS LETTERS, Vol 31, No 17, pp1461-1463 (1995)

[142] M. Matsumoto, A. Hasegawa and Y. Kodama. Adiabatic amplification of solitons by means of nonlinear amplifying loop mirrors. OPTICS LETTERS, Vol 19, No 14, pp1019-1021 (1994)

[143] M. Matsumoto, H. Ikeda and A. Hasegawa. Suppression of noise accumulation in bandwidth-limited soliton transmission by means of nonlinear loop mirrors. OPTICS LETTERS, Vol 19, No 3, pp183-185 (1994)

[144] F. M. Knox, P. Harper, P. N. Kean, N. J. Doran, and I. Bennion. Low jitter long distance pulse transmission near net fibre dispersion zero wavelength. ELECTRONICS LETTERS, Vol 31, No 17, pp1467-1468 (1995)

[145] M. N. Islam, C. E. Soccolich and J. P. Gordon. Soliton intensity-dependent polarization rotation. OPTICS LETTERS, Vol 15, No 1, pp21-pp23 (1990)

[146] V. V. Afanasjev. Soliton polarization rotation in fiber lasers. OPTICS LETTERS, Vol 20, No 3, pp270-272, (1995)

[147] R. H. Stolen, J. Botineau and A. Ashkin. Intensity discrimination pulses with birefringent fibers. OPTICS LETTERS, Vol 7, No 10, pp512-514 (1982)

[148] D. S. Govan, N. J. Smith, F. M. Knox and N. J. Doran. Stable propagation of solitons with increased energy through the combined action of dispersion management and periodic saturable absorbtion. JOURNAL OF THE OPTICAL SOCIETY OF AMERICA, Vol 14, No 11, pp2960-2966 (1997)

[149] D. S. Govan. Private communication

[150] A. Sahara, K. Suzuki, H. Kubota, T. Komukai, E. Yamada, T. Imai, K. Tamura, and M. Nakazawa. 40Gbit/s soltion transmission field experiment over 1,020km and its extension to 1360km using in-line synchronous modulation. Technical Digest of Optical Fiber Communication Conference, San Diego pp121-124 (1999)

[151] J. Brentel, P. A. Andrekson, E. Kolltveit, B. E. Bakhshi, J. Hansryd, P. O. Hedekvist, M.Karlsson, and J. Li. Single-wavelength 40Gbit/s Soliton field transmission experiments over 400km fibre without in-line control. Technical Digest of Optical Fiber Communication Conference, San Diego pp112-114 (1999)

[152] I. Morita, K. Tanaka, N. Edagawa, and M. Suzuki. 40Gbit/s single-channel soliton transmission over 10200km without active inline transmission control. European Conference on Optical Communication (Postdeadline), Madrid, (1998)

[153] I D Phillips, A Gloag, D G Moodie, N J Doran, I Bennion, and A D Ellis, "Drop and insert multiplexing with simultaneous clock recovery using an electroabsorption modulator", IEEE Photonics Tech. Lett. 10 (2), pp. 291-293 (Feb 1998)

[154] I Phillips, A Gloag, D G Moodie, N J Doran, I Bennion, and A D Ellis, "40 Gbit/s 'drop-and-insert' multiplexing with novel clock recovery using an electroabsorption modulator in a bi-directional configuration", 23rd European Conference on Optical Fibre Sensors, Edinburgh, pp81-84 (Sep 1997)

[155] I. Morita, M. Suzuki, N. Edagawa, S. Yamamoto, and S. Akiba. Single-channel 40Gbit/s, 5000km straight-line transission experiment using periodic dispersion compensation. ELECTRONICS LETTERS, Vol 33, No 8, pp698-699 (1997)

[156] I. Morita, K. Tanaka, N. Edagawa, S. Yamamoto, and M. Suzuki. 40 Gbit/s single-channel soliton transmission over 8600km using periodic dispersion compensation. ELECTRONICS LETTERS, Vol.34, No.19, pp.1863-1865 (1998)

[157] D. Nesset, M. F. C. Stephens, A. E. Kelly, C. Gilbertas, J. Reed, K. A. Williams, S. Bouchoule, R. Kashyap, A. D. Ellis and D. G. Moodie. 40Gbit/s transmission over 186.6km of installed fibre using mid span sprectral inversion for dispersion compensation. Optical Fiber Communication Conference, San Diego, (1999)

[158] U. Feiste, R. Ludwig, E. Dietrich, S. Diez, H. J. Ehrke, Dz. Razic, H. G. Weber. 40Gbit/s Transmission over 434km Standard-Fiber Using Polarisation Independent Mid-Span Spectral Inversion. (postdeadline Volume 3) European Conference on Optical Communications, Madrid, (1998)

[159] D. S. Govan, W. Forysiak, and N. J. Doran. Long-distance 40Gbit/s soliton transmission over standard fiber by use of dispersion management. OPTICS LETTERS, Vol 23, No 19, pp1523-1525 (1998)

[160] M. Nakazawa, E. Yoshida, E. Yamada, K. Suzuki, T. Kitoh and M. Kawachi. 80Gbit/s soliton data transmission over 500km with unequal amplitude solitons for timing clock extraction. ELECTRONICS LETTERS, Vol 30, No 21, pp1777-1778 (1994)

[161] S. Wen. Distributed erbium-doped fibre amplifier for soliton transmission. OPTICS LETTERS, Vol 19, No 1, pp22-24 (1994)

[162] D. S. Govan. Private Communication